STRUCTURAL EVOLUTION OF THE TWELVE MILE BAY SHEAR ZONE, GRENVILLE PROVINCE, ONTARIO, CANADA

Peter J. Regan

Submitted in partial fulfillment of the requirements
for the degree of Master of Science

Dalhousie University
Halifax, Nova Scotia
November, 2019

TABLE OF CONTENTS

LIST OF TABLES

LIST OF FIGURES

ABSTRACT

Shear zones are tabular structures of higher strain and vorticity relative to the country rock. Shear zones appear globally, at all scales, and commonly link together to form complex anastomosing patterns. The processes by which shear zones nucleate, propagate, and form networks have been studied extensively, but predominately in isotropic materials.

The Twelve Mile Bay shear zone, located in the ca. 1.0 Ga Grenville orogen in Ontario, Canada, is a shear zone system developed with anisotropic rocks of the interior Parry Sound domain (iPSD). Granulite facies layering of the southern margin of the iPSD is transposed by a series of increasingly connected amphibolite facies shear zones within a five kilometer wide zone of progressive deformation, preserving several stages of shear zone development, resulting in the regional-scale shear zone between the iPSD and the lower Go Home domain.

Outcrops were digitally imaged using innovative aerial photography and open source software to create high-resolution georeferenced aerial photo mosaics of several islands. Photo mosaics enabled quantitative measurement of strain along shear zones and their geometries at various stages of shear zone development.

Measurements show an increase in shear strain (γ_{avg}) proximal to the Twelve Mile Bay shear zone and reveal a bimodal distribution of extension directions, from NNE-SSW at the start of the zone of transposition, to E-W toward the Twelve Mile Bay shear zone where transposition is complete. Folds within wall rocks at several stages of transposition revealed that fold hinges originate in a steeply plunging orientation and are reoriented into the shallowly plunging, E-W oriented, regional extensional direction of the Twelve Mile Bay shear zone (~E-W).

This study proposes a conceptual model for the main stages of transposition along the southern margin of the iPSD: i) brittle fracture-filled pegmatite dykes introduced hydrated planes of weakness; ii) initial dextral shear zone developed along pegmatites; iii) sinistral shearing at a high angle to dextral shear zones that amplified pre-exisiting dextral shear zones and introduced internal wall rock deformation; iv) folded wall rock blocks are increasingly deformed and rotated into the regional extensional direction causing shear zone widening, which led to an increasingly linked shear zone network; and, v) complete transposition of iPSD layering to the shear zone fabric with rare pods of iPSD fabric.

LIST OF ABBREVIATIONS AND SYMBOLS USED

ABT	Allochthon Boundary Thrust
bPSD	basal Parry Sound Domain
CGB	Central Gneiss Belt
CMB	Central Metasedimentary Belt
D	Displacement
DEM	Digital elevation model
DGPS	Differential global positioning system
GFTZ	Grenville Front Tectonic Zone
iPSD	interior Parry Sound Domain
L	Lineation
lGH	lower Go Home Domain
lPSSZ	lower Parry Sound shear zone
PSD	Parry Sound Domain
R	Ellipticity
RRB	Retrogression and Reworking Boundary
RTK	Real-time Kinematic
S	Shawanaga Domain
S_1	PSD granulite facies fabric
S_2	TMBSZ amphibolite facies fabric
TMBa	Twelve Mile Bay assemblage
TMBSZ	Twelve Mile Bay shear zone
tp	Transposed gneiss unit
uGH	upper Go Home Domain
uPSSZ	upper Parry Sound shear zone
W	Width of a shear zone
α	Angle of an undeformed layer
α'	Angle of a layer deflected by a shear zone
β	Wall rock rotation
γ_{avg}	Average shear strain
γ_{bulk}	Bulk shear strain
γ_{max}	Maximum shear strain
θ'	Angle of the long axis of a strain ellipse

ACKNOWLEDGMENTS

I would like to thank several people who helped me along this journey of my graduate research. I could not have done it without your help, patience, and support.

First and foremost, I would like to thank my supervisor Dr. Nick Culshaw for his guidance through this process. I thoroughly enjoyed our time in the field and have many happy memories of time spent around Georgian Bay. Aside from helping with everything from structural geology to Grenville tectonics, Nick offered me constant optimism and encouragement, both of which were crucial in getting me over the line.

I would like to thank my examining committee, Dr. Djordje Grujic, Dr. Brendan Murphy, Dr. Chris Greene, and Dr. Yana Fedortchouk for chairing the defence. In particular I'd like to thank Djordje, as a member of my thesis committee and providing plenty of helpful comments to improve the thesis.

I would like to thank Mary and Ed Bartram who graciously let us use their little paradise as part of our study area. Sadly Ed passed away this year and will be sorely missed.

I would like to thank my friends and family for their encouragement and support in particular, my mother Debbie. Lastly I would like to thank Svieda Ma for her love, patience, and belief in me. I could not have done it without you.

CHAPTER 1: INTRODUCTION

1.1: Statement of problem

The goal of the study is to document macroscopic features of a shear zone network within the Grenville Province along Twelve Mile Bay, southern Ontario by creating detailed photo-maps of several islands representing progressive stages of the strain gradient within Twelve Mile Bay. Data can then be used to further characterize shear zones as they develop, for example, whether a shear zone widens with an increase of strain. The photo-maps allow quantitative data to be derived including shear zone width, displacement, shear zone density, and shear strain of shear zones. From previous studies it has been shown that propagation of shear zones into a network is accompanied by an increase in shear strain along individual shear zone segments (Carreras, 2001; Mancktelow and Pennacchioni, 2005; Schrank et al., 2008). The data collected from the Twelve Mile Bay shear zone (TMBSZ) was used to investigate if shear strain values increase as the complexity and geometry of an amphibolite facies shear zone network evolves.

1.2: Shear zones

Shear zones are planar zones of higher strain compared to the country rock that flanks them (Ramsay and Graham, 1970; Fossen, 2017). Shear zones appear globally, at all scales, and have been extensively studied as it has been recognized that shear zones play an important role in rock deformation, particularly in the lower crust (Ramsay and Graham, 1970; Gapais, 1989; Hudleston, 1999; Carreras, 2001; Fossen, 2017).

It should be noted that there is a distinction between shear zone systems, and shear zone networks. A shear zone system refers to a series of coeval shear zones which may, or may not, be linked together. A shear zone network however, explicitly refers to a group of shear zones that are kinematically linked to one another. A shear zone system may include several shear zone networks.

Many authors have described natural examples of anastomosing shear zone networks (Gapais et al., 1987; Bhattacharyya and Hudleston, 2001; Fusseis et al., 2006; Carreras et al., 2010; Ponce et al., 2013); however, exposures featuring multiple stages of shear zone development are rare. The Twelve Mile Bay shear zone (TMBSZ) provides an opportunity to study and document the processes by which shear zones nucleate, propagate, and link together into networks as it provides a strong example for empirical study. Understanding shear zone network geometries and their progressive development can lead to a better understanding of how bulk deformation is accommodated (Hudleston, 1999; Bhattacharyya and Czeck, 2008). These processes have widespread implications for the dynamics of major tectonic boundaries, localized deformation of the lower crust, and thereby orogenic development.

Much of the literature regarding shear zone networks is based on studies within isotropic rocks (Gapais et al., 1987; Pennacchioni and Mancktelow 2007; Schrank et al., 2008). This study features shear zone networks that have developed within strongly anisotropic rocks with varying contrasts in layer competence. It is important to recognize that shear zones in anisotropic rocks have specific properties that make them different from shear zones forming in isotropic rocks. The presence of pre-existing anisotropies is known to have a significant influence of the orientation, propagation and deformation style of shear zones (Ponce et al., 2013, and references therein). This study will focus on characterizing stages of amphibolite facies shear zone development within a granulite facies block during progressive deformation, and what effects pre-existing anisotropy have on shear zone system development.

1.3: Geologic Setting

The Grenville Province of the south-eastern Canadian Shield is a deeply eroded collisional orogenic belt (ca. 1.1 Ga) that developed during the formation of the supercontinent Rodinia (Hynes and Rivers, 2010). The Grenville Orogen was a large, hot orogen, comparable in scale to the modern day Himalayan Orogeny (Jamieson et al., 1995; Rivers, 2008). Wynne-Edwards (1972) divided the western Grenville Province into three distinct packages, the Grenville Front Tectonic Zone (GFTZ), the Central Gneiss Belt (CGB), and the Central Metasedimentary Belt (CMB). The Central Gneiss Belt is exposed along Georgian Bay, providing an excellent opportunity to study the mid-to-lower crust of a large, hot orogenic belt (Culshaw et al., 1997; Carr et al., 2004; Rivers, 2012).

The location of the Parry Sound domain (PSD), bounding shear zones, and neighboring lithotectonic domains within this study within the Grenville Province are located in Figure 1.1. The CGB is a large area that consists of several units of orthogneisses, migmatites, and supracrustal rocks separated from one another by regional-scale shear zones (Davidson, 1982; Culshaw et al., 1997). The Parry Sound domain is one such unit, with the lower Parry Sound shear zone (lPPSZ) separating the PSD from the underlying Shawanaga domain (S) to the north, and the Twelve Mile Bay shear zone (TMBSZ) separating the PSD from the underlying upper Go Home domain (uGH) (Culshaw et al., 2010). The lithotectonic domains of the CGB are interpreted as lower crustal thrust sheets that were stacked and exhumed during collision (Davidson, 1982; Culshaw et al., 1997; Carr et al., 2000; Jamieson et al., 2007).

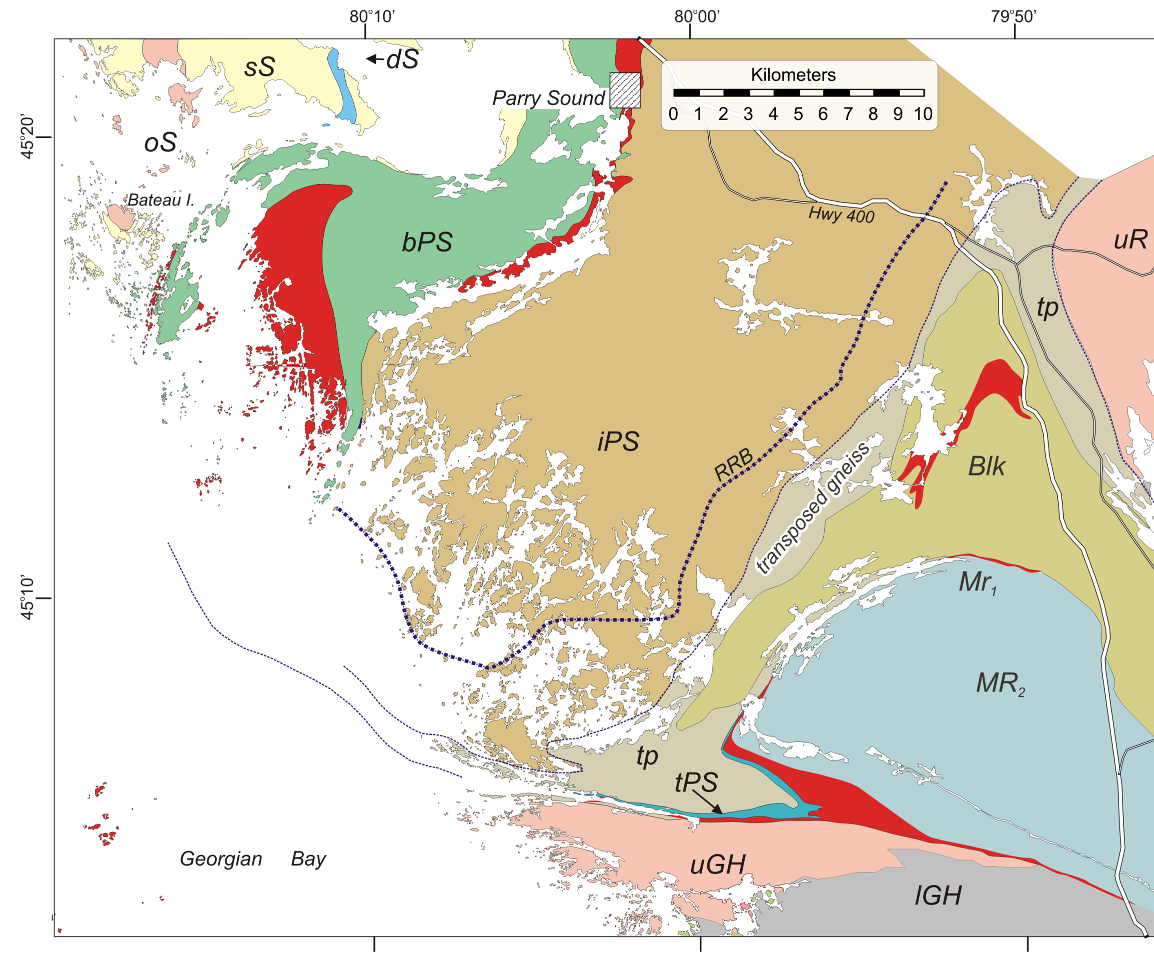

Figure 1.1: Geologic map of Georgian Bay, southern Ontario from Culshaw et al., 2010. Shawanaga domain: oS, Ojibway; sS, Sand Bay gneiss association; dS, Dillon schist. Parry Sound domain: bPS, basal Parry Sound; iPS, interior Parry Sound; tPS, Twelve Mile Bay assemblage; tp, transposed gneiss unit. Moon River domain: $MR_{1\text{-}2}$, interior subdivisions of Moon River domain. Domain of uncertain affinity: Blk, Blackstone gneiss association. Go Home domain: uGH and lGH, upper and lower.

The PSD along Twelve Mile Bay provides excellent opportunities to observe minor (metre-scale) and major (tens of metre-scale) shear zones across a strain gradient and the progressive development of the crustal-scale TMBSZ by shear zone network widening. Work by Culshaw et al. (2010) and Marsh et al., (2011a) concluded that the interior PSD retains its structure and fabric, but along its margins there is a zone of reworking caused by hydration and retrogression of granulite facies to amphibolite facies assemblages. Fluid emplacement is focused in linear corridors of fractures filled with pegmatite. Given the mineralogical and geochemical evidence for increased water content in the sheared rocks, it is thought that the shear zone network forms preferentially along these weakened zones. The granulite facies gneissosity of the PSD is reworked into the terrane bounding amphibolite facies TMBSZ. The TMBSZ is thought to have developed as part of a ductile shell that surrounded the rigid PSD during its transport from the lower crust through amphibolite facies migmatites (Culshaw et al., 2010; Marsh et al., 2011a; Marsh et al., 2011b).

The overprinting of one fabric over another is referred to as transposition, which is the superposition of a tectonic foliation on a pre-existing fabric. With progressive deformation the pre-existing fabric is isoclinally folded and dismembered leading to isolated fold hinges with axial planes parallel to the new foliation. Pre-existing fabric is transformed into a discontinuous banding parallel to the new foliation (Twiss and Moores, 2007). In this case we refer to transposition as the progressive development of amphibolite facies shear zones within a granulite facies protolith with gneissosity at a high angle to the transposed shear zone gneissosity. The southern margin of the iPSD with the TMBSZ is a strain gradient marked by the progressive increase of shear zone density and thickness, which may be accompanied by the linkage of shear zones into networks. Several islands situated within the strain gradient provide exposures of differing stages of transposition. At one end of the gradient is the interior PSD granulite striking NNE; at the other end is a new amphibolite fabric from transposed and reworked PSD gneissosity, striking W.

1.4: Proposed Study

The work done by Culshaw et al., (2011) highlighted the importance of documenting the early development of shear zone networks, but it is necessary to extend this work to investigate the evolution of such a network across a strain gradient. Strain transects can be analyzed using improved methods of quantifying shear strain for many sites along the Twelve Mile Bay strain gradient. By displaying the results of strain transects on highly accurate photo-maps, shear strain can be compared with qualitative features such as physical characteristics of the shear zone geometry, as well as other quantitative data, leading to a better understanding of the development of an amphibolite facies shear zone network within a granulite facies block.

Previous structural investigations have described Matches Island as a dextral shear zone system. As Matches Island is considered to be a juvenile developmental stage of the Twelve Mile Bay shear zone (Culshaw et al., 2011), the structural and kinematic interpretation of Matches Island has implications for the larger region in general. Observations made from new aerial imagery from Matches Island reveal that the W-E striking dextral shear zones are cross-cut by a wide N-S striking sinistral shear zone. Sinistral shear zones have also been noted on islands in the advanced stages of transposition (Culshaw et al., 2011; Marsh et al., 2011a), but the discovery of sinistral shear overprinting dextral shear as observed on Matches Island is evidence that sinistral shear may play a greater role in transposition than was previously thought. The discovery of sinistral shear zones in the early stages of transposition suggest that the Twelve Mile Bay shear zone has undergone either; i) two distinct phases of ductile deformation; or ii) deformation via a conjugate shear zone network; requiring a rethink of the regional kinematics of the Twelve Mile Bay shear zone.

The purpose of this study is to document and describe the structural evolution between the southern margin of the iPSD and the Twelve Mile Bay shear zone (Fig. 1.1). The study areas of Teddy Rock, Matches, PBW, Bartram's, and PBE islands represent various preserved stages of transposition with early stages to the N and advanced stages to the S. By investigating the structural evolution of the southern interior Parry Sound domain margin we hope to determine whether these juxtaposed sinistral and dextral shear zones within TMBSZ formed separately as two distinct phases of deformation, or together as a conjugate shear zone network. The style and development of shearing has direct implications for the regional kinematics for the emplacement of the Parry Sound domain.

1.5: Objectives

Short term

a) Develop a mapping method to accurately map complex structure
b) Document how shear zone systems develop in space, based on measurable physical characteristics (layering dimensions, linkage, and shear zone dimensions) and changes in shear strain.
c) Measure and calculate shear strain changes along individual shear zones showing changes in physical characteristics along their length; and bulk strain for areas incorporating several shear zones (in well-developed and poorly developed systems).
d) Characterize shear zones based on qualitative features such as fold development and the deformation of wall rock.

Long Term:

a) Provide insight on how progressive development of a shear zone network leads to a regional-scale shear zone formed at amphibolite facies within a layered granulite facies block.
b) Provide insights on the regional kinematics and strain partitioning of the Twelve Mile Bay shear zone.

CHAPTER 2: REGIONAL GEOLOGY

2.1: Introduction

The Grenville Province of southeastern Ontario reflects the mid- to lower crust of a deeply eroded collisional orogen active between ca. 980 and 1090 Ma (Hynes and Rivers, 2010). The Grenville Orogen (Fig. 2.1) is characterized by high-grade metamorphism, with widespread amphibolite- to granulite facies metamorphic rocks found throughout as well as localized eclogite and greenschist facies metamorphism (van Gool, 1992; Indares and Rivers, 1995). The complex tectonometamorphic history of the Grenville Orogeny has drawn comparisons to the modern day Himalayan orogen, and provides an opportunity to study the behavior of middle- to lower crust of a large hot collisional orogen (Jamieson et al., 1995; Wodicka et al. 1996; 2000; Gerbi et al., 2010).

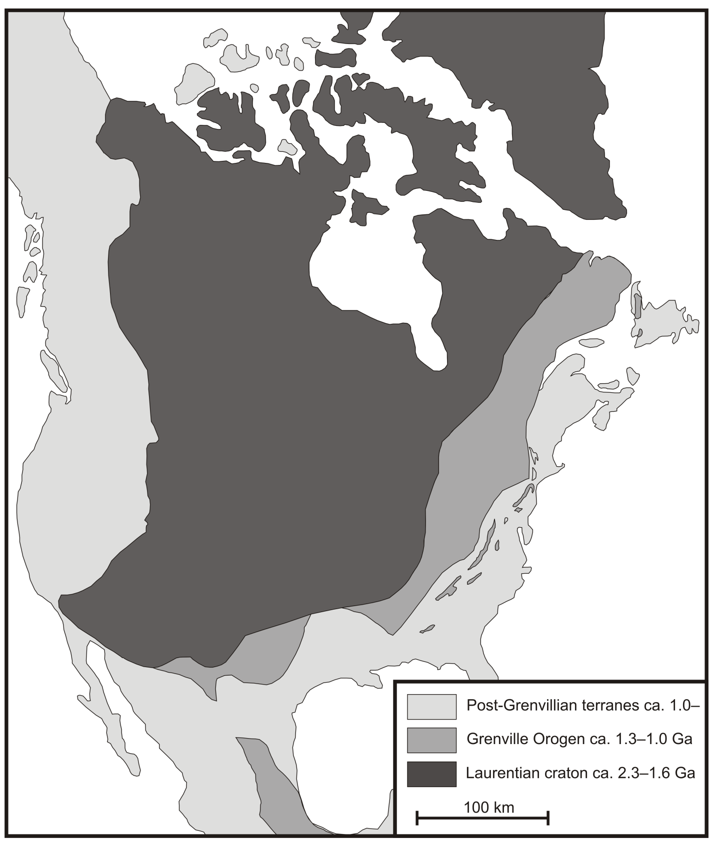

Figure 2.1: Extent of the Grenville Province, modified from Hoffman (1988).

The Grenville Orogeny was caused by the collision between Laurentia with another continent, which is thought to be Amazonia (Hoffman, 1988; Rivers, 2008) that took place between ca. 1090-980 Ma. The Grenville Province comprises reworked Archean and Paleo- to Mesoproterozoic rocks of Laurentian affinity, as well as rocks of exotic outboard terranes that accreted to the Laurentian margin during convergence (Rivers et al., 1997).

There are several time periods of thrusting and metamorphism that have been associated with the Grenville Province. Rivers and Corrigan (2000) divided the Grenville orogen into three distinct orogenic pulses: i) the Shawinigan phase, active from ca. 1190 – 1120 Ma; ii) the Ottawan phase, active from ca. 1090 – 1020 Ma; and iii) the Rigolet phase, active from ca. 1020 – 980 Ma. The Shawinigan pulse is associated with localized high-grade metamorphism and deformation in the southwest and central parts of the orogen, caused by the accretion of arc terranes to the Laurentian margin (Rivers et al., 2002). The Ottawan phase is characterized by widespread high-grade metamorphism throughout the Grenville Orogeny, caused by the main Grenvillian collision (Jamieson et al., 2010). The Rigolet phase features localized thrusting and metamorphism along the northwest margin of the orogeny, as well as localized extension due to post-convergent gravitational spreading (Jamieson et al., 2010; Rivers, 2012).

2.2: Regional Framework

The Grenville Province in Canada has been divided into two major lithotectonic units; i) the Parautochthonous Belt, consisting of reworked Archean-Mesoproterozoic rocks; and ii) the Allochthonous Belt, consisting of juvenile plutonic and supracrustal rocks (Rivers et al., 1989; Davidson 1995; Culshaw et al., 1997). The term allochthonous is used to imply far-travelled terranes rather than imply a genetic link to Laurentia, as the Allochthonous Belt is further subdivided into monocyclic and polycyclic units, with the former being exotic and the latter being Laurentian derived terranes (Rivers, 2012). Monocyclic refers to rocks that have only experienced Grenvillian metamorphism, while polycyclic refers to rocks that have experienced pre-Grenvillian metamorphism (pre- ca. 1200 Ma) (Wodicka et al., 2000; Culshaw et al., 2010). The Allochthon Boundary Thrust (ABT), a southeast-dipping crustal-scale décollement, separates the Allochthonous hanging wall from the Parautochthonous footwall (Rivers et al., 1989).

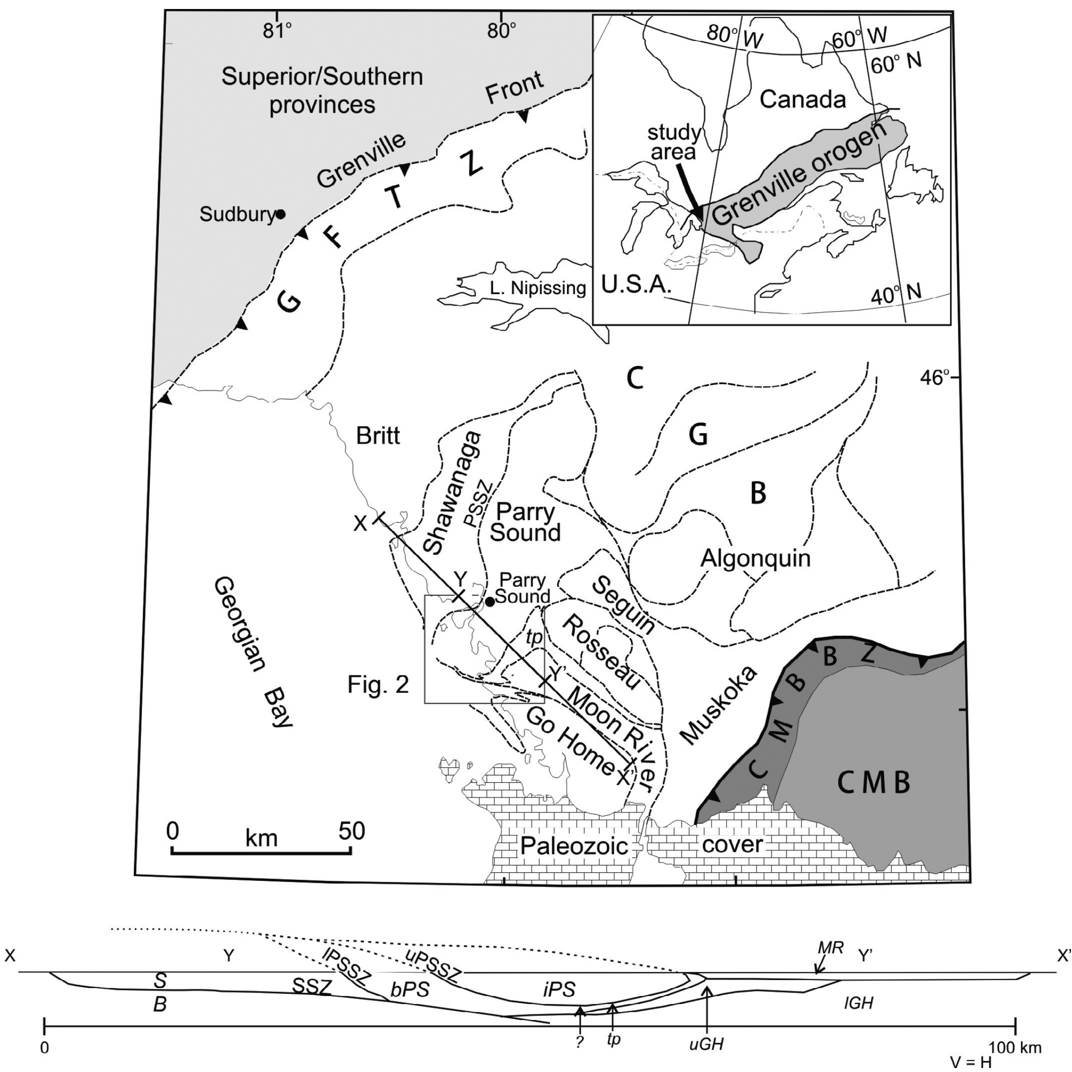

Figure 2.2: Geologic map of the Grenville Province of southestern Ontario. Lithotechtonic subdivisions (Wynne-Edwards, 1972): GFTZ, Grenville Front Tectonic Zone; CGB, Central Gneiss Belt; CMB, Central Metasedimentary Belt; CMBBZ, Central Metasedimentary Belt Boundary Zone. Subdomains of the southwestern CGB on cross-section X-X': B, Britt domain; S, Shawanaga domain; bPS, basal Parry Sound domain; iPS, interior Parry Sound domain; MR, Moon River domain; uGH, upper Go Home domain; lGH, lower Go Home domain. Other structures or tectonic units: lPSSZ, lower Parry Sound shear zone; uPSSZ, upper Parry Sound shear zone; SSZ, Shawanaga shear zone; tp, transposed gneiss. From Culshaw et al. (2010).

The Parautochthonous Belt is made up of polycyclic rocks that predominately originated from the Laurentian craton, and were subsequently reworked during Grenvillian orogenesis. In the western Grenville Province, the Parautochthonous Belt consists of granitoid plutons with a bimodal age distribution (ca. 1750-1600 and ca. 1500-1340 Ma (van Breeman et al., 1986; Corrigan et al., 1994) Rocks of the Parautochthonous Belt are comprised of pre-Grenvillian migmatites and granulites.

The Allochthononous Belt is divided into two sub-units: the Allochthonous Polycyclic belt, and the Allochthonous Monocyclic Belt. The Allochthonous Polycyclic rocks record pre-Grenvillian deformation, metamorphism, and plutonism, but has not been correlated with rocks of the parautochthon, although more recent works make this relationship no longer clear (Culshaw et al., 2016). The Allochthonous Monocyclic Belt comprises of predominately supracrustal and plutonic rocks that have no tectonometamorpic history prior to the Grenville orogeny (Rivers et al., 1989).

Numerical models hypothesize that the structure of the Grenville Province can be explained by mid- to lower-crustal ductile flow, which has been termed ductile or nappe flow (Beaumont et al., 2001; Culshaw et al., 2006). Nappe flow describes the lateral flow of a weak, viscous layer between two rigid bounding slabs in a response to a horizontal gradient in lithostatic pressure (Godin et al., 2006). Ductile flow provides a mechanism for the extrusion of the mid-to-lower crust in large, hot collisional orogens (Beaumont et al., 2001; Godin et al., 2006; Trap et al., 2011).

Nappe flow described by Jamieson et al. (2010) produced a series of numerical models to identify the controls on degree of metamorphism and ductile deformation during the Grenville Orogeny. Their stop-convergence model produces results that are comparable to the natural crustal structure and pressure-temperature characteristics. The model results show that lower-crustal blocks of the Allochthonous Belt underwent several hundred kilometres of displacement during mid-crustal flow, which is also supported by metamorphic and petrologic data (Wodicka et al., 2000; Jamieson et al., 2010).

Several classification systems of the Grenville Province have been introduced, such as Rivers et al. (1989), Culshaw et al. (1997), and Carr et al. (2000). The subdivision of the Grenville Province introduced by Wynne-Edwards (1972) is the most frequently used classification scheme in the literature for the southwest Grenville Province and will be used in this study. The Grenville Province is broken down into three parts: i) the Grenville Front Tectonic Zone (GFTZ), an orogen-scale thrust-sense shear zone bounding the Grenville Province with Laurentia; the Central Gneiss Belt (CGB), consisting of Laurentia-derived supracrustal continental margin sequences and associated plutons, reworked during orogenesis, which structurally overlies the GFTZ; and the Central Metasedimentary Belt (CMB), which is made up of post-1400 Ma continental arc terranes and basin sequences accreted to Laurentia during collision, and overlies the CGB. .

2.3: Central Gneiss Belt

The Central Gneiss Belt of the Grenville Province is regarded as an aggregate of structural domains of distinct tectonometamorphic histories, assembled under ductile conditions during the Grenvillian Orogeny (Davidson et al., 1986; Bussy et al., 1995). These lithotectonic domains have been interpreted as thrust sheets that are bounded from one another by crustal-scale shear zones (Fig. 2.2) (Culshaw et al., 1994; Culshaw et al., 1997; Carr et al., 2000; Hynes and Rivers, 2010). The domains of the CGB are predominately composed of granitoid gneisses metamorphosed at upper amphibolite to granulite facies, with peak metamorphic conditions in excess of 750°C and 10-13 kbar (Culshaw et al., 2010), which represents the mid-to-lower crust of a doubly thickened orogeny (Carr et al., 2000; Culshaw et al., 2010).

The Georgian Bay transect of the southwestern Grenville Province contains both Allochthonous and Parautochthonous belts of the CGB. The underlying Parautochthonous Belt is represented by the Britt domain, while the overlying

Allochthonous Belt is represented by the Shawanaga, Parry Sound, upper Go Home, lower Go Home, and Moon River domains (Fig. 2.3).

Below is a general summary of the lithotectonic domains found along the Georgian Bay transect of the Central Gneiss Belt, from lowest to highest structural level. The PSD and its bounding shear zones are the focus of this study and require more detail in the background geology, but regional context will be provided by also discussing neighboring domains.

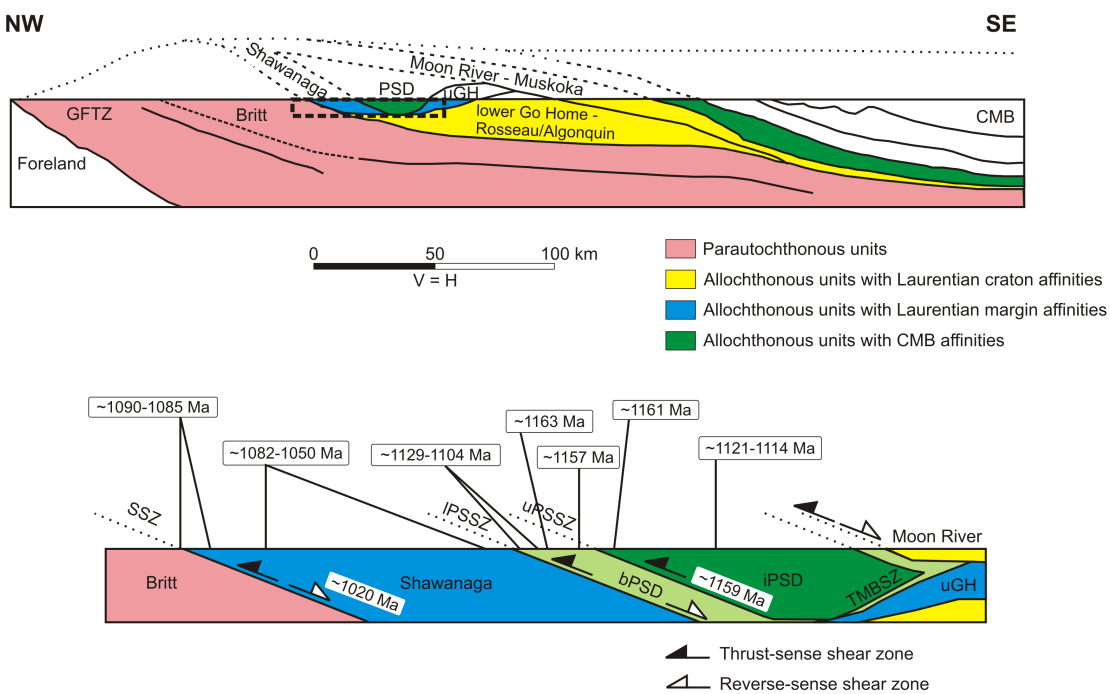

Figure 2.3: Cross-sections modified from Wodicka et al. (2000). **a)** Crustal-scale cross from the Grenville Front (NW) to the Central Metasedimentary belt (SE). **b)** Schematic cross-section of the Georgian Bay section of the Central Gneiss belt with approximate timing of thrusting and extension indicated. Cross-section b) is located by the dashed box in a).

2.3.1: Britt Domain

The Britt domain is a polycyclic parautochthonous unit at the base of the Central Gneiss Belt, overlying the GFTZ. Pre-Grenvillian metamorphism and deformation of orthogneiss and paragneiss occurred at ca. 1684 Ma, likely due to the accretion of the Labradorian terrane with a second phase of high-grade (625-700°C and 7.2-8.4 kbar) granulite facies metamorphism and leucosome development at ca. 1456 Ma during the Pinwarian deformation phase (Corrigan, 1990; Corrigan et al., 1994). Plutons ranging from granitic to tonalitic in composition were emplaced throughout the Britt domain between ca. 1460-1430 Ma (van Breeman et al., 1986; Corrigan 1990; Corrigan et al., 1994). Monazite and titanite grains of the Britt domain record a lower grade of Grenvillian metamorphic history of ca. 1080-1060 Ma, which represents the exhumation of the Britt domain during the Ottawan phase (Tucillo et al., 1992; Corrigan et al., 1994).

2.3.2: lower Go Home Domain

The lower Go Home domain is made up of strongly deformed metaplutonic rocks, with minor pelitic gneiss and marble, and coronitic metagabbro (Davidson et al., 1986; Culshaw et al., 1990). The metaplutonic rocks yield crystallization ages of ca. 1460 Ma (Krogh, 1991), while Nd model ages are as old as ca. 1.9 Ga (Dickin and McNutt, 1991), which shows that the lower Go Home domain has a pre-Grenvillian polycyclic history and affinity to Laurentia (Culshaw et al., 1997).

2.3.3: Shawanaga Domain

The monocyclic Shawanaga domain lies structurally above the polycyclic Britt domain in the nappe stack and is separated from the Britt domain by the Shawanaga shear zone. The Shawanaga domain underlies the northern margin of the Parry Sound domain, with the lower Parry Sound shear zone forming the boundary between the two units. The Shawanaga and lower Parry Sound shear zones converge on the southwestern margin of the lower Parry Sound domain where the extensional Shawanaga shear zone overprints the straight gneiss (a layered gneiss with indicators of high strain) of the lower Parry Sound shear zone shear zone (Culshaw, 2005).

The Shawanaga shear zone has a two-stage history, originally forming as a top to the northwest thrust-sense shear zone as a continuation of the province-wide Allochthon Boundary Thrust, the crustal-scale décollemont separating Parautochthonous and Allochthonous belts (Rivers et al., 1989; Culshaw et al., 1994;

Culshaw et al., 1997; Carr et al., 2000; Culshaw, 2005). The Shawanaga shear zone is then reworked into a high-grade extensional-sense shear zone with top-to-the-southwest kinematics (Ketchum et al., 1998; Culshaw, 2005).

The Shawanaga domain is characterized by pervasive partial melting of plutonic rocks forming extensive migmatitic units that have been divided into four lithotectonic assemblages. From highest to lowest structural level they are the: i) Lighthouse assemblage; ii) Sand Bay assemblage; iii) Ojibway assemblage; and iv) Shawanaga pluton (Culshaw et al., 1994, 1997, 2013).

Magmatic zircons from the Shawanaga pluton and detrital zircons from the Ojibway gneiss association yield crystallization ages ranging between ca. 1466 – 1346 Ma, indicating a Laurentian source (van Breeman et al., 1986; Wodicka et al., 2000; Slagstad et al., 2004). Recent U/Pb work done on detrital zircons in the Sand Bay and Lighthouse gneiss associations produced magmatic ages between ca. 1260 – 1250 Ma, with these constraints given by detrital zircon ages (Culshaw et al., 2013). Short-lived eclogite facies metamorphism is recorded within garnet-clinopyroxene rich rocks of the Shawanaga domain and yield ages of ca. 1090 – 1085 Ma (Ketchum & Krogh, 1997). This event has been interpreted as the deep burial or partial subduction of the Laurentian margin beneath the Central Metasedimentary Belt during the collision between Laurentia and exotic terranes (Hanmer and McEachern, 1992; Wodicka et al., 2000).

The thrusting of the Shawanaga domain along the Shawanaga shear zone is inferred to have taken place at ca. 1080- 1050 Ma, resulting in widespread amphibolite facies metamorphism throughout the domain, which was accompanied by deformation and partial melting (Slagstad et al., 2004). SHRIMP U/Pb analyses of zircons reveal the crystallization of leucosome took place between ca. 1067and 1047 Ma (Slagstad et al., 2004).

A ca. 1020 Ma post-orogenic extension reactivated the Shawanaga shear zone to become a major extensional, top-to-the-southwest shear zone (Ketchum et al., 1998; Wodicka et al., 2000). Post-tectonic pegmatites intrude the Shawanaga domain between ca. 990 and 956 Ma (Ketchum et al., 1998; Wodicka et al., 2000; Slagstad et al., 2004).

2.3.4: Parry Sound Domain

The Parry Sound domain is a monocyclic allochthonous unit comprised of granulite facies layered gneiss of metasedimentary and metaplutonic origins (Fig. 1.1) (Culshaw et al., 1997, 2010). Lithological and geochronological similarities between the PSD and the Central Metasedimentary Belt Boundary Zone have led to the interpretation that the PSD is an allochthonous nappe derived from material of the CMB (Wodicka et al., 1996, 2000; Marsh et al., 2013). Results of numerical models for the Georgian Bay section of the Grenville Province predict the transport of a detached nappe, supporting the idea that the PSD is a far travelled lower crustal nappe (Jamieson et al., 2010).

The PSD is a nappe stack that can be subdivided into several distinct units based on structural, lithological, geochronological data, each of which are separated from one another by nappe bounding shear zones. From lowest structural level to highest the units are; the lower Parry Sound shear zone (lPSSZ); basal Parry Sound domain (bPSD); upper Parry Sound shear zone (uPSSZ); and the interior Parry Sound domain (iPSD) (Fig. 2.3) (Culshaw et al., 1997).

On the northern margin of the Parry Sound domain the south-dipping lower Parry Sound shear zone separates the basal Parry Sound domain from the underlying Shawanaga domain, while the south-dipping upper Parry Sound shear zone separates the bPSD from the overlying interior Parry Sound domain (Culshaw et al., 2010). The upper and lower Parry Sound shear zones converge near the town of Parry Sound, where the upper and lower Parry Sound shear zones can be differentiated from one another the distinct lithological assemblages of their respective protoliths.

The southern margin of the interior Parry Sound domain is bounded by the underlying north-dipping Twelve Mile Bay shear zone. The regional-scale shear zone separates the interior Parry Sound domain from the underlying upper Go Home domain as well as the overlying Moon River domain (Culshaw et al., 1997; Carr et al., 2000).

The bPSD is the structurally lowermost unit of the PSD, located on the northwestern margin of the PSD (Fig. 1.1). The bPSD features metasupracrustal and orthogneissic rocks, with variably deformed anorthosite bodies, which vary in orientation but generally dip to the south beneath the interior Parry Sound domain (Fig. 2.3). The bPSD comprises mafic gneisses (possibly metavolcanic) interlayered with pelitic gneiss, quartzofeldspathic paragneiss, marble, and Armer Bay quartzite, which contains detrital zircons yielding ca. 1250 Ma maximum age of sedimentation (Culshaw et al., 2013). Along with metasedimentary material, the bPSD is interlayered with rocks of plutonic heritage in the form of tonalite-granodiorite orthogneiss, monzonitic orthogneiss, anorthositic gneiss, and gabbroic anorthosite (Culshaw et al., 1990; Wodicka et al., 1996; Marsh et al., 2011b).

The interior Parry Sound domain is made up of well layered to massive granulites facies orthogneiss, granitic through intermediate to mafic compositions. The NNE striking, steeply dipping, isoclinally folded centimetre- to metre-scale compositional layering typically alternates between mafic and felsic layers with a down-dip mineral lineation with no clear kinematic indicators (Marsh et al., 2011b).

The meso-scale structure of the interior Parry Sound domain (iPSD) reveals a granulite facies core, with a rim of amphibolite facies fabric that overprints granulite facies fabrics the Zone of Reworking, as mapped by Culshaw et al. (2010) in the transitional zone between the iPSD and the TMBSZ. The northern margin of the Zone of Reworking is the Retrogression and Reworking Boundary (RRB), the first sign of amphibolite facies overprinting the southern interior Parry Sound. The southern boundary is the transposed gneiss unit (tp), a highly transposed Parry Sound domain structure characterized by amphibolite facies shear zone foliation (Culshaw et al., 2010).

The five kilometre transect from the interior Parry Sound to the Twelve Mile Bay shear zone represents the strain gradient marked by the progressive reworking of interior Parry Sound domain derived material (Culshaw et al. 2010; Marsh et al., 2011a). The strain gradient spans the transition of interior Parry Sound domain granulite facies fabric, to variably transposed iPSD within the Zone of Reworking, culminating in the transposed gneiss unit, which is a member of the TMBSZ (Marsh et al., 2011a). The partial overprinting of granulite facies fabric by amphibolite facies shear zones is a part of the ductile shell of the interior Parry Sound domain (Fig. 1.1) (Culshaw et al., 2010; Gerbi et al., 2011; Marsh et al., 2011a).

The earliest stage of transpositions occurs immediately south of the RRB, where granulite facies layering is locally cut by quartz and feldspar veins that form at a high angle to granulite facies layering. Many mineralized fractures exhibit retrogression haloes, and show minor dextral strike-slip displacement (Culshaw et al., 2010; Marsh et al., 2011a). The degree of amphibolite facies overprinting increases with distance from the RRB, resulting metre wide amphibolite facies shear zones nucleating along tabular pegmatitic dykes. The shear zones widen and link together to create an increasingly connected network of amphibolite facies fabric, which culminates in the transposed gneiss unit, the uppermost unit of the nappe-bounding Twelve Mile Bay shear zone (Culshaw et al., 2010).

2.3.5: Twelve Mile Bay shear zone

The Twelve Mile Bay shear zone is a structurally heterogeneous, regional-scale shear zone system separating the PSD from the underlying Go Home domain. The Twelve Mile Bay shear zone is characterized by pervasive high strain amphibolite facies fabric, which dips north beneath the southern margin of the interior Parry Sound domain. The Twelve Mile Bay shear zones bound the interior Parry Sound domain from the underlying upper Go Home domain to the south, and the overlying Moon River domain to the east (Fig. 1.1) (Culshaw et al., 2010; Marsh et al., 2011).

The TMBSZ comprises of several distinct packages of north-dipping rock, all of which share a similar strain history as reflected by the common fabric. From north to south the packages are: i) the hydrated and reworked mafic-intermediate rocks of PSD derived material, termed the transposed gneiss unit in Culshaw et al. (2010); ii) the Twelve Mile Bay assemblage, a pelitic gneiss unit that shows lithologic similarities to the bPSD (Culshaw et al., 1989; Wodicka et al., 1996; Marsh et al., 2013); iii) anorthosite gneiss and iv) the strongly foliated migmatitic granitic orthogneiss of the upper Go Home domain (Marsh et al., 2013).

The transposed gneiss unit is the culmination of reworking of the interior Parry Sound domain, resulting in a completely transposed amphibolite facies fabric (Culshaw et al., 2010; Marsh et al., 2011a). High strains associated with the Twelve Mile Bay shear zone result in straight gneiss with alternating mafic and felsic compositional layering ranging from cm- to m-scale. The near homogenous amphibolite fabric is disrupted by mafic granulite facies pods of Parry Sound domain heritage (Fig. 2.4). The pods of relict mafic material preserve variably rotated granulite facies fabric, and rare patches of granulite facies mineral assemblages. The volumetrically dominant amphibolite facies fabric wrap around relict granulite facies pods forming shear folds on the margins of the granulite facies pods.

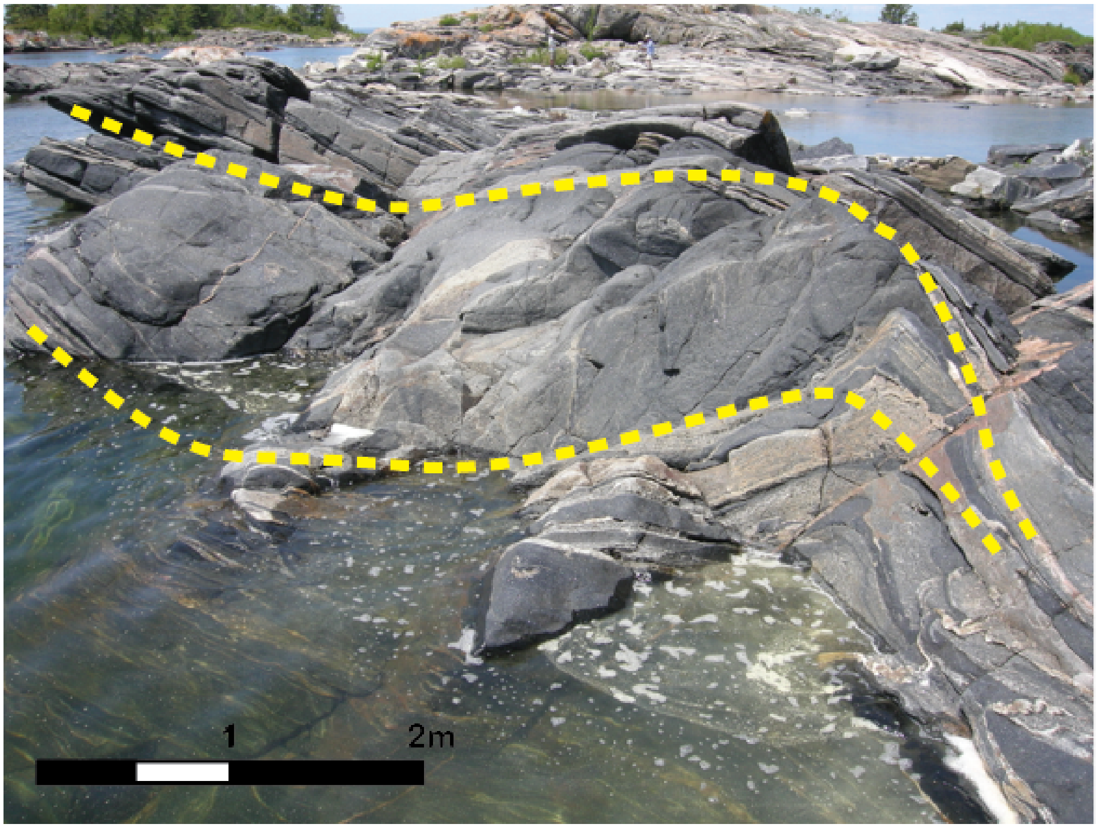

Figure 2.4: Field photo looking NW of a Parry Sound domain pod (outlined by dashed yellow lines) within the amphibolite facies transposed gneiss unit. Photo is from PBE Island, located on the boundary between the iPSD and tp units of Figure 1.1.

The Twelve Mile Bay assemblage includes pelitic gneiss, which contains an assemblage of garnet + biotite + plagioclase + K feldspar + sillimanite + pods of quartzofeldspathic material (Wodicka et al., 2000), along with associated plutonic bodies of amphibolite and anorthosite (Marsh et al., 2012). Estimated P-T conditions of paragneisses, amphibolites and anorthosites within the Twelve Mile Bay assemblage were found to be between ~7kbar/~820 °C and ~13 kbar/~940 °C (Wodicka et al., 2000; Marsh et al., 2011a). The lithology and P-T estimates of the TMBa are similar to results of the bPSD to the north (Wodicka et al., 1996; Culshaw et al., 1997; Marsh et al 2011).

2.3.6: Moon River domain

The monocyclic Moon River domain structurally overlies both the Parry Sound domain and the Go Home domain (Culshaw et al., 1997 and references therein). The Moon River domain is a large first-order synform that narrows towards the southeast, terminating in a southward-plunging tail (Schwerdtner et al., 2005, and references therein). The axial plane of the fold structure dips steeply towards the SW, with moderate to low plunging hinges that trend to the SE. Although the Moon River domain is comprised predominantly of amphibolite facies grey gneisses and amphibolites, there are examples of relict granulite facies blocks, suggesting an older high-pressure metamorphic history (Davidson et al., 1982; Schwerdtner et al., 2005; Culshaw et al., 2010).

The Moon River domain has been subdivided into two packages: the Moon River gneiss association and the Blackstone Lake gneiss association (Culshaw et al., 2010). The Moon River gneiss association contains uniform leucosome-rich pink and grey migmatites, whereas the Blackstone Lake gneiss association is made of grey gneisses of granodioritic composition with pink leucosomes (Culshaw et al., 2010).

A highly deformed segment of the Twelve Mile Bay assemblage has been traced into the Moon River structure (Culshaw et al., 1997). The TMBa marks the lower structural boundary of the Moon River domain, and transitions into Parry Sound domain derived material (Culshaw et al., 1997; Culshaw et al., 2010).

2.3.7: upper Go Home domain

The upper Go Home domain is a kilometre-scale first order antiform, which is bounded from the underlying Parry Sound domain by the Twelve Mile Bay shear zone (Schwerdtner et al., 2005; Culshaw et al., 2010).

2.4: Tectonic Assembly of PSD

The tectonic assembly and transport of the Parry Sound domain has a multistage history, which is summarized in Figure 2.5. The stages involve the building of the Parry Sound nappe stack on the Laurentian margin, the thrusting of the Parry Sound domain onto the Shawanaga domain, and subsequent post-convergence extension.

The formation of the PSD is interpreted to have occurred on the offshore margin of Laurentia, analogous to a collisions between several island arcs, given the pre-Grenville igneous ages (ca. 1450-1350 Ma) of plutons, related sedimentation (Carr et al., 2000). U-Pb zircon ages from the Parry Sound domain reveal igneous ages ranging from ca. 1436 – 1314 Ma (van Breeman et al., 1986; Wodicka et al., 1996; Wodicka et al., 2000), which is significantly younger than equivalent igneous ages within the Central Gneiss Belt (ca. 1800 – 1400 Ma) (Wodicka et al., 1996; Carr et al., 2000). Magmatic ages of the Parry Sound domain more closely resemble those of the Central Metasedimentary Belt (ca. 1450 – 1300 Ma), which is a composite arc belt formed offshore of the Laurentian margin (van Breeman et al., 1986; Wodicka et al., 1996; Culshaw et al., 1997; Carr et al., 2000). The Central Metasedimentary Belt shares geochronological and lithological similarities with the Parry Sound domain, leading to the interpretation that the Parry Sound domain formed alongside the Central Metasedimentary Belt on the Laurentian margin (Wodicka et al., 2000; Carr et al., 2000).

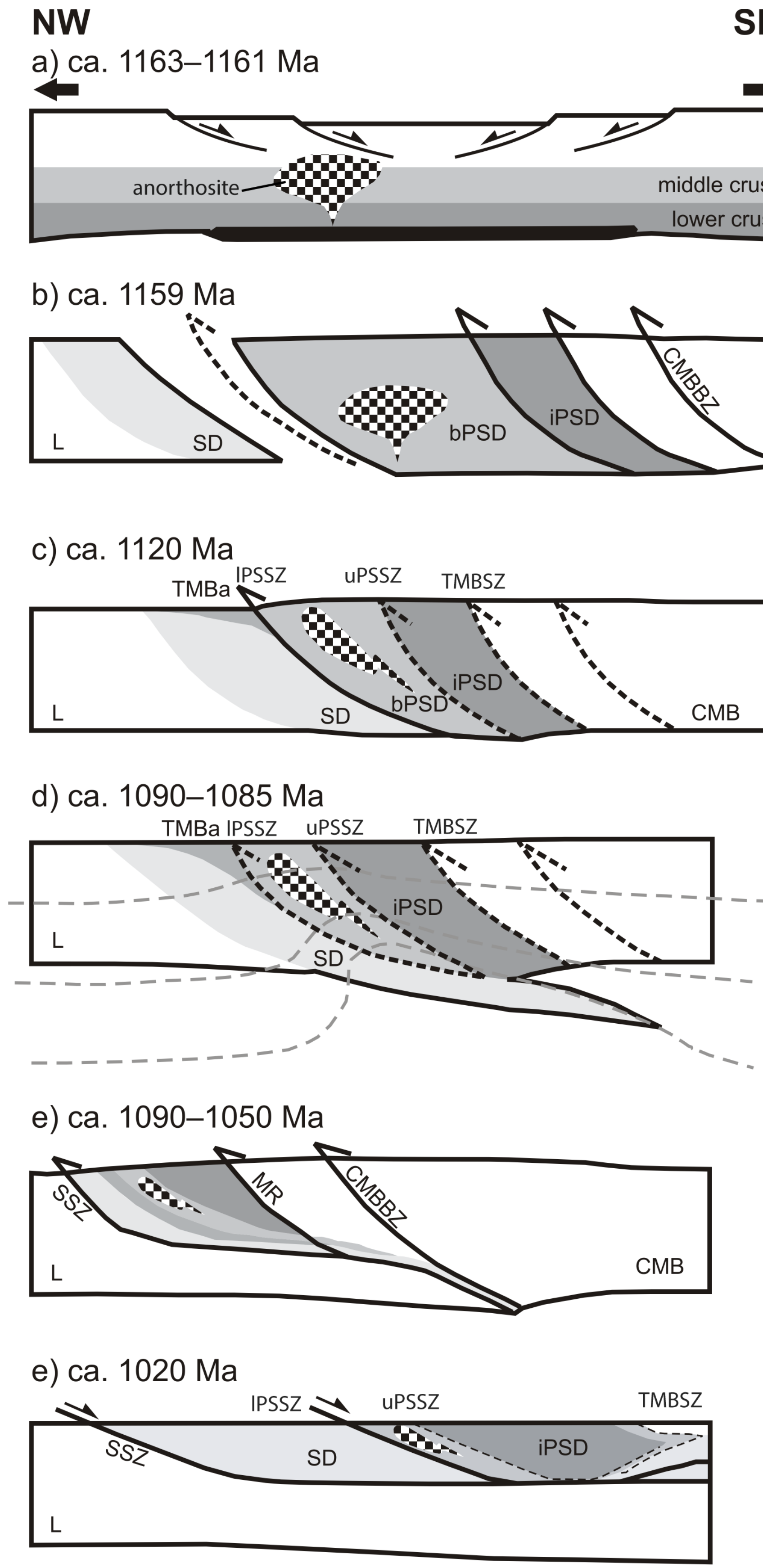
NW
SE
a) ca. 1163–1161 Ma
anorthosite
middle crust
lower crust
b) ca. 1159 Ma
L
SD
bPSD
iPSD
CMBBZ
c) ca. 1120 Ma
TMBa
lPSSZ
uPSSZ
TMBSZ
L
SD
bPSD
iPSD
CMB
d) ca. 1090–1085 Ma
TMBa
lPSSZ
uPSSZ
TMBSZ
iPSD
L
SD
e) ca. 1090–1050 Ma
SSZ
MR
CMBBZ
L
CMB
e) ca. 1020 Ma
lPSSZ
uPSSZ
TMBSZ
SSZ
SD
iPSD
L

Figure 2.5: Schematic representation of the tectonic evolution of the Parry Sound domain and Shawanga domain between ca. 1163 and 1020 Ma, modified from Wodicka et al. (2000). SD, Shawanaga domain; bPSD, basal Parry Sound domain; iPSD, interior Parry Sound domain; CMBBZ, Central Metasedimentary belt boundary zone; TMBa, Twelve Mile Bay assemblage; CMB, Central Metasedimentary belt; lPSSZ, lower Parry Sound shear zone; uPSSZ, upper Parry Sound shear zone; TMBSZ, Twelve Mile Bay shear zone; SSZ, Shawanaga shear zone. See text for detailed description.

The interior Parry Sound domain and the basal Parry Sound domain underwent granulite facies metamorphism at ca. 1163 Ma, along with the coeval emplacement of the Parry Island anorthosite (Fig. 2.5 a) (van Breeman et al., 1986; Wodicka et al., 2000; Culshaw et al., 2010; Marsh et al., 2012). The granulite facies metamorphism has been interpreted as being a response to an outboard collision between several arcs, forming an aggregate of composite arcs (Culshaw et al., 1997; Carr et al., 2000).

Shortly after reaching peak granulite facies conditions at ca. 1162 ma (van Breeman et al., 1986), the upper Parry Sound shear zone is initiated with the northwestward thrusting of the interior Parry Sound domain upon the basal Parry Sound domain at ca. 1160 – 1156Ma (Fig. 2.5 b) (van Breeman et al., 1986; Wodicka et al., 1996; Culshaw et al., 2010; Marsh et al., 2012). Thrusting along the upper Parry Sound shear zone coincides with amphibolite facies overprinting of granulite facies mineral assemblages within the upper part of the basal Parry Sound domain (Tuccillo et al., 1992; Wodicka et al., 1996; Culshaw et al., 2010). During transport along the upper Parry Sound shear zone, the interior Parry Sound domain began to develop leucosomes that yield crystallization ages of monazite ca. 1159 – 1152 Ma (Wodicka et al., 1996; Marsh et al., 2012), and zircon ca. 1146 ± 12 Ma (Marsh et al., 2012).

U-Pb analysis of zircons from a quartzite layer within the Twelve Mile Bay assemblage provide a maximum depositional age of ca. 1140 – 1120 Ma, representing the youngest metasedimentary unit in the Central Gneiss Belt. Detrital zircons from the same sample have bimodal age populations, indicating differing sources of sediment. The first population is at ca. 1146 Ma, which has been interpreted as an early stage of Granulite-facies metamorphism; with the second population being ca. 1069 Ma, which has been interpreted as a second phase of amphibolite facies deformation within the TMBSZ (Marsh et al., 2012). The age distribution of the detrital zircons indicates that source of sediment came from Laurentian as well as outboard terrane material. Therefore, the Twelve Mile Bay assemblage has been interpreted to have deposited on the Laurentian margin around the time of the initial collision between Laurentia and the outboard Parry Sound domain and other foreign terranes (Culshaw et al., 1997; Marsh et al., 2012).

Between ca. 1123 – 1116 Ma there is major amphibolite facies metamorphism recorded within the lower basal Parry Sound domain and interior Parry Sound domain, interpreted as the thrusting along the lower Parry Sound shear zone, resulting in the Parry Sound domain overriding the Shawanaga domain (van Breeman et al., 1986; Wodicka et al., 2000; Krogh & Kwok, 2005; Culshaw et al., 2010; Marsh et al., 2011b). Widespread amphibolite facies metamorphism at this time corresponds to the maximum age of the Grenvillian and Laurentian detrital zircon bearing Twelve Mile Bay assemblage. This relationship has led to the interpretation that the ca. 1120 Ma age represents the main phase of collision between Allochthonous and Parautothchonous belts (Wodicka et al., 2000; Marsh et al., 2011a).

Thrusting of the Parry Sound Domain onto the Laurentian craton at ca. 1120 Ma resulted in the overprinting of granulite facies assemblages by amphibolite facies fabrics due to cooling and decompression (Tuccillo et al., 1992; Wodicka et al., 2000). The Twelve Mile Bay assemblage underwent amphibolite facies metamorphism as the Parry Sound domain was thrust over it along the Twelve Mile Bay shear zone between ca. 1145-1100 Ma (Wodicka et al., 2000; Marsh et al., 2013). Pegmatite dykes syntectonic with thrusting and amphibolite facies metamorphism were emplaced within the interior Parry Sound domain between ca. 1105 – 1100 Ma introducing hydrous phases into previously dry granulite, initiating localized weakening along pegmatites within the interior Parry Sound domain (Culshaw et al., 2011; Marsh et al., 2011b). The Twelve Mile Bay shear zone yields metamorphic ages ranging from ca. 1120 – 1080 Ma, indicating that the age of transposed fabric is likely to be within the range of ca. 1105 Ma (first occurrence of syntectonic pegmatites) and ca. 1080 Ma (final stages of thrusting along the lower Parry Sound shear zone) (van Breeman et al., 1986; Tuccillo et al., 1992; Wodicka et al., 2000; Culshaw et al., 2011; Marsh et al., 2011b). There is widespread amphibolite facies metamorphism from ca. 1080 – 1035 Ma throughout the Central Gneiss Belt, with the exception of the Parry Sound domain and the Grenville Front Tectonic Zone (Culshaw et al., 1997; Wodicka et al., 2000).

CHAPTER 3: MAPPING METHODOLOGY

3.1: Introduction

The research objectives of this thesis focus on the quantifying shear zone geometric parameters such as wall rock layer thickness or shear zone width, as well as documenting stages of shear zone propagation. Measuring such parameters is impractical to do in the field due to time constraints, and working from ordinary photographs encounters camera distortion problems. Recent structural studies have applied photogrammetric techniques to create orthorectified photomosaics and 3D renderings of outcrops, these images/renderings can be taken back to a laboratory setting and analyze the images for spatial information (Bemis et al., 2014; Vollgger and Cruden, 2016; Tavani et al., 2016). In this study, a unique mapping method was developed to accurately image complex structure by systematically taking ultra-low aerial photographs and merging them together to create a single seamless image. The merged image, which we refer to as a photo-map, is an orthorectified, high resolution ultra-low aerial photograph. The photo-maps are used to accurately map shear zones, as well as provide qualitative data to characterize shear zone systems and accompanying structures during progressive deformation.

The primary advantages of the photo-map technique lies in the cm-scale precision and orthorectified view that allows for the collection of quantitative data, in this case, quantitative measurements of shear zone geometry. By pairing the photo-maps with GIS software, the photo-maps can be georeferenced so that quantitative data can be reliably measured directly from the photo-map, which in this case is predominately shear zone parameters. The quantitative data can then be used for strain analysis and geometrical studies to further characterize each outcrop.

3.2: Mapping Methods

To understand and accurately map several islands with highly complex structure, it was imperative to have detailed aerial photographs. Existing satellite images and regional aerial photographs do not provide the spatial resolution required to take precise measurements on the metre-centimetre-scale, so an innovative method was devised to create high resolution orthorectified photo mosaics. The creation of the photo-maps allowed for careful observation of the structurally complex outcrops, which ultimately led to the discovery of several new structures that otherwise were missed in a more conventional field study methodology. The method has three main components: i) digitizing a grid of markers, ii) photographing each grid square using the pole camera (modified from Swanson et al., 2006), and iii) mosaicking the photos together using open source software. The result is orthorectified ultra-low aerial photograph of key study locations.

It should be noted that while the photo-maps give a true profile view of an outcrop comprised of vertical layering, many of the outcrops studied do not have vertical layering. In such cases additional software was used to manipulate the image to the desired angle, such as a down-dip or down-plunge view.

3.2.1: The grid

In order to map the outcrops systematically, grids of numbered ceramic tiles (each ~10x10 cm) were arranged on each outcrop of interest. The grid was set up using a baseline rope and placing marker tiles down every 2 m using a tape measure. The study areas were predominately all low relief, allowing for the camera to be at a consistent height of approximately 4 m. Lines of the grid were constructed perpendicular to the baseline, again using a rope and placing tiles every 2 m. Creating and digitizing grids was done in the summer of 2013, with the majority of the photos shot during this time. The grid set up on Matches Island, the largest grid, used several baselines at differing orientations to image the large exposure. The tiles were laid down in a numbered sequence so that that the location of a particular photo could be easily determined by looking at the tile identification numbers. An example of the Matches Island grid is given in Figure 3.1.

The size and spacing of the tiles were designed so that for every photo of a grid square there would be sufficient overlap with the neighboring grid squares. Having a certain degree of overlap of photos is important for the photo stitching process and allows more tiles to be visible, placing tighter constraints on georeferencing the photo. The photos were taken so that two complete grid squares were visible, leading to approximately 50% overlap with the exception of the margins of the grid. The spacing of the tiles was measured by tape measure and is not exactly 2 m due to topography and human errors.

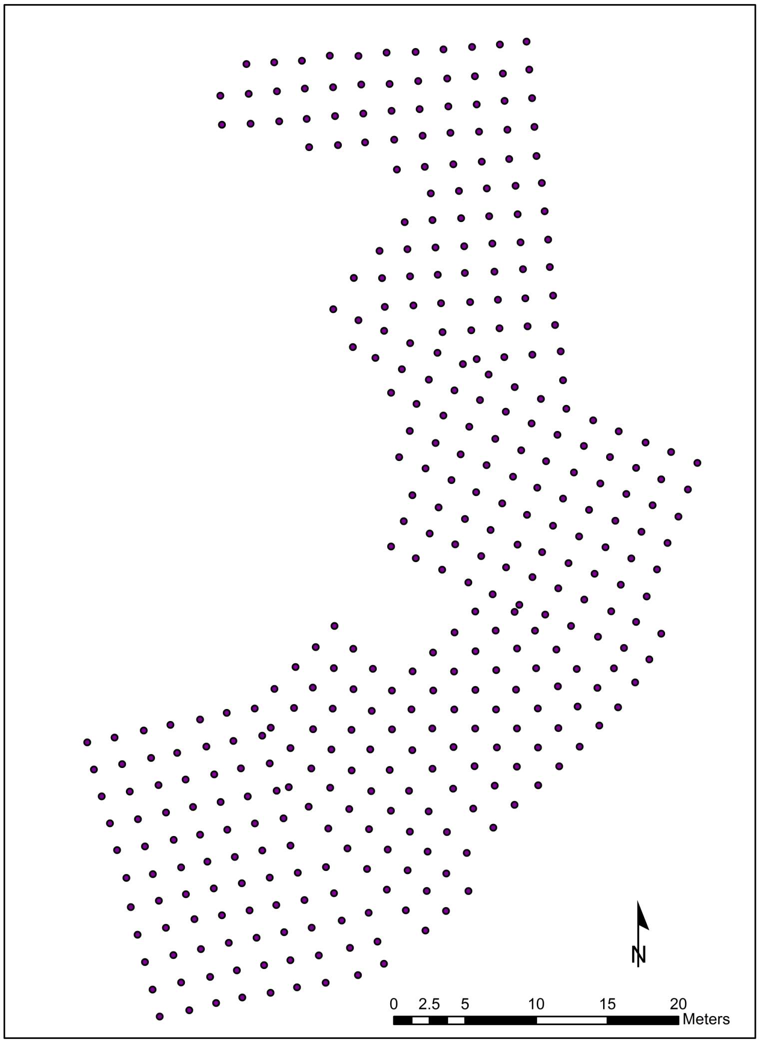

Figure 3.1: An example of the Matches Island grid digitized with ArcGIS. Black dots are tile markers spaced approximately 2 metres from one another.

3.2.2 Pole camera

The pole camera is attached to a 5 m telescoping aluminum pole by a gimbal mounted to one end. The pole camera rig was created in the Oceanography machine shop at Dalhousie University, and consists of three sections of hollow aluminum rods with each rod fitting inside the rod before it. The gimbal consists of a universal camera mount with a swing mechanism allowing the mounted camera to change pitch while the yaw is fixed. On the back of the gimbal there is an adjustable weight, allowing the control of the pitch of the lens. Each time the camera was placed on the gimbal, the weight would be adjusted so that the lens is oriented perpendicular to the ground, irrespective of the pole orientation.

Operation of the pole camera requires a minimum of two people, one to hold the pole steady and the other to line up the shot and take the photo using a remote trigger. The pole holder would stand at the base of two grid squares, allowing a minimum of six marker tiles to be within the camera's field of view to ensure that multiple marker points could be georeferenced (Fig. 3.2 a and b). The second person was responsible for the alignment of the camera, iteratively making adjustments to ensure that the shot was framed properly, and shooting the photograph with the remote trigger.

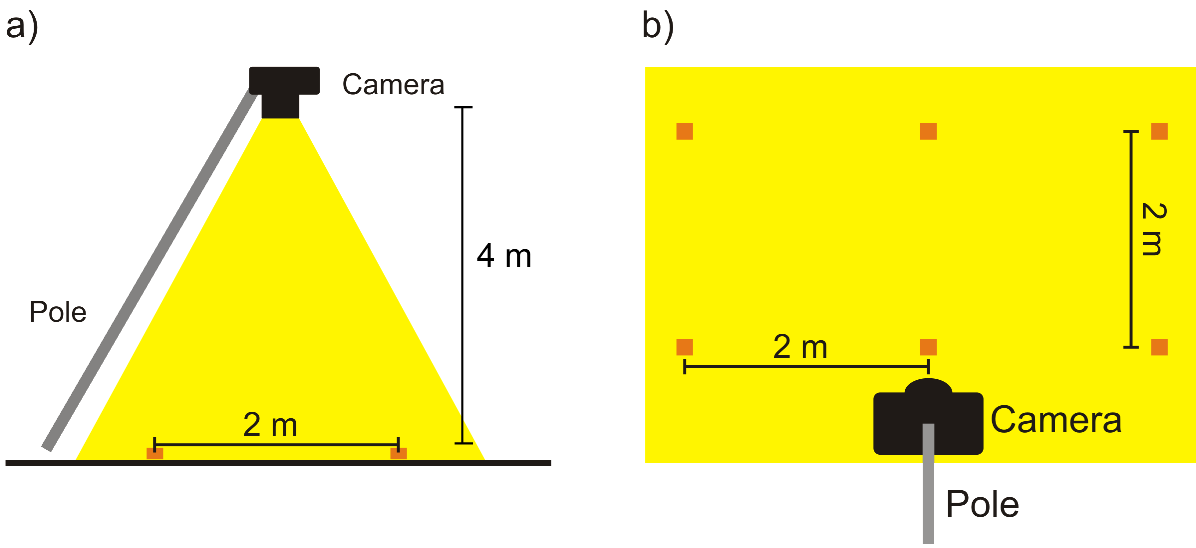

Figure 3.2: Schematic of the pole-camera setup in **a)** cross-section and b) plan view. Yellow polygon, field of view; grey, pole; black polygon, camera; orange square, marker tile.

The photos were taken with the camera positioned along a grid line, with two grid squares within the camera's field of view. Once a photo was taken, the setup would move along the gridline to the next set of squares. At the end of a gridline, the setup would move to the adjacent gridline and continue in the same back and forth manner. This movement was done so that the photos would contain enough overlap with neighboring photos so that they could be mosaicked.

3.2.3 Differential Global Positioning System:

The grid of ceramic tiles was digitized using a Leica differential global positioning system (DGPS), allowing centimetre-scale precision for georeferencing the photographs. The DGPS was comprised of two components, a base station and a mobile rover unit to gather real-time kinematic positioning (RTK) of specific locations. The base station records its own position while powered, but because the station remains fixed the entire time it effectively measures coordinate measurement fluctuations and computes corrections for each satellite signal. The base station transmits real-time corrections by radio link to the rover unit, allowing real-time centimetre-scale precision (Takac & Lienhart, 2008). The corrections are recorded on the base station, so if the radio connection between the base station and rover is disrupted, post-processing corrections can be made using the stored data in the base station.

The base station consisted of an antenna receiver, transmitter, Leica console, and two batteries all mounted on a tripod. Bartram's Island was chosen to be the site of our base station, as it is within the transmission range for each of the islands of interest, and was sheltered from the wind. The base station was visited every morning before running the rover, to put in freshly charged batteries and to ensure that the unit was receiving and transmitting data.

The rover unit consists of a Leica console and antenna within a backpack, connected to a pole-mounted receiver. The rover was used to digitize each grid tile by standing over the tile, placing the pole receiver directly on the tile, and storing the DGPS location, matching the DGPS point number with the unique tile number. This process was repeated for each marker tile in every grid.

During the digitization process, there were times when the link between the base station and the rover would become severed for a short period of time. The disruption in transmission means that the rover was no longer receiving RTK data from the base station, diminishing the accuracy of the spatial data. However, a post-processing correction can be applied to the data using Leica Geo Office software, which uses RTK data recorded in the base station data and applies it to the rover data; resulting in DPGS data with centimetre-scale accuracy.

3.3: Photo-merging

Many software suites that have the capability to produce orthorectified images from air photos require intricate data about the camera (e.g. angle between the lens and the ground) that are difficult to measure. Fortunately available from the open source software community there are three programs that complement each other to create orthorectified photo-mosaics, 3D models, and down-dip views. The photomerge workflow is shown in Figure 3.3., with two distinct streams; using MeshLab to produce downdip imagery; and using CMPMVS to produce orthorectified imagery.

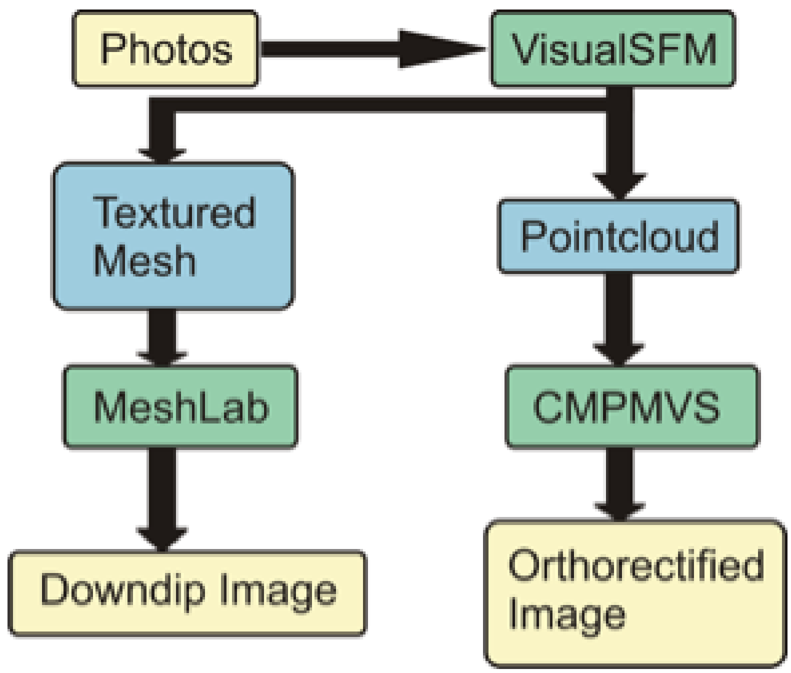

Figure 3.3: Photomerge workflow. Green, software; yellow, image; blue, 3D reconstruction data.

The first program VisualSFM© is a GUI application produced by Changchang Wu that reconstructs 3D objects by using image tie points. The software relates images to one another by recognizing common points in several images. These points are displayed in the interface if the point is detected in a minimum of three images, hence the need for a sufficient amount of overlap of photos (Fig. 3.2, b). The output of this file is a point cloud that can be viewed in 3D. The point cloud file from VisualSFM can be imported into Michael Jancosek's program, CMPMVS, which can be used to reconstruct the object, an outcrop in this case. CMPMVS produces a variety of meshes, masks, DEMs, and most importantly, an orthorectified photo.

In order to create a 3D model of the outcrop the point cloud file output of VisualSFM is opened with MeshLab, an open source program for the processing and editing of 3D meshes. Once the model is created in MeshLab, the model can be rotated and zoomed to the user's desire, which in our case was to rotate the model into the view of the foliation plane for a down-dip view.

Below there is a walkthrough of each program in order to produce a mesh, orthorectified photo, and a 3D model. With VisualSFM and CMPMVS there are several parameters regarding the geometry of image reconstruction that can be adjusted by the user, but in this case the default settings were used. These programs have specific system requirements, which can be viewed on each program's respective websites.

3.3.1: VisualSFM workflow:

To create a point cloud, first import the photos into VisualSFM by selecting "open+ multi images" from the file drop down (1, Fig. 3.3 a), and select a series of overlapping photos of the object that you would like to digitally reconstruct. Once the photos have loaded, select the option "compute missing matches + CTRL: match specified pairs" (2, Fig. 3.4 a), and then "compute 3D reconstruction" (3, Fig. 3.3 a). The 3D reconstruction results in several models of sparse pointclouds and camera angles that can be rotated around by right-clicking and dragging the cursor. The pixels in the pointcloud represent common points observed in at least 3 images that will be used to merge several photos together during image reconstruction, and the floating images represent the camera angle.

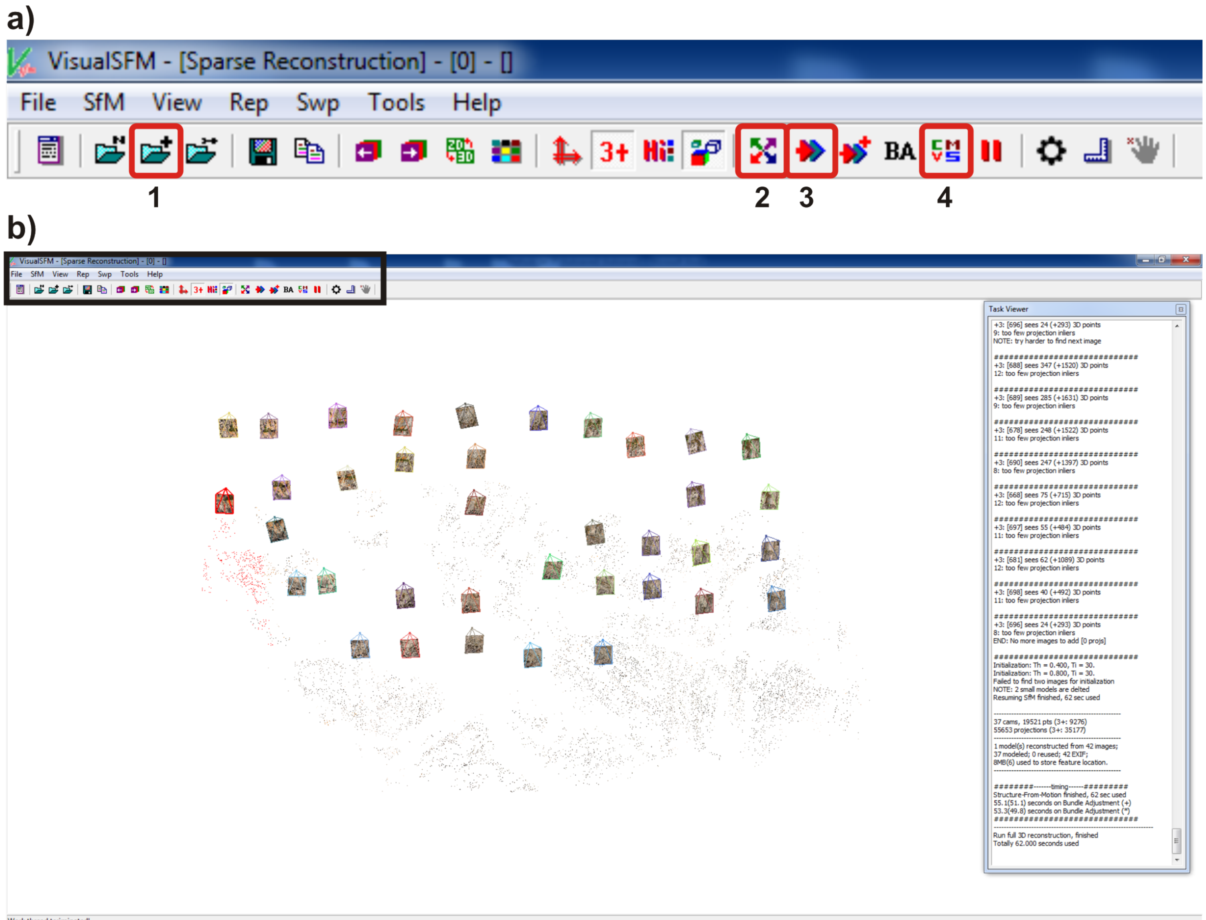

Figure 3.4: a) The VisualSFM toolbar with the indicated steps to produce a pointcloud from a set of images. 1, open multiple images; 2, compute missing matches; 3, compute 3D reconstruction; 4, run dense reconstruction. **b)** A screen grab of the software after running the compute 3D reconstruction task. The squares show the location of the camera that took an image, while the dots represent common points observed by multiple cameras.

Depending on how well the photos match up, several models can be toggled through by hitting the up and down arrows on the keyboard. It is best to have only one model, as it gives you one complete picture rather than several fragments, but sometimes it cannot be avoided because the photos are not fully merged. Typically there will be a small amount of photos that do not find matches, with one model containing the bulk of the matched photos, and the other model will have few photos associated with it. In this case, carry on the rest of the VisualSFM workflow, the model selection comes up in the CMPMVS workflow.

To then build the point cloud press the “run dense reconstruction” (4, Fig. 3.3 a), which will create dense pointclouds for each of the models the program has created. A save prompt will appear, and select the nvm.cmp file extension, and save to a desired folder. When the text “work thread terminated” appears in the bottom left hand corner, the file has saved. The result should be a folder containing subfolders of models numbered sequentially beginning with “00”. Within each model folder there is the data folder, containing the photos matched within that model and the mvs.ini file, which is the file that will be used in CMPMVS.

3.3.2: CMPMVS workflow

CMPMVS uses the dense pointcloud produced in VisualSFM to construct a series of 3D meshes, textured 3D models, and orthorectified photo-mosaics. Within the program files there are a series of text files that contain parameters the program will run. These parameters can be changed, and certain functions can be turned off to speed up processing time. The photomaps in this study were used with the default parameters, but with the “generate video frames” function turned off, which significantly speeds up the processing time.

CMPMVS runs and executes tasks in the windows command prompt (cmd). In order to run the dense pointcloud, the filepath of the folder containing CMPMVS.exe must be accessed in the command prompt. Once the correct directory is accessed type in the program, CMPMVS.exe, and the filepath of the pointcloud file with a space between the two. The pointcloud filepath will reflect where the pointcloud was saved, and how many models of matched photos were saved. For example, in Figure 3.4, C:\Users\User\Desktop\VSFMOut\test.nvm.cmp\00\mvs.ini is the filepath, with “test.nvm.cmp” being the folder created in VisualSFM, the subfolder “00” is the model number, and “mvs.ini” is the pointcloud file of that model number.

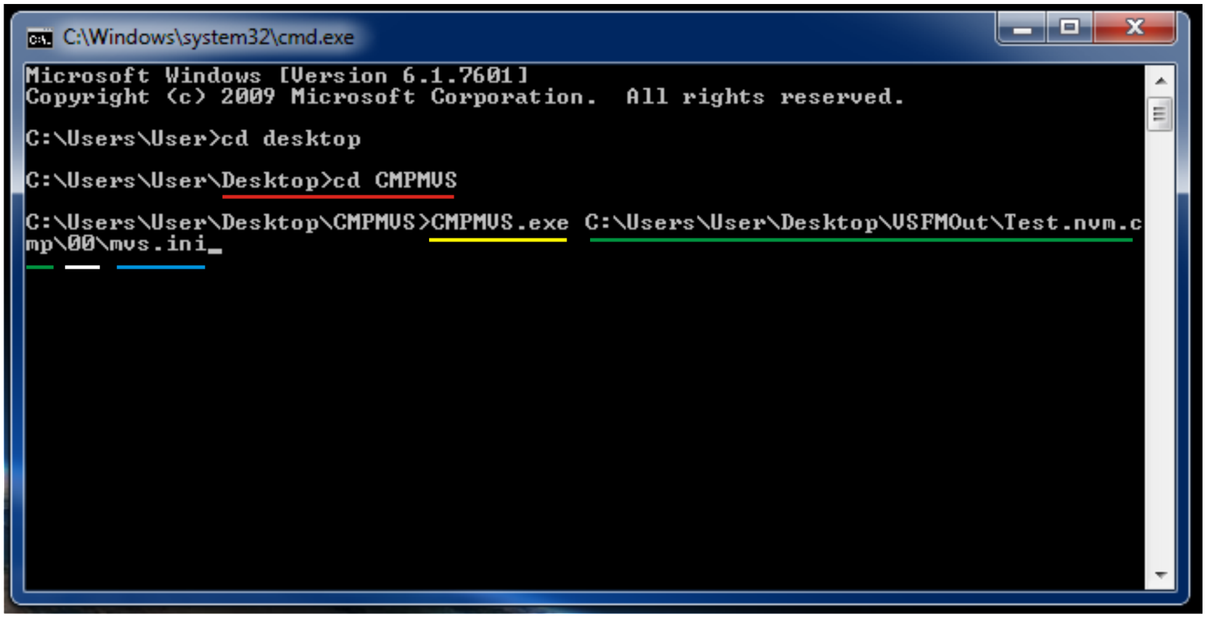

Figure 3.5: A screen grab of running a pointcloud file produced in VisualSFM with CMPMVS. Red, location of the CMPMVS folder; yellow, initiate CMPMVS.exe and select file; green, location of pointcloud file; white, pointcloud model number; blue, pointcloud file.

CMPMVS will run for several hours, depending on the volume of photos and whether other functions are switched off. The results will be saved in a folder called "_OUT" within a subfolder called "data" within the model filepath. The files of interest here are the DEM_orthophoto, the orthorectified photomosaic, and the .wrl and .ply extensions, 3D meshes.

3.3.3: Meshlab Workflow

Meshlab is used to create down-plunge/dip views of the photomaps by importing 3D meshes previously created with CMPMVS. To import a new mesh, click "file", "new mesh" and select either a .ply or .wrl file from the CMPMVS output folder. "meshAvImgTex.wrl" will be the largest mesh file, and will be the highest resolution. Once a mesh is selected, the mesh will be displayed and can be rotated to the desired angle. To capture the image of the down-plunge/dip view, click the photo icon, and select the output folder and resolution.

3.4: Spatial resolution and error

The spatial resolution of the photomaps ranged from 1.4 cm to 3 cm, depending on the size of the area being imaged. Matches Island was the largest area mosaicked, and yielded the lowest spatial resolution (1.4 cm). However, the large Matches Island mosaic was made up of five smaller mosaics that had spatial resolutions in the range of 2.5-2.8cm. This allowed for a higher precision of quantitative measurements when required if a feature was contained within one of the smaller mosaic. The size of the area being imaged on PBE, Bartram's, and PBW islands were relatively small compared to the large Matches Island photomap and had spatial resolutions in between 2.5-3cm.

To calculate error the tiles that were used as georeferencing markers were measured in photomaps using ArcGIS. The measured dimensions were compared with known tile dimensions (10x10cm, with 90° corners). Error was calculated using root mean square error, and was found to be ±0.54cm for distances and ±2.99° for angles.

CHAPTER 4: STRUCTURE

4.1: Introduction

This study examined several islands at various structural levels within the boundary zone along the southern margin of the iPSD (Fig. 4.1 a). The islands show a progressive transition from NNE-striking granulite facies fabric (Fig. 4.1 b) to a WNW-striking amphibolite facies fabric (Fig. 4.1 d) over the span of approximately five kilometres. This study takes a comprehensive look at several islands within this transition zone to provide an overview of the structural evolution of the tectonic boundary between the iPSD and the TMBSZ.

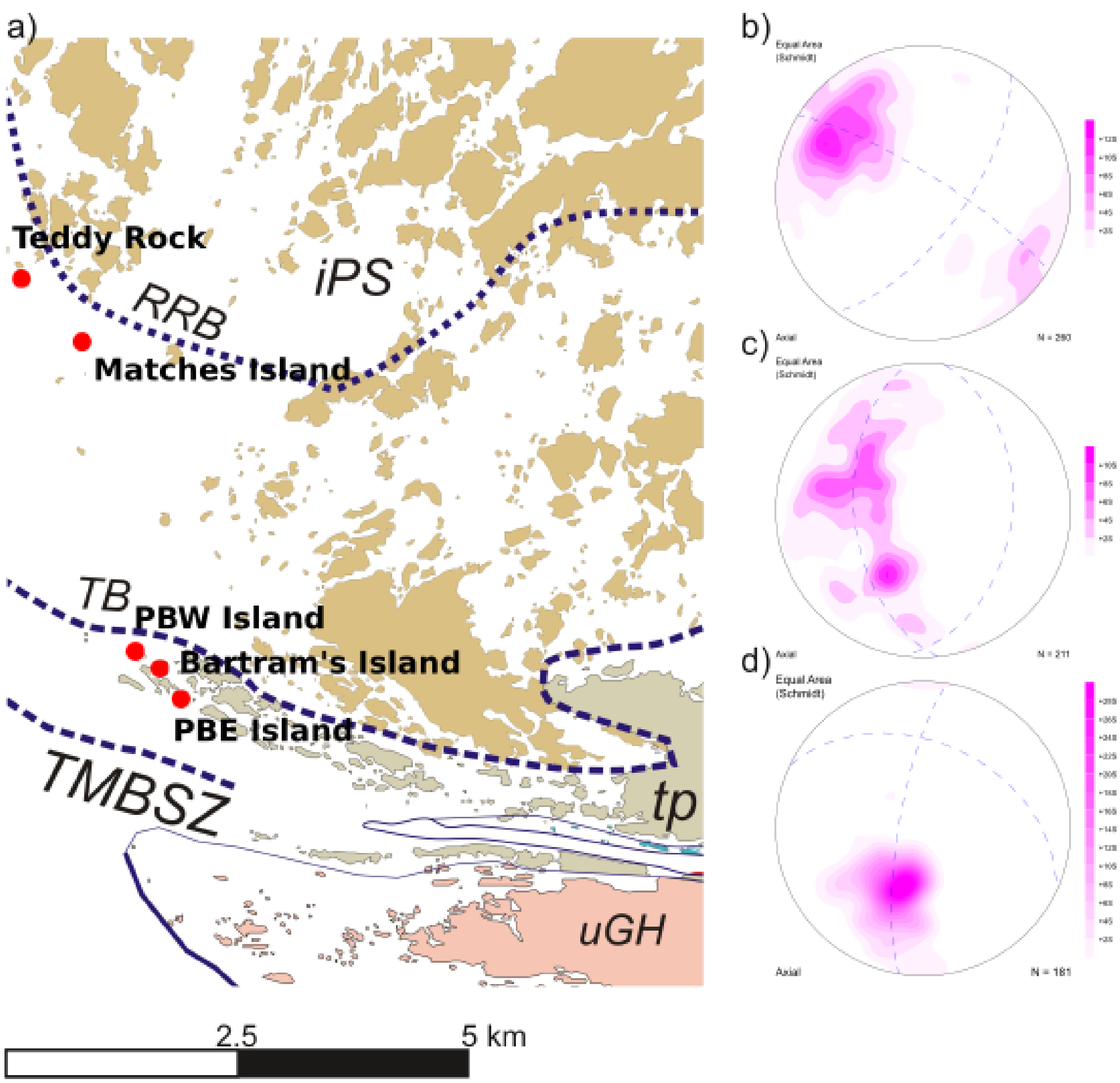

Figure 4.1: **a)** Geologic map of study area with island locations (red dots), from N to S: Teddy Rock, Matches Island, PBW Island, Bartram's Island, PBE Island. iPS, interior Parry Sound domain; RRB, retrogression and reworking boundary; TB, transposition boundary; tp, transposed unit; TMBSZ; Twelve Mile Bay shear zone; uGH, upper Go Home domain. **b)** Lower hemisphere equal area contoured projections showing both poles to foliations within iPS, **c)** between RRB and TB, and **d)** TMBSZ. Blue dashed great circles are best fit planes. Modified from Culshaw et al. (2010).

Throughout the zone of retrogression and reworking between the Retrogression and Reworking boundary (RRB) and the Transposition boundary (TB) (Fig. 4.1), the granulite facies foliation (S_1) deviates variably from the average orientation of the granulite facies foliation north of the RRB. Therefore, the term wall rock foliation is used to describe local relict granulite facies foliation of the iPSD (S_1), and the term original PSD fabric is used to refer to the regional orientation of granulite facies foliation north of the RRB.

Turning now to the geometry of wall rock separating shear zones, the term "wall rock block" refers to a metre-scale rectilinear area of wall rock material, which is bounded on two or more sides by shear zones. Wall rock blocks are grouped together by parallel shear zones forming corridors of granulite facies material, typically with high aspect ratios with longest axis of the wall rock block is aligned parallel to the surrounding shear zones. A package of wall rock blocks refers to multiple wall rock blocks alongside each other separated from one another by parallel shear zones. A "wall rock lozenge" refers to a lozenge-shaped area of wall rock material that is bounded on all sides by shear zones. Wall rock lozenges are typically found within shear zones themselves as isolated pods, or in close proximity to merging shear zones. The foliation preserved in wall rock lozenges commonly displays larger amounts of rotation and internal deformation than the foliation preserved in wall rock blocks.

The structural evolution of the southern margin of the PSD is characterized by the increased development of an amphibolite facies shear zone foliation that overprints the pre-existing granulite facies foliation (Culshaw et al., 2010, 2011; Gerbi et al., 2010; Marsh et al., 2011 a, 2013). The amphibolite facies shear zone foliation nucleates on leucocratic veins and pegmatite dykes orthogonal to the granulite facies foliation. These veins introduce fluid into the PSD, and initiate the retrogression reactions of pyroxene and garnet to aggregates of hornblende, biotite quartz and plagioclase (Culshaw et al., 2010, 2011; Marsh et al., 2011 a, 2013). The generalized balanced reaction to this process is as follows:

Cpx + Grt + Hbl_1 + Pl_1 + FeOx ± Opx ± Qtz = Hbl_2 + Pl_2 ± Bt ± Ttn ± Qtz (Marsh et al., 2011a)

A photomicrograph taken by Marsh et al. (2011a) documents the progressive overprint of granulite facies assemblages as proximity to the margin of the leucocratic vein decreases (Fig. 4.2).

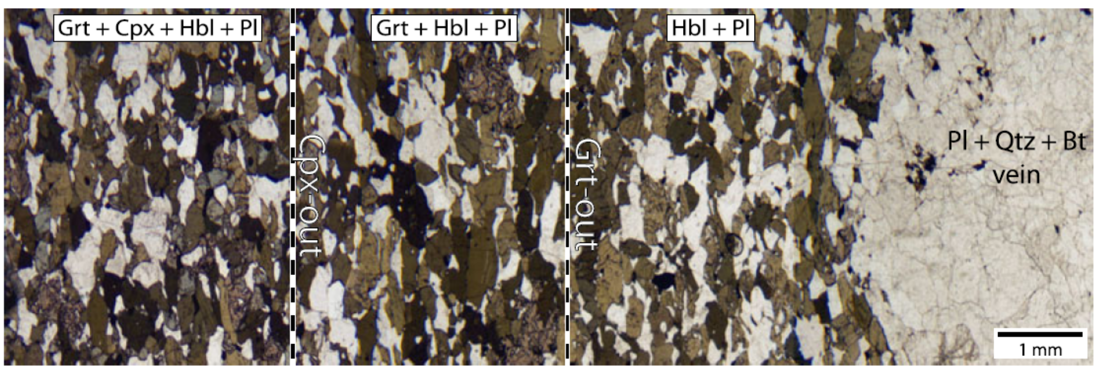

Figure 4.2: Photomicrograph of the margin of a pegmatite vein from Matches Island (Marsh et al., 2011 a). The microstructure shows the progressive replacement of granulite facies mineral assemblages (i.e. grt and cpx) by amphibolite facies mineral assemblages from left to right.

The ca. 1160 Ma gneissic foliation of the iPSD, S_1, is characterized by centimetre- to- decimetre-scale compositional layering, which typically alternates from felsic to mafic (Culshaw et al., 2010, 2011; Gerbi et al., 2010; Marsh et al., 2011a). The orientation of undeformed and unrotated iPSD gneissosity strikes WNW and dips sub-vertically (Fig. 4.1 b). The iPSD foliation is defined by coarse-grained, granoblastic/porphyroblastic microstructure that shows weak to moderate layer-parallel grain shape foliation (Fig. 4.3 a) (Marsh et al., 2011a).

The term shear zone foliation or amphibolite facies foliation is used when discussing S_2 rather than mylonitic foliation because the term mylonitic implies grain size reduction. In the early stages of transpression (i.e. Teddy Rock and Matches Island) grain size reduction in shear zones does not occur (Gower and Simpson, 1992).

On the margins of pegmatite veins (and later, shear zones) granulite facies assemblages are progressively replaced by recrystallized hornblende- and plagioclase-rich assemblages and begin to form a new foliation, S_2, (Fig. 4.2) (Marsh et al., 2011a). Zircons from syn-tectonic pegmatite veins yield ages of ca. 1100 Ma, constraining the age of the amphibolite facies foliation (Culshaw et al., 2011; Marsh et al., 2011b). The shear zone foliation is defined by straight polycrystalline quartz and plagioclase ribbons, as well as hornblende and biotite aggregates parallel to the foliation (Gower and Simpson, 1992; Marsh et al., 2011 a) (Fig. 4.3 b). A study that focused on the microstructural analysis of shear zones on Matches Island by Marsh et al. (2011a) concluded that the introduction of hydrous fluid combined with syn-kinematic reactions leaves dislocation creep and dissolution-precipitation creep of quartz and plagioclase as the likely deformation mechanisms.

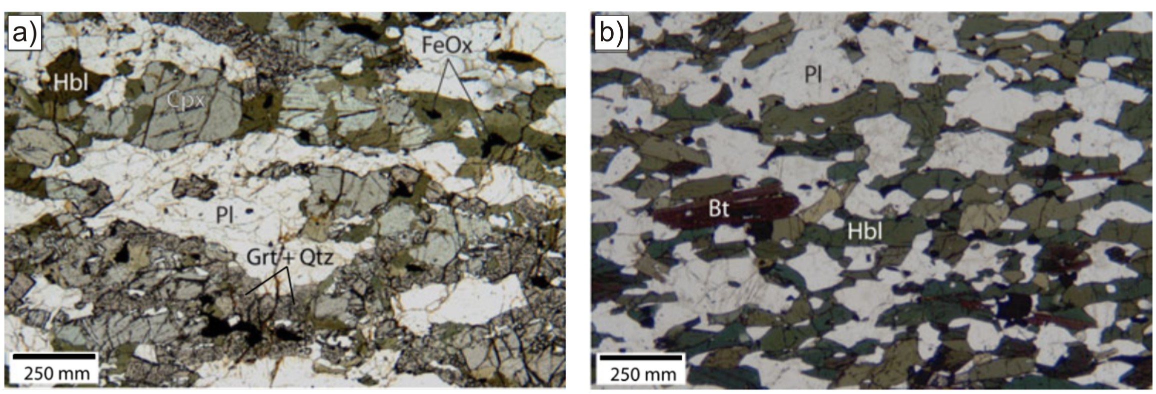

Figure 4.3: Photomicrographs representative of mafic wall rock and shear zone mineralogy and microstructure (Marsh et al., 2011a). a) Sample taken from a wall rock block on Matches Island with preserved granulite facies mineral assemblages and microstructure. b) A sample taken from shear zone on PBE Island with amphibolite facies mineral assemblages and microstructure.

Three types of lineations have been identified and are included in the following structural reports: down-dip mineral aggregate lineation of the iPSD, fold hinges (within wall rocks), and a hinge-parallel intersection lineation of S_1 on the S_2 foliation surface. There is a notable lack of a stretching lineation within amphibolite facies shear zones (Culshaw et al., 2011), therefore lineations found within amphibolite facies shear zone fabric (S_2) are likely the passively reoriented pre-existing lineations. The Bartram's Island outcrop provides an excellent example, as steeply plunging S_1 folds are progressively tightened and reoriented with proximity to shear zones. Reoriented fold hinges reveal the stretching direction of the TMBSZ to be approximately 080-20 (Fig. 4.1, d).

4.2 Teddy Rock:

Teddy Rock is located within the southern interior Parry Sound domain on the northern border of the Zone of Reworking, (the boundary zone between the southern interior Parry Sound domain and the Twelve Mile Bay shear zone) and ~750 m NW of Matches Island (Fig. 4.1). Teddy Rock was not studied at the level of detail as the other islands in the study and lacks a photomosaic map; however, Teddy Rock contains several examples of early shear zone development, such as initial orientations of wall rock and pegmatite/shear zones and bulk kinematics. Determining the initial orientations of such structures is imperative to understanding the evolution of the Twelve Mile Bay shear zone system. The relatively simple structure of Teddy Rock is illustrated effectively by the schematic map of Marsh et al. (2011 a) that has been slightly adapted here (Fig. 4.4).

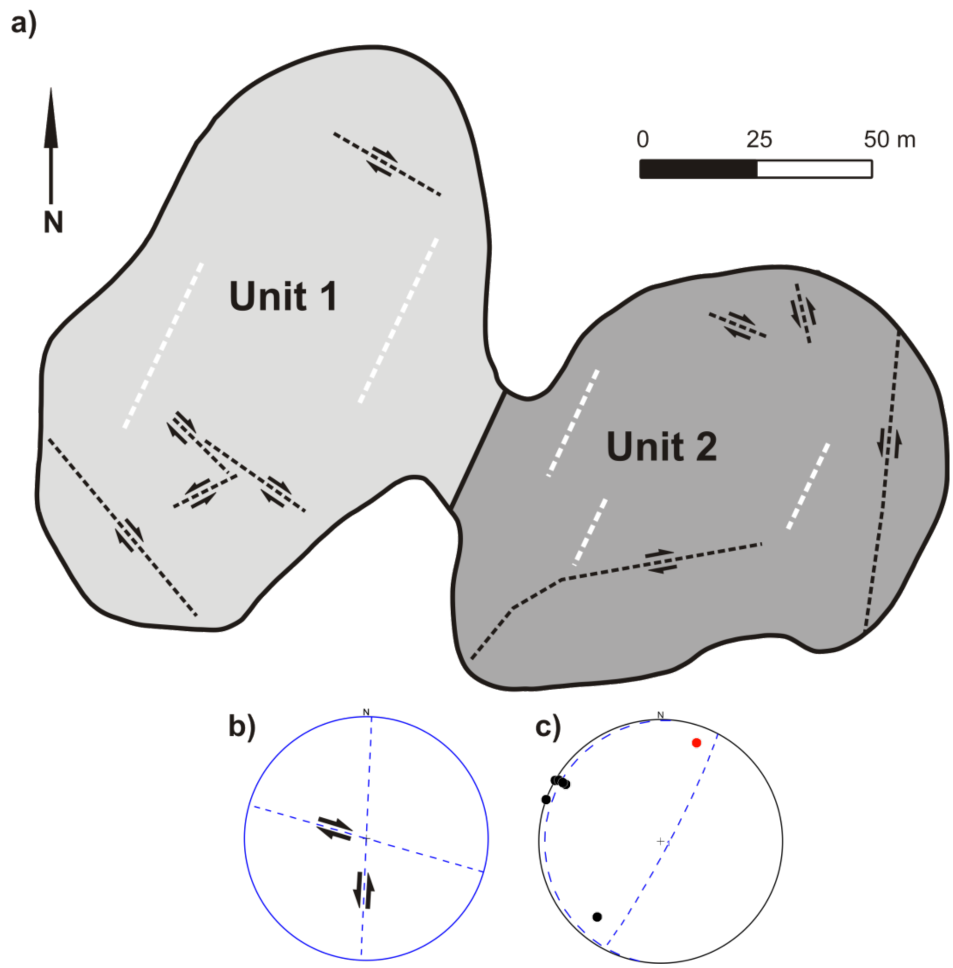

Figure 4.4: a) Schematic structural map of Teddy Island adapted from Marsh et al. (2011a). Unit 1, finely layered metasupracrustal sequence; Unit 2, thickly layered meta-mafic and granitic rocks; iPSD foliation, dashed white lines; pegmatite filled fractures exhibiting sheared offsets, dashed lines with kinematics indicated. **b)** Lower hemisphere equal area projections show average shear planes for both sinistral and dextral zones, and **c)** poles to wall rock foliation (black great circles), and a rotated wall rock block (red great circle).

Teddy Rock is made up of two units of granulite facies gneiss of metasupracrustal origins, with alternating garnetiferous and mafic layers. The western side (Unit 1) of the island hosts a finely layered metasupracrustal sequence and massive mafic granulites, whereas the eastern side (Unit 2) contains thickly layered (2-5m) meta-mafic and granitic rocks. Boudinaged mafic layers are common on the eastern side, with leucosome material infilling the boudin necks (Marsh et al., 2011a, 2011b). Granulite facies layering strikes NNE to N, typical of the interior Parry Sound domain.

Several leucocratic veins and pegmatite dykes were emplaced in various orientations and commonly show shear offsets along the vein margins. Pegmatite minerals such as plagioclase and k-spar porphyoblasts are deformed in areas of shearing (Marsh et al., 2011a).Fluids introduced into dry granulite facies country rock initiate a retrograde reaction, evidenced by the amphibolized margins of the veins and dykes (Culshaw et al., 2011; Marsh et al., 2011 a). The introduction of fluids via pegmatites and granitic veins play a vital role in weakening the dry granulite facies PSD (Gerbi et al., 2010; Culshaw et al., 2010). Figure 4.5 a and b feature outcrop photos of millimetre-centimetre-scale pegmatite filled cracks cut wall rock layering at a high angle. Shear strain nucleates along the weak amphibolized zone, leading to the development of centimetre-scale shear zones. Marsh et al.'s (2011a) structural map of Teddy Rock shows that pegmatite-focused shear zones display both sinistral and dextral motion. Shear zones of opposing kinematics strike at a high angle to one another; dextral shear zones strike ~ENE-WSW; and sinistral shear zones strike ~N, mimicking wall rock layering (Fig. 4.4 b, c).

The majority of shear zones on Teddy Rock are small-scale features, with shear zone widths and offsets in the centimetre- to decametre-scale range. However, there are rare examples of shear zones that are much wider and more developed than the millimetre-centimetre-scale primitive shear zones on the island (Fig. 4.5 c). One such outlier is a three metre wide pegmatite cored sinistral shear zone, located on the eastern side of the island within Unit 2. Within the shear zone there is a 1 m wide block of relict mafic wall rock. Compositional layering within the mafic block has been rotated during shearing (red circle, Fig. 4.4 c), as the mafic block layering no longer conforms to the regular N-NNE wall rock layering trend.

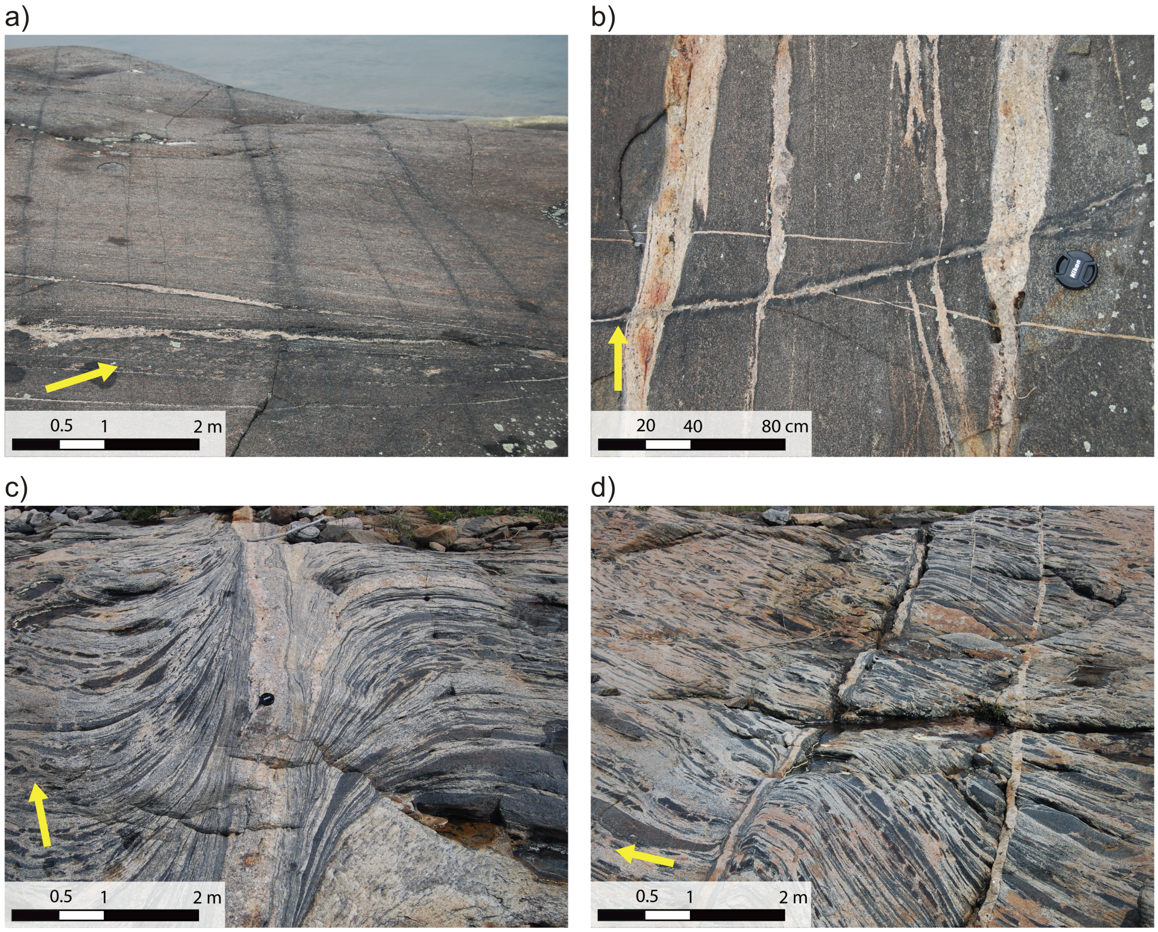

Figure 4.5: Field photos of Teddy Rock detailing the various stages of shear zone development. Photos taken by Chris Gerbi. **a)** Original iPSD granulite facies mafic wall rock with amphibolized fractures (oriented ~E-W in photo) at a high angle to layering (oriented ~N-S in photo). **b)** Pegmatite filled amphibolitized fractures begin to develop into small scale shear zone in massive mafic granulite. **c)** A strongly developed sinistral shear zone within the anisotropic Unit 1. d) A pair of pegmatite veins within Unit 1, with the vein to the left displaying weak sinistral displacement**.**

Teddy Rock showcases the first appearance of granulite facies structure being overprinted by amphibolite facies structure within the Twelve Mile Bay strain gradient (Culshaw et al., 2010; Marsh et al., 2011). Shear zone initiation is caused by millimetre- to- centimetre wide brittle fractures, which become amphibolized as the fractures widen and collect pegmatite fluid (Fig. 4.5 a) (Culshaw et al., 2010, 2011; Marsh et al., 2011a). When the fractures reach a critical width, and thereby critical volume of fluid, the fractures start to behave in a ductile manner (Fig. 4.5 b) (Culshaw et al., 2011). These shear zones can develop into decimetre- to -metre-scale structures (Fig. 4.5 c), and begin to segment the wall rock layering into corridors of wall rock blocks (Culshaw et al., 2011; Gerbi et al., 2010) (Fig. 4.5 d).

4.3: Matches Island

Matches Island is located within the northern extremity of the Zone of Reworking, the broad zone of reworking separating the southern interior Parry Sound domain and the Twelve Mile Bay shear zone (Fig. 4.1). The key features of Matches Island are the WNW-striking metre-scale pegmatite-cored amphibolite facies shear zones that overprint granulite facies layered gneiss of the interior Parry Sound domain. Partial overprinting of granulite facies fabric is further complicated by the deformation of dextral shear zones by sinistral shearing resulting in a complex curving network of shear zones (Fig. 4.6).

4.3.1: Macro-scale structure

Matches Island contains two lithological units on the island proper, and a third outcrops on a nearby islet to the southeast (Fig. 4.6) (Culshaw et al., 2011). Unit 1, the dominant lithology of the island is a layered granulite facies gneiss with alternating felsic and mafic layers, variably retrogressed to amphibolite facies (Marsh et al., 2011a, 2013). Felsic and mafic layers in wall rocks variably preserve granulite facies assemblages, especially in mafic layers, while felsic and mafic layers in shear zones are made up of amphibolite facies assemblages (Table 4.1). The wall rock mineral assemblages contain primarily granulite facies assemblages (although with variable retrogression), and the shear zones show an amphibolite facies mineral assemblage.

Table 4.1: Mineral assemblages of layering with Unit 1 (Culshaw et al., 2011; Marsh et al., 2011a). Mineral abbreviations from Kretz (1983).

Unit 1	**Shear Zone**	**Wall Rock**
Felsic layering	Pl ± ksp ± qtz ± hbl ± bt	Pl ± ksp ± opx ± qtz ± hbl ± bt
Mafic layering	Hbl ± pl ± bt ± qtz ± tnt	Pl ± cpx ± opx ± hbl ± grt


0
20
40 m
N
Fig. 4.15 a
Fig. 4.14 d
Fig. 4.8 c
Fig. 4.8 a
Fig. 4.15 c
Fig. 4.14 b
Fig. 4.15 b
Fig. 4.8 d
Fig. 4.14 c
Fig. 4.8 b
Fig. 4.14 a
Fig. 4.16 b
Fig. 4.15 d
Unit 1
Fig. 4.16 a
Fig. 4.11 a
Unit 2
Unit 3

Figure 4.6: An orthorectified aerial photo of Matches Island showing the lithologic units as outlined in Culshaw et al., 2011. Solid white lines, lithology boundaries; dashed white lines, uncertain lithology boundaries; dashed boxes, figure locations as indicated

Unit 2 is located on the southeastern margin of the island (Fig 4.6) and is comprised of a uniform amphibolite facies gneiss, which lacks mafic layers but contains concordant pink granitic layers dispersed throughout the grey gneiss. The mineral assemblage of Unit 2 reflects a package of rock that has been completely retrogressed from granulite facies to amphibolite facies, consisting largely of plagioclase, quartz, hornblende and biotite, with leucosome patches containing retrogressed pyroxene (Culshaw et al., 2011). Unlike Unit 1, the mineral assemblage does not vary from wall rock to shear zone (Culshaw et al., 2011). Similar to Unit 1, dextral shear zones are focused on pegmatite dykes that cut the gneissic layering, although shear zones are less frequent than in Unit 1. Large amplitude (0.5 to 1 metre) folds are common within Unit 2 panels, reflecting a lower competence contrast between mafic and felsic layers within Unit 2 than Unit 1.

Unit 3 is located 5m offshore to the southeast of Matches Island, and consists of a homogeneous amphibolite, although the presence of retrogressed pyroxenes within leucosomes indicates that a granulite facies heritage is likely (Culshaw et al., 2011). There are several prominent pegmatites emplaced nearly orthogonal to the host rock layering, consistent with the geometry observed on the mainland near Matches Island. Centimetre-scale dextral displacements are observed along the margins of the pegmatites and offset wall rock layering. Unit 3 contains the least internal deformation, and the orientation of wall rock layering is approximately the same as the original iPSD orientation north of the retrogression boundary (RRB, Fig. 4.1), therefore we assume Unit 3 to contain examples of the initial wall rock and initial fracture orientations.

The map view of Matches Island (which is approximately a down-dip view) shows that the lithological boundaries form a step-like pattern (Fig. 4.6). The two competent units (1 and 3) are separated from one another by a weak unit (Unit 2), which forms a half a boudin neck infill protruding into Unit 3 and two infill structures that flow into

Unit 1, each bounded by dextral shear zones along the boundary. Unfortunately, the full view of the boudinage structure is obscured by water so it is difficult to deduce the geometry. However, from the orientation of the decametre-scale boudinage, it appears to be NNE extension; i.e. layer parallel extension to original PSD orientation.

Rocks on Matches Island have two planar fabrics; i) granulite facies compositional layering inherited from the interior Parry Sound domain (S_1), and ii) amphibolite facies gneissosity within dextral shear zones (S_2). S_2 overprints S_1, within regularly spaced strongly localized shear zones (Fig. 4.6). Both fabrics are then variably overprinted by a broad, weakly localized sinistral shear, which rotates both S_1 and S_2 counterclockwise.

The detailed field work was focused within Unit 1, as highlighted by the yellow area within Figure 4.7, as this area provided the largest area free from boulder and vegetation cover, and provides a transect from weakly to strongly developed shear zones. The yellow area represents the coverage of highly detailed low level photographs as explained in the methods section. The rest of the island was imaged using a series of conventional aerial photos, as well as field photos.

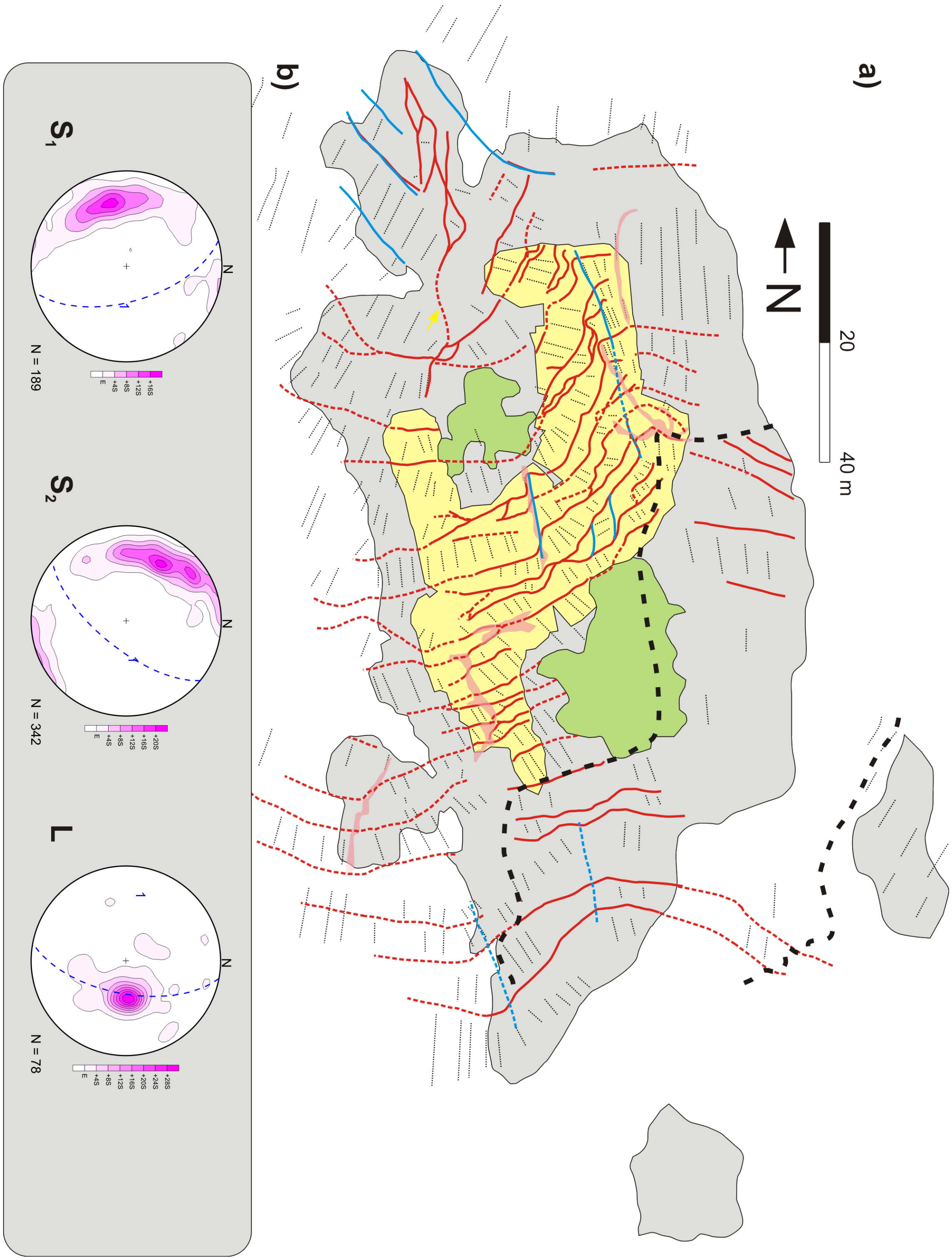
a)
N
20
40 m
b)
S1
N = 189
S2
N = 342
L
N = 78

Figure 4.7: Schematic structural map of Matches Island. Thick dashed black lines, lithology bounds; thinly dashed black lines, iPSD layering (S_1); solid red lines, mapped dextral shear zones (S_2); dashed red lines, inferred dextral shear zones; solid blue lines, mapped sinistral shear zones; dashed blue lines, inferred sinistral shear zones; green polygon, vegetation; yellow polygon, trace of photomosaic area; pink polygon, concordant granitic layers. **b)** Lower hemisphere equal area projections showing poles to wall rock layering (S_1), poles to shear zone layering (S_2), and hinges and linear features (L). Blue dashed great circles are best fit planes.

4.3.2: Wall Rock Layering

The wall rock layering of Unit 1 is made up of large (~2 x 5 m) predominately mafic wall rock blocks containing original granulite facies mineral assemblages. Wall rock layering within Unit 1 predominantly consists of NNE striking, sub-vertical granulite facies gneissic foliation. Structure of wall rock layering is shown in Figure 4.7 b, which gives an average wall rock layering orientation for Matches Island of 345/60 (blue dashed great circle). The poles to wall rock foliation cluster along a single great circle, rotated around the first eigenvalue (labeled 1 on stereonet), which corresponds to measured linear features. .

There is considerable variability of the orientation of the wall rock foliation across the island due to the rotation of wall rock blocks, some of which deviate significantly from original iPSD layering. In extreme cases wall rock layering has been rotated up to 90° from the original iPSD layering. The progressive rotation of granulite facies foliation (dashed black lines) can be seen in Figure 4.7. This variability associated with shearing will be discussed in further detail in Chapter 5.

The amphibolite facies biotite gneiss layers in Unit 2 are rheologically weaker than the granulite facies counterparts of Unit 1, resulting in a competency contrast within Unit 2 between the biotite-rich and felsic layers. This folding of Unit 2 wall rocks during shearing results in large amplitude open folds. The folded wall rock of Unit 2 is particularly evident on the eastern side of the island in Figure 4.6. Although wall rock blocks can be observed in Unit 2, folding of wall rock panels combined with poorly developed shear zones form a more chaotic pattern than the structure observed in Unit

1. The style of deformation within Unit 2 is similar to that described by Culshaw (2005), where wall rock develops drag folds as it is sheared.

Unit 3 was not studied in detail. It is made up of homogeneous wall rock panels with little to no internal deformation. The orientation of wall rock layering of Unit 3 closely compares to interior Parry Sound domain layering, and can be used as a reference to wall rock layering from original iPSD layering.

4.3.3: Dextral shear zones

Within Unit 1 amphibolite facies dextral shear zones dissect granulite facies wall rock layering at a high angle, resulting in an orthogonal relationship between the two structures. Shear zones are strongly localized and range from centimetre to decametre-scale in width. The simplest structure within Unit 1 is the 'ladder and rung' structure, where granulite layering (ladder rungs), are overprinted by dextral shear zones (Fig. 4.8 a, b). Dextral shear zones are concentrated within Unit 1 and are regularly spaced at approximately 2 m intervals.

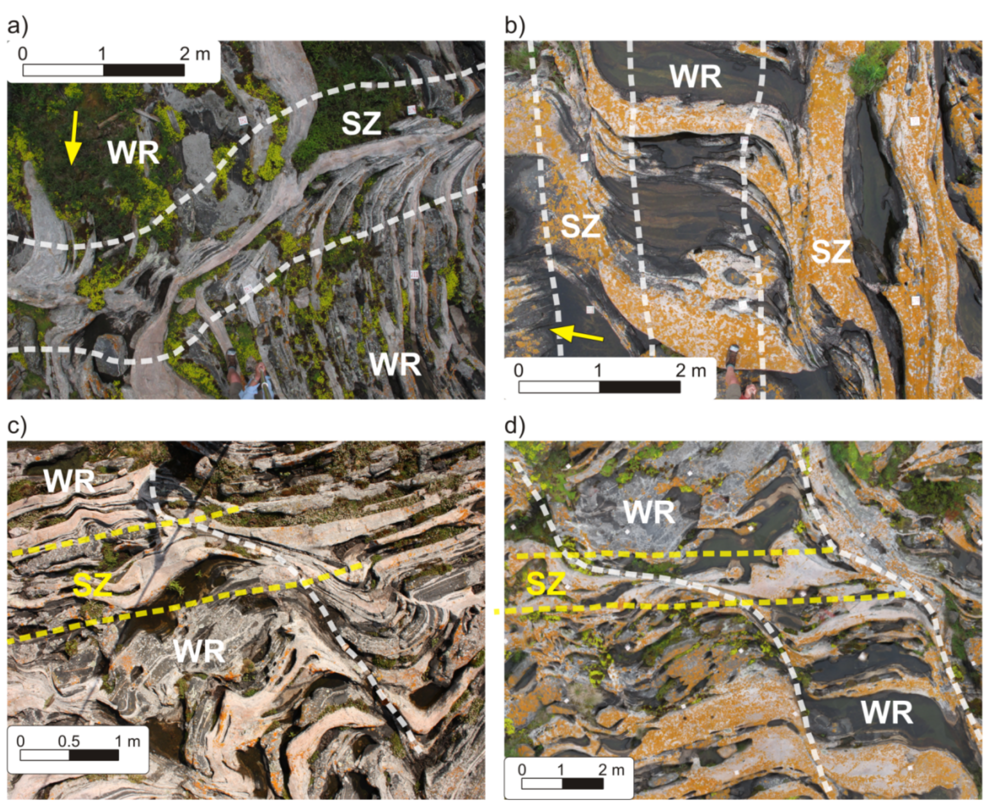

Figure 4.8: Examples of shear zones in Unit 1. White dashed line, dextral shear zone; yellow dashed line, sinistral shear zone; WR, wall rock; SZ, shear zone; yellow arrow, north. **a)** and **b)** are examples of dextral shear zones overprinting wall rock layering, while **c)** and **d)** are examples of discrete sinistral shear zones overprinting wall rock layering and dextral shear zones. See Figure 4.6 for locations.

Dextral shear zones within Unit 2 are much less common and behave in a different style than their Unit 1 counterparts. There are only four dextral shear zones, which are defined by the presence of a pegmatite core, displacement, and thinning of incoming layering. Several structures within Unit 2 that were mapped as shear zones are now interpreted as asymmetric folds due the to relatively weaker amphibolite facies wall rocks of Unit 2. The reinterpretation was based on the absence of pegmatite and lack of displacement along the previously mapped shear zones. Units 1 and 2 are separated from one another by a dextral shear zone (Fig. 4.6, 4.7).

Dextral shear zones in Units 1 and 2 show the same rotational pattern as wall rock layering, resulting in a broad sigmoidal curve when seen at the decametre-scale (Fig 4.6, Fig. 4.7). The least rotated dextral shear zones originate with a WNW orientation and are variably rotated, resulting in NNE striking dextral shear zones in areas of maximum rotation. This orientation is consistent with undeformed cm-scale pegmatite veins observed on Teddy Rock and several other sites on the southern iPSD, indicating that the original vein orientation is WNW. Shear zone terminations are common along the W and E side of the island, as evidenced by undeformed and unrotated pegmatites in the shallow water. As far east as Unit 3 there are pegmatite veins and display dextral displacement in their original orientation that display a combination of brittle and ductile deformation.

An island-wide summary of dextral shear zones is given in figure 4.7 c, which shows a series of steeply dipping shear zones of variable strike. The data display a loose cluster around a common direction/orientation, but strongly clusters along a common great circle. The rotational axis measured from dextral shear zones, labeled as 1 on Figure 4.7 (S_1), is nearly identical to the rotational axis of wall rock layering. These axes coincide with the strong cluster of shear zone and wall rock hinges shown in Figure 4.7

(L), which is evidence that wall rock layering and dextral shear zones are part of a cylindrical system and rotate around a common axis.

4.3.4: Sinistral shear zones:

There are two styles of sinistral shear zones on Matches Island; discrete sinistral shear zones, and a broad zone of sinistral rotation bounded by discrete shear zones (Fig. 4.9). The two styles of shear form a larger master shear system, where discrete sinistral shear zones flank broad sinistral shear zones, and act as discrete slip planes (Fig 4.9). Sinistral shear zones overprint both wall rock and dextral shear zones leading to two possibilities; either sinistral and dextral shear zones developed together as a conjugate network; or the sinistral event postdates dextral deformation.

Discrete sinistral shears are comparable to dextral shear zones as they exhibit localization, and commonly nucleate on thick felsic wall rock layering (Fig. 4.8 c, d). Broad sinistral shear zones, illustrated in Figure 4.9, strongly differ in style from their dextral counterparts in that the broad sinistral shear zones are diffuse, and do not focus on pegmatite veins. The rotation of both wall rock and dextral shear zones observed from map pattern (Fig. 4.7 a) is attributed to a decametre-scale sinistral shear zone that strikes approximately north-south (Fig 4.9).

In Unit 1 there is a broad sinistral shear zone running roughly N-S (Fig. 4.9). The broad sinistral shear zone is approximately 20 m wide and bounded to the W and E by narrow bands of discrete sinistral shear zones. The midpoint of the broad sinistral shear also coincides with the maximum rotation of wall rock and dextral shear zones, which maintain their original orthogonal relationship. It is within this broad sinistral shear where the most internal deformation of wall rock blocks occurs.

Discrete sinistral shear zones differ from broad sinistral shear zones in scale and degree of strain localization. Discrete sinistral shear zones occur as centimetre- to-metre-scale zones of highly localized deformation. Discrete sinistral shear zones typically form along strike of thick felsic wall rock layers creating several discontinuous segments, reminiscent of en echelon arrays (Fig. 4.8 d). It is unclear if discrete sinistral shear zone nucleation sites are pre-existing thick felsic layers within the granulite facies blocks, or if they are concordant granitic sills.

Within Unit 2 there is a 20 m wide sinistral shear zone located on the southern point of Matches Island (Fig. 4.7 a). Due to the more complex structure associated with the widespread buckling of wall rock within Unit 2, discrete bounding shear zones are difficult to image. However, pegmatite veins visible offshore in shallow water can be easily traced from E (within Unit 3) to W. The pegmatites swing from their original orientation into a sigmoidal pattern, defining the boundaries of the broad sinistral shear.

Matches Island is made up of a series of wall rock blocks separated by shear zones (that originated on pegmatite filled fractures) that strike orthogonal to granulite facies layering. The shear zones curve anticlockwise, reaching a maximum rotation of approximately 90° from regional PSD orientation close to the center of the island before returning to the regional PSD orientation. The wall rock panels rotate with the shear, leaving their orthogonal relationship with the shear zones intact. The wall rock blocks that have undergone the most rotation (i.e. the center of Unit 1, Fig 4.6, Fig 4.9, Block B) tend to have the most well developed shear zones, demonstrated by a transect across Unit 1.

Figure 4.9 shows three blocks of differing wall rock and shear zone orientation, A, B and C. Block A is slightly rotated from its original orientation and features weakly developed shear zones with low displacements. Block B shows a much higher degree of rotation than that of Block A along with wider shear zones with larger displacements. The rotation of wall rock and fracture orientations peaks within Block B and leads to a series of features that accompany the widening of shear zones. On the block B/C margin, a highly deformed felsic layer separates Block B from the less rotated Block C, which is comparable to Block A in terms of degree of rotation. Unit 2 also follows this pattern but is less obvious due to wall rock folding and poor shear zone development.

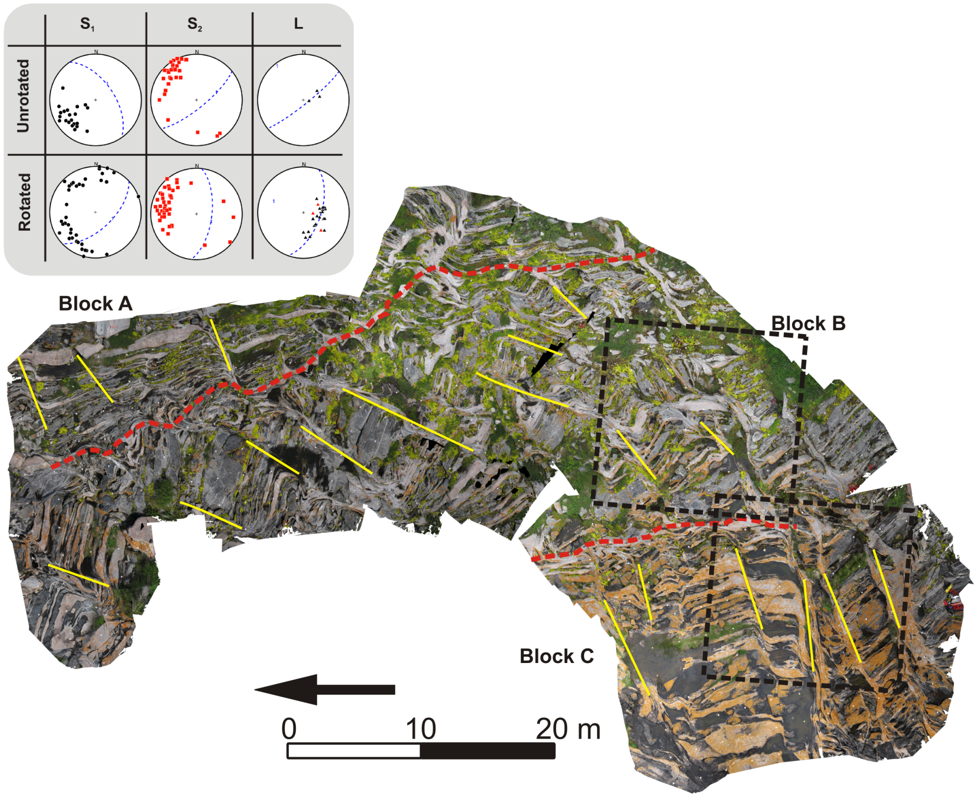

Figure 4.9: Photomosaic of Matches Island displaying rotational boundaries (part of yellow polygon, Fig 4.6). Red dashed lines, rotational boundaries; solid yellow lines, pegmatite filled dextral shear zone orientation; black dashed boxes, Figure 4.10 locations.

Space problems caused by the rotation of rigid wall rock blocks appear to be resolved by the emplacement of ~1 m thick granitic sills of undetermined relative age. It is possible that the granitic sills are fed by the original fracture filling pegmatites that formed orthogonal to layering, because the granitic sills commonly intersect the pegmatite-cored dextral shear zones (Fig 4.10), but it is unclear whether these intersections are pre- or syn-shear. These granitic sills are typically found between zones of different rotational regimes and can be considered as rotational boundaries (Fig. 4.10 a) that accommodate rotational strain by displaying ductile dextral offsets (Fig. 4.10 b). Shear zones are not observed in wall rocks until the wall rock and pegmatite rotate anticlockwise. In Figure 4.11 a there are two rotational boundaries; to the west of the westernmost boundary there is no sinistral rotation or shear zones. It is only after crossing the westernmost granitic sill in Figure 4.10 a do we observe the onset of sinistral rotation and dextral shear zones.

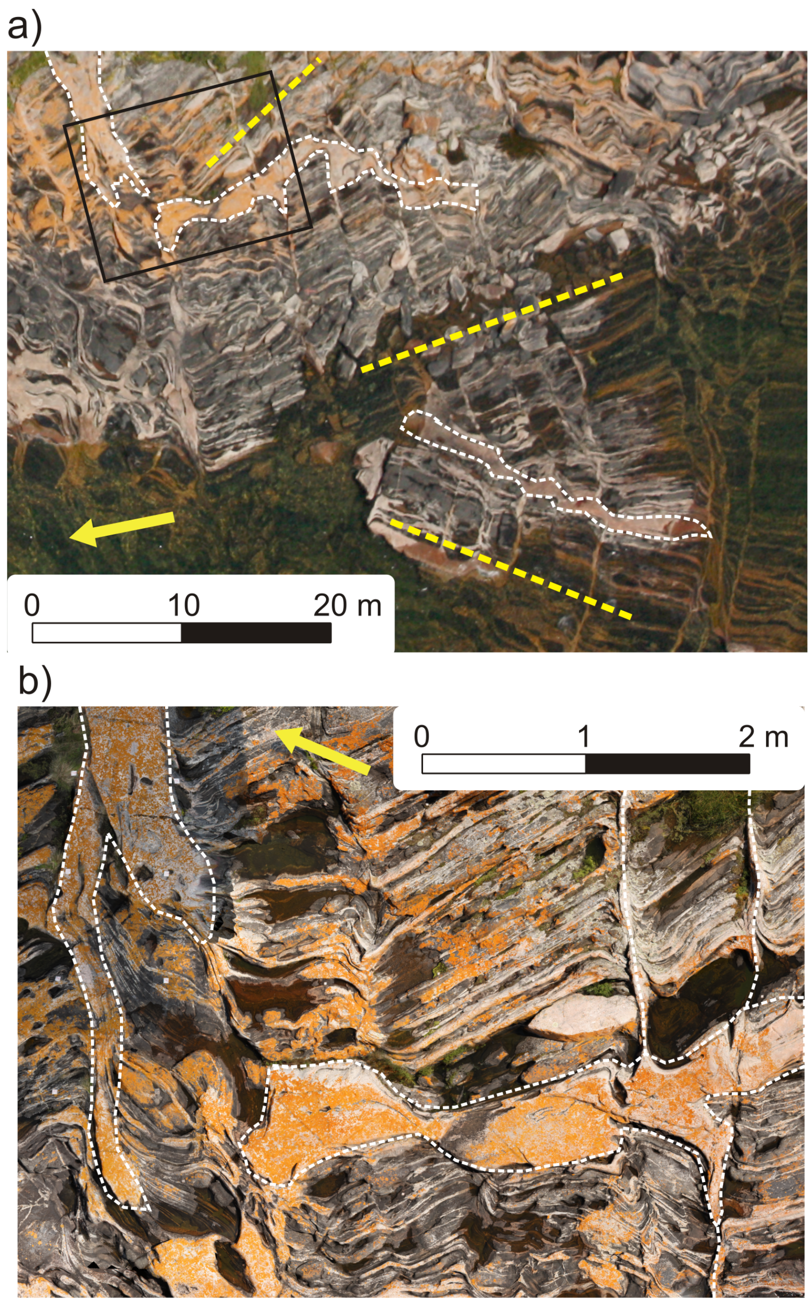

Figure 4.10: Granitic sills along rotational boundaries. Granites, white dashed lines; average wall rock strike of a rotational regime, yellow dashed lines; b location, black box. **a)** Pegmatitic granites concordant to layering act lie along rotational boundaries and themselves develop ductile deformation that accommodates rotation and maintains compatibility between panels. **b)** At the breaks in rotational domains, the pegmatitic granites appear to be fed by pegmatites normal to layering.

Zones of rotated wall rock layering are also laterally separated from one another by wedge-like blocks of highly deformed wall rock lozenges bounded by well-developed shear zones (Fig. 4.11). Like the concordant granitic sheets, the wedged material acts as a rotational boundary, allowing the wall rock layering and shear zones in the panels flanking the wedges to remain orthogonal.

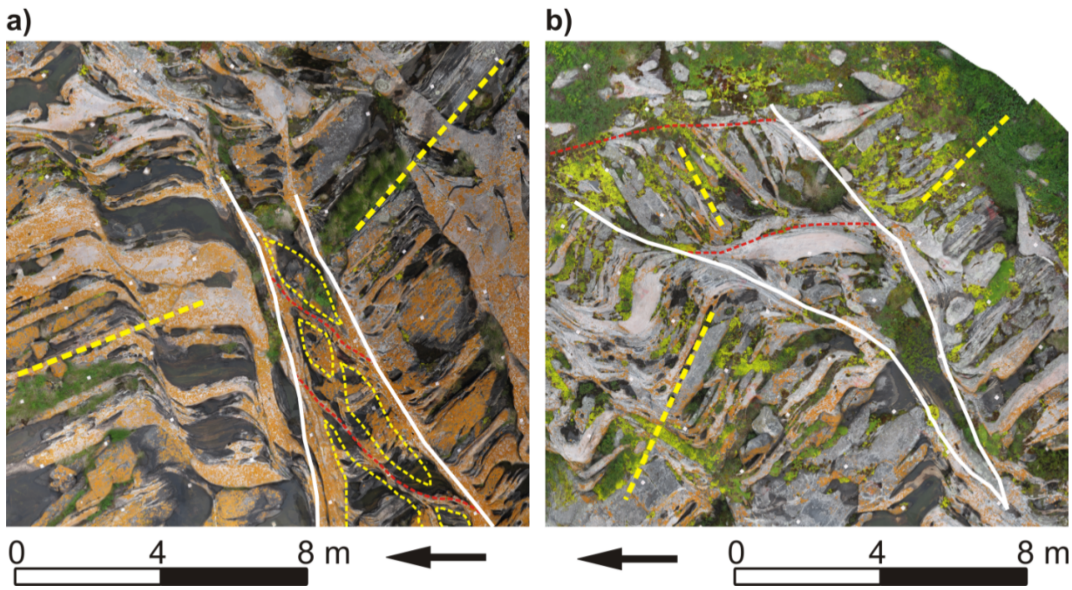

Figure 4.11: Examples of wedges separating zones of rotated wall rock layering, see Fig. 4.10 for locations. Solid white lines, wedge outline; yellow dashed lines, wall rock orientation; red dashed lines, linked dextral shear zones; yellow dashed polygons, deformed wall rock.

The extent of shear zones on Matches Island is governed by the rotation of wall rocks. On the eastern and western margins of the island there are packages of unrotated rock (Fig. 4.6, Fig. 4.7). The pegmatites within the unrotated packages show little to no sign of ductile deformation or displacement. Dextral shear zones along pegmatites occur only when the packages of rock have rotated.

In the northwest of the island, a small patch of rubble obscures a potentially key outcrop. To the east of the rubble there is a zone of highly rotated wall rock panels and strongly developed shear zones; to the west is a zone of unrotated wall rock panels and weakly developed shear zones (yellow arrow, Fig. 4.7). A layer-parallel shear zone lies along the unrotated domain along strike to the rubble, and is the obvious boundary between the domains of contrasting rotation and strain. The layer-parallel shear zone shows apparent dextral motion at the boundary of the unrotated and rotated domains. The N-S strike of the dextral shear zone is an unusual orientation for dextral shear zones, which normally strikes ~E-W.

4.3.5: Folds

Fold hinges on Matches Island show a strong uniform orientation, with hinges plunging nearly vertically. Axial planes show symmetric to asymmetric fold geometry, dipping near vertical and striking either ~NNE or WSW. The structural summary of fold hinges on Matches Island is illustrated by Figure 4.7 d. The strong cluster of fold hinge data indicates a cylindrical system folding of S_1 (Fig. 4.7 b, c.).

Fold development within Unit 1 is concentrated within the broad sinistral shear zone, folds nucleate and the axial planes of which are approximately perpendicular to one another. The axial traces form a bimodal pattern, with buckle fold axial traces oriented NNE, and scar fold axial traces show much more variability, with a fan like rotational pattern from north to south (Fig. 4.12).

The relatively low competence contrast of the amphibolite facies wall rock of Unit 2 compared to the granulite facies wall rock of Unit 1 permits wall rock layering to fold before shearing, contrasting with the fold style of Unit 1 (Culshaw et al., 2011). Widespread folding of wall rock layering results in symmetrical open folds with amplitudes ranging from decimetre- to metre-scale, indicating the introduction of a pure shear component. Within the broad sinistral shear zone of Unit 2 the pre-existing wall rock folds are affected by shearing, which causes the axial traces of the folds to rotate anticlockwise, while the interlimb angles decrease to reflecting the tightening of the fold. Sheared folds show a weak transition to an ‘s-type’ asymmetry. Folds located outside the broad sinistral shear zone have an average axial trace trending ESE-WNW, with an average interlimb angle of 109°, whereas folds within the broad sinistral shear have an average axial trace nearly NNE-SSW, with an interlimb angle of 30°.

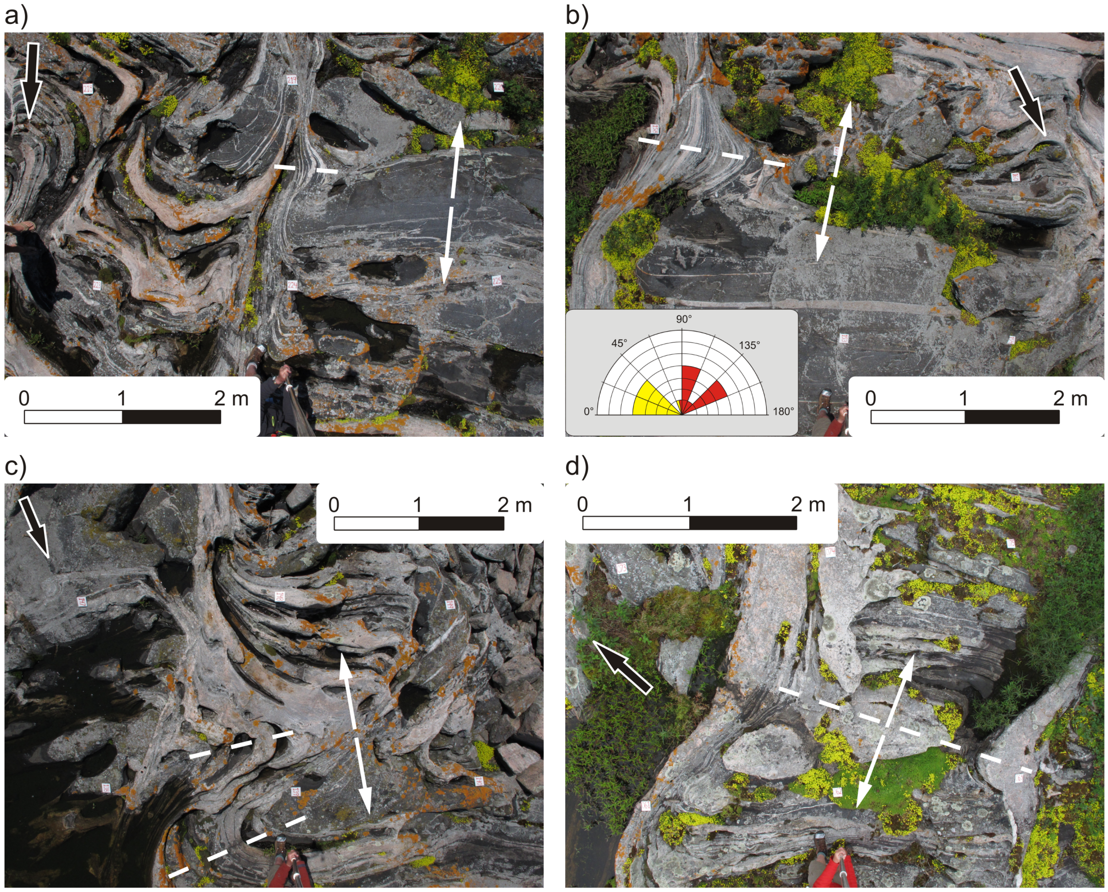

Figure 4.12: Examples of folds within shear zones within Unit 1 on Matches Island. Axial trace, white dashed line; inferred extensional direction, white arrow. **a)** A weakly developed fold within a shear zone, note the folded wall rock panel to the left. **b)** A strongly developed fold flowing around a mafic panel. **c)** Scar fold amplified with rotation of wall rock block. **d)** A strongly developed fold between two mafic wall rock panels.

4.3.6: Anastomosing shear zones

Unit 1 of Matches Island provides several examples of anastomosing shear zones. The junctions of one or more shear zones are of great interest to this study, as many of the structural complexities occur at the location of these shear zone merges, such as deformed wall rock panels and folds that can be reworked or partially preserved following increasing strain. Culshaw et al. (2011) divided shear zone merges into two categories, i) sub-parallel minor shear zones, linking established shear zones, and ii) established shear zones merging to form a single thick shear zone. There are fewer examples of anastomosing shear zones within Unit 2 due to the poorly developed shear zones. Figure 4.13 shows examples of type-i and type-ii shear zone merges.

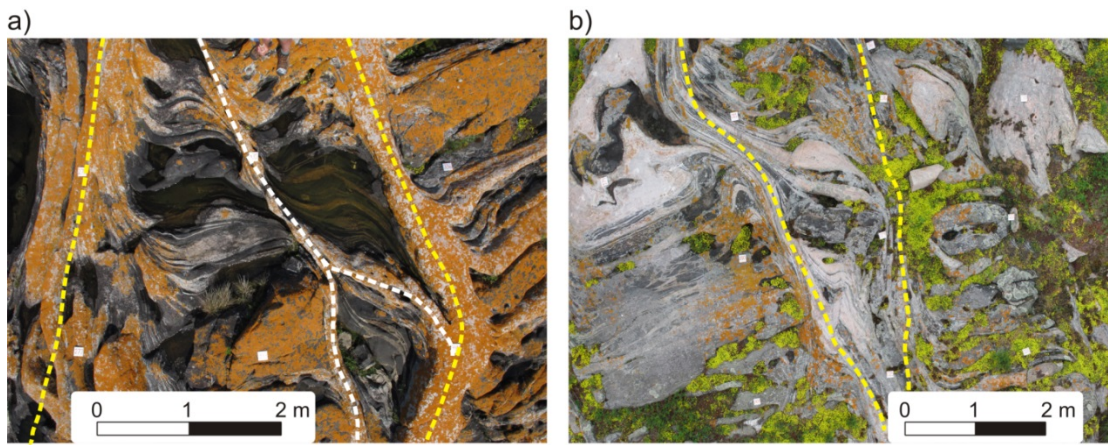

Figure 4.13: Examples of shear zone merges within Unit 1 on Matches Island. Yellow dashed line, established shear zone; white dashed line, new, sub-parallel shear zone. **a)** A type-i shear zone merge, where the two established shear zones are joined by new shear zones, forming several sigmoidal wall rock lozenges. **b)** A type-ii shear zone merge, where the two established sub-parallel shear zones merge together to form a single wide shear zone.

The established shear zones on either side of the highly deformed blocks are thick (0.5-1 m wide) pegmatite cored dextral shear zones. Sub-parallel shear zones develop along pegmatite veins within the wall rock panel, dissecting the wall rock panel into smaller segments. These new shear zones are much narrower than the established shear zones, ~10-25 cm wide, but may split to form a small network of anastomosing shear zones. The wall rock foliation of the resulting dissected wall rock blocks generally do not fold, but wall rock foliation is variably rotated towards the shear plane. This results in a several small wall rock panels of varying deformation state, which are also observed in the wall rock wedges (Fig. 4.11). With increasing strain it is likely that the sub-parallel shear zones may merge with other shear zones in the manner of type ii shear zone merges.

The wall rock panel between the merging shear zones becomes increasingly tapered as the margins are incorporated into the bounding shear zones. Wall rock layering within the collapsing panel may develop folds or simply rotate into the shear plane. In the example the collapsing wall rock panel does not develop strong folds but the neighboring wall rock panel does.

There is a third possible shear zone merge; high-angle sinistral-dextral junctions. Sinistral overprinting of dextral shear zones establishes a timing relationship, leading to the hypothesis that broad sinistral shear zones cause antithetic dextral shear zonesand that sinistral and dextral shear zones were approximately coeval. Junctions between discrete sinistral and dextral shear zones are associated with the folding wall rock, and subsequent wall rock panel collapse. The majority of shear zone merges occur within the broad sinistral shear zone, which is likely related to the higher frequency of S_1 folding and providing more opportunities for anastomosing shear zones.

4.3.7: Summary

Matches Island represents an initial stage of transposition in the Twelve Mile Bay strain gradient. Despite the development of a strongly localized shear zone network, the island still preserves granulite facies mineral assemblages and structure. Matches Island provides the first appearances of linked shear zones, buckled granulite facies wall rock layering, and scar folds. Kinematic analysis from decametre-scale boudins (i.e. Unit 3), and buckle/scar fold hinge orientations give a NNE extensional direction.

4.4: PBW Island

Situated just south of the transposition boundary, PBW Island consists of widespread amphibolite facies Twelve Mile Bay shear zone fabric, with wider shear zones and higher proportions of S_1 transposed parallel to S_2 than Matches Island (Fig. 4.14). Predominant dextral and localized sinistral shear zones appear nearly coplanar, with sinistral overprinting dextral structures, consistent with overprinting observations on Matches Island.

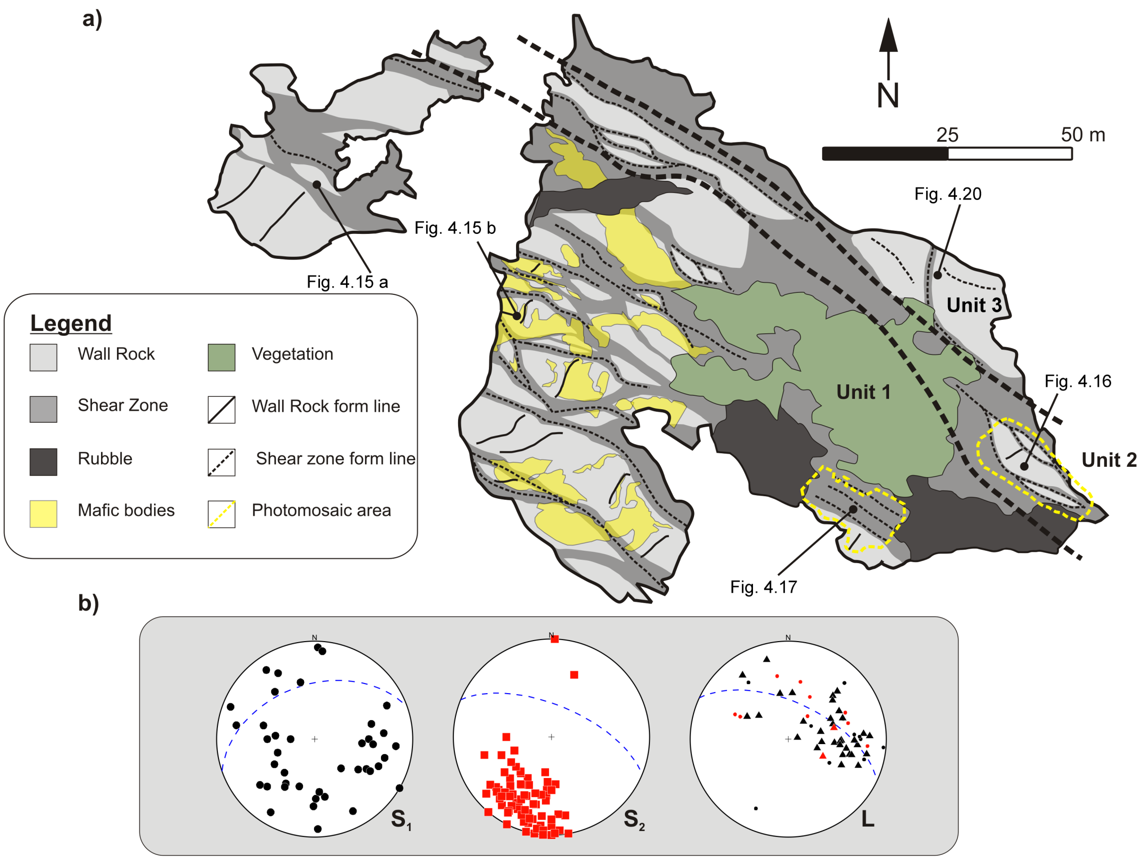

Figure 4.14: a) Schematic structural map of PBW Island. Light grey, wall rock; dark grey, shear zone; black, rubble; green, vegetation; yellow, mafic bodies; black lines; wall rock layering form lines; thin dashed black lines, shear zone layering form lines; thick dashed black lines, lithological boundaries; dashed yellow lines, photomosaic area. **b)** Lower hemisphere equal area projections showing poles to wall rock foliation (S_1), poles to shear zone foliation (S_2), and fold hinges and lineation (L). Legend for linear features net: black triangle, wall rock fold hinge; red triangle, shear zone fold hinge; black dot, wall rock lineation; red dot, shear zone lineation, blue dashed great circle, best fit plane.

4.4.1: Macro-scale structure

PBW Island is made up of two units, which slightly differ from lithological compositions found at Matches Island. Felsic layers on Matches Island are granitic, but one PBW Island felsic layers are granodiorite to tonalite in composition; i.e hornblende+ biotite+ quartz+ plagioclase within shear zones and wall rock, with relict porphyroblasts of primary garnet and orthopyroxene (mantled by hornblende, plagioclase, biotite and/or quartz) occasionally found within wall rock blocks reflecting granulite facies remnant assemblage (Marsh et al., 2011 a). The distinguishing difference between the units is the m-scale layer thickness (Fig. 4.15) and presence of mafic granulite facies dykes that truncate wall rock foliation within the most areally extensive unit on the SW side of the island (Fig. 4.14).

Unit 2, located on the NE side of the island closely resembles the lithology of Unit 1 on Matches Island, and as a result, has a similar structure in both geometry and scale, i.e., centimetre-to- decimetre-scale wall rock foliation. Wall rock foliation alternates from mafic to felsic with a higher proportion of mafic layers that tend to be thicker than their felsic counterparts. Figure 4.16, a photomosaic map, is a representative section of the structure of Unit 2, with a tapered, thinly layered wall rock block bounded on either side by thick shear zones. The shear zones on either side of the tapered wall rock block converge to form a single, wide shear zone, similar to shear zone merges observed on Matches Island. The wall rock panels within Unit 2 frequently featurefolds, another distinguishing characteristic shared with Unit 1 on Matches Island.

Unit 3 is located on the NE of the island and consists of amphibolite facies layering oriented parallel to the dominant shear zone orientation (Fig. 4.14a). The amphibolite facies fabric is subsequently cross-cut by shear zones, but this unit was not investigated in detail in this study.

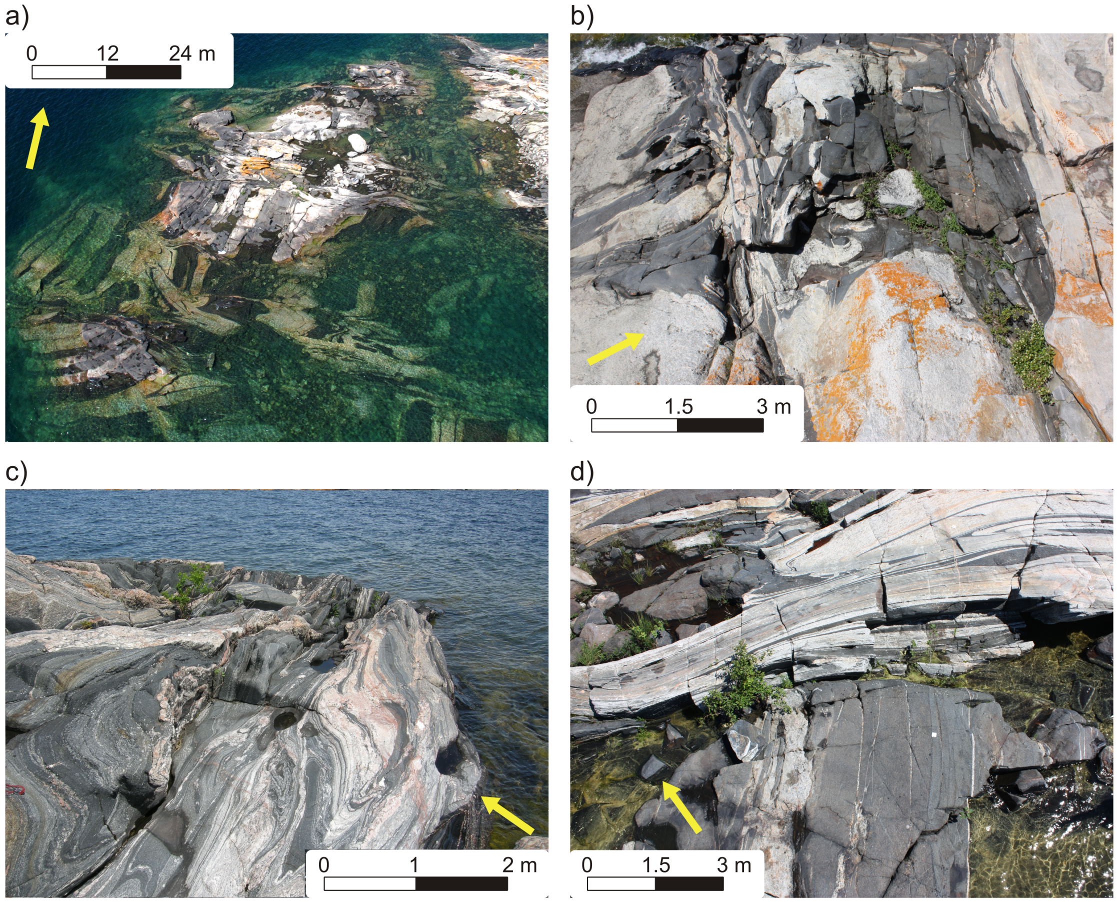

Figure 4.15: Examples of multi-scale shear zones and wall rock lozenges on PBW Island. See Figures 4.17 for photo locations. **a)** Thickly layered wall rock blocks and bounding shear zones located in the shallow water to the northwest of the island. **b)** Thickly layered wall rock panels typical of Unit 1 and relatively thin bounding shear zones. **c)** Composite shear zone within Unit 2. **d)** Massively layered mafic wall rock panel surrounded by a strongly developed shear zone.

Unit 1, located on the SW side of PBW Island, geometrically similar to Unit 2, is complicated by the presence of large (10-20 m wide) granulite facies dykes that intrude into the tonalitic country rock (Fig. 4.14, yellow polygons). The presence of dykes within Unit 1 results in massive wall rock blocks (10-20 m wide), which in turn influences the width and spacing of shear zones. The shear zones in this area show predominately dextral shear sense.

There are several examples of apparent sinistral motion, which appear in centimetre-scale shear zones. The relative timing of the sinistral and dextral shear zones is unknown, as there were no examples of one set overprinting the other in the field. There is one example of apparent down-dip displacement of wall rock layering in the vertical plane along a dextral shear zone. However, the down-dip displacement is very small (centimetre-scale), there was also a lack of stretching lineation and occurrence of such a structure was isolated and unrepresentative of the shear zone system.

Composite shear zones to refer to metre- to- decametre-wide shear zones ranging from 1 to 5 metres in width, of interlinking shear zones and small blocks of variably deformed and rotated wall rock material (Fig. 4.15 c). The orientation of sub-shear zones within a composite shear zone can vary, as the shear zone layering deflects around the competent wall rock material. Composite shear zones are commonly found in Unit 1 of PBW Island, particularly in the northwestern side of the island.

Composite shear zones in Unit 1 commonly feature very thickly layered wall rock blocks (5-10 m wide). These large, thickly layered wall rock blocks show little signs of internal deformation and preserve interior Parry Sound domain fabric and in some cases original granulite facies mineral assemblages. The best examples of decametre-scale wall rock blocks come from shallow water exposures to the W of the island that can be seen in aerial photographs (Fig. 4.15 a). Undeformed wall rock foliation strikes NNE, consistent with the original iPSD fabric. Figure 4.16, a photomosaic map, is a representative section of the structure of Unit 2, featuring wall rock blocks with metre-scale layer thickness.

The decametre- to- hectometre-scale structure of PBW Island is made up of wall rock panels (of varying scale, depending on lithology), and strongly developed amphibolite facies shear zones with widths ranging from metre- to- decametre-scale. The decametre-scale structure is governed by lithology, with low amplitude open folds developing in the thinly layered wall rock panels of Unit 2. Unit 1 features thickly layered wall rock layering that leads to the development of large-scale wall rock panels. Such folds do not develop in wall rock layering of Unit 2, likely because of the very thick layer thicknesses that are common. In general, the wall rock panels are lozenge shaped rather than rectangular wall rock blocks observed on Matches Island. The strong deformation of wall rock blocks results in a highly variable wall rock orientation (S_1), and in turn the orientations of the now well-developed shear zone fabric (S_2) are nearly parallel (Fig 4.14, b).

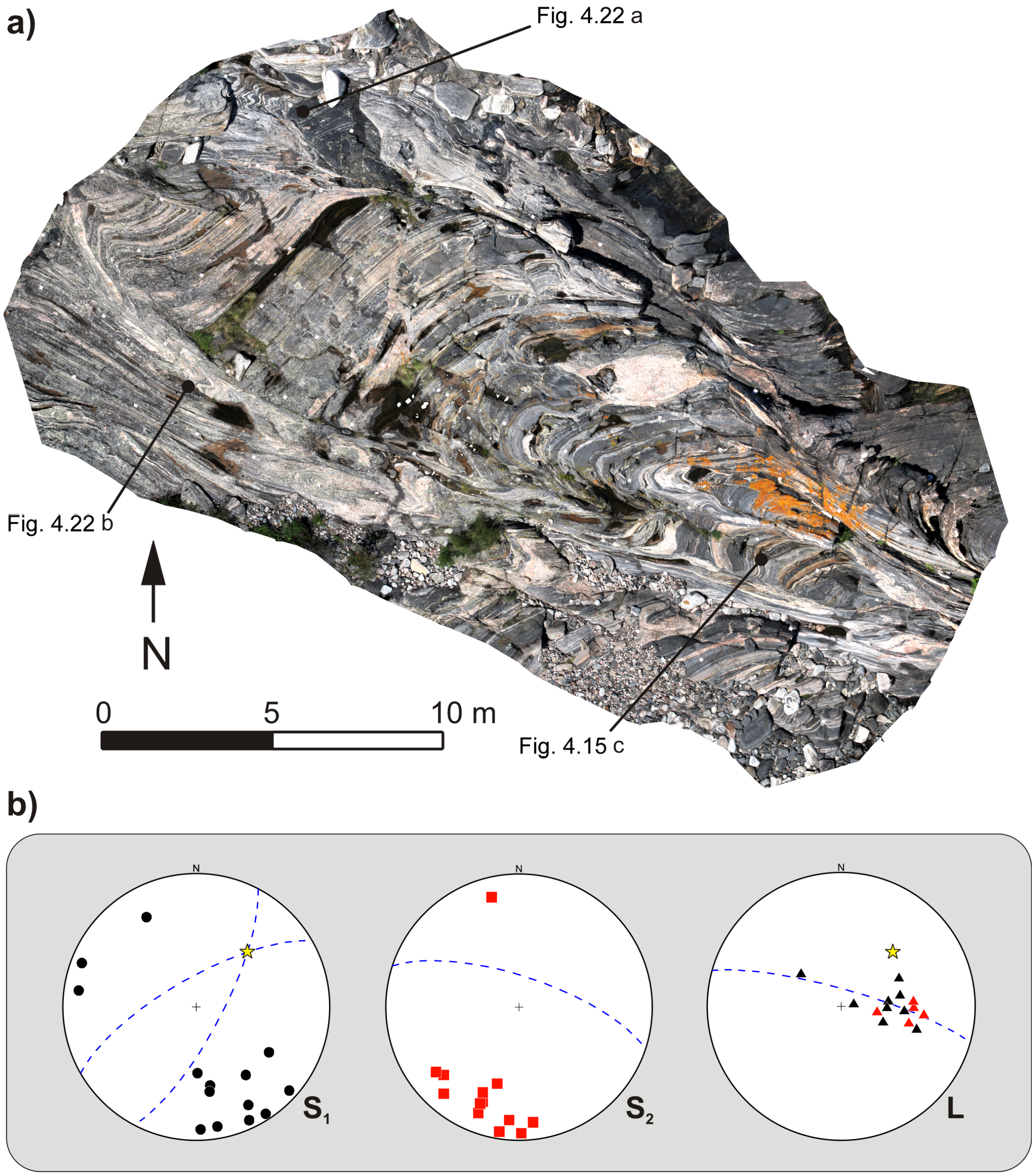

Figure 4.16: a) Photo-map of a wall rock lozenge bounded by thick shear zones on either side within Unit 2. Note the sub-shears and lozenges towards the tapered ends of the wall rock panel. See Figure 4.17 for location. **b)** Lower hemisphere equal area projections showing poles to wall rock foliation (S_1), poles to shear zone foliation (S_2), and fold hinges and lineation (L). Yellow star, inferred fold axis from S_1 net; red triangle, shear zone fold hinge; black triangle, wall rock fold hinge; blue dashed great circle, best fit plane to poles (for S) and to lineations (for L).

a)

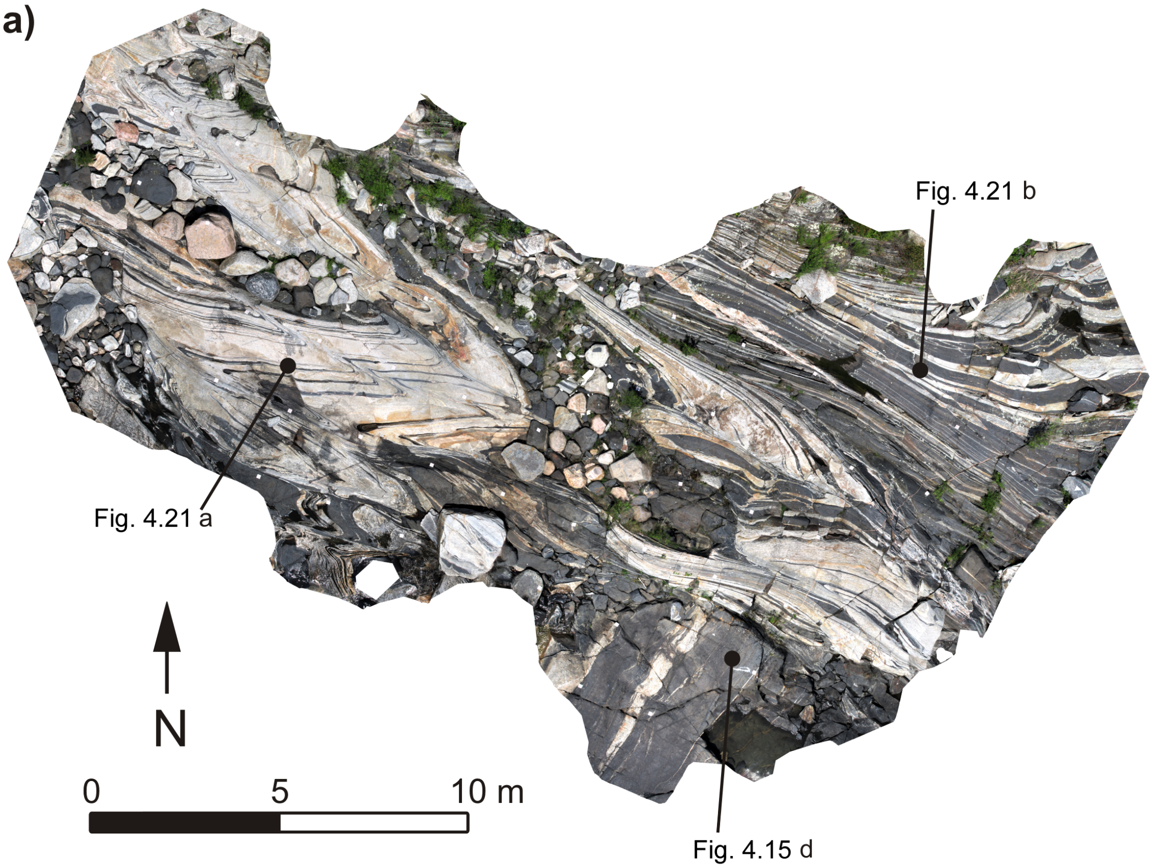

b)

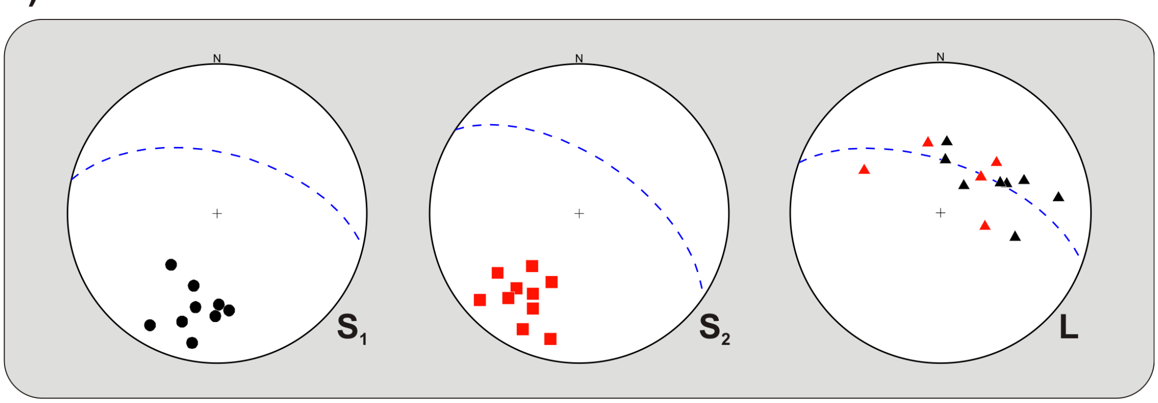

Figure 4.17: a) Photo-map of a wall rock lozenge within Unit 1. See Figure 4.14 for location. **b)** Lower hemisphere equal area projections showing poles to wall rock foliation (S_1), poles to shear zone foliation (S_2), and fold hinges and lineation (L). Red triangle, shear zone fold hinge; black triangle, wall rock fold hinge; blue dashed great circle, best fit plane to poles (for S) and to lineations (for L).

4.4.2: Wall rock foliation

Wall rock foliation is much more chaotic on PBW than observed on Matches Island. This stereonet pattern is in part due to the seemingly random orientation of dykes on the western side of the island, and widespread buckling of wall rock in Unit 2 on the eastern side. Orientation of wall rock layering ishighly variable and does not form a strong pattern (Fig. 4.14, S_1).

In Unit 2 (Fig. 4.16), there is a metre- to- decametre- scale wall rock lozenge with wide shear zones bounding it. Within the lozenge there are several sub-lozenges separated from one another by centimetre- to decimetre-scale shear zones that show dextral motion. The wall rock foliation of the sub-lozenges shows a clear bimodal orientation (Fig. 4.16, b), which is due to the fold development within Unit 2. Fold development is concentrated towards the narrow tips of the wall rock lozenge, where there are also an increased amount of smaller scale shear zones.

The photomap example of Unit 1, Figure 4.17, displays a small segment of competent mafic wall rock that preserves interior Parry Sound domain structure (Fig. 4.15 d). The remainder of the outcrop is a series of highly rotated wall rock panels that are cut by centimetre- to decimetre-scale shear zones. Not only is S_1 layering transposed but so are linear features indicating homogeneous simple shear. While the wide shear zones bounding the outcrop show dextral motion, there are many examples of sinistral shear sense on smaller scale structures that postdate dextral shear zones. The wall rock layering within the photomap area shows an average E-W trend, closely resembling the shear zone orientation (Fig. 4.14 b), reflecting the lack of preserved interior Parry Sound structure within the outcrop.

The better examples of preserved wall rock layering within Unit 1 come from the western side of the island. Thickly layered metre-scale wall rock blocks show little signs of internal deformation (Fig. 4.15 a, b), and preserve granulite facies fabric, shown by stereonet in Figure 4.18, and in some cases granulite facies mineral assemblages (Marsh et al., 2011 a). However, deformed wall rock blocks and mafic dykes of chaotic orientations introduce outliers in Figure 4.18 despite the strong N-S trend.

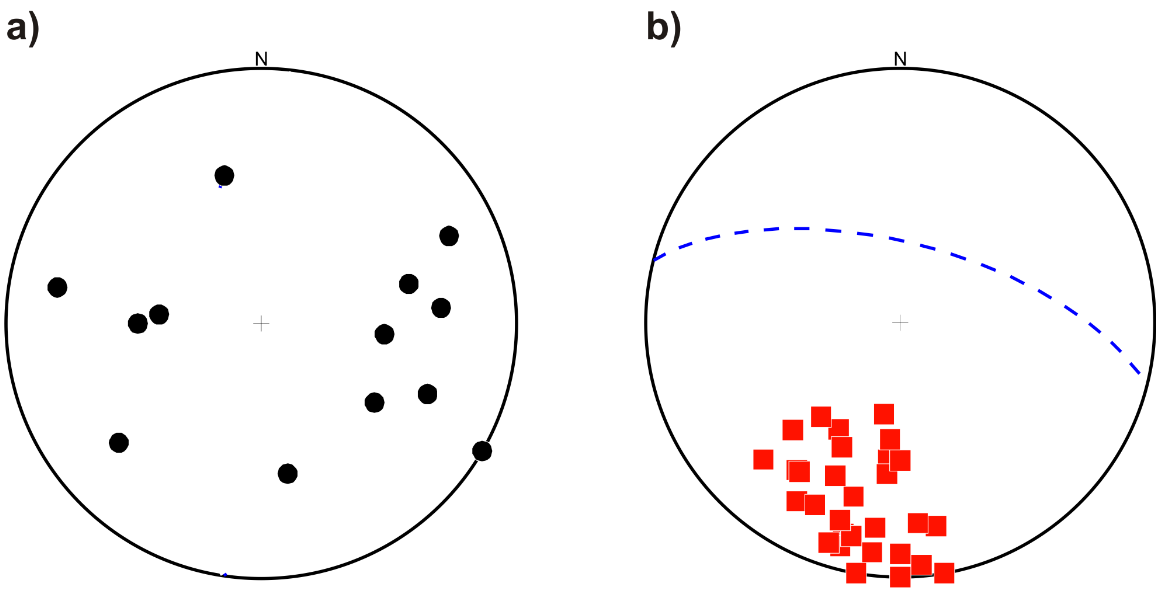

Figure 4.18: Structure of Unit 1 excluding the photomap area. Lower hemisphere equal area projections of **a)** poles to wall rock foliation and **b)** poles to shear zone foliation. Blue dashed great circle, best-fit plane to poles.

4.4.3: Shear Zones

Shear zone foliation attitudes measured across PBW Island show a homogeneous orientation, with poles to shear zone foliation show a strong cluster around a common direction (Fig. 4.14 b, S_2). The data cluster is comparable to the regional Twelve Mile Bay shear zone trend. Individual outcrops in both Unit 1 and Unit 2 show the same pattern of a strong cluster that corresponds to the regional shear plane (Figs. 4.16 b, 4.17 b).

4.4.4 Shear zone kinematics:

In areas of high strain, lozenge geometry can be useful to determine shear zone kinematics (Ponce et al., 2013). Deflections of wall rock layering within lozenges show predominately dextral movement in horizontal plane. However, lozenge geometry can be unreliable as a kinematic indicator on PBW Island as many wall rock layers are tightly folded upon entering shear zones, leaving the sense of movement enigmatic. The several shear zones that do show obvious movement record predominately apparent dextral motion but there are several examples of sinistral and an isolated example normal kinematics as well (top to the NW).

Structural data collected from shear zones of obvious kinematics are plotted that differentiate sinistral and dextral displacements (Fig. 4.19). The average shear planes (dashed blue great circles, Fig. 4.19) of each data set are approximately coplanar, and both are close to the average orientation of shear zones across the whole island (compare with S_2, Fig. 4.14 b).

In an additional attempt to determine decametre-scale kinematics, shear zone associated lineations were plotted on a stereonet (Fig. 4.19 b). The data group around a great circle that is approximately the Twelve Mile Bay shear zone plane, similar to that of the fold hinges (Fig. 4.14 b) but there is no cluster around a common direction, leading to no discernible stretching direction from lineations. This is likely due to a component of oblique or down dip movement, rather than pure strike-slip displacement.

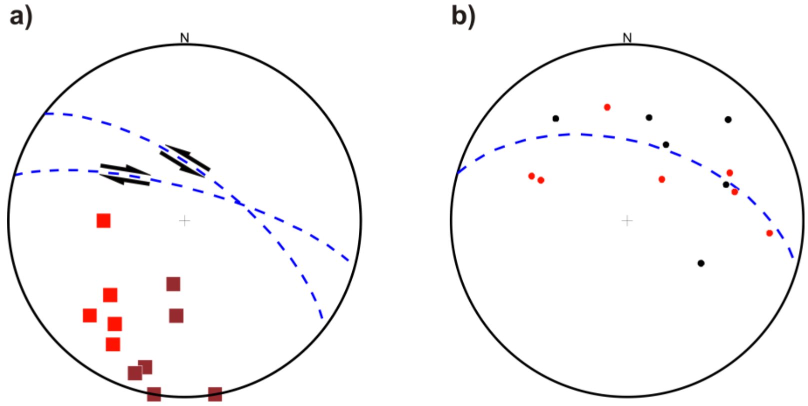

Figure 4.19: Sinistral and dextral shear zone foliations. **a)** Poles to shear zone foliation of indisputable kinematics. Red boxes, poles to sinistral shear zone foliations; maroon boxes, poles to dextral shear zone foliations; blue dashed great circles, average shear planes (kinematics indicated). **b)** PBW Island lineations (predominately intersection or ridging along shear zones). Red circle, shear zone lineation; black circle, wall rock lineation; blue dashed line, average shear plane.

4.4.5: Sinistral Shear zones

Towards the eastern side of Unit 2 there is a curved sinistral shear zone that cross-cuts Unit 3 (Figure 4.20). Gerbi et al. (2010) and Marsh et al. (2011 a) mapped the unit as a wall rock block, but the structure of the unknown unit Unit 3 more closely resembles other shear zones found on the island. The layering of Unit 3 (black symbols, Fig. 4.20) is parallel to other shear zones on the island, but is cut by a curved sinistral shear zone. On the western end, the sinistral shear zone cuts layering at a high angle before curving to conform to the regional shear plane, S_2. The shearing of the unknown unit can be explained by three possibilities: i) the unknown unit is highly rotated wall rock; ii) there is an additional straight gneiss unit that was previously unmapped; or iii) late sinistral shearing cross-cuts established shear zones.

Figure 4.20: A curved sinistral shear zone (black dashed line) cross-cuts Unit 3 (see text for possibilities). Shear zone foliation is indicated by red symbols on map and poles to the foliation are indicated by red boxes on stereonet, while unknown unit foliation is indicated by black symbols on map and black boxes poles to foliation on stereonet.

In the photomap area of Unit 1 (Fig. 4.17) there are several examples of cm-scale sinistral shear zones overprinting both wall rock layering and shear zone fabric. Figure 4.21 a features thickly layered wall rock panels that show clockwise rotation attributed to nearby dextral shearing. The rotated wall rock foliation is cut by several centimetre-scale pegmatite-cored shear zones, which show sinistral displacement. Figure 4.21 b shows a portion of a ~4 m wide, strongly developed transposed planar fabric as a result of dextral shearing. The transposed fabric is cut at a low angle by cm-scale pegmatite-cored sinistral shear zones. The sinistral shear zones in both Figure 4.21 a and b are parallel, striking WNW, at a low angle to dextral shear zone fabric, consistent with observations shown in Figure 4.19 a.

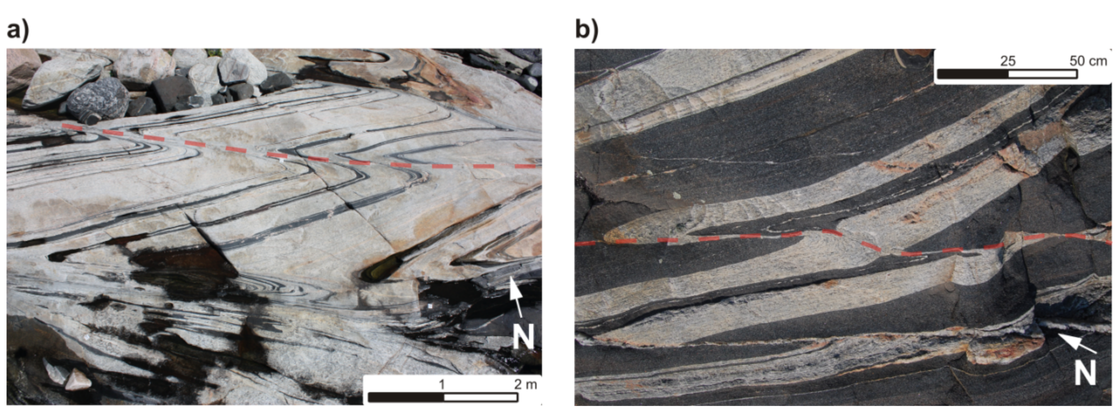

Figure 4.21: Field photos of late sinistral shear zones (dashed red lines) in Unit 1 overprinting wall rock rotated by dextral shearing. See Fig. 4.17 for photo locations.

4.4.6: Anastomosing shear zones

The photomap area of Unit 1 (Fig. 4.17) is representative of how shear zones merge within Unit 2. The large wall rock tapers to the northeast and to the southwest forming a lozenge. As the wall rock tapers the sub-parallel bounding shear zones converge and form a single, wide shear zone (Fig. 4.17). In addition to the established shear zones, there are several centimetre-scale width shear zones that develop within the lozenge towards the tapered ends, further segmenting the lozenge. The smaller sub-parallel shear zones branch off from the wall rock-bounding shears and form sub-parallel to the master shear zone orientation. The sub-shear zones may link back to the master shear zone at the tapered end of the wall rock forming an isolated sub-lozenge, or may terminate before reaching the tapered end.

The majority of shear zone merging in Unit 1 is concentrated on the western end of PBW Island. The area consists of the metre-scale wall rock panels that are bounded by thick (0.5-5 m) composite shear zones. Typically shear zones link in a similar fashion to those in Unit 2, with shear zones converging at the tapered margins of wall rock lozenges. However, there are some subtle differences in the style by which shear zones link together. There are few examples of sub-parallel shear zones, likely due to the scale of the layering within wall rock blocks. The shear zones form an anastomosing pattern around isolated wall rock lozenges (Fig. 4.16)

4.4.7: Folds

Fold hinge orientation data collected within the photomap for folded shear zone foliations (red triangles) and folded wall rock foliations (black triangles) are displayed in Figure 4.14 b (L). Both shear zone and wall rock fold hinges cluster around a common direction, 080-30, which is congruent with the regional axis of the Twelve Mile Bay shear zone. In the Unit 2 photomap (Fig. 4.14), interior Parry Sound domain layering is folded into open to close folds with centimetre-scale amplitudes. The axial trace is approximately parallel to the strike of the shear zone foliation and perpendicular to the regional shortening direction. Folds commonly develop in the centimetre-scale felsic layering within a particularly mafic-rich sub-lozenge (Fig. 4.22 a).

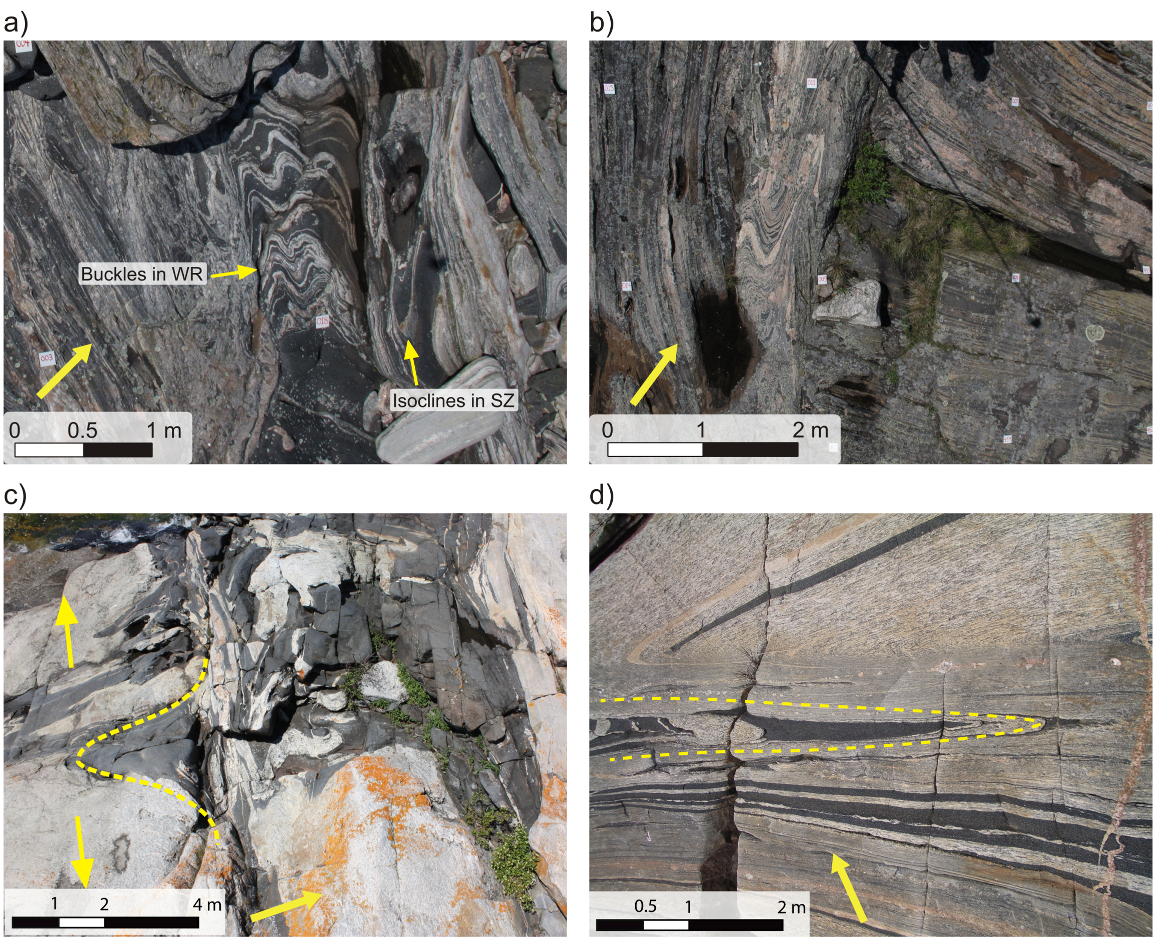

Figure 4.22: Field photos of folds in different stages of development. See Fig. 4.14 for photo locations. **a)** Open to close folds within a wall rock panel within Unit 2 that are adjacent to isoclinal folds in a neighboring shear zone. **b)** The tightening of a folded wall rock foliation as the wall rock lozenge is incorporated into the shear zone. **c)** A boudinage structure develops within a shear zone during extension perpendicular to wall rock layering. Arrows indicate extensional direction. **d)** Isoclinal fold of a nearly completely transposed wall rock block (yellow-dashed line) within a wide shear zone with the axial plane approaching parallelism with the shear zone.

4.4.8: *Summary*

Layer thickness has a profound effect on how the rock behaves mechanically and is thought to dictate the thickness and spacing of shear zones, analogous to how layer thickness dictates fracture spacing (Bai and Pollard, 2000). The contrasting scales of layer thickness between Unit 1 and Unit 2 result in two contrasting structural styles. Unit 1 feature widely spaced shear zones and a notable lack of folds within wall rocks, while Unit 2 features closely spaced shear zones and folded wall rock foliation. The presence or absence of buckle folds in wall rock blocks depends on the maximum wall rock layer thickness. Buckle folds are more likely to be observed within the thinly layered wall rock packages of Unit 2 as thinner layer thicknesses will produce buckle folds with wavelengths smaller than the width of the block.

4.5: Bartram's Island

Bartram's Island (Fig. 4.23) lies to the south of the Zone of Reworking within the Twelve Mile Bay shear zone (see Fig. 4.1 for island location). While the outcrops chosen to study on Bartram's Island reflect the minority of the fabric on the island, the majority of which is now predominantly Twelve Mile Bay shear zone fabric (S_2), the selected outcrops provide examples of wall rock collapse and transposition of granulite facies layering (S_1) into amphibolite facies shear foliation (S_2). The structure of Bartram's Island has been broken down into two outcrops featuring examples of low strain lozenges that are approximately 10 metres from one another. Orthorectified photomosaics were created for the two target outcrops. The structure of both outcrops was inspected in detail; however, the remaining structure of the island was not investigated due to lack of exposure of preserved wall rock.

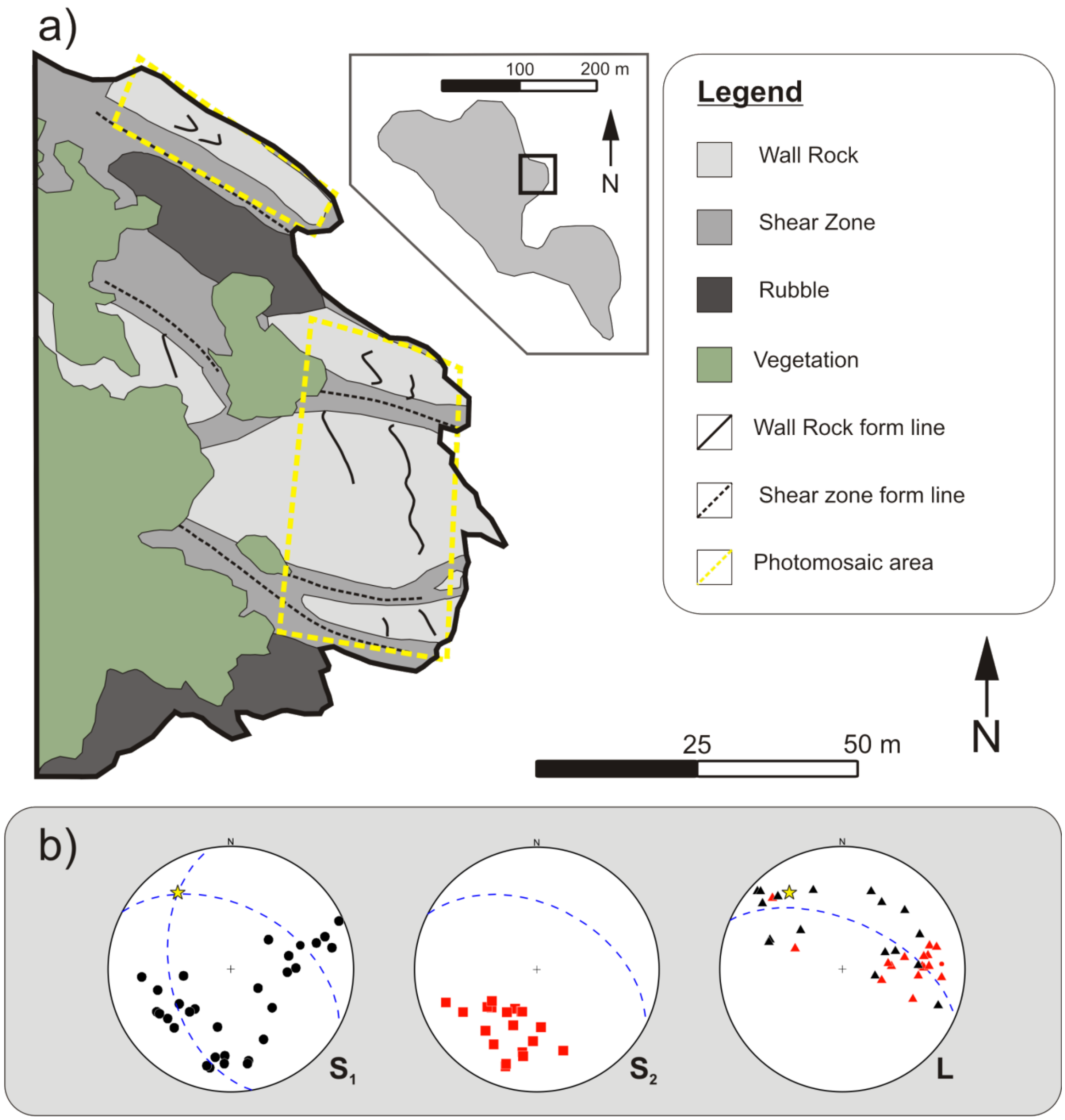

Figure 4.23: a) Schematic structural map of Bartram's Island outcrop. **b)** Lower hemisphere equal area projections for poles to wall rock foliation (S_1), poles to shear zone foliation (S_2), and fold hinges and lineations (L). Inset on map shows the location of the study site on Bartram's Island. Black symbol indicates wall rock structure, and red symbol indicates shear zone structure. Yellow star, inferred fold axis of wall rock foliation from S_1 net; Triangle, fold hinge; blue dashed great circle, average plane.

4.5.1: Macro-scale structure

The lithology of Bartram's Island is an amphibolite facies layered gneiss, with alternating felsic and mafic layers, and containing a similar mineral assemblage to other studied islands, with the notable lack of granulite facies relics within wall rock blocks. Outcrop A (Figure 4.24), is made up of several wall rock panels in varying states of transposition, bounded by amphibolite facies shear zones. Outcrop B (Fig 4.25) features a strongly folded wall rock panel that is bounded by two shear zones. Outcrop A contains excellent examples of drag folds, shear zone merges, and contrasting layer thickness.

4.5.2: Wall rock foliation

There is a significant variability of wall rock foliation orientations due to the development of folds. Poles to wall rock layering show a bimodal distribution pattern with best-fit great circles constructed for each limb, the intersection of which is an interpreted fold axis (S_1, Fig. 4.23 b). One population represents a limb with an average orientation close to initial granulite facies foliation, although the foliation has undergone anticlockwise rotation from its initial orientation. The other population represents a limb that has been affected by shearing, as the sheared limb cluster closely resembles the poles to shear zone foliation cluster (S_2, Fig. 4.23 b).

a)

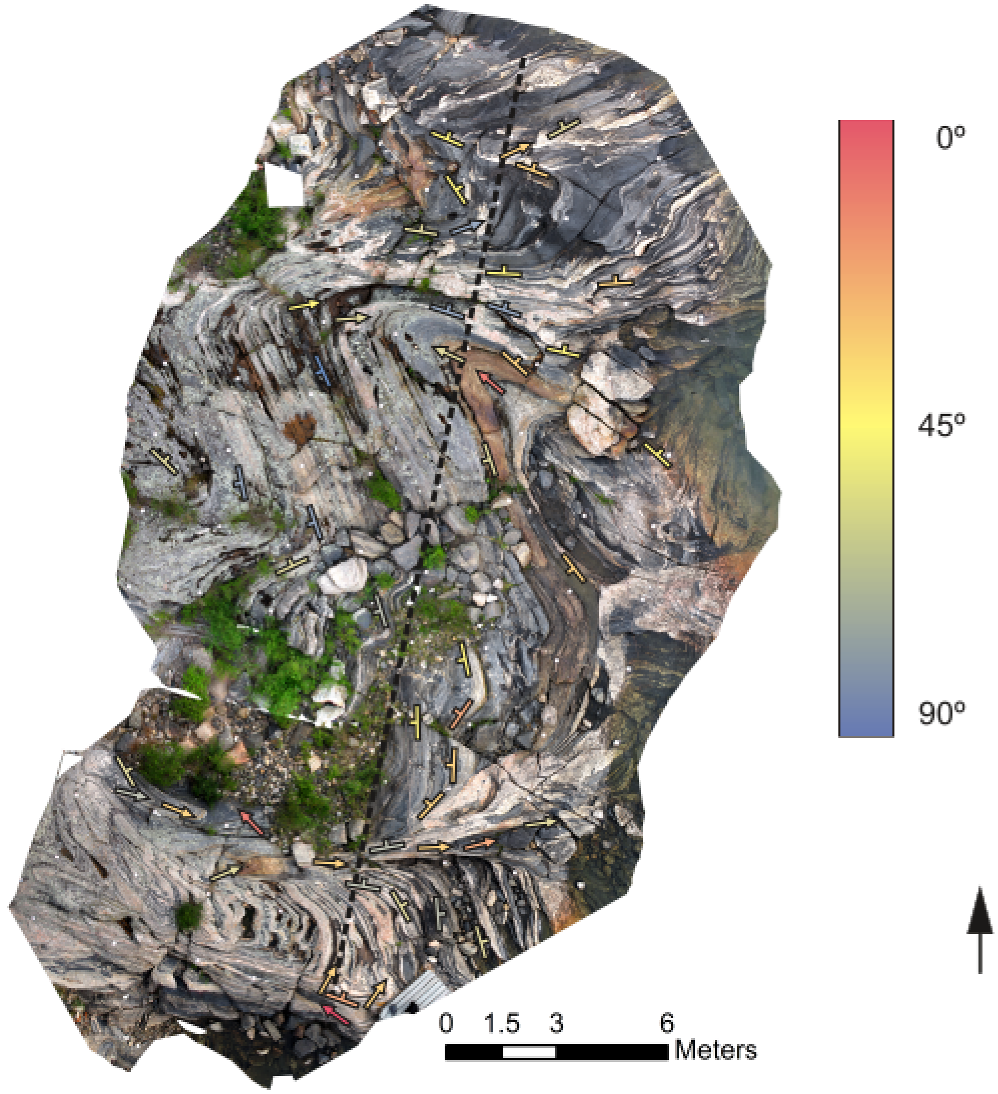

b)

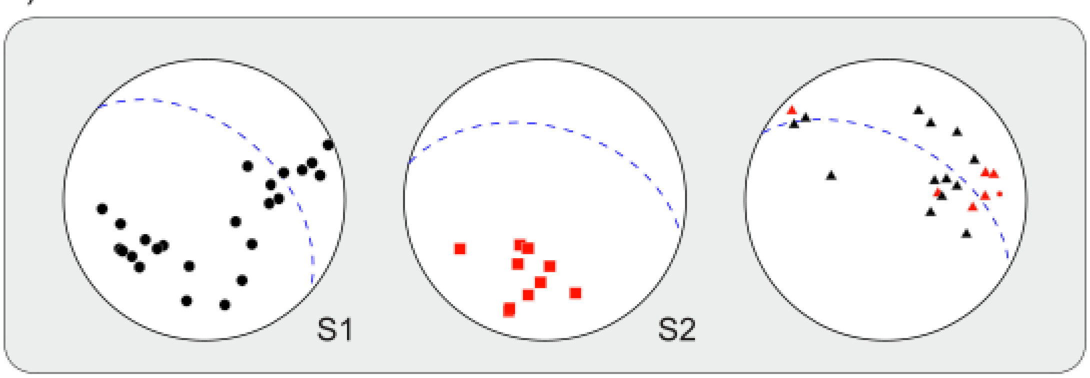

Figure 4.24: Structural overview of Outcrop A of Bartram's Island. **a)** Photomosaic map of Outcrop A with structure. Structural symbols are colored based on dip. See Fig. 4.26 for location. **b)** Lower hemisphere equal area projections for poles to wall rock foliation (S_1), poles to shear zone foliation (S_2), and fold hinges and lineations (L). Red triangle, shear zone fold hinge; black triangle, wall rock fold hinge; blue dashed great circle, best fit plane.

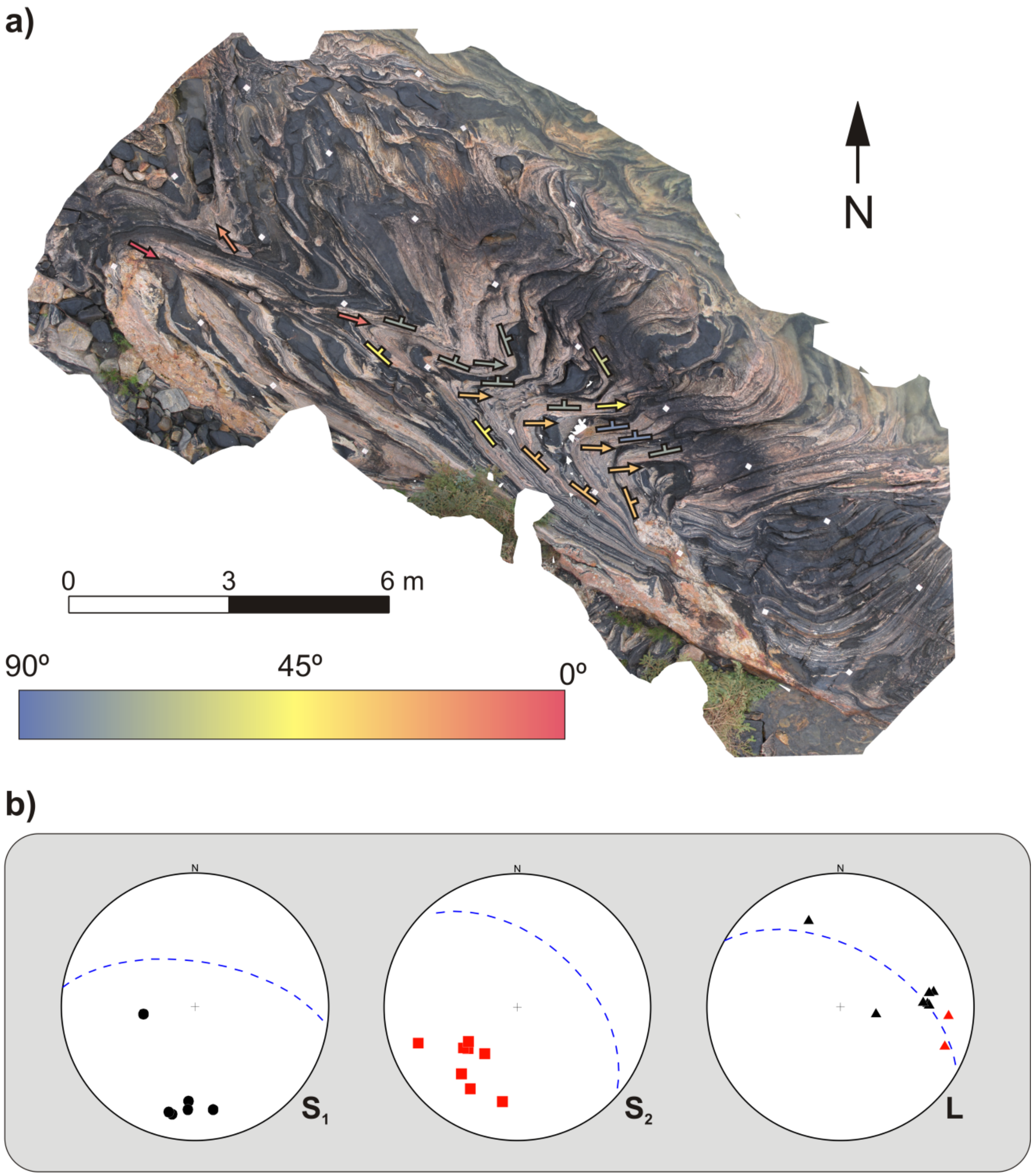

Figure 4.25: Structural overview of Outcrop B of Bartram's Island. **a)** Photomosaic map of Outcrop B with structure overlain. Dip degrees given by color ramp. See Figure 4.26 for location. **b)** Lower hemisphere equal area projections for poles to wall rock foliation (S_1), poles to shear zone foliation (S_2), and fold hinges and lineations (L). Red triangle, shear zone fold hinge; black triangle, wall rock fold hinge; blue dashed great circle, best fit plane.

There is significantly less wall rock by area exposed on Bartram's Island than observed on previous islands. Outcrop A is an outlier in that it contains one large well preserved wall rock block, flanked by two smaller wall rock blocks that are not as well preserved (Fig. 4.24). The wall rock blocks are folded and are lozenge-shaped rather than appearing as blocky as seen on Matches and PBW islands, which indicates a further stage in wall rock deformation and transposition.

A cross-section of Outcrop A (Fig. 4.26) is perpendicular to shear zone foliation, and sub-parallel the strike of wall rock foliation. The shear zones dip beneath wall rock panels and may merge at depth to form a three-dimensional network of interconnected shear zones, a typical pattern of anastomosing shear zones (Mancktelow and Pennacchioni, 2005; Fusseis et al., 2006; Carreras et al., 2010) The section line parallel to shear zone layering runs obliquely to the large fold in outcrop A (Fig. 4.24).

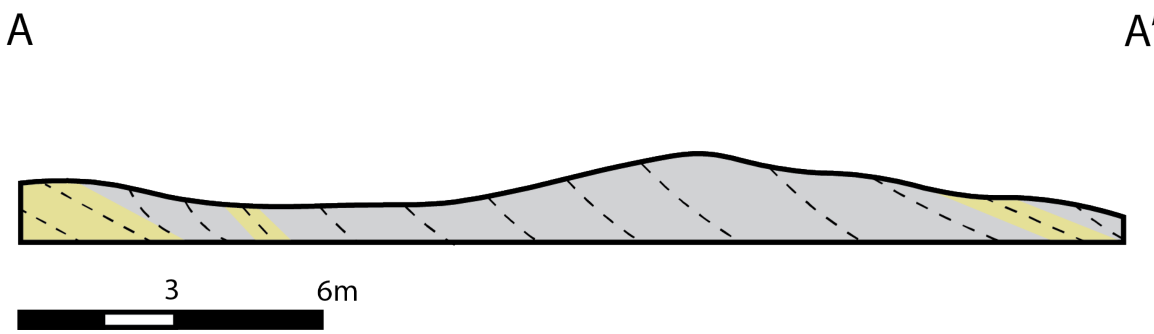

Figure 4.26: Cross-sections of outcrop A, perpendicular to the strike of shear zone folation and the fold hinges. Yellow, shear zone; light grey, wall rock; dashed line, apparent dip of folation to the section line. See Figure 4.24 for cross-section line.

4.5.3: Shear zones

Strongly localized amphibolite facies dextral shear zones overprint the variably retrogressed wall rock panels at a high angle, similar to the geometry observed on other islands. The shear zones range from 2-6 m in width, and commonly contain isoclinal folds in their cores. Figure 4.26 b displays shear zone foliation data (S_2) that loosely clusters around a common point, resulting in average shear zone orientation on Bartram's Island to be 300/40°, similar to the average orientation of the Twelve Mile Shear zone fabric.

The kinematics of shear zones on Bartram's Island are predominantly dextral, with two examples of sinistral shear zones. The first sinistral shear zone is the pegmatite cored shear zone in outcrop B (Fig. 4.25 a), whereas the second one appears in outcrop A. The sinistral shear zones are roughly coplanar with their dextral counterparts. Figure 4.27 shows the shear zone within outcrop A that displays dextral motion to the north and sinistral motion to the south. At the core of the shear zone there is a series of isoclinal folds that decrease in interlimb angle to the west, culminating in the remnants of a poorly preserved wall rock block. The presence of this predominately assimilated wall rock block shows that this type of shear zone with ambiguous kinematics can arise because of the merging of a multiple shear zones.

Shear zones on Bartram's Island display linking behavior in addition to the sinistral-dextral merge discussed earlier. There are far fewer examples than on previous islands, likely due to the relative low abundance of wall rock panels on Bartram's Island. Within outcrop A, a prominent wall rock panel tapers and folds, allowing the two bounding shear zones to merge into a single shear zone (Fig. 4.27)

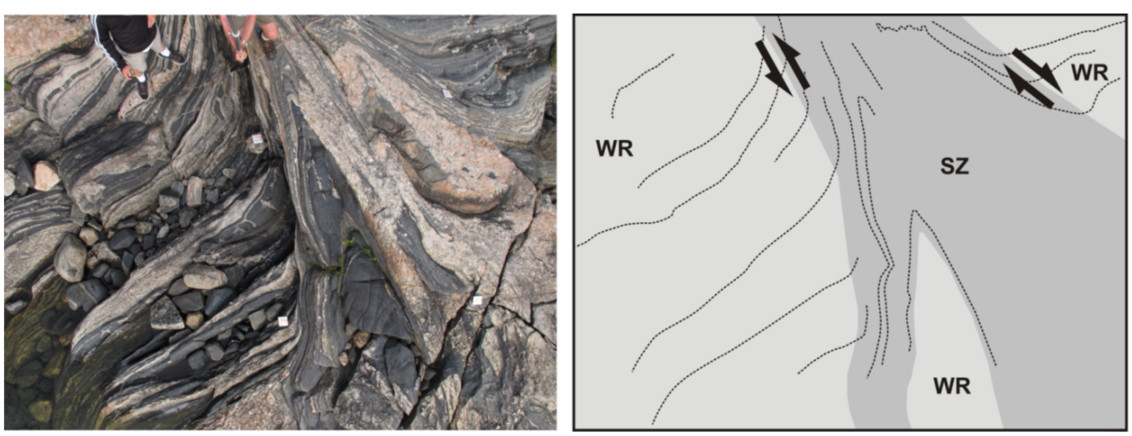

Figure 4.27: Pole camera photo **(a)** and schematic line drawing **(b)** of a shear zone with opposing kinematics within outcrop A. The southern side of the shear zone is sinistral, while the northern side is dextral. A highly deformed mafic wall rock block is situated at the core of the shear zone is folded into an isoclinal fold.

4.5.4: Folds

Bartram's Island features folds with a wide variety of fold geometries and orientations. The fold hinges, while variable, do form a loose girdle that is similar in orientation to the Twelve Mile Bay shear zone plane (Fig 4.23, b). Low amplitude, gentle to open folds of metre-scale wavelength are observed within wall rock blocks of Outcrop A. The wall rock in Outcrop B is strongly deformed, resulting in low amplitude open folds that generally show a 'z-type' asymmetry (Fig. 4.25). High amplitude, tight to isoclinal folds are found on the margins and within the cores of shear zones in Outcrop A and B (Fig. 4.24; Fig. 4.25)

4.6: PBE Island

PBE Island is located to the south of the Transposition Boundary and along strike from PBW and Bartram's islands and, of the three islands, it lies closest to the high strain core of the Twelve Mile Bay shear zone (Fig. 4.1 for location). PBE Island represents the latter stages of transposition with the dominant fabric being amphibolite facies straight gneiss formed by the coalescence of centimetre-scale shear zones into decametre-scale shear zones. The amphibolite facies lithology that makes up PBE Island is formed from shearing of Parry Sound domain derived material, as evidenced by several relict low strain pods within the shear zone preserving Parry Sound domain structures.

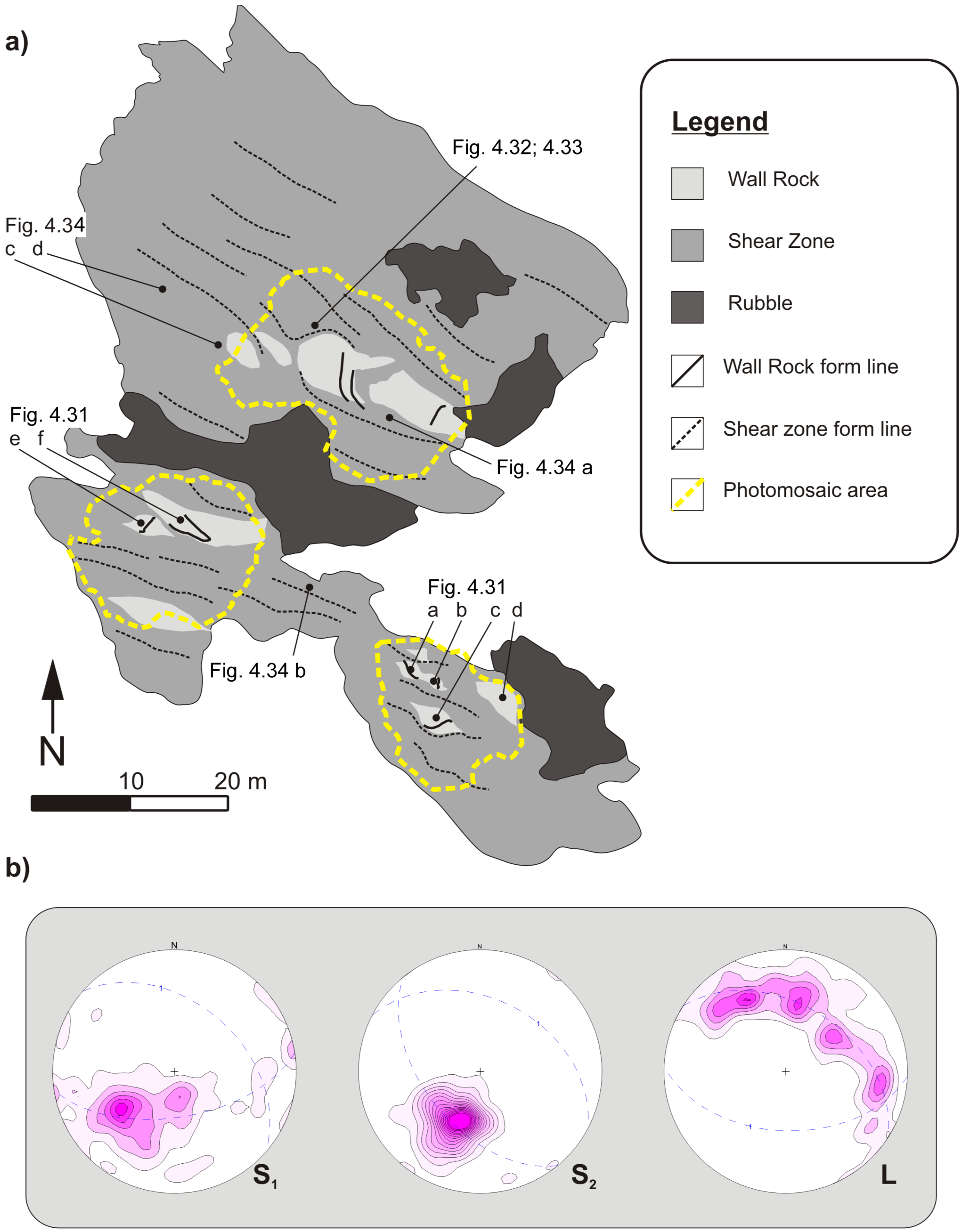

Figure 4.28: a) Schematic structural map of PBE Island. Light grey, relict interior Parry Sound domain lozenges; grey, shear zone; dark grey, obscured by rubble; solid black line, wall rock form line; dashed black line, shear zone form line; dashed yellow line, photomap area. **b)** Lower hemisphere equal area projections showing poles to wall rock foliation (S_1), poles to shear zone foliation (S_2), lineations (L), and best-fit great circles (blue dashed lines).

4.6.1: Macro-scale structure

PBE Island is made up of a similar multilayer package to Unit 1 of Matches Island, Unit 1 on PBW Island, and the study area of Bartram's Island. The package consists of an orthogneiss in the southwest with compositional layering alternating from mafic to tonalitic. The northwest side of the island consists of layered granulites of mixed origins, including some garnetiferous metasedimentary layers. The thickness of the layering is centimetre-to-decimetre scale, with no prominent outliers or subunits. The rocks on the island have been thoroughly retrogressed from granulite to amphibolite facies, with a notable lack of granulite facies mineral assemblages even within low-strain pods.

PBE Island is characterized by nearly homogeneous northeast-dipping amphibolite facies straight gneiss, typical of the regional-scale Twelve Mile Bay shear zone (Fig. 4.28 b). The near homogenous fabric contains several low-strain lozenges of interior Parry Sound domain fabric of a variety of scales and orientations. The presence of low-strain pods within the near homogenous straight gneiss provides a clear genetic link between the Twelve Mile Bay shear zone and the interior Parry Sound domain material.

Structure preserved in the low-strain pods is highly variable (Fig. 4.28 b, S_1), with a weak cluster of poles to wall rock layering around the regional shear trend, illustrating the pervasive influence of the Twelve Mile Bay shear zone. Decametre-scale shear zone orientations (Fig. 4.28 b, S_2) closely resemble the foliation of the Twelve Mile Bay shear zone, indicating the homogeneity of shear zone fabric at this location. Lineations and fold hinges strongly spread along a great circle, indicating that linear features are formed or rotated into the shear plane that is approximately the Twelve Mile Bay shear zone.

4.6.2: Wall rock foliation

The best examples of preserved wall rock lozenges are found within the central PBE Island (Fig. 4.28 a), and shown in detail as a photomap in Figure 4.29. The central island region features two wall rock panels bounded by strongly developed and penetrative shear zones. The western wall rock panel shows the most resistance to deformation and rotation of all lozenges on the island, retaining the north striking, steeply dipping compositional layering typical of the interior Parry Sound domain. The eastern wall rock panel is separated from the western wall rock panel by a shallowly-dipping shear zone, which shows significant rotation from the interior Parry Sound domain orientation with very shallow dips in contrast with the vertical layering typical of the interior Parry Sound domain.

a)

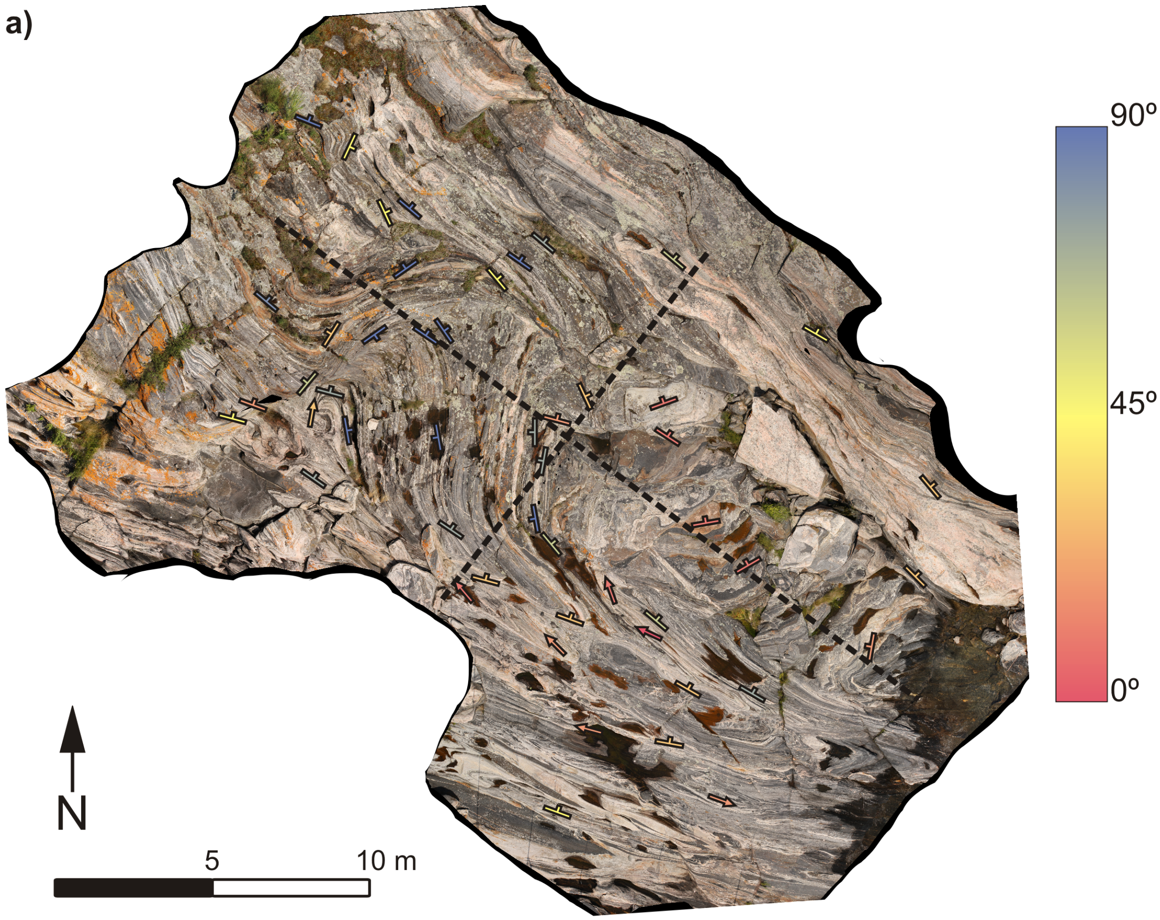

b)

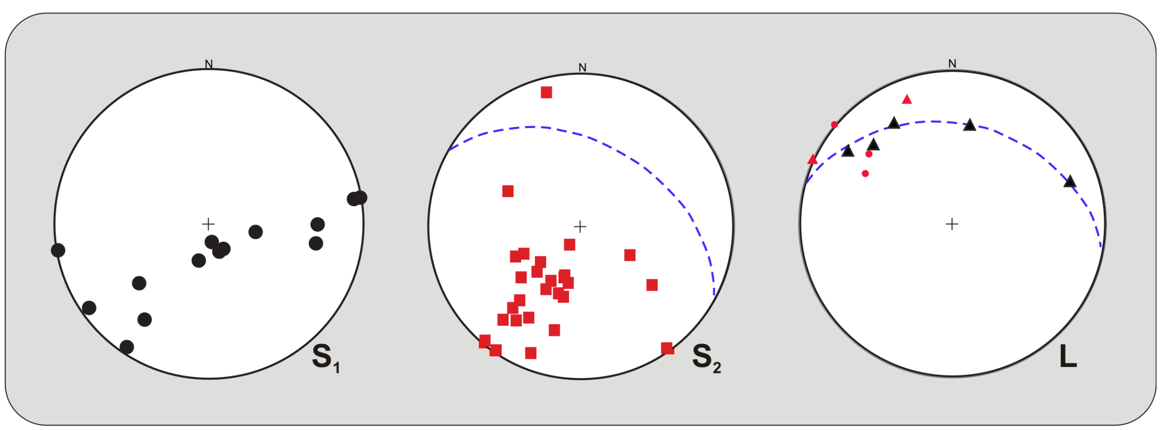

Figure 4.29: a) Orthorectified photomap of the central area of PBE Island with structure indicated. Structure is color coded based on dip. Strike and dip symbol indicates foliation and arrow indicates fold hinge. Dashed lines are the cross-section lines (see Fig. 4.33). **b)** Lower hemisphere equal area projections showing poles to wall rock foliation (S_1), poles to shear zone foliation (S_2), and lineations (L). Red triangle, shear zone fold hinge; black triangle, wall rock fold hinge; blue dashed great circle, best fit plane.

Preserved interior Parry Sound domain wall rock layering on the southern and eastern ends of PBE Island is virtually non-existent (Fig. 4.30). There are few examples of original granulite fabric preserved in small mafic pods that are volumetrically insignificant within the now 10's of metre wide shear zone. The wall rock layering is very uniform, approaching the regional shear plane (Fig. 4.30 c).

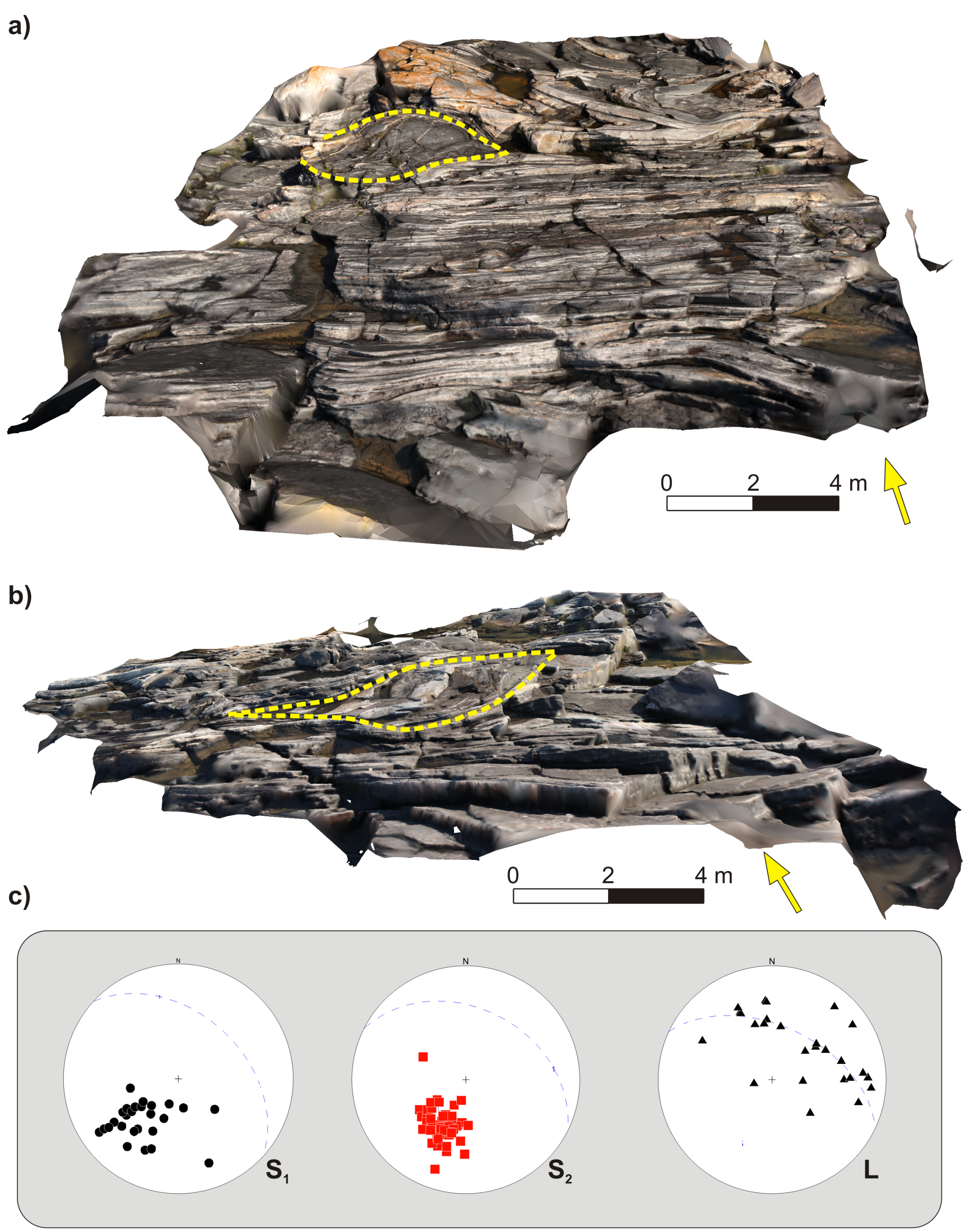

Figure 4.30: a) Down-dip photomaps of **a)** the southern end of PBE Island and **b)** islet along strike from a. Yellow dashed line indicates wall rock panels. **c)** Lower hemisphere equal area projections showing poles to wall rock foliation (S_1), poles to shear zone foliation (S_2), and lineations (L). Blue dashed great circle, best fit plane

Low-strain pods that preserved iPSD fabric found on the southern margin of PBE Island were studied in detail to determine the orientation of wall rock. The low strain pods form sigmoidal lozenges of competent mafic material that has resisted deformation to varying degree (Fig. 4.30). The orientation of wall rock layering within the lozenges varies significantly, which is not surprising given the widespread deformation and rotation is occurring all around them (Fig. 4.30 c, S_1; Fig. 4.31 g). However, the variably deformed interior Parry Sound domain structure preserved within the low-strain lozenges spreads along a great circle indicating rotation around a lineation oriented ~060-30 (Fig. 4.31 g).

The rotation of wall rock layering around a common pole is observed in the structure collected within the photomap area of the central island (Fig. 4.29 b) and individual wall rock lozenges along the southern end of the island (Fig. 4.31 g). However, the rotational pole of the central island differs from the rotational pole of the southern island. There are several possible explanations to explain this discrepancy but the two most likely are; i) the central island contains a greater amount of less deformed wall rock blocks, and the rotational axis has not yet been rotated into the preferred orientation (similar to PBW and Bartram's Island); ii) the central island stereonet reflects a fold interference pattern.

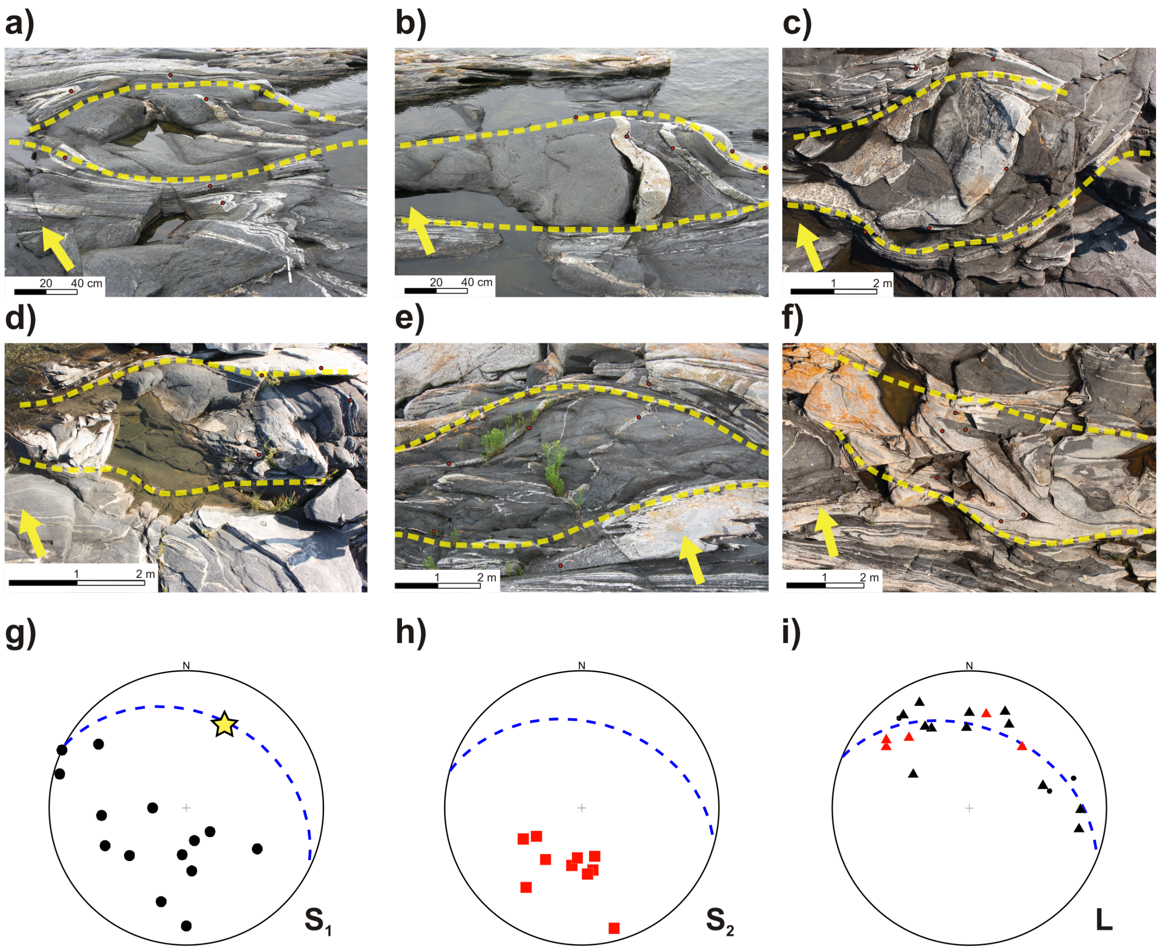

Figure 4.31: a-f) Wall rock lozenges within straight gneiss of the southern end of PBE Island. See Figure 4.1 for individual lozenge locations. **g)** Lower hemisphere equal area projections showing poles to wall rock foliation within wall rock lozenges (S_1) with inferred rotational axis (star), **h)** poles to shear zone foliation (S_2), and **i)** lineations (L). Red triangle, shear zone fold hinge; black triangle, wall rock fold hinge; blue dashed great circle, best fit plane.

4.6.3: Shear zones

The southern end of PBE Island and the islet to the east is made up of almost entirely Twelve Mile Bay shear zone fabric (Fig. 4.28 a). Due to the moderate dip of the Twelve Mile Bay shear zone fabric, the orthorectified photo-maps display skewed geometries. To remedy this, down-dip photo-maps were constructed (see Methodology chapter), which yield accurate geometrical representation.

In the photomap area of the central island (Fig. 4.29 a) the north-dipping amphibolite facies shear zone shows areas of distinct variability that could be attributed to flowing around competent the large wall rock panels. Despite this local variability, shear zone foliations form a strong cluster, representing the regional shear plane (Fig. 4.29 b).

In the northwest of the central island photomap, steeply dipping shear zone foliation abruptly swings ~90° around a large wall rock block (Fig. 4.32). A small segment of shear zone locally deflects around a large wall rock block and merges back with the main shear zone foliation. The deflected shear zone cross-cuts gneissic shear zone foliation parallel to the main shear zone trend.

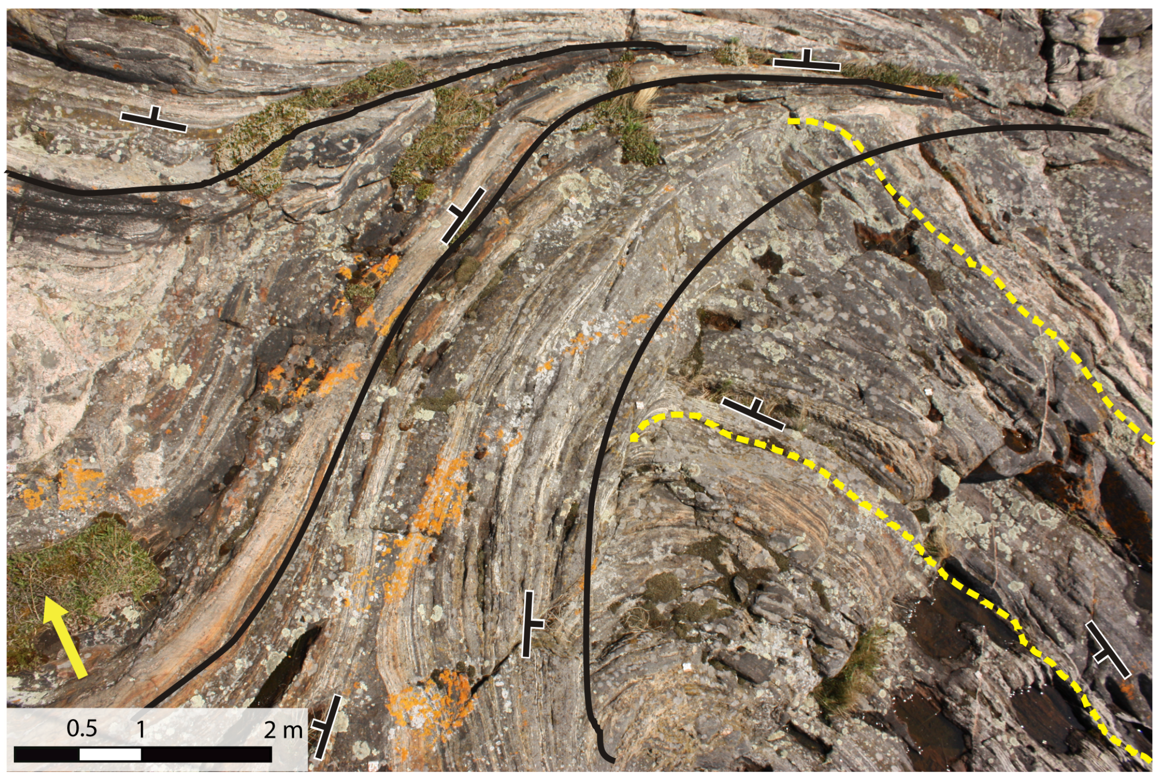

Figure 4.32: A close up of a shear zone deflecting around a wall rock panel from the central outcrop of Fig. 4.29. The deflected shear zone truncates older foliation. Black line; shear zone foliation trace; yellow dashed line, wall rock foliation trace.

A cliff section within the central island area combined with the map view provides a rare three-dimensional view of the interaction between shear zone and wall rock. Figure 4.33 is a down-plunge view of the cliff outcrop, where the shear zone foliation (on the high ground and cliff) transitions into wall rock panel (low ground). The cliff section reveals the complex overprinting pattern relating to folding in three dimensions, showcasing the variability in shear zone layering orientation on the margin of the wall rock panel. On the cliff face itself, the characteristic Twelve Mile Bay shear zone fabric can be seen dipping moderately to the north and beneath the wall rock panel. To the west there is a wedge shaped block of folded wall rock that strikes parallel to the regional shear zone foliation, but is much steeper than what would be expected for a shear zone (red dashed line, Fig. 4.33). To east of the wedge, the deflected shear zone segment deviates significantly from the regional shear zone orientation, dipping moderately to the northwest overlying the wall rock panel. The cross-section reveals a complex flow pattern of ductile material around the competent wall rock panel, resulting in the shear zone foliation locally deflecting to envelope the wall rock panel.

The southern end of PBE Island and the islet to the east is dominated by north-dipping shear zone foliation (Fig. 4.30). These two outcrops are along strike from one another and are deemed to be of the same lithology and structure. Both outcrops show nearly homogenous straight gneiss with volumetrically insignificant pods of highly rotated and folded wall rock panels (yellow dashed lines, Fig. 4.31). Structural data collected within the region confirm the structural homogeneity of the fabric with a strong cluster of poles consistent with a shear zone foliation orientation of ~320/40, the approximate orientation to the regional trend of the Twelve Mile Bay shear zone.

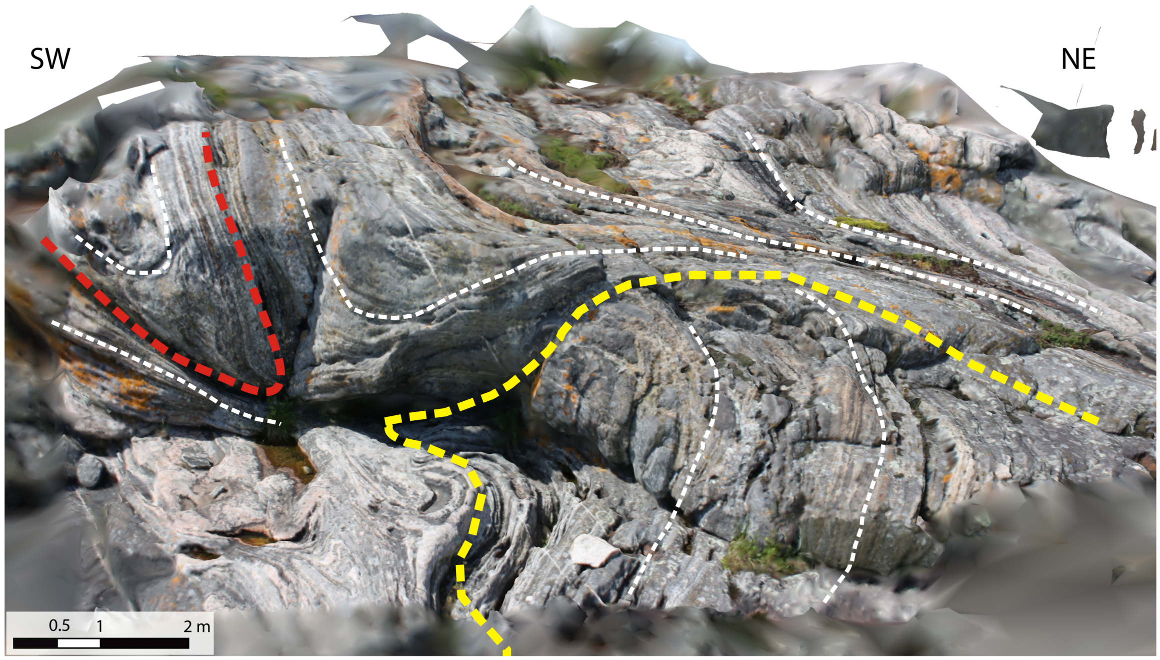

Figure 4.33: Down-plunge view of the cliff section within the central island outcrop, see Fig. 4.28 for location and scale. Folded wedge, red dashed line; wall rock panel, yellow dashed line; fabric form lines, white dashed lines. Shear zone fabric to the south of the folded wedge underlies the wall rock panel.

4.6.4: Folds

Folds within both shear zone and wall rock foliation are common throughout the island, with fold hinges oriented within the regional shear plane (Fig. 4.28 b, L). Folds in wall rock lozenges have typically moderate-to-shallow northwest plunging hinges. The folds found in wall rock lozenge commonly low-amplitude open folds that are likely buckles folds and reoriented in response to shearing. Folds found within shear zones are similar in hinge orientation, with hinges commonly plunging shallowly to the northeast. The shear zone folds, however, exhibit tight to isoclinal fold geometry that reflect the tightening of wall rock folds. The development of folds within shear zone largely depends on the pre-existing fold orientation and asymmetry, with examples of tightening of pre-existing folds during deformation (Fig. 4.34 a).

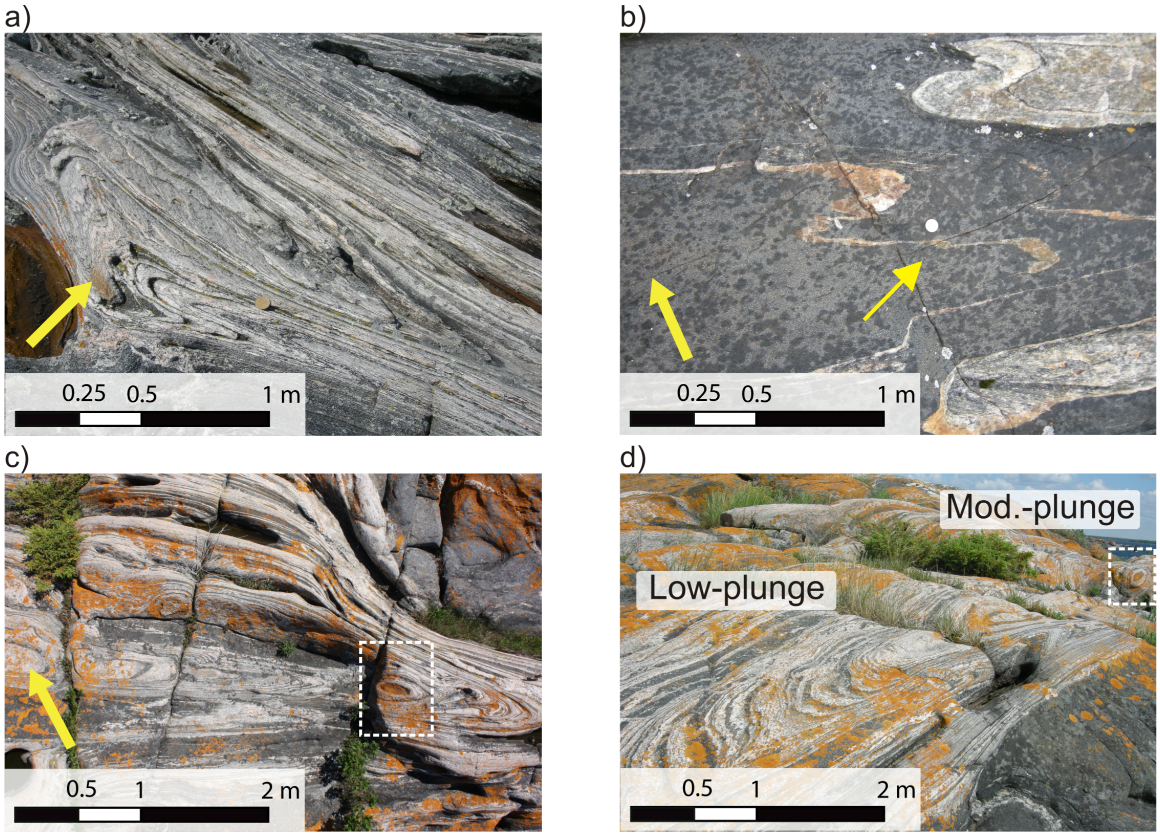

Figure 4.34: Field photos of folds within shear zones on PBE Island. See Figure 4.28 for photo locations. **a)** A shallowly-plunging isoclinal fold forms a ridge-like intersection lineation, coin for scale. **b)** The thinning of pre-existing fold limb during tightening within a shear zone (yellow arrow), coin for scale. **c)** The transition from a steeply plunging-hinge, to **d)** a low-plunging hinge, is a doubly plunging fold. White dashed box in b and c indicate reference point.

4.7: Twelve Mile Bay shear zone

There was no detailed study on the core of the Twelve Mile Bay shear zone conducted as the on the segment of the shear zone that abuts the Parry Sound domain, as the structure is relatively simple. Homogenous strain results in a strongly foliated north dipping amphibolite facies fabric (Fig. 4.1). A cliff section along the northern shore of Twelve Mile Bay reveals an anorthosite layer that possesses a similar geometry to that found on Matches Island (Fig. 4.38). Dextral-sense fractures are truncated by a large sinistral sense shear zone. The orientation of the anorthosite layering is rotated anticlockwise in a similar fashion to what was observed on Matches Island.

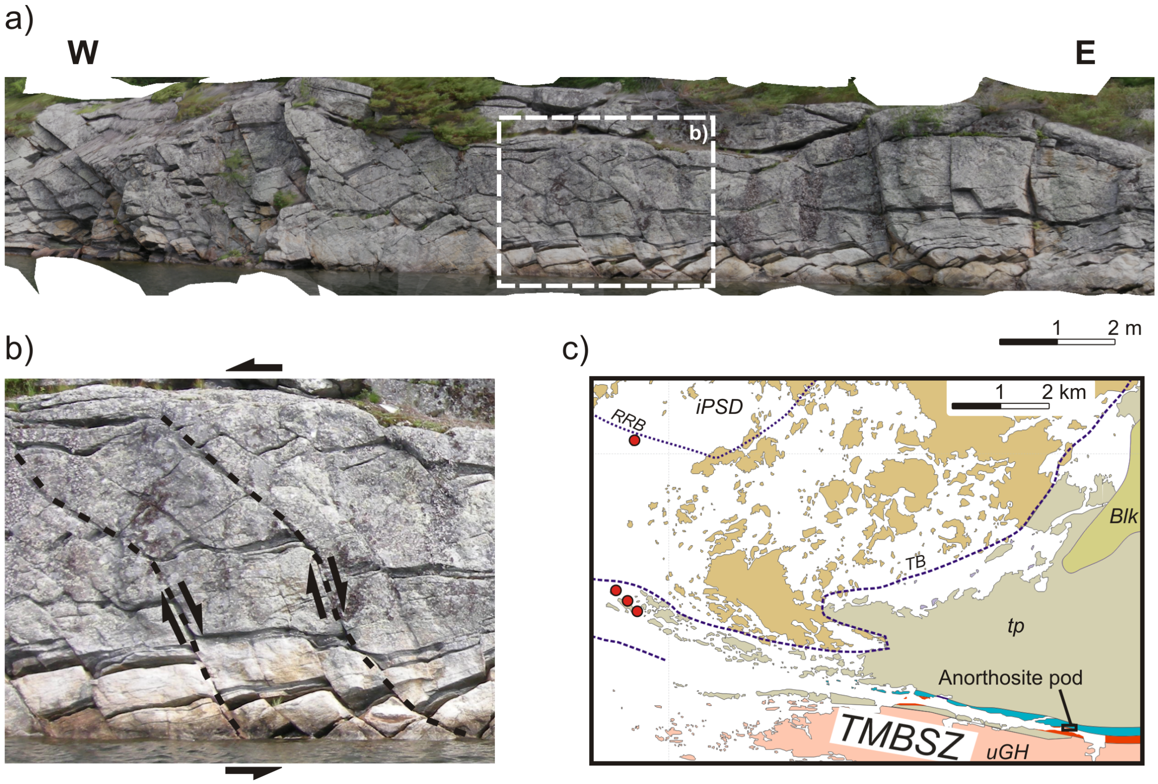

Figure 4.35: Fault/shear zone geometry of anorthosite blocks within the Twelve Mile Bay shear zone**. a)** Photomosaic of anorthosite pod cliff section along Twelve Mile Bay shear zone. **b)** Detail of a), featuring a similar shear zone geometry as observed on Matches Island. Dashed lines are faults/shear zones with top-to-the-east movement. **c)** Location of anorthosite pod (black box) with other study areas indicated (red dots).

CHAPTER 5: QUANTITATIVE ANALYSIS

5.1: Simple shear strain analysis

Matches, PBW, and Bartram's islands were assessed for shear strain within the Zone of Reworking (Fig. 4.1) in an effort to characterize deformation within shear zones and to test efficacy of the mapping method by comparing strain results of different methods. The results of the strain analysis were used to compare differences in strain values along individual shear zones, to distinguish distinct strain domains, and to compare strain values across islands for both individual shear zone segments and bulk strain. Strain ellipses were produced and used to create strain maps that provide insight on variations in strain patterns at both individual shear zone and island scale, and the local kinematics.

The most comprehensive strain analysis was conducted on Matches Island because of the high quality and extent of shear zone exposure that allowed use of both the displacement width method and the angle method. These two methods of shear strain analysis (Ramsay and Graham, 1970; Fusseis et al., 2006; Sassier et al., 2009) were used to calculate values for shear strain along a shear zone segment. Both methods were used for as many shear zones segments as possible so that direct comparisons could be made between results.. Shear strain values for both metre-scale dextral shear zones and island-scale sinistral shear zones were calculated using these methods. The other islands considered suitable for strain analysis were PBW Island and Bartram's Island.

In the following section on shear strain analysis, several terms will be initially clarified. The term "average shear strain" (γ_{avg}) refers to the total shear strain calculated across a shear zone, and will be used most frequently. "Maximum shear strain" (γ_{max}) is reserved for the shear strain at a point within the shear zone and is used exclusively with the angle method (Ramsay and Graham, 1970; Fusseis et al., 2006). The term bulk shear strain (γ_{bulk}) is simply the average shear strain (γ_{avg}) calculated across multiple parallel shear zones and combined to create a value of shear strain that is representative of the area traversed by the shear zones (Culshaw et al., 2011).

5.1.1: Simple shear strain calculations

Shear strain within a shear zone can be determined by a number of methods. In this study, two different methods were explored to calculate shear strain on individual shear zone segments; the angle method (Ramsay and Graham, 1970; Ramsay and Huber, 1987; Fusseis et al., 2006; Sassier et al., 2009) and the displacement method (Ramsay and Huber, 1987) (Fig. 5.1). Both methods work under the assumption of plane strain and constant volume simple shear and were used in tandem on Matches Island allowing for the results of the methods to be directly compared. The lack of wall rock deformation on Matches Island indicates a near simple shear system, and therefore these methods are appropriate. In the cases of PBW and Bartram's Island, there is very likely a pure shear component, which would lead any strain calculated using these methods to be a minimum estimate of strain. In addition to calculating shear strain for individual shear zone segments bulk shear strain was also calculated using a modified version of the displacement method (for a simple shear) (Ramsay and Huber, 1987).

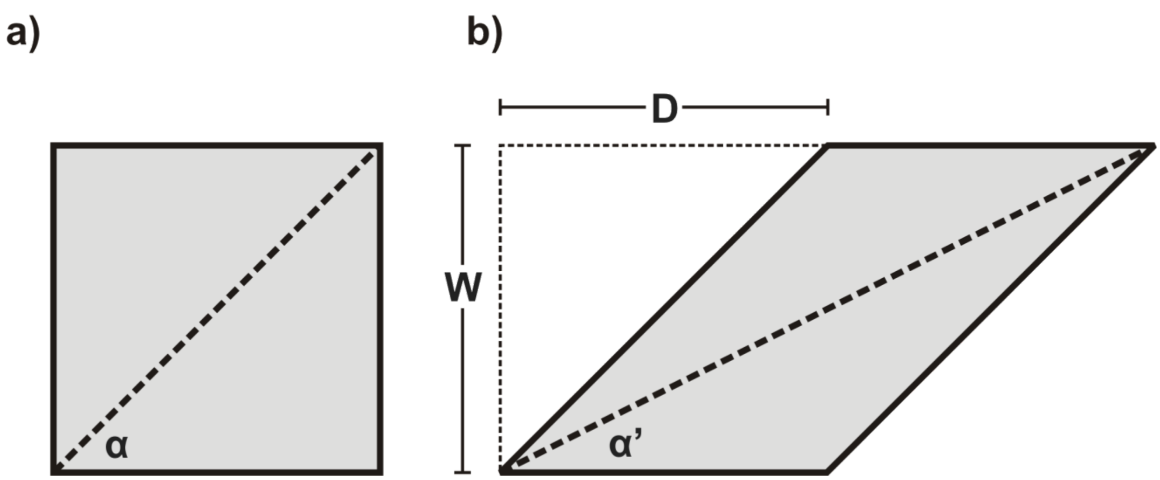

Figure 5.1: The geometry of the rotation of a marker layer, modified from Ramsay & Huber (1983). **a)** The undeformed state with a marker layer at an angle to a shear zone, α. **b)** After undergoing a simple shear, α becomes α', where the displacement (D) and

width of the shear zone (W) can be measured. Alternatively, displacement can be calculated once shear strain and shear zone width are determined.

The angle-method comprises measuring the change in angle of a layer, with respect to the shear plane. The shear planes are assumed to be parallel to shear zone boundaries. Due to the variable orientations of dextral shear zone boundaries on Matches Island, each individual shear zone segment selected for strain analysis has a local shear plane. The sinistral shear zones on Matches Island do not show the variability their dextral counterparts do, and so an island-scale shear plane was determined and used for the sinistral shear zone strain analysis. The angle method was also used to calculate the island-scale sinistral shear strain on Matches Island by measuring the change of original angle of dextral shear zones to the chosen shear plane within the island-scale shear zone. Strain analysis using the angle method can be conducted using equation (i) from Ramsay and Graham (1970):

$$\cot(\alpha') = \cot(\alpha) - \gamma_{max} \qquad \text{(i)}$$

where α is the initial angle of a layer, α' is the final angle (in radians) of a layer, and γ_{max} is the maximum shear strain at a given point (Fig. 5.2). The angle method was the most robust method for calculating shear strain on individual shear zone segments, and was successfully completed on each island chosen for strain analysis.

Both the displacement method and the angle method for calculating shear strain require clear shear zone boundaries. In an effort to be consistent, shear zone boundaries are defined at the deflection of wall rock foliation past a threshold angle. Shear zone boundaries were determined by measuring the deflection of wall rock foliation from a baseline orientation representative of the wall rock and constructing foliation isogons. In this study, when the deflection of the wall rock foliation exceeds 10° from the wall rock initial orientation, it is judged to be in a shear zone boundary.

The angles α and α' were measured using the dimension function within CorelDraw from different layers along a transect perpendicular to the boundaries of a shear zone segment. A polyline was constructed parallel to the shear zone boundary of the shear zone segment to act as the baseline from which all angles were measured. A second polyline, perpendicular to the first, was used to measure the distance of each α' measurement to produce a strain transect across the shear zone segment. A single value of α was measured on the wall rock margin and was compared against various measurements of the angle α' measured within the shear zone boundary using equation (i). Figure 5.2 a) illustrates the angle method; the α value was measured on wall rock layering, and various α' values are measured across the width of the shear zone (red dots). This process was repeated until there was a continuum of measured α' values across the shear zone. This allowed for the calculation of γ_{max} using equation (i) at several points across the shear zone.

a) b)

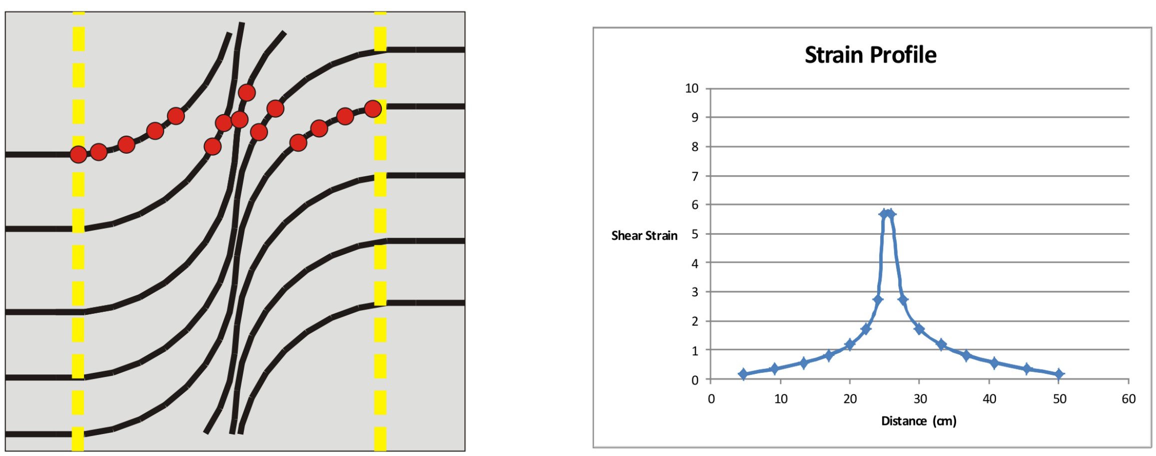

Figure 5.2: Example of measuring deflected foliation for calculating shear strain using the angle method. **a)** A transect of α' across a shear zone (red dots), within the shear zone boundaries (yellow lines). **b)** Strain results of the transect from a), plotted against distance to yield the strain profile of the shear zone.

The γ_{max} calculation is extremely sensitive to α and α', therefore inaccuracies of angular measurements can cause large errors in maximum shear strain, which subsequently affects the estimate of average shear strain. The γ_{max} value changes drastically for α' values less than 5°. In Figure 5.3, there is a hypothetical set of α' values plotted against the resulting γ_{max} values. For the majority of the strain profile, there is a small increase in γ_{max} for every increment of α’. The problems begin around values of α’ less than 5°, there are very large increases in γ_{max} values for the same increments of α’. This leads to the conclusion that the difference between α’ values smaller than 5° are inconsequential because the misjudgment of an angular measurement by a single degree could significantly change the result, therefore, α’ values of less than 5° were not used in the γ_{max} calculations, therefore the maximum measured shear strain is not always the maximum actual shear strain.

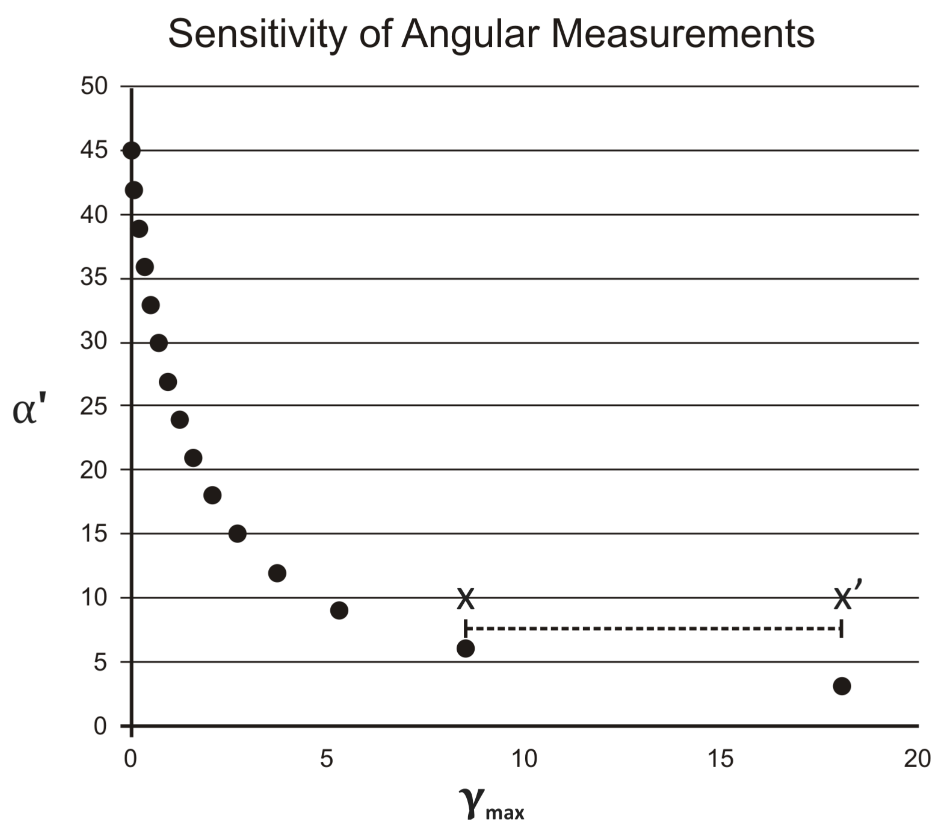

Figure 5.3: Sensitivity of angular measurements. α = 45, α’ is varied in increments of 2°.

Strain profiles (a plot of shear strain against distance across a shear zone) can be used to determine whether a shear zone has widened or narrowed during progressive shear, which can indicate transpression/transtension and whether a shear zone has experienced strain softening or strain hardening (Means, 1995). According to Means’ (1995) model, a shear zone that is widening is strain hardening vice versa for a shear zone that is narrowing. Strain profiles can be constructed (Fig. 5.2 b) to calculate average shear strain (γ_{avg}) by integrating the area under the strain profile curve (Fusseis et al., 2006). Previous studies that feature strain quantification typically use only one method of calculating strain (Mohanty and Ramsay, 1994; Fusseis et al., 2006; Sassier et al., 2009). By using both the displacement method and the angle method along the same shear zone segment, the results can be compared to ensure reasonable results and to calibrate error.

The displacement method consists of measuring the shear offset of a marker layer and the width of the shear zone that has displaced it. The displacement method is described by equation (ii) (Ramsay and Huber, 1987):

$$\gamma_{avg} = \frac{displacement}{width} \qquad \text{(ii)}$$

where γ_{avg} is the average shear strain across a shear zone, displacement is the offset of a marker layer in metres, and width is the width of the shear zone in metres.

The displacement method was used to calculate shear strain for both sinistral and dextral shear zones. Wall rock layering was used as the displaced marker layer when calculating the shear strain of dextral shear zones, as they form perpendicular to the wall rock layering. When calculating shear strain for sinistral shear zones, dextral shear zones themselves were used as the displaced marker as they are overprinted at a high angle by the sinistral shear zones.

The measurements for the displacement of marker layers and widths of shear zones were created on a separate layer of the same CorelDraw file as the angle method. After identifying a marker layer that can be traced across a shear zone, two points are marked where the marker layer intersects each shear zone boundary. The shear zone width was simply the distance between the boundaries, measured perpendicular to the shear zone boundary (Fig. 5.4 a). The displacement of the marker layer was measured as the straight-line distance between the two points parallel to the shear zone boundary (Fig. 5.4 a).

The displacement method was the more limited method for calculating shear strain, as it requires a recognizable displaced marker layer. Matches Island was the only study site that proved to be suitable for this method.

The bulk shear strain, γ_{bulk}, across an area containing several shear zones, can be calculated by the displacement method by tracing a marker layer across several shear zones (Fig. 5.4 b). When employing the displacement method to calculate γ_{bulk}, the shear zone width was measured from the midpoint of the displaced layer rather than the edge of a shear zone when calculating γ_{avg} for a single shear zone. This measurement was useful when discussing and comparing shear strain values on an island- or unit-scale rather than individual shear zones (Culshaw et al., 2010).

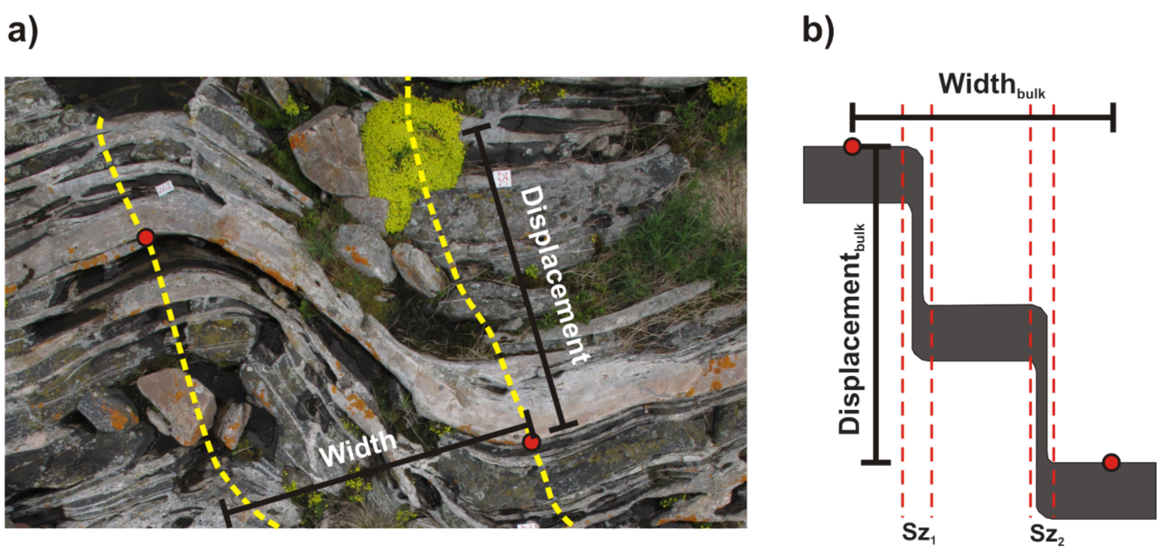

Figure 5.4: a) Example of the displacement width method on a natural shear zone. Shear zone boundaries are given by the yellow dashed lines, and the intersection of a marker layer and the shear zone boundaries are red circles. **b)** A schematic of the displacement width method to calculate bulk strain, in this example across two shear zones (red dashed lines). The intersection of the marker layer and the midpoint of the outside wall rock panels are given by red circles.

For each strain analysis (both individual and bulk), a strain ellipse was constructed that contributed to creation of strain maps. To calculate ellipticity (R) and the orientation of the strain ellipse (θ'), the deformation matrix (D) must be evaluated to determine the eigenvalues (Fossen and Tikoff, 1993).

$$D = \begin{bmatrix} k_x & \tau \\ 0 & k_y \end{bmatrix} \qquad \text{(iii)}$$

Where τ is effective shear strain, k_x is pure shear and k_y is $1/k_x$. To evaluate the deformation matrix (D) for a simple shear, k_x and $k_y = 1$, and $\tau = \gamma_{avg}$ resulting in a simplified matrix.

The ratio of the long axis to the short axis is the ellipticity of the strain ellipse (R), which is calculated using equation (iv) (Fossen, 2010):

$$R = \frac{\sqrt{\lambda_{11}}}{\sqrt{\lambda_{22}}} \qquad \text{(iv)}$$

where λ_{11} and λ_{22} are the eigenvalues of the deformation matrix, D or bulk deformation matrix, D_{bulk}. The orientation of the long axis of the strain ellipse can be determined by using equation (v) (Fossen, 2010):

$$\theta' = \tan^{-1}\left(\frac{\Gamma^2 + {k_x}^2 - \lambda_{11}}{-k_y\tau}\right) \qquad \text{(v)}$$

The parameters in equation (v) are for a general shear. For a simple shear k_x and $k_y = 1$, and $\tau = \gamma_{avg}$.

5.1.2: Matches Island dextral shear zones displacement method results

Figure 5.5a shows the schematic map of the photomap area of Matches Island overlain with strain ellipses calculated using the displacement method for strain of individual dextral shear zones in Unit 1. The strain ellipses clearly show three distinct clusters: i) a low strain cluster on the northeast extent of Fig. 5.5, with the maximum extension direction trending northeast; ii) a high-strain cluster in the center, with a maximum extension direction trending north; and iii) a low-medium strain cluster on the southwest of Fig. 5.5, with a maximum extension direction trending northeast. See Appendix A for a list of values of γ_{avg}, R and θ‘ for individual shear zones. The long axes of the strain ellipses show an anticlockwise rotation toward the NNE direction with increasing shear strain.

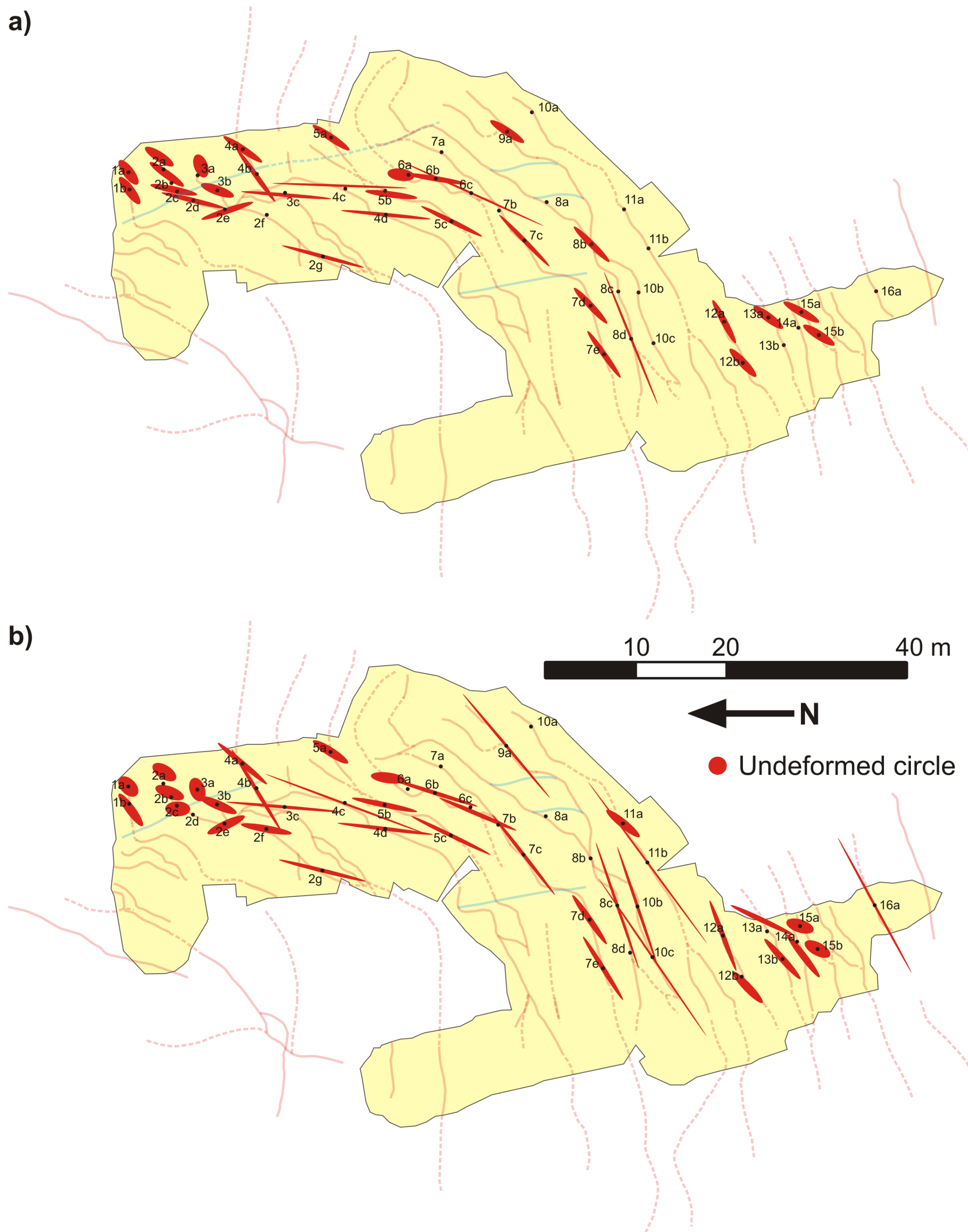

Figure 5.5: Shear strain map of dextral shear zones on Matches Island. Yellow polygon, photomosaic area; red solid lines, dextral shear zones; red dashed lines, inferred dextral shear zones; red ellipse, strain; black dot, location of strain measurement. **a)** Strain ellipses constructed using values calculated using the displacement method and **b)** strain ellipses constructed using values calculated using the angle method. Strain ellipses with ellipticity values larger than 100 were not plotted (black dots without ellipses). See Appendix A for values of γ_{avg}, R and θ' for each individual shear zone segment.

5.1.3: Matches Island dextral shear zones angle method results

Strain ellipses calculated using the angle method for shear strain of dextral shear zones largely mirrors the pattern determined by the displacement method (Fig. 5.5 b). The strain pattern created from the angle method shows a central high-strain zone flanked by a low strain zone to the east and a low-high strain zone to the west. One significant difference between the two strain patterns is the magnitude of strain produced in the high-strain zone in the angle method (γ_{avg}) is much larger than those produced using the displacement method. The values of shear strain calculated for dextral shear zones on Matches Island are displayed in Appendix A.

The angle-method also enables the production of a strain profile, the shape of which can be used to characterize whether a shear zone is strain softening or strain hardening (Hull, 1988; Mitra, 1992; Means, 1995). There is a pronounced shift in the strain profiles across the sinistral shear zone that separates clusters of strain ellipses (Fig. 5.5). Strain profiles from Block A exhibit broad, flat-topped curves with no clearly defined peak typical of Type I (widening) shear zones (Means, 1995). A representative strain profile of Block A is shown in Figure 5.6 a. Strain profiles from Block B feature strong well developed peaks that correspond to large shear strains, indicating a small 'active' zone of deformation typical of Type II (thinning) shear zones (Means, 1995). Figure 5.6 b shows a representative strain profile of the high strain shear zones of Block B.

a) b)

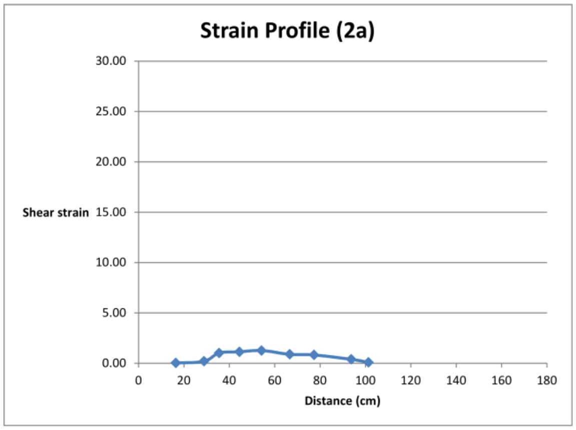

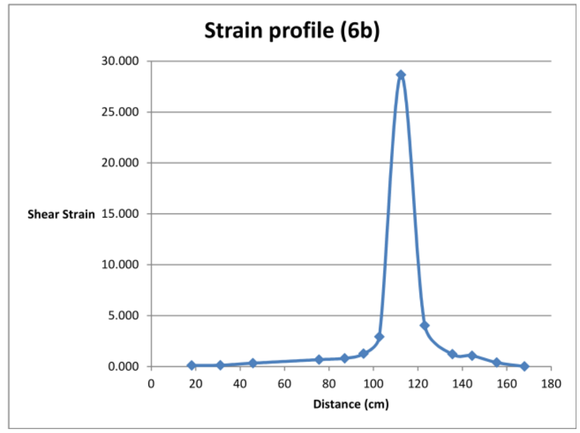

Figure 5.6: Examples of strain profiles produced using the angle method to calculate shear strain. **a)** A low strain example from Block A and **b)** a high-strain example from Block B. Note that scale is the same for direct comparison. See Fig. 5.5 for shear zone locations.

5.1.4: Matches Island sinistral shear zones displacement method results

Strain analysis of sinistral shear zones was calculated using displacement and deflection of dextral shear zones by sinistral shear zones, and widths of either the broad sinistral shear zone (black dashed lines, Fig. 5.7) or discrete width of an individual shear zone. The results of the strain analysis using the displacement method produced varying results (Fig. 5.7). The sinistral shear zone boundaries were drawn parallel to observable discrete sinistral shear zones (blue dashed lines). Discrete sinistral shear zones (dark blue ellipses, Fig. 5.7) were found to have shear strains from between 2 and 3. Strain calculations based on measurements from the broad sinistral shear zone (light blue ellipses, Fig. 5.7) produced shear strains of less than 1, which was to be expected given the observable layer deflections are low. Despite the magnitude difference in shear strain, ϑ' values oriented strain ellipses of discrete sinistral shear zones and the broad sinistral shear zone in a consistent orientation ~NNE, which also agrees with the orientation of strain ellipses determined by the analysis of dextral shear zones (Fig. 5.5).

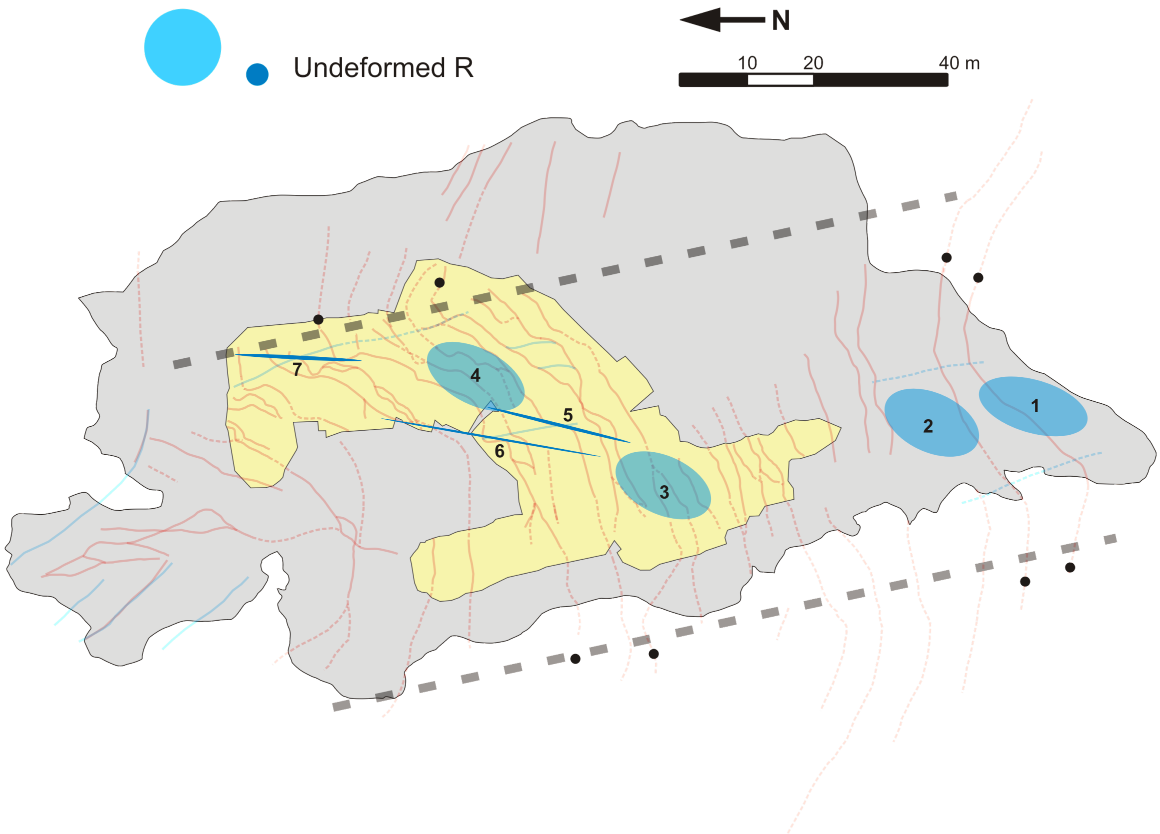

Figure 5.7) Strain map of sinistral shear zones on Matches Island using the displacement method. Grey polygon, island area; yellow area, photomap area; red lines, dextral shear zones; blue lines, sinistral shear zone; black dashed lines, sinistral shear plane; light blue ellipse, strain ellipse for broad sinistral shear zone; dark blue ellipse, strain ellipse for discrete sinistral shear zone; black dots, displacement markers for broad sinistral shear zones. See Table 5.1 for values of γ_{avg}, R, and θ'.

Table 5.1) Shear strain results of sinistral shear zones using the displacement method on Matches Island. See Figure 5.6 for locations of bulk shear. SZ ID, shear zone identification; γ_{avg}, average shear strain; type, broad or discrete sinistral shear zone; R, ellipticity; θ', orientation of long axis of the strain ellipse.

SZ ID	Type	γ_{avg}	R	θ'
1	Broad	0.72	2.02	-35.13
2	Broad	0.46	1.58	-38.52
3	Broad	0.50	1.64	-37.95
4	Broad	0.63	1.86	-36.26
5	Discrete	2.16	6.49	-21.43
6	Discrete	2.86	10.09	-17.47
7	Discrete	1.92	5.52	-23.05

5.1.5: Sinistral shear zones angle method results

The results of strain calculations of sinistral shear zones on Matches Island using the angle-method are displayed in Table 5.2, and as a map (Fig. 5.8). The angle method produced notably higher values of shear strain, with a much higher variance of values. Calculations based on measurements from the southern end of Matches Island (SZ 1-6, Table 5.2) result in much lower shear strains than shear strain values calculated in the middle of the island (SZ 7-8, Table 5.2), a result that is consistent with results from dextral shear zone analysis as well as field observations. Once again, the resulting strain ellipses yield a stretching direction of ~NNE.

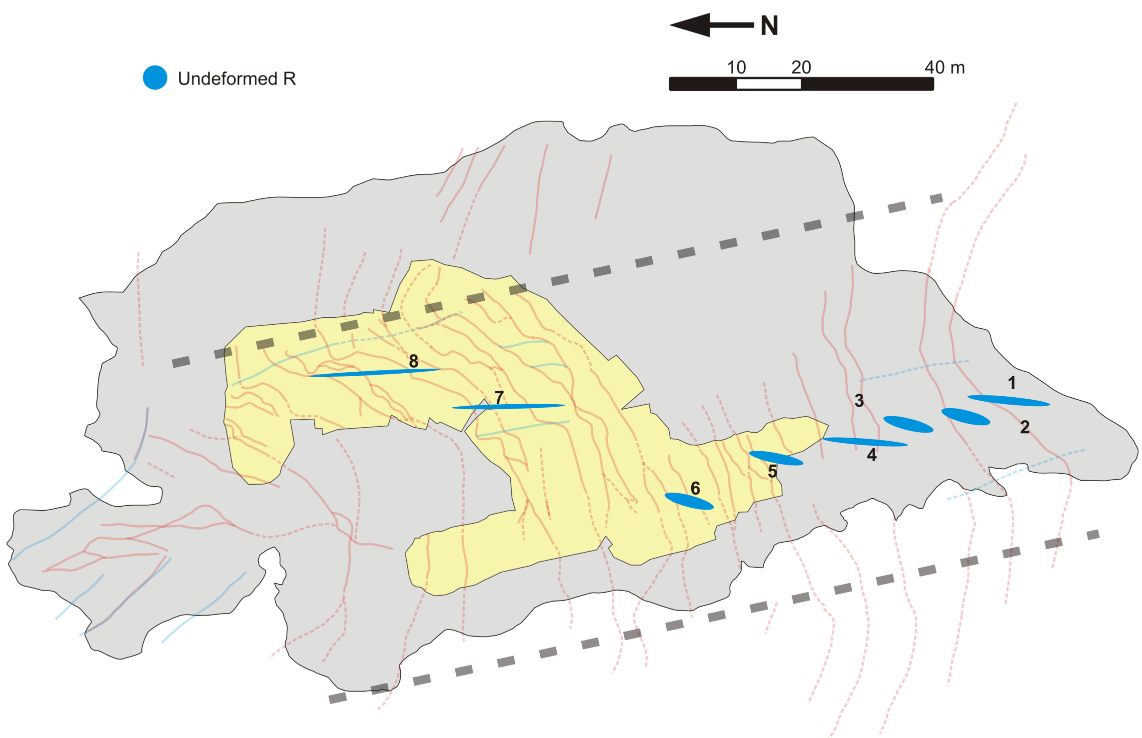

Figure 5.8) Strain map of sinistral shear zones on Matches Island using the angle method. Grey polygon, island area; yellow area, photomap area; red lines, dextral shear zones; blue lines, sinistral shear zone; black dashed lines, sinistral shear plane; light blue ellipse, strain ellipse for broad sinistral shear zone; dark blue ellipse, strain ellipse for discrete sinistral shear zone. See Table 5.2 for values of γ_{avg}, R, and θ'.

Table 5.2) Bulk strain results of Matches Island. See Figure 5.8 for locations of bulk shear. SZ ID, shear zone identification; γ_{bulk}, bulk shear strain; R, ellipiticy; θ', orientation of long axis of the strain ellipse.

SZ ID	γ_{avg}	R	θ'
1	2.96	10.66	-17.03
2	1.51	4.03	-26.48
3	1.62	4.38	-25.54
4	3.34	13.07	-15.46
5	1.92	5.50	-23.09
6	1.58	4.28	-25.81
7	4.66	23.66	-11.62
8	5.32	30.28	-10.30

5.1.6: Matches Island bulk strain results

The displacement method was also used on Matches Island to calculate bulk shear strains of larger areas, by evaluating displacement across multiple neighboring dextral shear zones. The results of bulk strain analysis can be used to further characterize strain domains, as well as derive strain data that can be used in the method by Horsman and Tikoff's (2005) of evaluating bulk strain with a pure shear component. The results of the bulk strain are shown as ellipses on a strain map (Fig. 5.9), and accompanied by Table 5.3. The γ_{bulk} results show that Block B contains the highest degree of deformation, while Blocks A and B are zones of lower strain. The major exception is shear zone 5_{bulk}, which despite being in the supposed low strain Block C shows the highest γ_{bulk} value. The unexpectedly high value of shear zone 5_{bulk} can be explained by the presence of the major dextral shear zone, which cuts across the island and has highest values of shear strain associated with it.

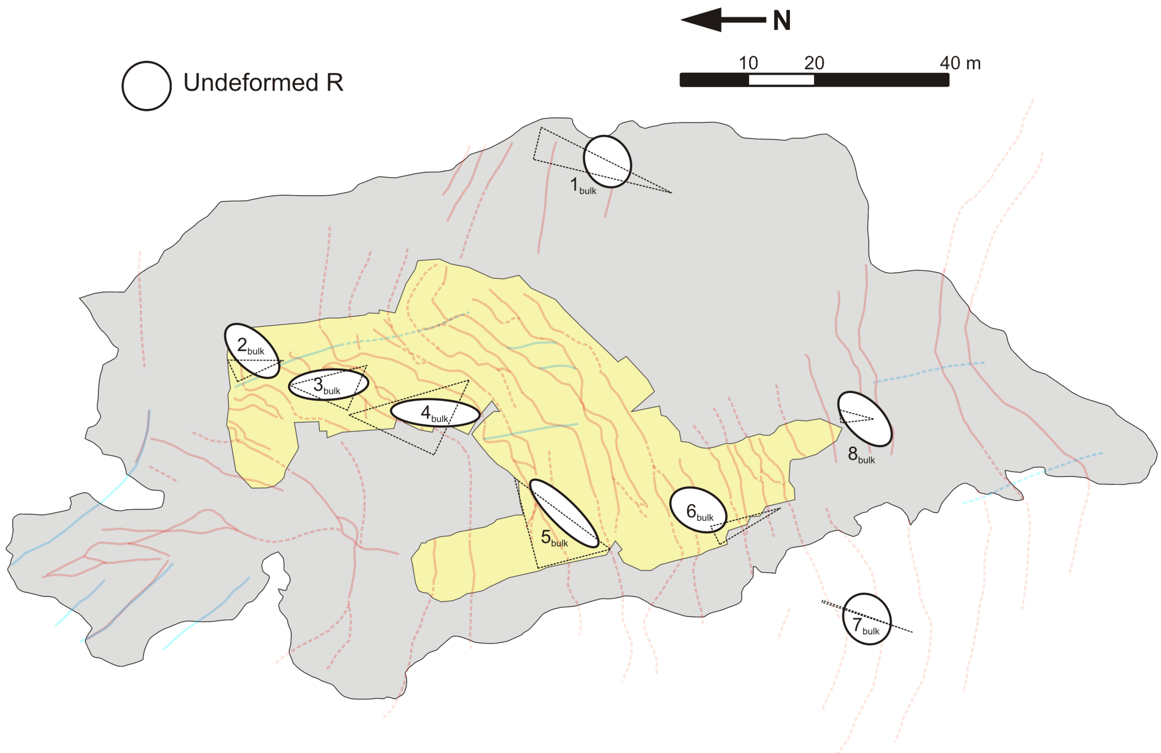

Figure 5.9) Bulk strain map of Matches Island. Grey polygon, island area; yellow polygon, photomosaic area; red lines, dextral shear zones; blue lines, sinistral shear zones; black dashed lines, bulk displacement markers; grey ellipses, bulk strain ellipses. See Table 5.3 for bulk strain values. The bulk displacement markers are constructed as triangles with the hypotenuse being the straight-line displacement distance, and the other sides of the triangle being the displacement parallel to the shear zone boundary and width of the bulk strain.

Table 5.3) Bulk strain results of Matches Island. See Figure 5.9 for locations of bulk shear. SZ ID, shear zone identification; γ_{bulk}, bulk shear strain; R, ellipticity of the strain ellipse; θ', orientation of long axis of the strain ellipse; block,

SZ ID	γ_{bulk}	R	θ'	Block
1_{bulk}	0.08	1.08	-43.84	A
2_{bulk}	0.47	1.59	-38.42	A
3_{bulk}	1.00	2.62	-31.70	B
4_{bulk}	1.19	3.09	-29.65	B
5_{bulk}	1.24	3.24	-29.07	C
6_{bulk}	0.35	1.42	-40.02	C
7_{bulk}	0.10	1.10	-43.59	C
8_{bulk}	2.06	1.76	-36.99	C

5.1.7: PBW Island angle method results

Strain analysis on PBW Island was limited to the angle method due to the lack of obvious displacement marker layers. Strain analysis was conducted on an outcrop that was imaged used the photomap technique (Fig. 4.19). The location of shear zone segments selected for strain analysis are plotted on the outcrop photomap (Fig. 5.10), with the magnitudes of shear strain shown in Table 5.4. The results show consistently high strain shear zones, with propagating sub-parallel shear zones showing relatively lower shear strains. The angle method was conducted on the least deformed region of the island (Fig. 4.17). Although the results may not be representative of the remainder of the island, they give a minimum strain estimate as well as a direct comparison to strain results from other islands.

The resulting R values calculated for each shear zone segment analyzed are very large (>100), and can be seen in Table 5.4. The orientation of the long axis of the strain ellipses (θ’) were also calculated and displayed in Table 5.4 with θ’ values typically <5°, leading to strain ellipses approaching parallelism with shear planes, with strain ellipses oriented in WNW.

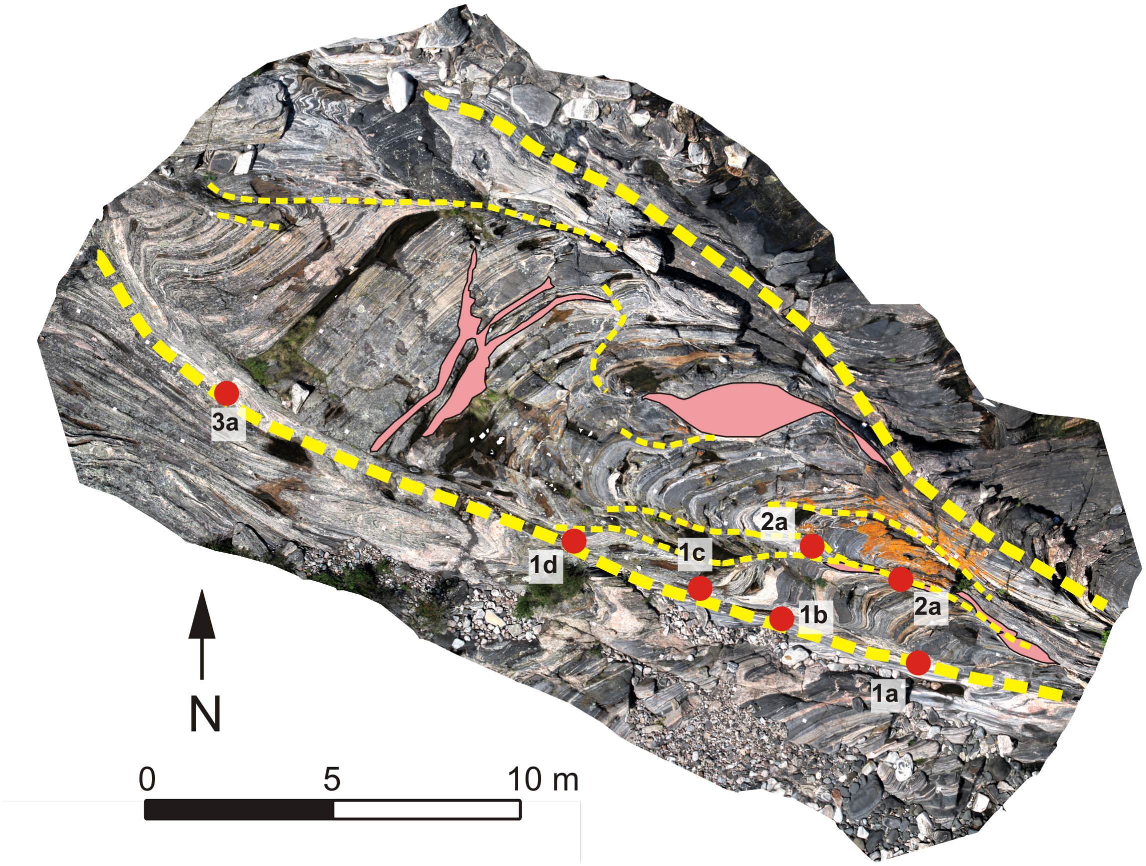

Figure 5.10: Locations of strain analysis on PBW Island. For location of outcrop see Fig. 4.17 and 4.19. See Table 5.4 for results. Thick yellow dashed lines, shear zones on margin of wall rock block; thin yellow dashed lines, sub-shear zones within the wall rock block; pink polygons, syntectonic (?) pegmatite; red circles, shear zone segment identification.

Table 5.4: PBW Island strain analysis results. All shear strains were calculated using the angle method. γ_{avg} values were used to calculate R and θ'. See Fig. 5.10 for shear zone locations.

SZ ID	γ_{avg}	R	θ '
1a	11.06	124.37	-5.12
1b	28.14	794.12	-2.03
1c	15.75	250.20	-3.62
1d	17.21	298.22	-3.31
2a	11.16	126.57	-5.08
2b	11.20	127.43	-5.06
3a	30.80	950.90	-1.86

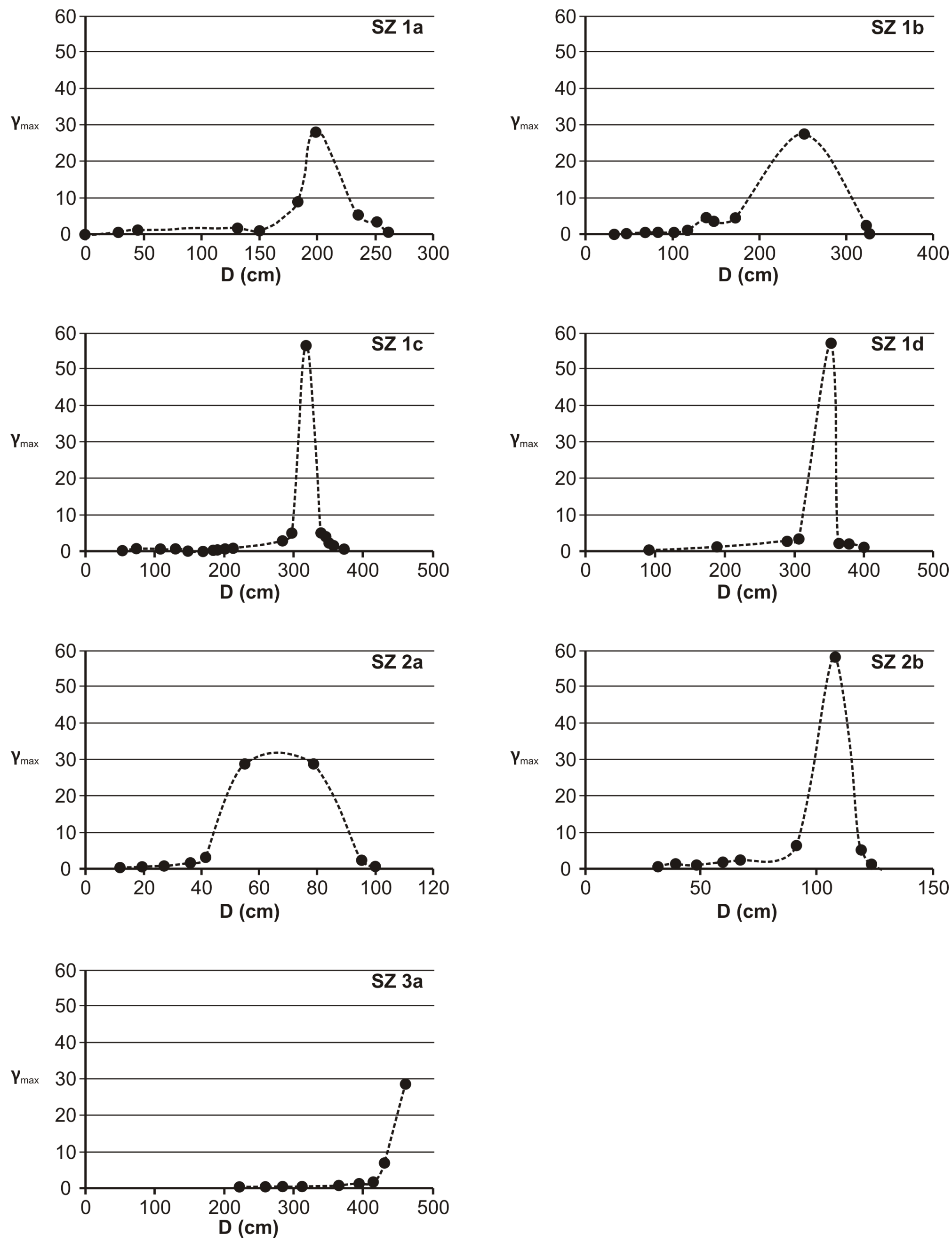

Figure 5.11: Strain profiles of shear zones within the photomap area of Unit 2 of PBW Island. Shear zone segment identification is in the top right of each graph. See Fig. 5.10 for shear zone segment locations. Black dot, data point; dashed line, best-fit curve. See Appendix A for data.

The strain profiles produced from strain data collected from PBW Island predominately display narrow zones of very high shear strains (Fig. 5.11). The narrow strain profile peaks observed closely resemble Means' (1995) model of thinning shear zones. Each maximum shear strain exceeds 25, indicating very strongly localized high strain shear zones. Shear zone segment 3a is a half profile, as the layering becomes approximately parallel to the shear zone boundary and the other side of the shear zone is not imaged. The last data point of the strain profile (Fig. 5.11, 3a) represents the last point at which the layering was not parallel to the shear zone boundary.

5.1.8 Bartram's Island angle method results

Strain analysis on Bartram's Island was also limited to the angle method due to the lack of displacement markers. The locations of shear zone segments analyzed are shown in Figure 5.12, and corresponding results in Table 5.5. Many of the shear zones analyzed featured wide high strain cores with shear zone foliation forming parallel to the shear plane, as well as isoclinal folds nested within the high strain cores. The presence of isoclinal folds within the shear zones made it difficult to construct a complete strain transect across a shear zone. Strain profiles of transects of one half of a shear zone are shown in Figure 5.13. The strain profiles consistently show very steep gradients in shear strain, and often feature small oscillations in strain values that reflect folding prior to reaching the high strain core.

SZ ID	γ_{avg}	R	θ '
1a	8.14	68.24	-6.89
1b	8.94	81.91	-6.28
1c	3.39	13.42	-15.62
1d	2.70	9.18	-18.89
2a	3.34	13.08	-15.82
2b	2.22	6.78	-21.99
2c	6.77	47.81	-8.25
3a	6.30	41.67	-8.84
3b	4.89	25.87	-11.23
3c	6.09	39.06	-9.13
4a	9.41	85.53	-6.14
4b	3.88	17	-13.87
4c	1.49	3.97	-28.75
5a	1.50	4.00	-28.64

Table 5.5: Bartram's Island strain analysis results. All shear strains were calculated using the angle method. γ_{avg} values were used to calculate R and θ'. See Fig. 5.12 for shear zone locations.

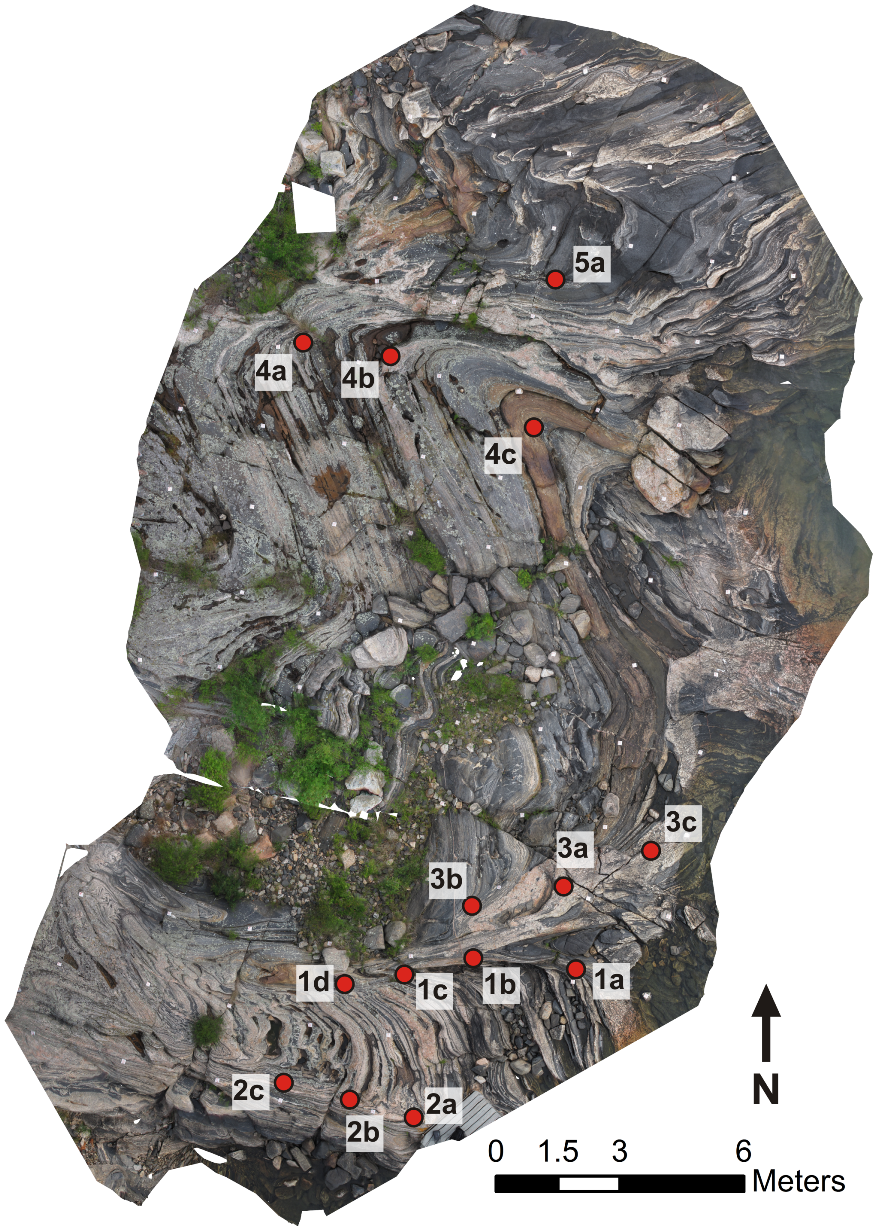

Figure 5.12: Locations of strain analysis on Bartram's Island. For location of outcrop see Fig. 4.17 and 4.19. See Table 5.5 for results. Red circles, shear zone segment identification. See Table 5.5 for γ_{avg} results.

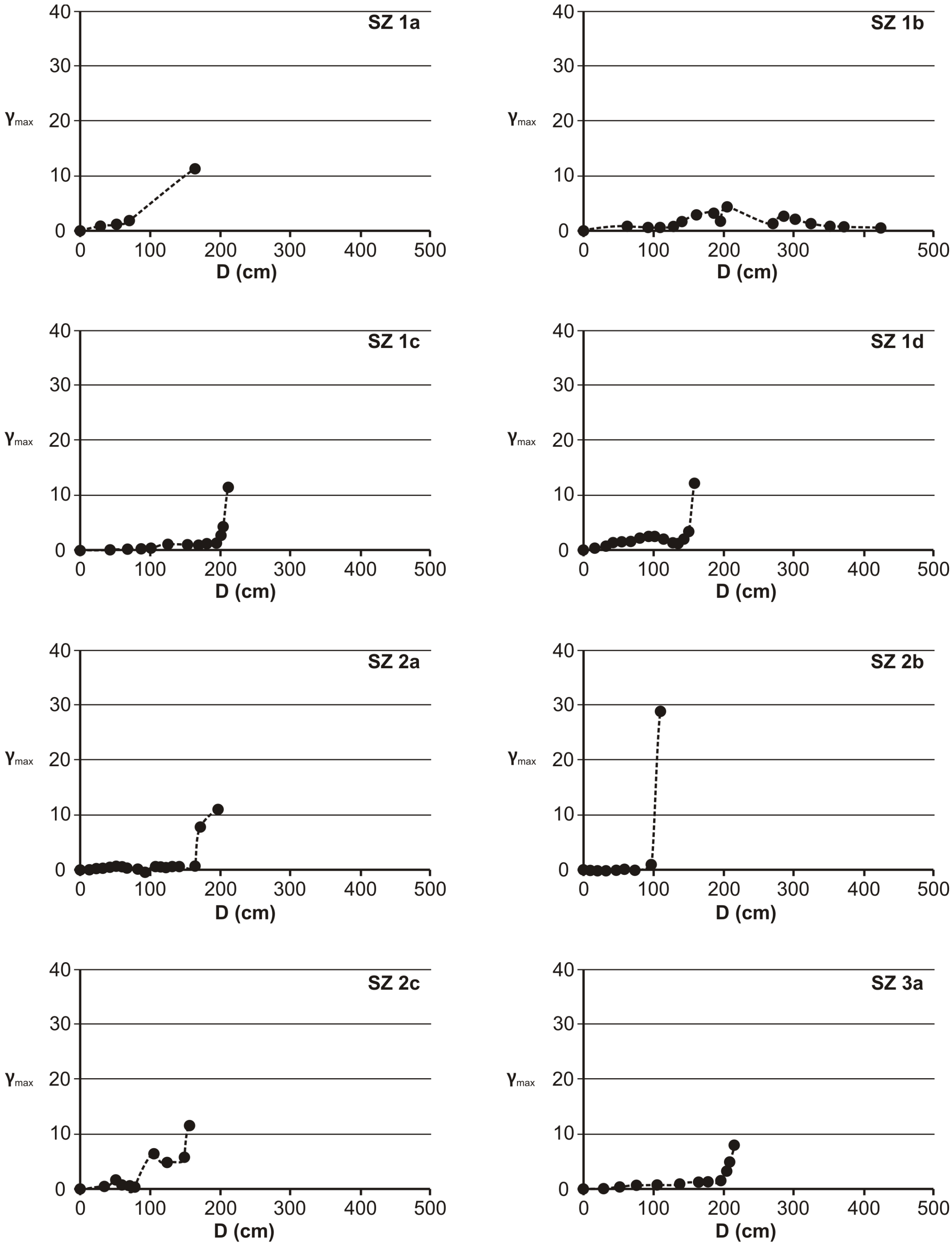
SZ 1a
SZ 1b
SZ 1c
SZ 1d
SZ 2a
SZ 2b
SZ 2c
SZ 3a
γ_{max}
D (cm)
0
10
20
30
40
100
200
300
400
500

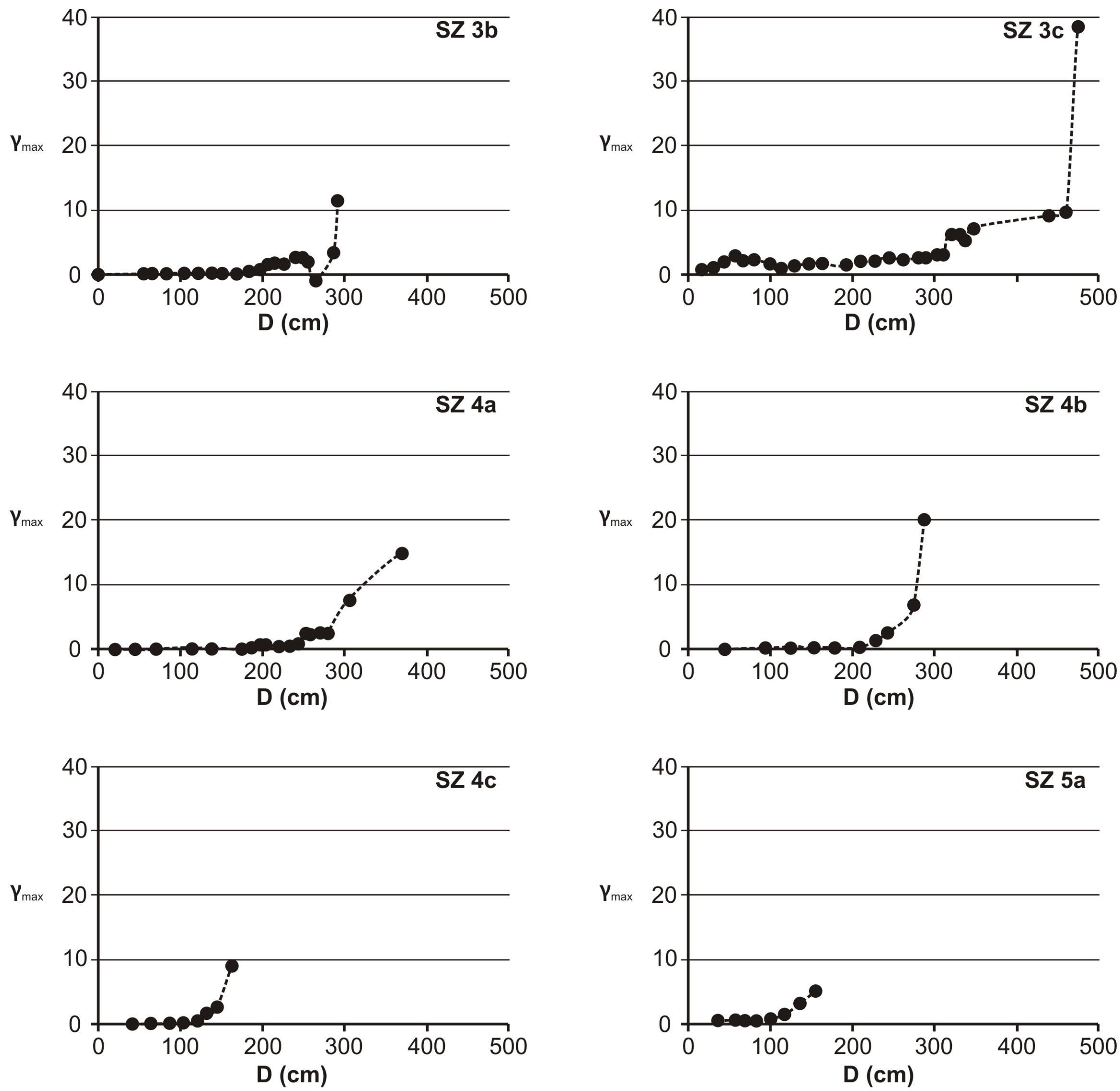

Figure 5.13: Strain profiles of shear zones within the photomap area of Bartram's Island. Shear zone segment identification is in the top right of each graph. See Fig. 5.10 for shear zone segment locations. Black dot, data point; dashed line, projected curve. See Appendix A for data.

The absence of complete strain transects of shear zones on Bartram's Island makes the calculation of γ_{avg} a minimum estimate. In an attempt to remedy this, strain transects on the opposite side of a shear zone segment have been paired together to create a 'composite' strain profile (Fig. 5.14). This was done by matching two strain profiles from two sides of the same shear zone, measuring the distance between the final points and connecting the strain profiles. Three composite strain profiles were constructed, 1a-3a, 1b-3b, and 4c-5a. Two of the three composite strain profiles (1a-3a, 4c-5a) feature very wide (> 150 cm) high strain cores resulting in values of γ_{avg} greater than 10 (Table 5.6). However, the data from the high strain core are sparse causing the peak of the strain profile to be poorly constrained. Strain results from Bartram's Island show that thick shear zones result in large values of shear strain and large displacements.

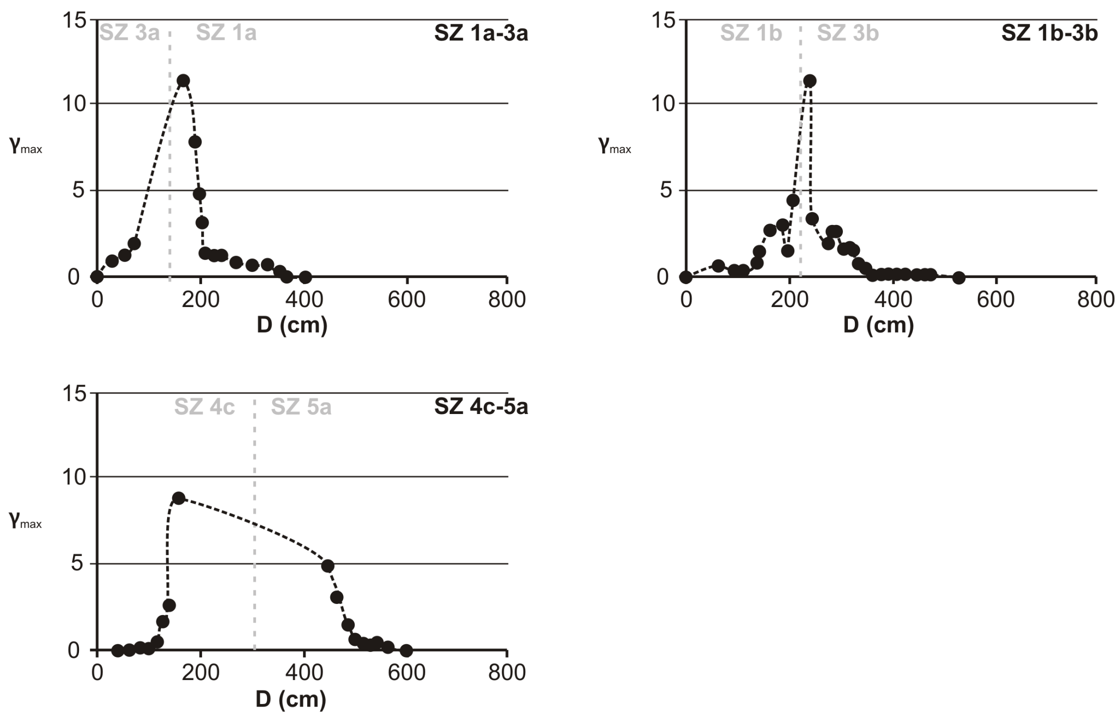

Figure 5.14: Composite strain profiles of shear zones within the photomap area of Bartram's Island. Shear zone segment identification is in the top right of each graph. See Fig. 5.10 for shear zone segment locations. Black dot, data point; dashed line, best-fit curve; grey dashed line, divide between two profiles. See Appendix A for data.

Table 5.6: Bartram Island strain analysis results for composite strain profiles. All shear strains were calculated using the angle method. γ_{avg} values were used to calculate R and θ'. See Fig. 5.11 for shear zone locations.

SZ ID	γ_{avg}	R	θ '
1a-3a	11.28	129.23	-4.97
1b-3b	7.28	54.98	-7.68
4c-5a	22.86	524.58	-2.37

The one complete strain profile that was collected was SZ 1b (Fig. 5.13), and had a γ_{avg} value of 8.94, similar to results obtained using the composite strain profiles. Shear zone segment 4c-5a is an outlier, as the γ_{avg} result is much larger than the γ_{avg} results from other two composite strain profiles and individual shear zone segments. However, the shear zone segment 4c-5a has a very wide high strain core (~200 cm) much larger than the other composite strain profiles. Therefore, the γ_{avg} must be very large with such a wide high strain core.

5.1.9: Strain analysis discussion

Strain analysis results of dextral shear zones on Matches Island show a consistent strain pattern. Both methods indicate that dextral shear zones located in Block B generally have much larger shear strains than Blocks A and C. The pattern of strain ellipses produced by analysis of individual dextral shear zones, with strain ellipses increasing in ellipticity and anti-clockwise rotation with proximity to Block B suggests an island-scale heterogeneous sinistral shear zone, with a shear plane that strikes approximately N-S. As mentioned, the angle method consistently produced higher values of shear strain when compared to shear strains calculated using the displacement method for the same shear zone segment.

The γ_{avg} results of the displacement method were plotted against the γ_{avg} results of the angle method (Fig. 5.15); where each point represents an individual shear zone segment that had been analyzed by each method. The ideal result would be a slope of 1; however, the results show that the slope is ~0.82. The slope of the line indicates that either the angle method overestimates γ_{avg}, or that the displacement method underestimates γ_{avg}. While this poses a problem in terms of the uncertainty of assigning a γ_{avg} value to a particular shear zone segment, it could perhaps be used as a guide for estimating an error to the magnitude of shear strain.

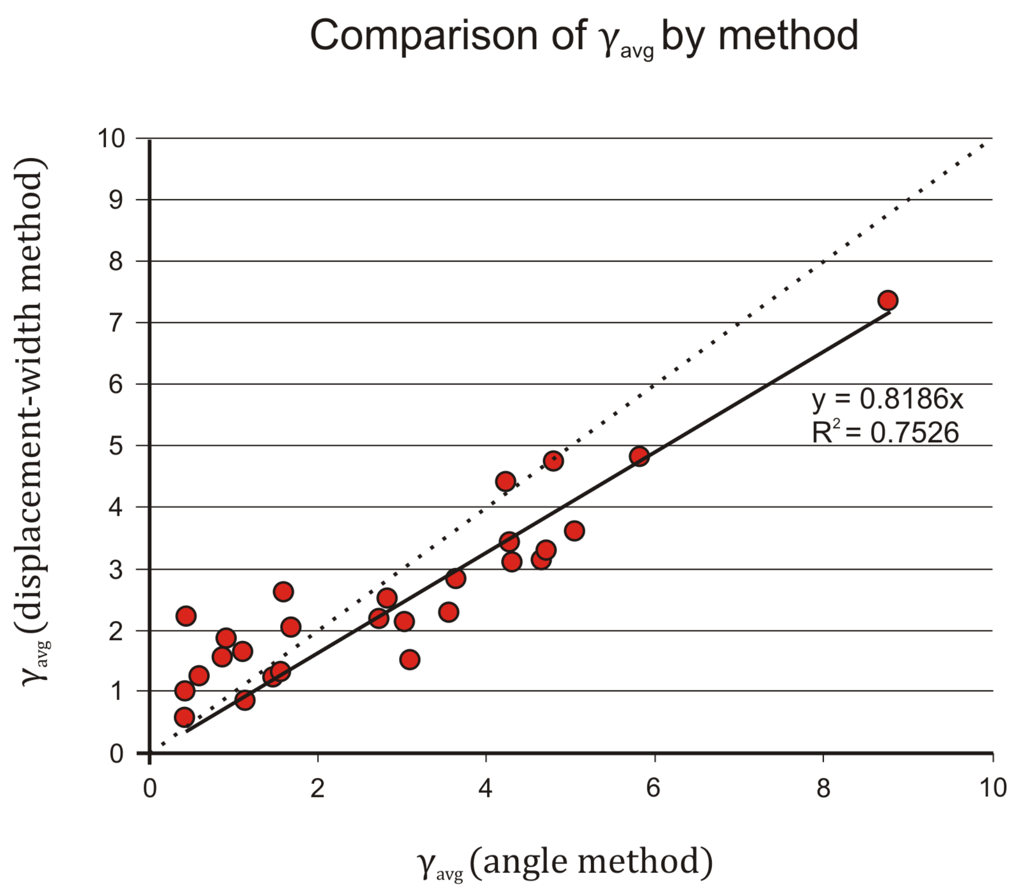

Figure 5.15: Shear strain (γ_{avg}) calculated by the displacement method against the angle method. Dashed line is for y = x.

Strain analysis results of sinistral shear zones (Fig. 5.7/5.8) reaffirmed the strain pattern established from dextral shear zones; with the long axis of strain ellipses oriented approximately N-S. Both methods agree on the orientation of the sinistral strain ellipses and once again the angle-method produces higher magnitudes of shear strain.

A potential reason for a large discrepancy between the sinistral γ_{avg} calculated using the angle-method and the displacement method is the lack of clear boundaries for sinistral shear zones. The angle-method is very sensitive to the orientation of the shear zone boundaries. Figure 5.16 presents three examples of shear zone boundaries and how the change in boundary selection affects the corresponding strain profiles. The strain profiles show different maximum shear strains, which would have a more pronounced effect on wider shear zones. The point is that even a reasonable amount of uncertainty of the shear zone boundaries (±5 °) can drastically affect the result of γ_{max} for wide shear zones.

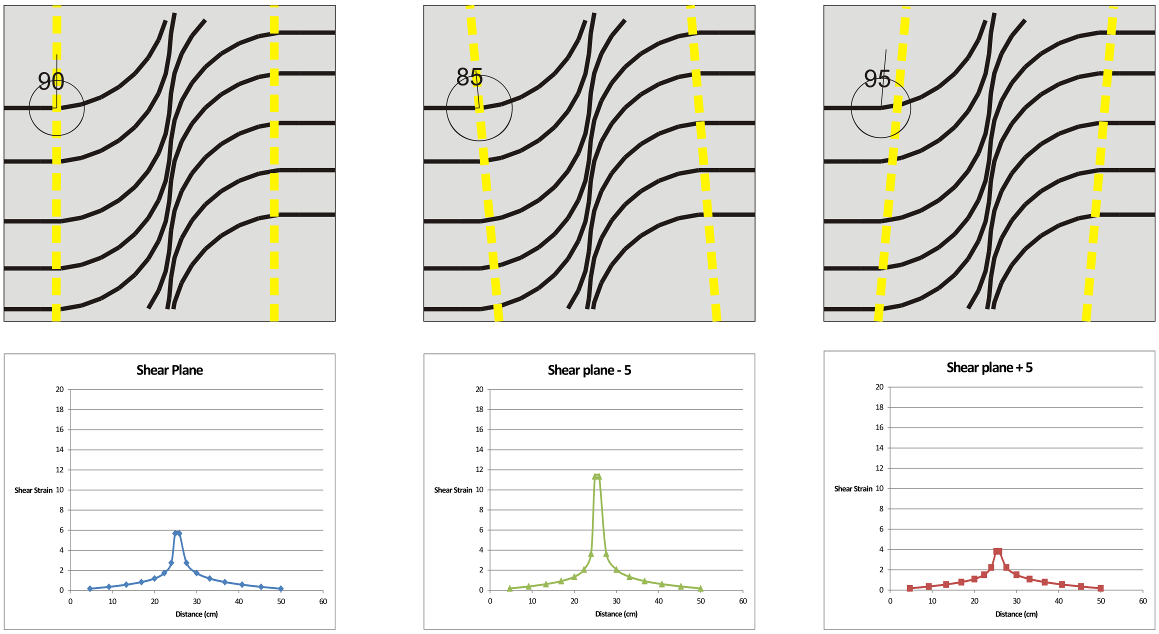

Figure 5.16: Maximum shear strain sensitivity with varying shear zone boundary orientations. **a)** The true shear zone boundary for this example and corresponding strain profile. **b)** The shear zone boundary misidentified by 5° counterclockwise and **c)** 5° clockwise and corresponding strain profiles.

While one could argue that the selection of shear zone boundaries also poses a problem for dextral shear zones, it would have a much smaller effect on the resulting strain calculation because dextral shear zone have clearly defined boundaries and a narrow core of high strain material. The problems for calculating strain within the island-scale sinistral shear zones using the angle method is that the shear zones are very wide (~20-40 m) resulting in a wider high strain core, and the shear zone boundaries are much less clearly defined than dextral shear zones.

Strain analysis of shear zones on PBW Island show much higher shear strains on individual shear zone segments than Matches Island. The strain pattern is also very uniform with the long axis of the strain ellipse trending in the WNW direction, approximately parallel to the regional stretching direction of the Twelve Mile Bay shear zone. While the magnitude of γ_{avg} may not be representative of the remainder of the island, the orientation of the strain ellipse is. The strike of shear zones across the entire island is fairly constant, and so the long axis of the strain ellipse approaching parallelism to the strike of shear zones would be representative of the island.

The strain analysis shows that the maximum values of γ_{avg} are found along the margin of the large wall rock block in Figure 5.10. Cm-scale shear zones that widen into the wall rock produced γ_{avg} values significantly lower than those analyzed on the wall rock margin. The results of the strain analysis and the structural observations of the marginal and interior shear zones suggest that the marginal shear zones are more developed and pre-date the interior shear zones. This is an important point as it shows that an advanced stage of transposition wall rock blocks are being continually deformed by the introduction of small sub-shear zones, as was the case for early stages of transposition.

A closer look at the interior of the wall rock block in Figure 5.10 reveals there to be many cm-scale shear zones that form sub-parallel to the dominant shear zones. The sub-parallel shear zones show a variety of orientations and kinematics and often are linked together and splay off from the main boundary shear zone. There are two possibilities for this kind of shear zone geometry of sub-shear zones: i) the sub-shears developed as sub-parallel offshoots of the major bounding shear zones, or ii) the development of a conjugate shear zone system. In this particular outcrop, the former explanation seems more likely due to the sub-parallel and linking nature of the sub-shear zones to the master shear zones, as well as the lack of evidence of any sub-shear zone overprinting another sub-shear zone of opposing kinematics, which would be indicative of a conjugate shear zone system (Ramsay and Huber, 1987).

Strain analysis of shear zones on Bartram's Island revealed γ_{avg} values larger than results from Matches Island, and on par with the results from PBW Island. However, because the γ_{avg} values on Bartram's Island were calculated using composite strain profiles and the small sample size make the Bartram's Island data set far from ideal.

However, the resulting high values of shear strain on Bartram's Island are supported by field evidence. Marker layers often cannot be traced across shear zones, implying displacements greater than the dimensions of the photomap area (ca. 20m).

Despite the challenges with the γ_{avg} results, direct comparisons can be made between the true strain profiles from Bartram's Island with strain profiles from the other study areas. The Bartram's Island strain profiles most resemble strain profiles from PBW Island. Both sets feature drastic increases in γ_{avg} values in a very short distance towards the center of the shear zone, indicative of strongly localized high strain zones. One feature that is common throughout the Bartram's Island strain profiles is the oscillation of the profile prior to reaching the peak. This feature is noticeably absent within the PBW Island data set. The oscillation of the strain profile is attributed to asymmetric folds that form on the margins of shear zones, as described in the structural overview of Bartram's Island (Chapter 4).

The γ_{avg} values calculated from shear zones on Matches, PBW, and Bartram's islands match the regional strain pattern of the Twelve Mile Bay shear zone, with lower γ_{avg} values found on Matches Island than on the other islands. Despite not obtaining many results on Bartram's Island, there were enough similarities in the γ_{avg} values calculated from composite strain profiles to the true strain profiles to results that were obtained from Bartram's Island, and from PBW Island γ_{avg} results.

Matches Island was the only site of the strain analysis study that had distinct sets of sinistral and dextral shear zones that could be assessed for magnitude of strain. The dextral shear zones on Matches Island showed both greater magnitude and degree of localization compared to sinistral shear zones. Although there are rare occurrences of sinistral shear zones on both PBW and Bartram's islands, they are parallel with dextral shear zones and are indistinguishable from dextral shear zones in terms of shear zone widths and localization.

The stretching directions determined by the orientation of strain ellipses for PBW and Bartram's islands were both approximately parallel to the strike of the Twelve

Mile Bay shear zone (~E-W). The strain pattern on Matches Island revealed a bulk extension in the NNE-SSW direction, approximately parallel to the strike of the original granulite facies layering of the iPSD. However, the stretching direction on Matches Island is sub-horizontal whereas the stretching direction on PBW/PBE has a down-dip component as evidenced by the regional plunge.

The horizontal bulk stretch of Matches Island differs significantly from the inferred regional stretching direction parallel to the Twelve Mile Bay shear zone. While it is possible that the progressive change in stretching direction from Matches Island to PBE Island is constant, the evidence that has been gathered from the outcrops available suggests a bimodal pattern. The stretching direction on Matches Island appears to coincide with the stretching direction of the large sinistral shear zone that are oriented N-S through the center of the island (Fig. 5.9). This observation leads to the hypothesis that the anomalous regional structure and stretching direction found on Matches Island is governed by sinistral motion.

5.2: Shear Zone Geometry

In an effort to understand the seemingly uniformly spaced shear zones found on Matches, PBW and Bartram's islands, individual wall rock panels were analyzed to determine what physical characteristics influence the spacing of shear zones. Bai and Pollard (2000a; 2000b) used the ratio of layer thickness to fracture spacing to characterize fracture saturation in layered rocks, with the caveat that their study entails fractures in sedimentary rocks in the brittle domain. Studies have shown that brittle fractures act as ductile shear zone nucleation sites (Davidson et al., 1994; Mancktelow and Pennacchioni, 2005; Culshaw et al., 2010). This study uses the photomaps of several different areas to measure shear zone spacing and maximum layer thickness to determine whether the fracture (and ultimately shear zone) spacing pattern follows the model advocated by Bai and Pollard (2000a; 2000b).

5.3.1: Methods

The parameters that were necessary to measure to test the fracture/spacing relationship were thickness of wall rock layering, shear zone spacing (measured from center of shear zones), and shear zone thickness. Several measurements of each parameter were made along shear zones from each of the islands to determine any trends regarding shear zone geometry.

The analysis of wall rock geometry used the alternating mafic and felsic layers found at varying scales within the study area as the basis of layer thickness. Wall rock layering thickness was measured by first creating a down-dip image of the outcrop and importing the image into a graphics program (in this case CorelDraw was used, but any graphics program that has a dimensional analysis tool can be used). A baseline was drawn perpendicular to wall rock layering in the middle of the wall rock panel. Layer thickness was then measured using the dimension tool along the base line and recorded in an Excel spreadsheet.

To determine the width of the shear zone, inclination isogons were constructed parallel to wall rock layering strike. Where the wall rock layering deviates more than 10° from the inclination isogon a point was marked. This procedure was repeated for several marker layers along a shear zone. The shear zone boundaries were constructed by connecting the points at which the layering deviated. The spacing of shear zones was measured from the midpoint of one shear zone to the midpoint of the neighboring shear zone, perpendicular to the shear zone boundary.

5.3.2: Results

Layer thickness of wall rock blocks are displayed as frequency plots for each island (Fig. 5.17), the data of which can be found in Appendix B. Matches Island had the most photomap area, which allowed for the results to be viewed in greater detail. Frequency plots of layer thicknesses from different zones within Unit 1 on Matches

Island are shown in Figure 5.17, with the divisions being the same three block model as used previously.

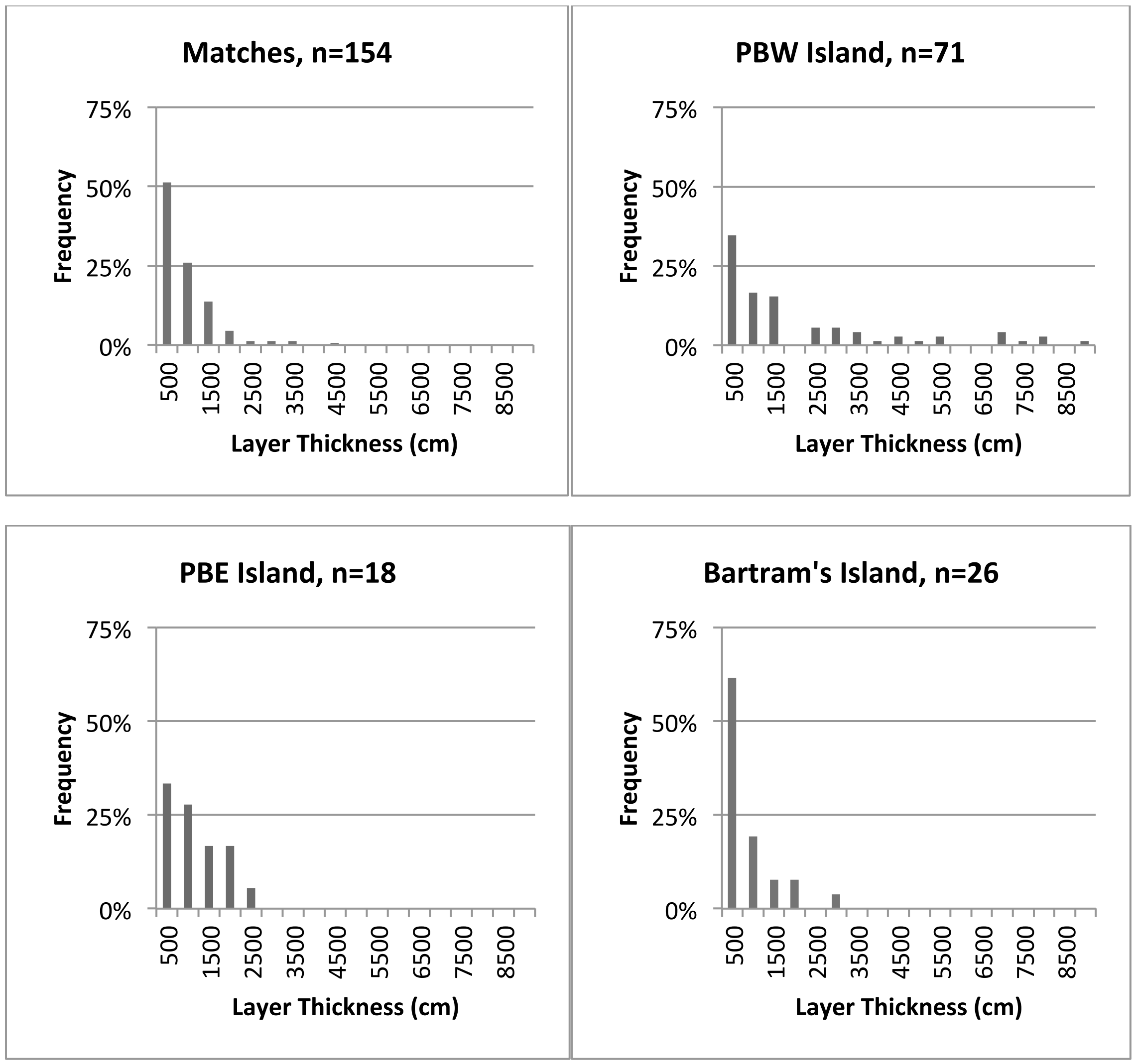

Figure 5.17: Wall rock layer thickness frequency plots. Bin size is 500 cm.

Comparing the wall rock layer thickness frequency charts of each island (Fig. 5.17) it is clear that Matches, PBE and Bartram's islands are made up of packages of comparable layer thickness. All islands show a high concentration of 0 to 1 metre thick layers, and typically do not exceed 3 metres. The outlier of the group is PBW Island, which features a high proportion of layer thickness greater than 3 metres. This pattern can be explained by the presence of two distinct lithological units on PBW Island; Unit 1, a very thickly layered gneiss which is noticeably absent from the other islands; and Unit 2, which is comparable in layer thickness to the other islands.

The results of shear zone spacing measurements are shown as frequency plots and are grouped by island in Figure 5.18. The plots show a wide variance of shear zone spacing island to island and also within islands. Matches and PBE islands both feature one strongly defined peak, while PBW and Bartram's island are bimodal. Despite the variances, nearly all of the plots share a common peak occur at the 3 metre interval.

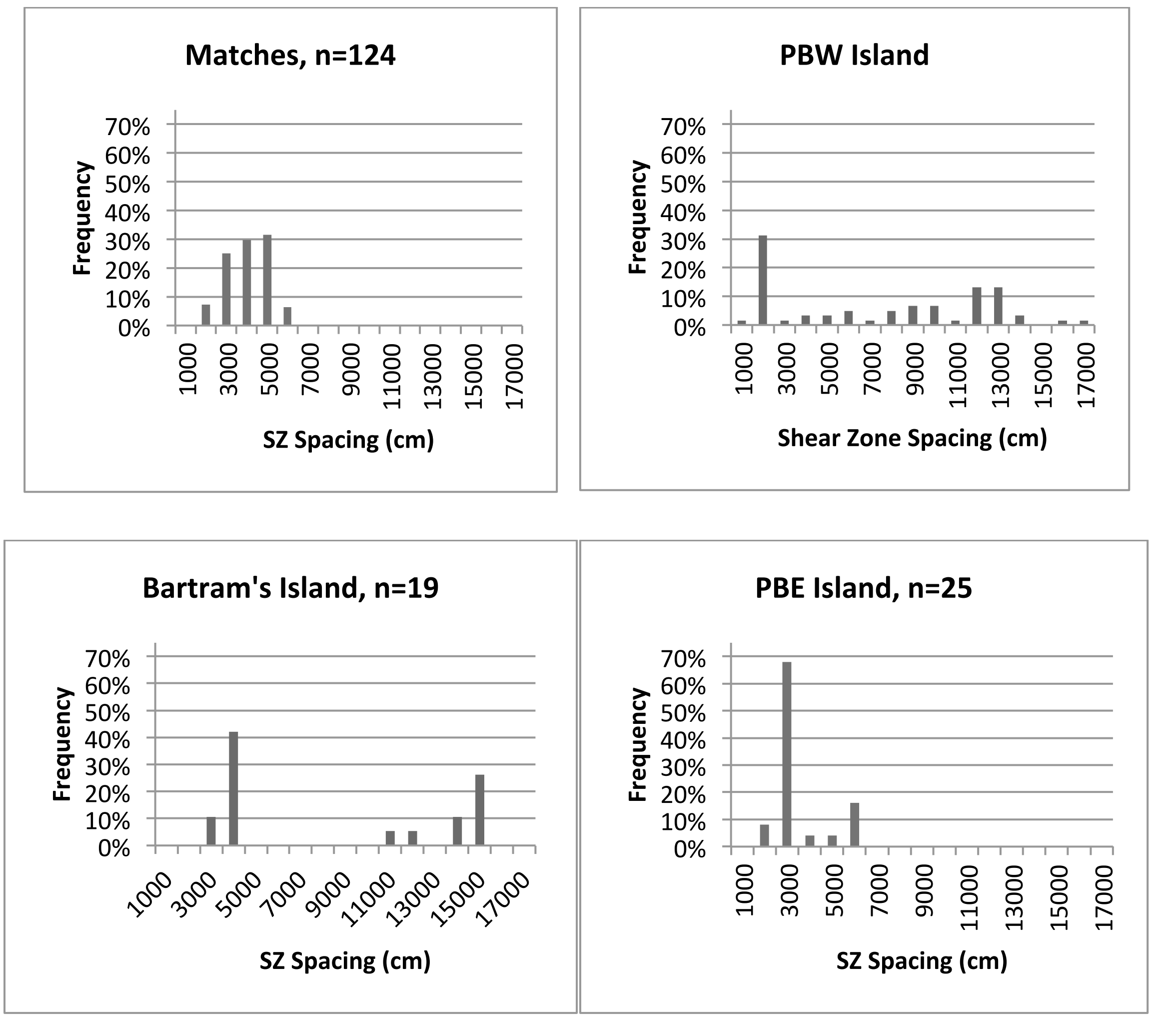

Figure 5.18: Shear zone spacing frequency charts.

5.3.3: Discussion

The aforementioned wall rock layer thickness data was plotted against shear zone spacing to determine if there was a clear relationship between the two. The data were condensed so that one datum represents a single wall rock block, where the average shear zone spacing of that block was plotted against the maximum layer thickness within the same block. The rationale behind this was that the shear zone spacing is generally constant, and so an average would be an appropriate representation.

Plotting the average shear zone spacing against maximum wall rock layer thickness reveals that the thicker the layer, the larger the shear zone spacing (Fig. 5.19). The data have been divided into three groups, undeformed wall rock blocks, deformed wall rock blocks, and anorthosite, with each data point representing a single wall rock block. The data in Figure 5.19 a and b are obtained from measurements taken from various wall rock blocks from Matches, PBW, Bartram's, and PBE islands. The data from Figure 5.19 c are from measurements taken from an anorthosite layer within the Twelve Mile shear zone. The anorthosite layer was included in this analysis as it has a similar geometry observed on Matches Island (i.e. antithetic fractures developed in response to a bulk shear), has a variety of layer thicknesses, but features brittle fractures filled by leucosomes rather than ductile shear zones.

The undeformed wall rock blocks (Fig. 5.19 a) form a strong linear trend (R^2 = 0.8689), and show that the spacing of shear zones increases along with the maximum layer thickness. The deformed wall rock blocks (Fig. 5.19 b) form a much looser cluster than their undeformed counterparts. However, apart from one outlier, the deformed wall rock panels follow the same general trend as the undeformed wall rock blocks. If the outlier is removed, the trend line of the deformed wall rock panels becomes closer to that of the trend line of the undeformed wall rock blocks and the R^2 value changes from 0.0019 to 0.0436. Data collected from the anorthosite pod (Fig. 5.19 c) also form a strong linear trend (R^2 = 0.7955) and follow the same general pattern as the other two analyses.

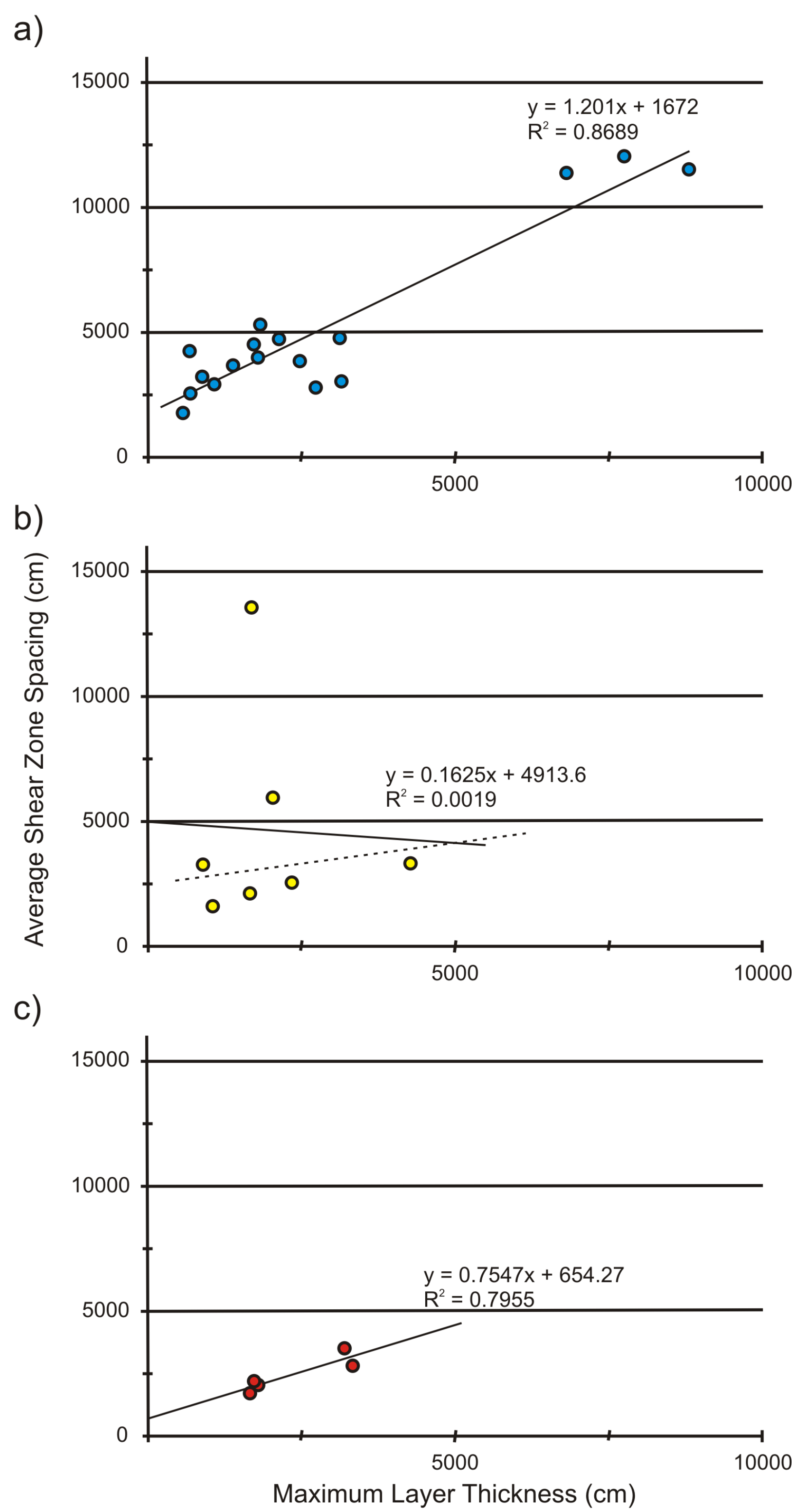

Figure 5.19: Maximum layer thickness plotted against average shear zone spacing of a) undeformed wall rock blocks, b) deformed wall rock blocks, and c) anorthosite unit. Black lines, linear trendlines; dashed black line, trendline with outlier omitted.

The slope of the undeformed wall rock trend line is ~1.2, which would be the average shear zone spacing to layer thickness ratio. Bai and Pollard (2000a) use the ratio of spacing to layer thickness to determine the degree of fracture saturation. Spacing to layer thickness of 1.2 corresponds to the Range I classification, which can be interpreted as the fractures not yet reaching saturation level (Bai and Pollard, 2000a). This leads to the interpretation that brittle fracturing proceeded shearing by a very short time period.

A brief pulse (or pulses) of brittle deformation is unusual at the granulite- to-amphibolite facies, and a possible explanation is melt-enhanced embrittlement. Melt-enhanced embrittlement is a deformation mechanism whereby deep crustal rocks will undergo brittle rather than ductile deformation due to the introduction of melt which increases the pore-fluid pressure and causes rocks to fracture (Hollister and Crawford, 1986; Davidson et al., 1994). In the aforementioned studies, conjugate leucocratic dykes are cited as the nucleation site of shear zones. In this study, the leucocratic dykes can be substituted with pegmatitic dykes that are commonly found within the study area, however there are no clear examples of conjugate pegmatitic dykes.

Interestingly, the data from deformed wall rock blocks and the anorthosite unit form a weak trend line below the undeformed wall rock block data. The trend lines defined by the deformed wall rock and anorthosite data are not strongly linear, and both have slope less than the undeformed wall rock trend line. This pattern indicates that the shear zone spacing becomes narrower relative to the maximum layer thickness with internal deformation of the wall rock block, a result which is not unexpected given that wall rock blocks often undergo layer-parallel shortening. The introduction of wall rock deformation is where the ductile fractures and subsequent shear zones discussed in this work differs from the brittle fractures discussed in Bai and Pollard (2000a).

Many studies on the evolution of shear zones also indicate a decrease in spacing between shear zones until they eventually merge together (Carreras, 2000; Fusseis et al., 2006). It is then not surprising that deformed wall rock blocks become significantly more closely spaced than the undeformed wall rock blocks for layers of equal thickness. The data produced in this study suggest that the spacing of amphibolite facies pegmatite cored shear zones is determined by the maximum layer thickness via fracturing systematics.

5.3: Expected displacement of shear zones

The rotational patterns of trains of wall rock blocks described on Matches Island are strikingly similar to the 'domino' or 'bookshelf' style faulting, which have been noted previously in other high strain brittle regimes (Mandl, 1984; Harris, 2003; Ponce et al., 2013). Bookshelf style structures are characterized by the development of antithetic displacements that form at a high angle to the bulk strain direction (Fig. 5.20).

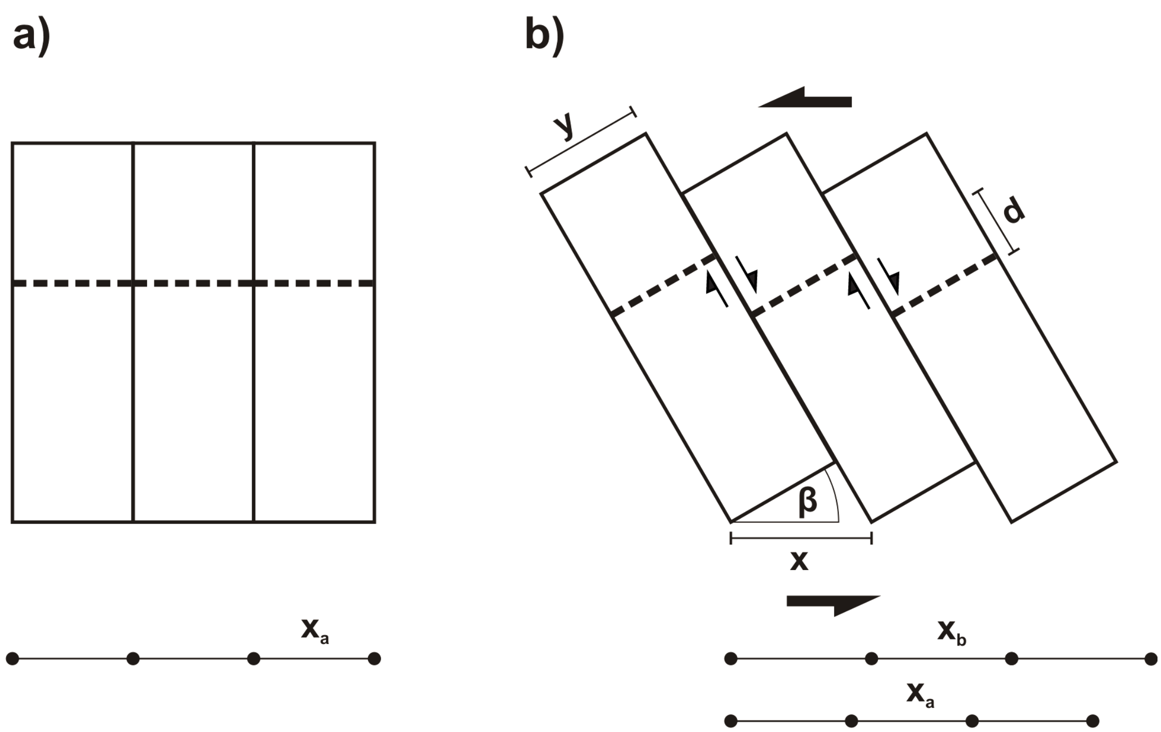

Figure 5.20: Ductile bookshelf conceptual model. **a)** Undeformed state with pre-existing lineaments and **b)** after a sinistral shear strain. y, shear zone spacing; x, wall rock marker point distance; d, displacement, β, wall rock rotation; dashed line, displacement marker layer.

In studies of poly-phase deformation it is imperative to demonstrate timing relations. Analyzing strain along antithetic shear zones can be used as a proxy for such timing relations by determining how much shear strain was due to simple rotation, and how much shear strain was independent of rotation. The model presented consists of wall rock blocks subjected to a sinistral rotation, as expected in a broad sinsistral shear zone such as Block B, resulting in antithetic dextral shear zones (Fig. 5.20). The ductile bookshelf model provides a possible explanation for the rotation of wall rock layers and shear zones, as well as the anomalously high shear strains found within the core of Matches Island. Furthermore, the bookshelf model can be used to calculate how much displacement would occur along slip planes (i.e. in this case, shear zones) given a finite rotation. This 'expected displacement' for a finite rotation can then be compared with displacements measured in natural shear zones using the photomaps. The comparison between the two displacements can be used to test the hypothesis that dextral shear zones on Matches Island are antithetic shear zones that formed due to rotation within the sinistral shear zone of Block B.

5.3.1: Methods

The model set up is shown in Figure 5.20, where a series of blocks undergo increasing amounts of anticlockwise rotation in response to a bulk sinistral shear. In the model set up the blocks rotate around the bottom left node of each wall rock block, which remains in contact with the rotational boundary. There are three key parameters that are used to determine displacement; angle of wall rock rotation (β); width of wall rock block (y); and the width of the interface between the lower left nodes of the wall rock blocks (x).

The geometric relationship of wall rock rotation, shear zone spacing, and expected displacement is expressed in equation (vii):

$$d = y(\tan(\beta)) \qquad \text{(vii)}$$

where d is displacement, y is the width of the wall rock block, and β is the rotation of the wall rock block. Using this expression, a graph was produced for a range of wall rock block widths showing how d changes with respect to β (Fig. 5.21). The graph shows that wider wall rock blocks will have greater displacement than a thinner wall rock block under the same rotation.

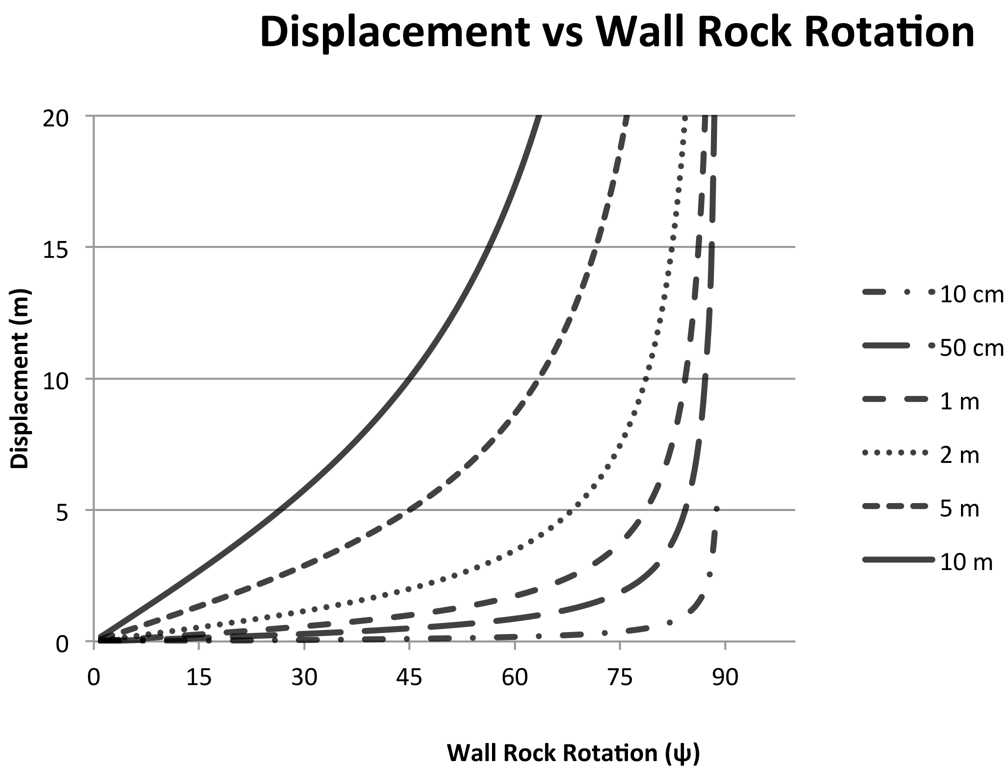

Figure 5.21: Displacement curves for various shear zone spacings. The curves clearly show that the displacement will increase for a greater block widths under the same rotational conditions.

The key model parameters were collected from natural shear zones using the photomap of Matches Island. The rotation of wall rock layering was measured using the angle between wall rock layering immediately adjacent to the shear zone segment and unrotated wall rock layering on the island to the southeast of Matches Island (Fig. 4.6, Unit 3).

5.3.2: Results

The results of the expected displacement calculations are displayed in Table 5.7, along with measured displacement, wall rock block width and wall rock rotation from the same shear zone segment. The results are also broken down by zones and displayed on the graph in Figure 5.22.

Table 5.7: Measured displacement results for Matches Island shear zones. See Figure 5.6 for shear zone locations. Expected displacement calculated using eq. (vii), measured displacement used from displacement-width strain analysis (Appendix C).

SZ ID	Rotation	SZ Spacing (m)	Exp. Disp (m)	Meas. Disp (m)
1a	35	4.29	3.00	1.76
1b	38	5.22	4.08	3.94
2b	55	4.29	6.12	2.85
2c	79	3.35	17.25	2.19
4a	68	5.93	14.67	6.67
5a	62	1.40	2.64	5.85
2e	115	5.85	12.54	5.07
2g	93	4.37	83.32	12.37
4b	51	4.29	5.30	7.73
4c	102	4.44	20.91	17.23
4d	98	6.08	43.27	15.23
5b	95	2.11	24.06	5.45
5c	81	2.50	15.75	6.76
6a	84	2.18	20.77	2.16
6b	98	2.50	17.75	10.19
6c	91	3.59	205.48	8.17
7c	83	2.57	20.96	8.39
8b	56	4.60	6.82	11.67
7d	48	5.22	5.80	4.79
7e	50	6.08	7.25	6.04
8d	42	3.12	2.81	19.04
13a	68	4.37	10.81	2.62
12b	54	2.42	3.33	3.38

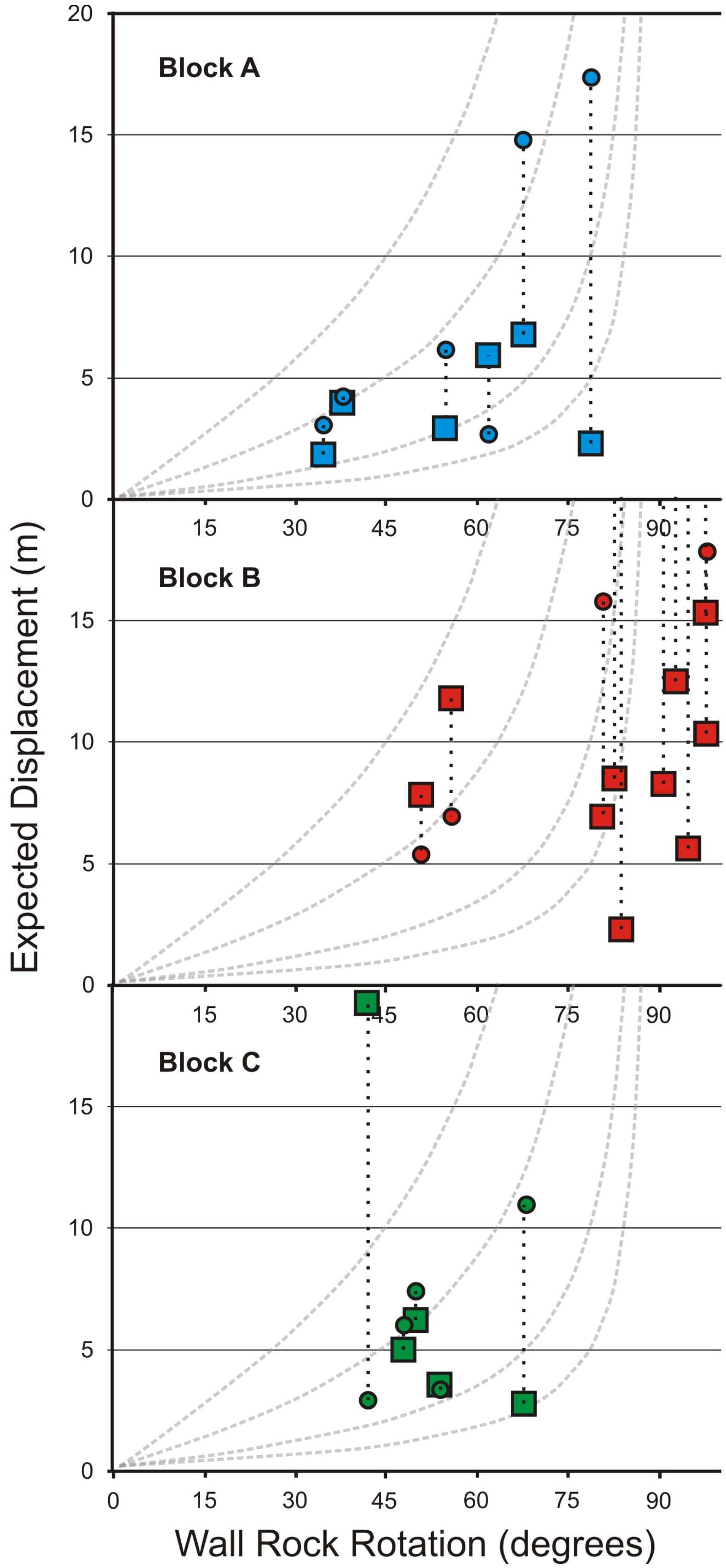

Block A
Block B
Block C
Expected Displacement (m)
Wall Rock Rotation (degrees)
0
5
10
15
20
0
15
30
45
60
75
90

Figure 5.22: Comparison of measured displacement with model calculated displacement results for Matches Island. Squares, measured displacement; circles, model calculated displacement; black dashed lines, tie lines of paired results; grey dashed lines, curves of various shear zone spacing.

A comparison between the expected displacement results with measured displacements from the same shear zone segment tests the accuracy of the ductile bookshelf model. The results are mixed in this respect; with many shear zone segments featuring lower values of measured displacement than the expected displacement for the measured rotation and spacing width. The shear zone segments that have a larger degree of rotation often grossly overestimate the expected displacement with respect to the measured value. Such overestimations indicate that there was either displacement that occurred prior to rotation (in the case of larger displacement than expected), or body rotation without slip (in the case of smaller displacement than expected).

5.3.3: Discussion

The results of expected displacement compared to the matching measured displacement value are ambiguous. The expected displacements calculated for shear zone segments featuring wall rock rotation of less than 60° closely matched the measured displacements. Shear zone segments that had undergone rotation of 60° or more showed much more variation, and commonly overestimates displacement by double or treble the measured value.

The majority of the shear zone segments that have experienced greater than 60° of rotation are located within Block B. As documented qualitatively in the Matches Island Structure chapter and quantitatively within the strain analysis of Matches Island, Block B is the area where the internal deformation of wall rock blocks is most prevalent. This is an important point to consider, as the simple block model does not account for a dynamic geometry, such as stretching along dextral shear zones or internal deformation of wall rock blocks.

Due to the poor results of expected displacement for wall rock blocks of high rotations, the ductile-bookshelf model needs to be refined. However, the results of expected displacement for wall rock blocks rotated less than 60° were similar to the measured displacements. Therefore, we propose that the ductile-bookshelf model operates as originally outlined until wall rock rotations reach 60° from the original wall rock orientation. Upon reaching this critical angle, additional mechanism(s) to lengthen the wall rock block and dextral shear zones in the stretching direction must begin instead of, or in addition to ongoing slip along dextral shear zones. Possible deformation mechanisms include stretching along dextral shear zones, folding of wall rock blocks, passive non-body rotation, volume change, and the introduction of pure shear.

Internal deformation of wall rock blocks is well documented in the structural outline of Matches Island in Chapter 4, and is shown to be concentrated in Block B. Block B features localized boudinaged wall rock blocks that indicate stretching towards the bulk sinistral shear zone direction. And if there is stretching present within wall rock blocks, then there must also be stretching within dextral shear zones to maintain strain compatibility or there must be some volume loss and strain partitioning between the wall rock and shear zone. In addition to wall rock/shear zone stretching, the majority of drag folds observed in Unit 1 of Matches Island are located in Block B.

The evidence for wall rock deformation within Block B and subsequent lack of wall rock deformation outside of Block B indicates a significant change in deformation style. These observations coupled with the accuracy of the expected displacement results for wall rock blocks of low rotation angles leads us to the conclusion that the change in deformation style switches from a simple ductile bookshelf model to a more dynamic geometry in Block B. The dynamic geometry model introduces localized stretching in the wall rocks and shear zones, as well as buckle folds within wall rock layering. Slip may also continue along dextral shear zones.

In the preceding results, the values of expected displacement were found to be generally higher than the values of measured displacement. There was one notable outlier to this trend; shear zone segment 8d within Block C shows a measured displacement significantly larger than the calculated expected displacement. This particular shear zone has been found to have large magnitudes of shear strain (Fig. 5.5), and is a major shear zone on Matches Island, as it is one of the only examples of a shear zone which can be traced offshore.

One possible explanation for the discrepancy between the measured and expected displacement for this shear zone segment is that this dextral shear zone pre-dated sinistral deformation (Fig. 5.23). In this case, a dextral shear zone would nucleate along a pegmatite (Fig. 5.23 b). This displacement would intensify with sinistral deformation in a manner similar to other dextral shear zones, causing the expected displacement to be much lower than the measured displacement (Fig. 5.23 c). The arrangement and timing of shear zones in Figure 5.23 results in a higher measured displacement of shear zone 2 than the expected displacement using the ductile bookshelf model. Field observations support this relative timing as sinistral shear zones have been observed cross-cutting dextral shear zones in the field, but not the other way around.

D_1 in Figure 5.23 could caused either be an early dextral shear zone of the Matches Island shear zone system, or an inherited shear zone that is unrelated to the Matches Island shear zone system and reactivated.

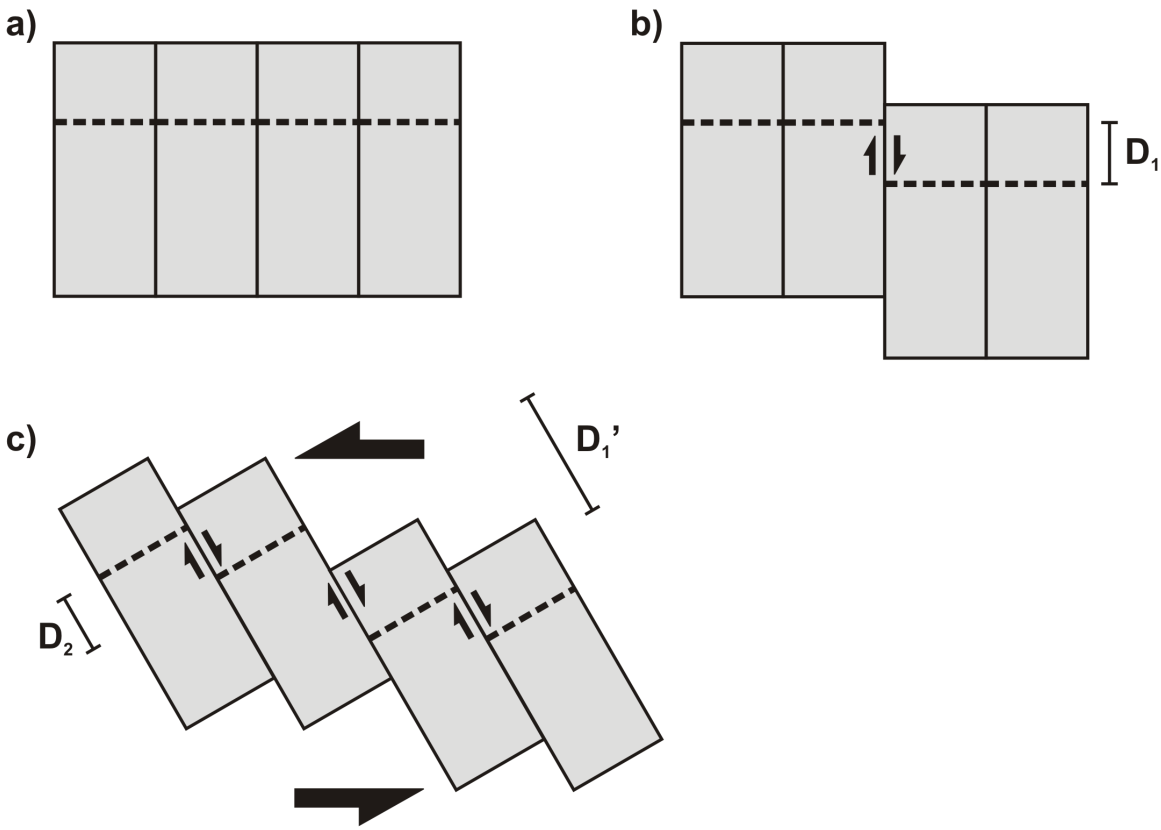

Figure 5.23: a) Initial undeformed model set up. **b)** A dextral shear zone activates along a slip plane prior to sinistral deformation, resulting in the offset marker D_1. **c)** Sinistral deformation results in additional antithetic shear zones that form dextral offsets (D_2), as well as the intensification of displacement along the pre-existing shear zone causing D_1 to become D_1'. Shear zone spacing is 2 m, and rotation is 30°. The spacing between the blocks is strongly dependent on the maximum layer thickness.

CHAPTER 6: DISCUSSION

6.1: Introduction

In the following sections, conceptual models are presented to explain the structural evolution of each island, as well as the regional-scale shear zone network as a whole. The model takes into consideration structural data, such as foliation and fold hinge data, as well as shear strain and volume loss estimates. The models are intended to document how the method of transposition can vary within the same system given changes in key parameters such as strain, initial orientation of anisotropy and thickness of previous anisotropies, and rheology.

6.2: Fold interpretation

Throughout the structural study of Matches, PBW, Bartram's, and PBW islands four distinct types of folds were identified: lobe, scar, buckle folds, and shear folds. All of which are passive folds, with the exception of buckle folds.

Lobe folds are passive folds that form when thinned wall rock layering near a shear zone boundary is deflected around more competent material, usually an amphibolite block. Lobe folds are commonly observed to deform S_1 layering and are often found adjacent to wall rock blocks that bounded by a pair of shear zones (Fig. 6.1).

Scar folds are open passive folds that appear to be flow features of shear zone foliation (S_2) with the shear zone foliation filling in spaces between wall rock blocks that have been pulled apart by extension, similar to a boudin neck. Scar folds are commonly observed between competent mafic blocks in zones of highly rotated wall rock blocks.

Buckle folds develop in wall rock blocks with strong mechanical anisotropy, and can be identified by the variation of wavelength to layer thickness. In some cases buckle folding can be demonstrably proven, but often buckle folding is suspected but unable to be proven due to not having a fully developed wavelength or lack of layers of different thickness.

Shear folds are the reworking of any of the aforementioned fold types in shear zones, and are characterized by pre-existing lineations deformed into a great circle pattern in response to deformation and tight-to-isoclinal fold geometry.

6.2.1: Matches Island

Matches Island features passive folding and features lobe, scar, and shear folds. There are also examples of buckle folds on Matches Island, but demonstrable buckle folds are rare and only found in wall rock blocks that display a variation of layer thickness. Figure 6.1 takes a close up look at the variety of folds found on Matches Island within Unit 1.

Tight to isoclinal shear folds are observed within shear zone foliation, but are likely from the reworking of buckle folds. Isoclinal folds within shear zones have been interpreted to represent the tightening of an open buckle fold formed during strong deformation of folded wall rock blocks (Culshaw et al., 2005; Carreras, 2005). Whether a fold is tightened or unfolded by shearing depends on a number of factors such as sense of movement, pre-shear orientation of panel layer, shear plane orientation, and vorticity (Carreras, 2005).

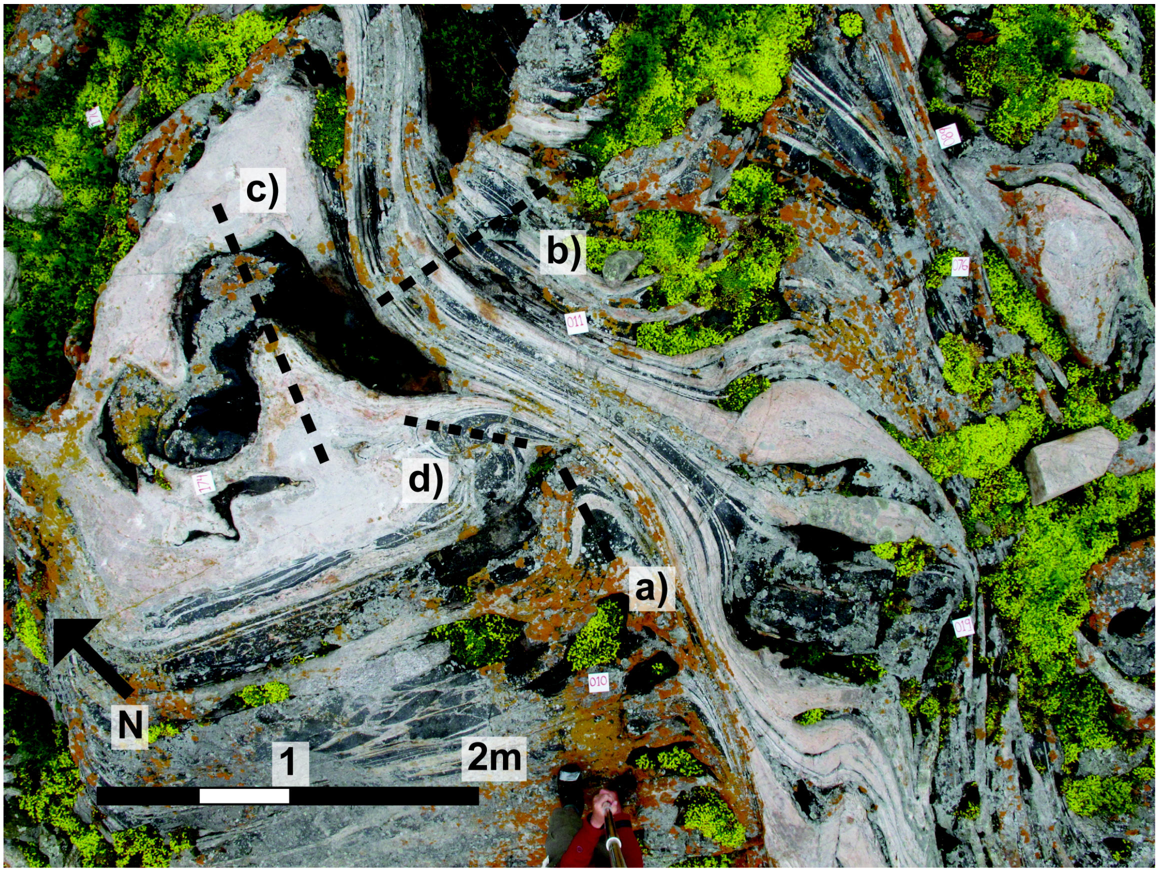

Figure 6.1: Examples of folds within Unit 1 on Matches Island, with axial traces of folds indicated by the dashed black line. **a)** A lobe fold forming as wall rock layering is folded around a competent amphibolite layer on the way into the shear zone. **b)** A weakly developed scar fold forming perpendicular to **c)** a large amplitude buckle fold within a felsic layer as shear zone merge to the south.

Lobe, scar, and buckle folds share a clear spatial association and it is likely they are part of the same system, as the rotating wall rock blocks will experience compression and extension. However, buckle folds are much more common and it appears that lobe and scar folds require the presence of large blocks of competent material to achieve the rheological contrast and/or mechanical anisotropy required to induce passive folding (Carreras, 2005).

The broad sinistral shear zone on Matches Island causes rotation of wall rock blocks, which introduces compression in the WNW direction and extension in the NNE direction. Folds subsequently form under these conditions, with buckle folds forming in layered wall rock and drag folds forming in the shear zone foliation. The deforming and extending wall rock blocks leave a space to be filled within the boudin necks, which are filled by sheared material and show a deflection of shear zone foliation Forming scar folds. These demonstrate that dextral shear zones and adjacent wall rocks are stretched during sinistral shearing and rotation.

6.2.2: PBW Island

PBW Island features lobe and scar folds, although scar folds are rare and are restricted to the massively layered wall rock blocks of Unit 1 (Fig 6.2). Buckle folds are by far the most common folds observed on PBW Island, especially in the thinly layered Unit 2. Buckle folds are similar in orientation to lobe folds found in wall rock blocks, with the axial trace of both fold varieties forming approximately parallel to bounding shear zones. However, buckle folds can be differentiated from lobe folds due to wavelengths varying with the thickness of the folded layer.

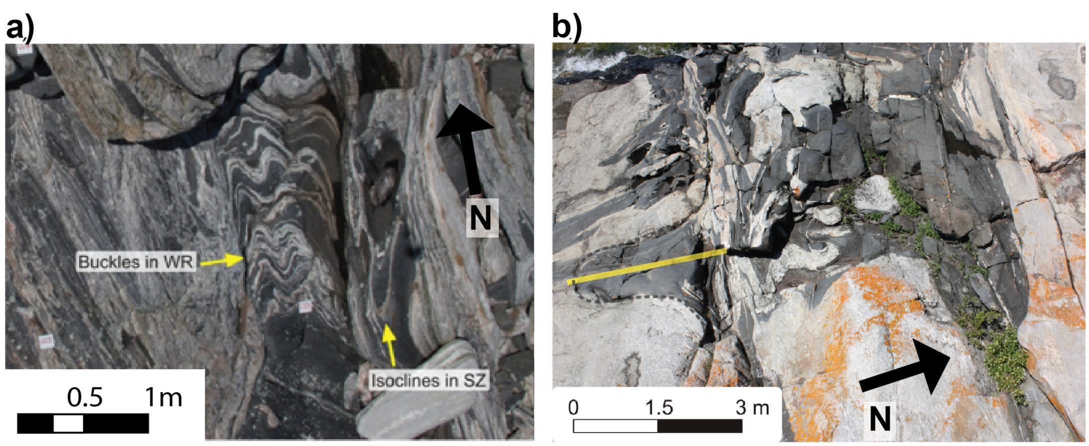

Figure 6.2: Examples of folds on PBW Island. Yellow line, axial trace; black dashed line, fold form line. **a)** Buckle folds form within Unit 2 wall rock layering. **b)** Scar fold developed in massively layered wall rocks of Unit 1.

Buckle folds in PBW commonly develop in wall rock layering between closely spaced shear zones in both Unit 1 and 2. In the photomap area of Unit 1, open buckle folds show both s- and z-fold asymmetries, however the s-fold asymmetry is much more common. Buckle folds in the photomap area of Unit 2 are much tighter than their Unit 1 counterparts with interlimb angles approaching 30°, with distinct z-fold asymmetries.

Buckle fold axial traces form approximately parallel to shear zone foliation and perpendicular to the regional shortening direction.

Buckle folds are more common in the thinly layered Unit 2, where buckle folds with sinuous open to close folds with centimeter-scale amplitudes form in wall rock layering. Buckle folds are observed in either wall rock blocks that have centimeter-scale felsic layering, or close to shear zone merges (Fig. 6.2). The orientations of buckle folds form in roughly the same orientation, or are rotated into the same direction as lobe folds, with fold hinges approaching 080-30 and axial planes approximately parallel to the shear zone foliation.

Isoclinal shear folds within shear zones are common in both Units 1 and 2 on PBW Island typically occur on the sheared margins of wall rock panels and within shear zones themselves. Isoclinal shear folds form by the tightening of either lobe or buckle folds as deformation becomes more pervasive.

6.2.3: Bartram's Island

The outcrops studied on Bartram's Island feature folded wall rock blocks with a wide variety of hinge orientation, fold asymmetry, interlimb angle, and wavelength. There are also clear examples of wall rock folds being reoriented and tightened with proximity to shear zones; therefore Bartram's Island is an excellent case study on fold evolution within the Twelve Mile Bay system.

Bartram's Island features open, low amplitude buckle folds within wall rock blocks, with fold hinges plunging shallowly to the NW. Buckle folds show variably strong fold asymmetries, with both 's' and 'z' fold asymmetries present, examples of which are common in Outcrop B (Fig. 4.28). Buckle folds within wall rock blocks are differentiated from lobe folds by observing the variation of wavelength with layer thickness, as the buckle fold hinges cannot be distinguished from lobe folds based on fold hinge orientation. Buckle folds are observed as symmetrical, open, low amplitude folds.

Shear folds are commonly observed within shear zones, with the interlimb angle of the fold generally decreasing with proximity to the shear zone core. Shear folds are deformed lobe and buckle folds, and show a wide variety of fold hinge orientations and fold geometries as they are interpreted as being a transitional phase between a wall rock fold and an isoclinal shear zone fold. Isoclinal fold hinge data show a strong cluster around a common direction 080-20 representing the regional hinge orientation of the Twelve Mile Bay shear zone.

Bartram's Island features the clearest examples of how folds develop in wall rock blocks and are reworked by shear zones, and therefore is the ideal case study to understand fold evolution. Fold hinge data has been divided into three categories based on their fold tightness; (i) open-close folds, (ii) tight folds, and (iii) isoclinal folds.

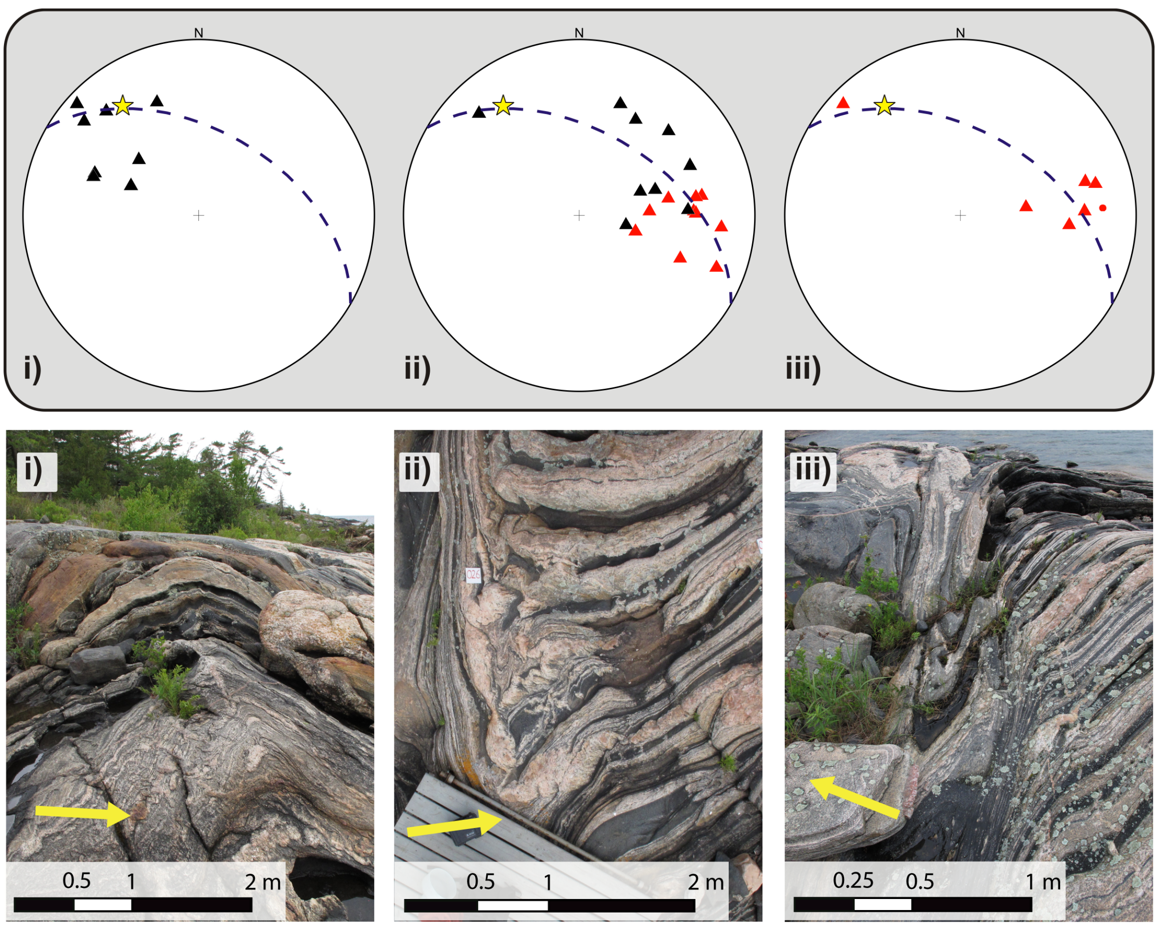

Figure 6.3: Lower hemisphere equal area projections for different types of fold hinges; i) open-close folds, ii) tight folds, and iii) isoclinal fold hinges. Black symbol indicates wall

rock, and red symbol indicates shear zone. Field photos are examples of each hinge class.

Open-close folds are considered to be the earliest stage of fold development on Bartram's Island, expressed as lobe and buckle folds within wall rock blocks. Outcrop A preserves open folds as well as tight folds. The hinge orientations, of which can be used to understand how the folds behave upon entering a shear zone. On a stereonet open-close fold hinges cluster around a common point at 310-30, indicating a cylindrical fold shape (Fig 6.3).

Tight folds are a transitional stage in fold development between the open-close folds and isoclinal folds, and are located on the boundary of wall rock and shear zone. Tight folds begin to become asymmetrical, reflecting their progressive deformation, with examples of both 's' and 'z' asymmetries. The fold hinge data of tight folds have a large spread, reflecting their state in progressive reorientation, but loosely cluster along the great circle that represents the local shear zone orientation (Fig 6.3 ii).

Isoclinal folds are limited to the cores of shear zones and are formed by the tightening and reworking of pre-existing folds incorporated into the shear zone. The isoclinal fold hinge data cluster around a common direction of 080 -20 (Fig 6.3) with the exception of an outlier.

Figure 6.3 illustrates the origin and subsequent fate of folds on Bartram's Island. The initial shallowly plunging open buckle folds are formed within wall rock blocks with the introduction of shear zones, likely in the fold system described for Matches Island. As shear zones progressively grow and incorporate wall rock within them, wall rock folds begin to deform. Interlimb angles decrease yielding tighter folds and fold asymmetries begin to arise. Fold hinges are reoriented towards the preferred direction (~080-20), while the axial planes rotate from near vertical to parallel with the shear zone foliation. Finally, when a fold is fully incorporated into a shear zone the fold has tightened up into an isoclinal fold. The resulting fold hinge of the isoclinal folds within shear zones are now reoriented into the regional extensional direction, 080-20.

6.2.4: PBE Island

With shear zone foliation now being the dominant fabric, folds are predominately tight –to- isoclinal shear zone related folds with hinges plunging shallowly to the northeast. There is still some variation in shear zone fold hinge orientations. The central island outcrop features a thick shear zone that borders the southern margin of the wall rock panels and contains several examples of shallowly plunging isoclinal folds within shear zones as well as moderately plunging folds. Northwest plunging folds commonly display s-fold asymmetries and form ridge-like hinges.

Within this zone, there is an area of tightly folded wall rock with moderately plunging fold hinges. These folds transition into folds with low–plunging hinges that have been rotated into the shear plane. The doubly-plunging nature of this fold system could either represent a later refolding event, sheath folds, or more likely, a unique stage of fold hinge reorientation due to a less common initial fold geometry.

6.2.5: Summary:

The evolution of folds within the Twelve Mile Bay shear zone system begins with buckle and lobe folds in a near simple shear setting, with rare scar folds forming in specific settings. As the system develops, higher shear strains, likely along with a pure shear component, wall rock folds are reworked by shear zones, resulting in isoclinal shear folds within in the cores of shear zones as well as the reorientation of fold hinges. The presence of isoclinal folds within a shear zone often represents the thickening of the shear zone by the assimilation of folded wall rock (Carreras et al., 2005).

6.3: Effect of anisotropy

Shear zones in anisotropic materials have been studied (Culshaw, 2005) and modeled extensively (Pennacchioni & Mancktelow, 2007; Carreras et al., 2013), and show high degree of complexity. Mechanical anisotropies under ductile strain leads to buckle folding and strain partitioning. Consequently, anisotropy plays a significant role in the structural architecture of the Zone of Reworking, where buckle folding is common and strain partitioning is likely, and from the results of this study, anisotropy dictating shear zone geometry.

Qualitatively, it was observed that there was a stark contrast in the scale of shear zone and wall rock blocks from PBW Island Unit 1, and the other islands. This study quantitatively demonstrates how layer thickness effects fracture, and by proxy, shear zone spacing. Shear zone spacing increases with an increase in maximum layer thickness of a wall rock block. Using Bai and Pollard 's (2000a) study on fracture spacing as a guide, fractures may have not yet reached saturation. As a result, brittle fracturing, as observed on Teddy Rock, must have happened over a short period of time, possibly by melt-enhanced embrittlement (Hollister and Crawford, 1986).

In the block model of bookshelf style faulting that is hypothesized as present on Matches Island the shear zone spacing is shown to have an effect on shear strain in antithetic dextral shear zones. If the findings regarding layer thickness affecting fracture spacing are correct, then layer thickness also plays a role in determining shear strain in these specific shear zones.

6.4: Absence of a stretching lineation

The lack of a stretching lineation or any notable elongate shape fabrics within individual shear zones within the Twelve Mile Bay shear has long been a problem. This problem is not limited to this study area, but has been well documented in shear zones that display an oblate strain fabric (Baird and Hudleston, 2007). The lack of an elongate strain fabric can be explained by three possibilities: i) volume loss; ii) localized flattening of shear zones; or iii) overprinting of a pre-existing strain fabric.

The removal of material from within the core of a shear zone by syn-kinematic fluids has been cited as the mechanism that produces oblate strain fabrics (Ring, 1999; Mohanty and Ramsay, 1994; Baird and Hudleston, 2007). The result of volume loss should lead to an oblate strain ellipsoid, and could explain the absence of a stretching lineation within a shear zone.

Shear zones typically show chemical variations from their country-rock due to providing a conduit for metamorphic fluids to travel through. This scenario has lead to many studies to quantify the amount of volume loss by using geometry (Mohanty and Ramsay, 1994), geochemistry (Grant, 1986; Ring, 1999), or the combination of the two (Srivastava and Hudleston, 1995; Baird and Hudleston 2007). It has been shown that shear zones can undergo extreme changes in volume, with reported losses of more than 50% are common throughout the literature (Mohanty and Ramsay, 1994; Srivasta and Hudleston, 1995; Baird and Hudleston 2007).

The isocon method (Grant, 1986) major element concentrations from wall rock and shear zone samples are constructed are plotted against one another and to identify the components that have remained immobile during deformation. The assumption is that some components will behave differently whilst undergoing a volume change. A line of best fit is constructed along the immobile elements and relative gains and losses in volume are determined by deviation from the best-fit line. Marsh et al. (2011b) produced two isocon charts of chemical data collected within wall rock and an adjacent shear zone on Matches and PBW Island, both of which show an isocon best fit line with a slope of ~1, indicating low mobility of elements along the line. The results of the isocon plots suggest that shear zones both on Matches and PBW islands have not undergone any significant change in volume.

6.5: Structural evolution

Several conceptual models have been proposed to explain the structural evolution of each island, as well as the regional-scale shear zone network as a whole. The models take into consideration structural data, such as foliation and fold hinge data, as well as shear strain and anisotropy. The models are intended to document how the method of transposition can vary within the same system given changes in key parameters such as strain, orientation and thickness of previous anisotropies, and rheology.

6.5.1: Matches Island conceptual model

The conceptual model for Matches Island that takes into account the kinematics and geometry of observations made in the field. The Matches Island shear system is interpreted as a large-scale sinistral shear zone that amplifies displacement along pre-existing dextral shear zones, and triggers the initiation of smaller-scale antithetic dextral shear zones. Opposing shear zones developed synchronously rather than a late sinistral overprint of earlier dextral shears. The earliest evidence of shear zones are mm-scale pegmatite filled brittle fractures with weak shearing showing dextral motion (Fig. 4.4), but the model suggests that the fracturing and subsequent dextral motion is in response to bulk sinistral kinematics. Our model closely resembles the geometry of Matches Island (Fig. 6.4), and can provide explanations for many of the features observed.

We begin with undeformed block of granulite facies interior Parry Sound domain with steeply dipping NNE striking layering and down-dip mineral lineation (Fig. 6.4 a). An initial deformation begins to affect the granulite facies block causing fractures to develop within the granulite facies block, approximately at right angles to interior Parry Sound domain layering (Fig. 6.4 b). With continued sinistral shear the fractures develop into continuous ~50 cm thick, regularly spaced planar features (Fig. 6.4 c).

Sinistral shearing causes a zone of both wall rock layering and pegmatite to be rotated anticlockwise. To maintain strain compatibility the rotated zone must accommodate some of the sinistral deformation while keeping the wall rock layering undeformed to both satisfy the assumption of simple shear as well as field observations. It has been well documented that the introduction of pegmatite fluid initiates retrogression reactions within the granulite facies block, forming amphibolized margins around pegmatites (Culshaw et al., 2011; Marsh et al., 2011a). The introduction of fluid into dry a granulite facies block also has implications on the rheology. Gerbi et al.'s (2010) two-phase viscous numerical models of natural shear zone and wall rock geometries show that an order of magnitude of weakening is required to develop the observed shear zone network geometry. With this in mind, it is the pegmatites that act as planes of weakness and accommodate strain resulting in antithetic dextral shear zones (Fig. 6.4 d).

However, there is a space problem that occurs on the margins of the rotational boundaries during sinistral shearing. Strain compatibility is maintained by two possibilities that can work in tandem, or independently of one another. The first option is that the wall rock accommodates strain by folding, while the second option is that concordant granitic layers that commonly form along rotational boundaries are fed by pegmatites and are syn-kinematic. The first option of folding wall rock near these rotational boundaries is demonstrable, as seen in Figure 4.11, while the second is more speculative as there are no clear cross-cutting relations to relatively date the concordant granitic layers.

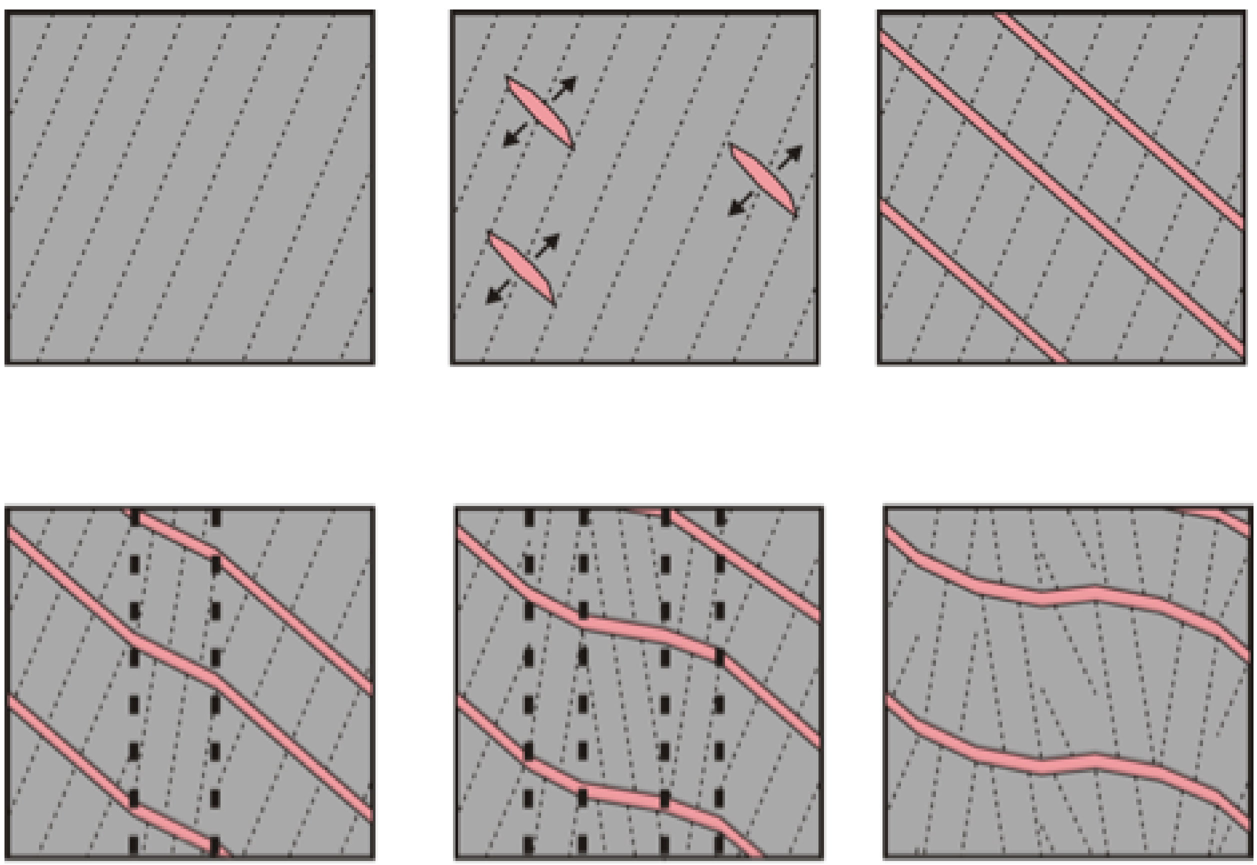

Figure 6.4: Conceptual model of the structural development of Matches Island. **a)** Undeformed iPSD layering. **b)** NE extension initiates extensional pegmatite-filled fractures that form at a high angle to iPSD layering. **c)** Continued NE extension sees the

development of continuous planar pegmatite-filled fractures. **d)** N-S sinistral shearing rotates wall rock layering, and initiates antithetic dextral shearing along pegmatites layers. **e)** Development of N-S sinistral shearing forms several packages of rotated wall rock, with rotation and strain increasing towards the center of the sinistral shear zone. **f)**

These rotational bounds are also prone to developing discrete en echelon sinistral shear zones at the same scale as dextral shear zones. The discrete sinistral shear zones typically form along concordant granitic layers or felsic layering parallel to the master shear zone. Shearing affects nearby folded wall rock showing thick/thin limb relations.

As sinistral shear continues a portion of wall rock rotates anticlockwise. To accommodate this rotation the pegmatites act as slip planes forming weakly developed dextral shear zones along them. Such a rotation causes a space problem at the rotational boundaries, which can be attributed to sinistral shearing and subsequent rotation to make space and concordant granitic layers to infill vacated space.

With increased strain more zones of rotated wall rock panels will form, with discrete sinistral slip occurring along rotational domain boundaries. We infer that these discrete sinistral shears nucleate on concordant granitic layers. The resulting strain pattern of our conceptual model is comparable with the natural strain patterns for calculated shear strain on Matches Island.

6.5.2: Bartram's area conceptual model

PBW, Bartram's, and PBE islands all share the same basic structural characteristics, with minor variations unique to each island. Therefore, the conceptual model presented here represents all three islands, which will be referred to collectively as Bartram's area conceptual model. The Bartram's area conceptual model is a continuation of the Matches Island model, as the islands are likely points on a continuum. The shear zone system observed in the Bartram's area consists of predominantly NW-SE trending dextral shear zones with wall rock layering appearing approximately orthogonal to shear zone foliation. The wall rock layering is locally weakly deformed by buckle folds and wall rock is segmented into lozenges. The major differences from Matches Island are the change of shear zone trends, commonly deformed wall rock blocks/lozenges, and locally on PBW Island, the presence of a massively layered unit further complicated by the presence of mafic dykes.

As PBW Island is situated on the margin of the TMB shear zone, its structure is reflective of a higher strain regime than Matches Island. In this 'gap' between Matches Island and PBW, the whole system is rotated counterclockwise, as evidenced by the now NE-SE striking wall rock foliation and the shear zones approaching parallelism with the regional scale TMB shear zone. This clockwise rotation is compatible with the Matches Island conceptual model, as broad sinistral shearing can induce counterclockwise rotation.

During this phase of rotation shear zones are intensified, with greater values of shear strain, become more sinuous, and greater degrees of wall rock deformation. It is with the increased deformation of wall rock that shear zones can begin to merge and dissect wall rock blocks, forming large shear interconnected shear zone networks.

6.6: Relative timing of shear zones

It is clear from numerous field observations that sinistral shear zones overprint dextral shear zones. There are two distinct possibilities regarding the genesis of the two sets of shear zones, i) they formed in two distinct deformation events, or ii) they formed synchronously as conjugate pair with the sinistral shear zones being the dominant set.

In the former scenario, immediately following brittle fracturing and pegmatite-emplacement a deformation event occurred resulting in WNW striking dextral shear zones. Initial dextral shear zones are low strain, with examples from Teddy Rock (Chapter 4.2) commonly showing cm-scale displacement. However, there are outliers, with rare meter wide, high strain dextral shear zones occurring at neighboring islands to Teddy Rock (Culshaw, personal communication, 2019). A second deformation event initiates sinistral shear zones at a high angle to the dextral set and overprint them. As shown by the ductile bookshelf model, sinistral shearing at a high angle to the initial dextral set amplifies the strain along dextral shear zones as well as introduces wall rock deformation and stretching along dextral shear zones. The absolute timing of shear zones, ca. 1100Ma, is from U/Pb geochronology of zircon grains from pegmatite dykes found to be, which were interpreted as syn-kinematic (Marsh et al., 2011b). This date is a good constraint for dextral shear zones, as they are most likely syn-kinematic with pegmatite emplacement. However, as the sinistral shear zones are not focused on pegmatites the best absolute age constraint of a sinistral deformation event is post ca. 1100 Ma.

In the conjugate shear zone scenario, immediately following brittle fracturing and pegmatite emplacement dextral and sinistral shear zones develop during the same deformation event. The orientation of pegmatite dykes favors dextral shear zone development, and therefore dextral shear zones are more prevalent in early stages. There are notable problems with interpreting kinematics from conjugate ductile shear zones (Carreras et al., 2010). It has been demonstrated that the maximum shortening direction can either be parallel to the acute bisector (Lamouroux et al., 1991), or the obtuse bisector (Ramsay, 1980; Gapais et al., 1987). Field observations of folds give evidence of what the shortening direction should be on a specific outcrop. With this in mind, we can use stereonets of conjugate sets of shear zones (Fig. 4.4b; Fig. 4.19) to approximate the regional kinematics. This results in using the acute bisector between the sets of shear zones to find extensional directions. The resulting geometry is an extensional direction NNW/SSE for Teddy Rock and Matches Island and WNW/ESE extensional direction for PBW Island. This geometry is compatible with the strain analysis results, which predicted similar extensional directions based on strain ellipse orientation. In this situation, both sets of shear zones would be constrained by Marsh et al. (2011b)'s ca. 1100Ma zircon date.

6.7: Stages of transposition

The main stages of the transposition of granulite facies Parry Sound domain layering into amphibolite facies Twelve Mile Bay shear zone foliation have been recognized using field observations and structural data.

The initial stage of transposition is fracture initiation and pegmatite dyke emplacement, resulting in a retrograde reaction along dyke margins causing planes of weakness (Culshaw et al., 2010; Gerbi et al., 2010; Marsh et al., 2011a). Cm-scale dextral shear zones nucleate on the pegmatite weakened planes and begin the transposition process. Teddy Rock is a prime example of this stage of transposition.

A sinistral shearing, either a later event or a dominant set of a conjugate pair, is introduced at a high angle to the initial dextral shear zone set and amplifies dextral shear zones (Fig. 5.23). Wall rock deformation is initiated, with wall rock layering developing buckle folds and boudinage. Blocks of wall rock and dextral shear zones are rotated together counterclockwise in accordance with an overall sinistral shear sense.

Complete retrogression of wall rock blocks allows for continued wall rock deformation, and folded wall rocks begin to be reoriented into a preferred orientation (Fig. 6.3). This degree of wall rock deformation results in widespread linking of shear zones, and increasingly isolated and deformed wall rock blocks.

The complete stage of transposition is a near homogeneous amphibolite facies shear zone fabric with isoclinal folds. The last vestiges of Parry Sound domain fabric are highly folded and rotated small mafic lozenges (Fig. 4.31).

6.8: Future work

In the future it would be useful to expand the study to include other islands to broaden the understanding of how the Twelve Mile Bays shear zone system developed. Future work must, in order to gain a more complete understanding of the TMB shear zone, include parts of the zone of transposition that have not been studied in detail. The area between Matches Island and PBW Island is such a zone that, although it has been mapped regionally (Culshaw et al., 2010), has not had its key outcrops picked apart. This area is important because it links Matches Island, which is close to the beginning of the transposition, and PBW, which is within the Twelve Mile Bay shear zone. The area should supply structural data that illustrates how Matches Island structures evolve to those found in transposed Parry Sound domain gneiss within Twelve Mile Bay shear zone.

One of the main questions that a key exposure could answer is how the bulk stretching direction changes. In the early stages of transposition on Teddy Rock and Matches Island the bulk extensional direction was determined to be NNW/SSE. In the advanced stages of transposition on PBW, Bartram's, PBE islands, and the Twelve Mile Bay shear zone the bulk extensional direction was found to be approximately E/W. The current model explaining this change is that the system exists as a continuum, progressively rotating into the Twelve Mile Bay shear zone. Finding a new island in a transitional phase of transposition could provide key structures to help refine the model.

Such transitional outcrops would contain a greater areal percentage of wall rock than shear zone. This is important because it is the progressive deformation of wall rock material is the focus of this study, and having more exposures of wall rock/shear zone interactions will lead to greater understanding of this process. Also, an exposure with a greater amount of wall rock material suggests that the outcrop would be an early-to-transitional stage of transposition, and not an advanced stage like PBW, Bartram's, and PBE islands.

The degree of internal wall rock deformation would also be a good indicator of where an exposure would lie along the transpositional spectrum. Matches Island for instance, has proportionally greater wall rock material than shear zone material, but relatively little internal wall rock deformation. An ideal transitional exposure would have similar wall rock to shear zone proportions as Matches Island, but a greater degree of internal wall rock deformation, such as on Bartram's Island.

The ideal location to expand the study would be somewhere between Matches Island and PBW Island. PBW, Bartram's, and PBE islands are within a kilometer of each other, and nearly within the Twelve Mile Bay shear zone. With these islands being so proximal to the main structure they are at an advanced stage of shear zone development. There is a gap of approximately three kilometers between Matches Island and PBW Island and several islands that could be suitable candidates to find more exposures that display an intermediary stage of transposition. Exposures towards the core of the Twelve Mile Bay shear zone could also be investigated to identify outcrops of completely transposed Parry Sound domain material with emplaced anorthosite layers within it, as seen in Fig. 4.39. Studying the range and geometries of such layers could possibly give insight into the kinematics of the Twelve Mile Bay shear zones history post-transposition.

Another Island to consider including in the study is Cone Island, which is situated a kilometer west of PBW Island. Cone Island is at a relatively advanced stage of transposition, so it wouldn't solve the problem of getting a greater resolution of the stages of transposition. What it would offer is studying the influence of mafic dykes on shear zones, and possibly using dykes as an additional marker layer to calculate shear strain. It pairs with PBW as a lower strain version of deformation of transposing PSD gneiss that contains mafic dykes. Srivastava and Hudleston's (1995) method of calculated shear strain and volume loss required two marker layers to be traced through a shear zone. By finding a suitable exposure on Cone Island, it would be possible to calculate additional shear strains, as well as determine whether shear zones on Cone Island were subject to volume loss.

The study of additional islands would be of course be limited by exposure and access (there are many privately owned islands in the area). The task of mapping any islands in the future could potentially be done faster and more accurately than before by using drone technology. There are many commercially available drones now that have been specifically designed for accurately mapping areas, and include onboard GPS systems that can be programmed to fly specific patterns. In addition, included software can process orthorectified mosaics, point clouds, and meshes to create a digital outcrop. This would drastically reduce time spent conducting the photo-mapping procedure that was implemented in this study, allowing more time to study more islands or to collect structural measurements and observations.

APPENDIX A: Shear strain results

Island	SZ ID	y avg (disp.)	y avg (angle)	y max (angle)	R (disp.)	R (angle)	Theta ' (disp.)	Theta' (angle)
Matches								
	1a	1.58	0.10	2.75	4.14	1.06	26	43
	1b	1.28	0.02	1.40	3.19	1.01	28	45
	2a	0.62	0.61	1.26	1.66	1.64	36	37
	2b	0.51	0.94	0.84	1.49	2.29	38	33
	2c	1.54	0.46	1.42	4.01	1.42	26	38
	2d	7.84	8.83	19.49	63.97	80.52	7	6
	2e	9.00	1.61	6.27	83.45	4.23	6	26
	2f	4.92	2.24	14.55	26.68	6.87	11	21
	2g	5.05	4.24	19.26	27.94	20.36	11	12
	3a	0.86	0.44	1.34	2.11	1.39	33	39
	3b	2.89	1.58	4.90	10.41	4.14	18	26
	3c	5.25	5.84	11.45	30.10	36.64	11	9
	4a	1.40	3.02	11.31	3.55	11.23	27	17
	4b	1.75	4.70	14.16	4.75	24.52	25	11
	4c	7.63	8.77	14.25	60.76	79.38	7	6
	4d	-	4.81	19.05	-	25.58	-	11
	5a	2.04	1.69	3.49	5.97	4.54	22	25
	5b	2.50	2.84	18.99	8.20	10.09	19	18
	5c	3.22	4.28	9.34	12.51	20.69	16	12
	6a	0.85	1.14	5.30	2.08	2.79	33	30
	6b	3.26	4.31	28.65	12.81	20.93	16	13
	6c	4.81	4.01	28.62	25.63	18.41	11	13
	7a	-	13.19	19.71	-	175.25	-	4
	7b	7.89	9.87	28.51	64.77	99.82	7	6
	7c	2.68	8.73	28.57	9.19	78.76	18	6
	7d	2.26	2.74	18.99	7.00	9.51	21	18
	7e	2.25	3.64	11.36	6.95	15.46	21	14
	8a	16.83	9.82	28.81	282.62	98.75	3	6
	8b	-	42.53	57.34	-	1768.70	-	1
	8c	-	6.89	28.50	-	50.09	-	8
	8d	7.38	43.13	57.31	57.05	1819.29	8	1
	9a	1.41	7.00	4.72	3.58	51.61	27	8
	10a	-	20.34	28.65	-	410.19	-	3
	10b	-	6.27	28.60	-	41.90	-	9
	10c	-	14.80	57.34	-	219.62	-	4
	11a	-	1.71	8.07	-	4.61	-	25
	11b	-	17.54	57.13	-	306.47	-	3
	12a	2.28	3.58	19.55	7.09	15.01	21	14
	12b	1.34	1.13	19.17	3.36	2.76	28	30
	13a	1.55	3.09	14.44	4.03	11.64	26	16
	13b	-	2.86	11.77	-	10.22	-	17

	14a	-	2.31	10.14	-	7.24	-	20
	15a	1.86	0.90	3.29	5.22	2.21	23	33
	15b	1.01	0.88	3.77	2.45	2.16	32	33
	16a	-	7.96	19.12	-	65.85	-	7
PBW								
	1a	-	11.06	28.17	-	124.40	-	
	1b	-	51.39	56.22	-	2577.50	-	
	1c	-	18.00	56.71	-	322.63	-	
	1d	-	22.63	56.69	-	506.40	-	
	2a	-	12.14	28.41	-	148.98	-	
	2b	-	11.07	57.29	-	124.53	-	
	3a	-	50.63	28.35	-	2502.02	-	
Bartram's								
	1a	-	0.94	28.53	-	2.29	-	
	1b	-	0.71	4.38	-	1.81	-	
	1c	-	0.19	11.40	-	1.13	-	
	1d	-		12.08	-	1.00	-	
	2a	-		11.27	-	1.00	-	
	2b	-		28.79	-	1.00	-	
	2c	-		11.27	-	1.00	-	
	3a	-		2.37	-	1.00	-	
	3b	-		11.27	-	1.00	-	
	3c	-		11.38	-	1.00	-	
	3d	-		57.13	-	1.00	-	
	4a	-		14.68	-	1.00	-	
	4b	-		19.57	-	1.00	-	
	4c	-		8.84	-	1.00	-	
	5a	-		4.85	-	1.00	-	

APPENDIX B: Shear zone spacing data

SZ ID		Rotation	SZ Spacing map	SZ Spacing Real	Max Width
1	a	35	0.55	4.29	5.22
1	b	38	0.67	5.22	5.22
2	a	55	0.55	4.29	4.29
2	b	79	0.43	3.35	4.29
3	a	23	0.65	5.07	5.93
3	b	24	0.56	4.37	5.93
3	c	28	0.61	4.76	5.93
3	d	68	0.76	5.93	5.93
4	a	10	0.58	4.52	5.46
4	b	12	0.7	5.46	5.46
4	c	35	0.34	2.65	5.46
4	d	62	0.18	1.40	5.46
5	a	3	0.34	2.65	3.12
5	b	39	0.4	3.12	3.12
5	c	66	0.39	3.04	3.12
7	a	71	0.55	4.29	4.29
7	b	66	0.55	4.29	4.29
14	a	10	1.62	12.63	12.63
14	b	20	1.3	10.14	12.63
14	c	22	1.3	10.14	12.63
14	d	54	0.99	7.72	12.63
15	a	13	0.65	5.07	5.07
15	b	19	0.49	3.82	5.07
15	c	43	0.57	4.44	5.07
15	d	37	0.45	3.51	5.07
1	c	129	0.15	1.17	2.57
1	d	98	0.33	2.57	2.57
1	e	76	0.29	2.26	2.57
1	f	98	0.22	1.72	2.57
2	c	96	0.48	3.74	6.24
2	d	115	0.75	5.85	6.24
2	e	101	0.8	6.24	6.24
2	f	92	0.77	6.00	6.24
2	h	83	0.7	5.46	6.24
2	i	76	0.7	5.46	6.24
2	j	93	0.56	4.37	6.24
3	e	51	0.55	4.29	6.78
3	f	106	0.35	2.73	6.78
3	h	102	0.57	4.44	6.78
3	i	98	0.78	6.08	6.78
3	j	100	0.87	6.78	6.78
3	k	69	0.77	6.00	6.78

3	l	57	0.69	5.38	6.78
4	e	74	0.09	0.70	4.13
4	f	95	0.27	2.11	4.13
4	h	95	0.31	2.42	4.13
4	i	120	0.38	2.96	4.13
4	j	87	0.38	2.96	4.13
4	k	78	0.29	2.26	4.13
4	l	81	0.32	2.50	4.13
4	m	66	0.36	2.81	4.13
4	n	58	0.43	3.35	4.13
4	o	52	0.53	4.13	4.13
5	d	78	0.39	3.04	3.59
5	e	84	0.28	2.18	3.59
5	f	98	0.32	2.50	3.59
5	g	91	0.46	3.59	3.59
5	h	64	0.43	3.35	3.59
5	i	51	0.35	2.73	3.59
5	j	52	0.26	2.03	3.59
6	a	95	0.53	4.13	4.13
6	b	97	0.37	2.88	4.13
6	c	70	0.3	2.34	4.13
6	d	97	0.22	1.72	4.13
6	e	69	0.15	1.17	4.13
6	f	72	0.19	1.48	4.13
6	g	58	0.21	1.64	4.13
6	h	83	0.33	2.57	4.13
6	i	62	0.33	2.57	4.13
6	j	61	0.51	3.98	4.13
6	k	112	0.47	3.66	4.13
7	c	89	0.28	2.18	5.85
7	d	83	0.26	2.03	5.85
7	e	78	0.27	2.11	5.85
7	f	88	0.31	2.42	5.85
7	g	90	0.42	3.27	5.85
7	h	97	0.63	4.91	5.85
7	i	80	0.74	5.77	5.85
7	j	67	0.75	5.85	5.85
7	k	56	0.59	4.60	5.85
8	a	92	0.41	3.20	4.99
8	b	57	0.42	3.27	4.99
8	c	89	0.26	2.03	4.99
8	d	62	0.45	3.51	4.99
8	e	59	0.64	4.99	4.99
14	e	64	0.96	7.49	7.49
14	f	48	0.8	6.24	7.49

14	g	67	0.49	3.82	7.49
14	h	65	0.47	3.66	7.49
14	i	75	0.57	4.44	7.49
15	e	67	0.52	4.05	8.81
15	f	71	0.52	4.05	8.81
15	g	74	0.67	5.22	8.81
15	h	94	0.83	6.47	8.81
15	i	76	0.91	7.10	8.81
15	j	73	1.01	7.88	8.81
15	k	86	1.13	8.81	8.81
3	m	128	0.7	5.46	8.89
3	n	54	0.81	6.32	8.89
3	o	58	0.97	7.56	8.89
3	p	59	1.14	8.89	8.89
3	q	58	0.2	1.56	8.89
3	r	62	0.47	3.66	8.89
3	s	40	1.11	8.65	8.89
4	p	103	0.25	1.95	2.65
4	q	46	0.34	2.65	2.65
4	r	50	0.31	2.42	2.65
6	l	75	0.6	4.68	8.19
6	m	51	0.61	4.76	8.19
6	n	48	0.67	5.22	8.19
6	o	46	0.71	5.54	8.19
6	p	50	0.78	6.08	8.19
6	q	39	0.77	6.00	8.19
6	r	55	0.86	6.71	8.19
6	s	50	0.88	6.86	8.19
6	t	44	0.95	7.41	8.19
6	u	32	0.83	6.47	8.19
6	v	52	0.94	7.33	8.19
6	w	38	1.05	8.19	8.19
6	x	9	0.94	7.33	8.19
7	l	92	0.42	3.27	3.35
7	m	38	0.43	3.35	3.35
7	n	42	0.41	3.20	3.35
7	o	42	0.4	3.12	3.35
7	p	40	0.38	2.96	3.35
7	q	22	0.25	1.95	3.35
8	f	64	0.39	3.04	4.29
8	g	51	0.55	4.29	4.29
8	h	46	0.48	3.74	4.29
8	i	37	0.36	2.81	4.29
8	j	63	0.33	2.57	4.29
8	k	44	0.25	1.95	4.29

9	a	68	0.56	4.37	5.07
9	b	59	0.65	5.07	5.07
9	c	56	0.61	4.76	5.07
9	d	50	0.38	2.96	5.07
9	e	42	0.27	2.11	5.07
10	a	62	0.45	3.51	6.16
10	b	51	0.43	3.35	6.16
10	c	57	0.47	3.66	6.16
10	d	57	0.79	6.16	6.16
10	e	18	0.33	2.57	6.16
10	f	6	0.54	4.21	6.16
11	a	48	0.22	1.72	2.50
11	b	74	0.26	2.03	2.50
11	c	63	0.22	1.72	2.50
11	d	43	0.32	2.50	2.50
11	e	19	0.29	2.26	2.50
11	f	4	0.3	2.34	2.50
12	a	44	0.83	6.47	7.17
12	b	56	0.88	6.86	7.17
12	c	27	0.92	7.17	7.17
12	d	17	0.9	7.02	7.17
13	a	65	0.3	2.34	4.29
13	b	43	0.38	2.96	4.29
13	c	18	0.5	3.90	4.29
13	d	31	0.55	4.29	4.29
13	e	20	0.48	3.74	4.29
13	f	22	0.48	3.74	4.29
14	j	69	0.75	5.85	6.39
14	k	40	0.59	4.60	6.39
14	l	28	0.82	6.39	6.39
14	m	23	0.8	6.24	6.39
15	l	48	1.16	9.04	9.04
15	m	14	0.91	7.10	9.04
15	n	17	0.8	6.24	9.04

APPENDIX C: Calculated displacement results

SZ ID	Rotation	gamma	d map	d real	d calc	Unit	Zone
1	35	0.67	0	0.00	0.40	1	A
	38	0.72	0.32	2.50	1.20	1	A
	129	15.11	0.64	4.99	0.26	1	B
	98	2.24	0.69	5.38	1.66	1	B
	76	1.46	0.95	7.41	7.88	1	B
	98	2.24	1.71	13.33	11.40	1	B
2	55	1.02	0	0.00	0.14	1	A
	79	1.54	0.19	1.48	0.58	1	A
	96	2.14	0.43	3.35	0.59	1	B
	115	3.89	0.58	4.52	0.60	1	B
	101	2.41	0.7	5.46	1.11	1	B
	92	1.96	0.88	6.86	1.53	1	B
	83	1.65	1.08	8.42	2.56	1	B
	76	1.46	1.35	10.53	2.63	1	B
	93	2.00	1.58	12.32	9.73	1	B
3	23	0.45	0	0.00	1.55	1	A
	24	0.47	0.63	4.91	1.54	1	A
	28	0.54	0.89	6.94	2.07	1	A
	68	1.28	1.15	8.97	3.73	1	A
	51	0.95	1.51	11.77	2.38	1	B
	106	2.77	1.7	13.26	2.51	1	B
	102	2.47	1.88	14.66	12.58	1	B
	98	2.24	2.6	20.27	4.65	1	B
	100	2.35	2.82	21.99	5.98	1	B
	69	1.30	3.08	24.02	4.45	1	B
	57	1.06	3.26	25.42	14.86	1	B
	128	12.24	3.8	29.63	4.22	1	C
	54	1.00	3.94	30.72	18.08	1	C
	58	1.08	4.49	35.01	11.23	1	C
	59	1.10	4.8	37.43	20.52	1	C
	58	1.08	5.32	41.48	21.72	1	C
	62	1.15	5.82	45.38	88.41	1	C
	40	0.76	7.52	58.64	220.47	1	C
4	10	0.16	0	0.00	0.79	1	A
	12	0.21	0.45	3.51	0.96	1	A
	35	0.67	0.67	5.22		1	A
	62	1.15	0.97	7.56	2.04	1	A
	74	1.41	1.21	9.43	3.78	1	B
	95	2.09	1.56	12.16	3.14	1	B
	95	2.09	1.8	14.04	1.59	1	B
	120	5.14	1.91	14.89	2.16	1	B
	87	1.78	2.05	15.98		1	B

	78	1.51	2.29	17.86	3.92	1	B
	81	1.59	2.5	19.49	5.98	1	B
	66	1.23	2.79	21.75	6.40	1	B
	58	1.08	3.07	23.94	5.20	1	B
	52	0.97	3.28	25.58	3.66	1	B
	103	2.54	3.42	26.67		1	C
	46	0.86	3.65	28.46	8.27	1	C
	50	0.93	3.93	30.64	-60.21	1	C
5	3	-0.03	0	0.00	0.26	1	A
	39	0.74	0.26	2.03	0.79	1	A
	66	1.23	0.52	4.05	1.38	1	A
	78	1.51	0.79	6.16		1	B
	84	1.68	1.15	8.97	1.33	1	B
	98	2.24	1.29	10.06	4.00	1	B
	91	1.92	1.64	12.79	2.29	1	B
	64	1.19	1.81	14.11	3.14	1	B
	51	0.95	2.02	15.75	6.74	1	B
	52	0.97	2.41	18.79		1	B
6	95	2.09	0	0.00	0.13	1	B
	97	2.19	0.18	1.40	0.50	1	B
	70	1.32	0.4	3.12	0.69	1	B
	97	2.19	0.58	4.52	1.37	1	B
	69	1.30	0.83	6.47	1.78	1	B
	72	1.36	1.07	8.34		1	B
	58	1.08	1.37	10.68	2.29	1	B
	83	1.65	1.57	12.24	2.60	1	B
	62	1.15	1.77	13.80	2.46	1	B
	61	1.13	1.94	15.13	3.85	1	B
	112	3.41	2.18	17.00	3.74	1	B
	75	1.43	2.39	18.64		1	C
	51	0.95	2.61	20.35	7.14	1	C
	48	0.90	2.94	22.92	6.72	1	C
	46	0.86	3.22	25.11	9.82	1	C
	50	0.93	3.59	27.99	14.65	1	C
	39	0.74	4.08	31.81	14.75	1	C
	55	1.02	4.52	35.24		1	C
	50	0.93	4.94	38.52	18.12	1	C
	44	0.83	5.39	42.03	18.79	1	C
	32	0.62	5.82	45.38	25.64	1	C
	52	0.97	6.36	49.59	15.23	1	C
	38	0.72	6.66	51.93	26.38	1	C
	9	0.14	7.15	55.75		1	C
7	71	1.34	0	0.00	0.11	1	A
	66	1.23	0.17	1.33	0.51	1	A
	89	1.85	0.4	3.12	0.73	1	B

	83	1.65	0.59	4.60	1.59	1	B
	78	1.51	0.87	6.78	1.85	1	B
	88	1.81	1.11	8.65		1	B
	90	1.88	1.28	9.98	4.23	1	B
	97	2.19	1.65	12.87	3.02	1	B
	80	1.56	1.87	14.58	4.22	1	B
	67	1.26	2.14	16.69	5.74	1	B
	56	1.04	2.46	19.18	7.19	1	B
	92	1.96	2.81	21.91		1	C
	38	0.72	3.16	24.64	13.58	1	C
	42	0.79	3.67	28.62	14.63	1	C
	42	0.79	4.15	32.36	10.41	1	C
	40	0.76	4.46	34.78	13.78	1	C
	22	0.43	4.84	37.74	-91.33	1	C
8	92	1.96	0	0.00		1	B
	57	1.06	0.4	3.12	2.97	1	B
	89	1.85	0.96	7.49	3.10	1	B
	62	1.15	1.31	10.21	9.22	1	B
	59	1.10	2.02	15.75	12.72	1	B
	64	1.19	2.71	21.13	13.31	1	C
	51	0.95	3.28	25.58		1	C
	46	0.86	3.62	28.23	10.98	1	C
	37	0.70	3.99	31.11	10.35	1	C
	63	1.17	4.31	33.61	21.57	1	C
	44	0.83	4.91	38.28		1	C
9	68	1.28	0	0.00	0.86	1	C
	59	1.10	0.47	3.66	3.19	1	C
	56	1.04	1.02	7.95	5.92	1	C
	50	0.93	1.6	12.48	11.92	1	C
	42	0.79	2.37	18.48	-21.90	1	C
10	62	1.15	0	0.00	2.19	1	C
	51	0.95	0.75	5.85	4.29	1	C
	57	1.06	1.29	10.06	8.34	1	C
	57	1.06	1.95	15.20	21.92	1	C
	18	0.34	3.07	23.94	20.15	1	C
	6	0.06	3.82	29.79	-56.89	1	C
11	48	0.90	0	0.00	1.45	1	C
	74	1.41	0.61	4.76	2.85	1	C
	63	1.17	1.05	8.19	7.51	1	C
	43	0.81	1.74	13.57	22.82	1	C
	19	0.36	2.98	23.24	19.04	1	C
	4	0.00	3.71	28.93		1	C
12	44	0.83	0	0.00	2.13	1	C
	56	1.04	0.74	5.77	4.45	1	C
	27	0.52	1.3	10.14	7.04	1	C

	17	0.32	1.87	14.58		1	C
13	65	1.21	0	0.00	0.94	1	C
	43	0.81	0.49	3.82	2.81	1	C
	18	0.34	0.98	7.64	5.50	1	C
	31	0.60	1.54	12.01	23.09	1	C
	20	0.39	2.88	22.46	12.47	1	C
	22	0.43	3.39	26.43		1	C
14	10	0.16	0	0.00	5.52	2	A
	20	0.39	1.19	9.28	11.35	2	A
	22	0.43	2.08	16.22	7.89	2	A
	54	1.00	2.52	19.65	9.86	2	A
	64	1.19	2.98	23.24	14.51	2	B
	48	0.90	3.55	27.68	16.72	2	B
	67	1.26	4.11	32.05	15.21	2	B
	65	1.21	4.56	35.56	14.46	2	B
	75	1.43	4.95	38.60	19.00	1	B
	69	1.30	5.42	42.26	16.17	1	C
	40	0.76	5.79	45.15	41.19	1	C
	28	0.54	6.64	51.77	41.02	1	C
	23	0.45	7.39	57.62		1	C
15	13	0.23	0	0.00	2.75	2	A
	19	0.36	0.84	6.55	3.44	2	A
	43	0.81	1.26	9.82	4.55	2	A
	37	0.70	1.66	12.94	3.48	2	A
	67	1.26	1.91	14.89	4.48	2	B
	71	1.34	2.19	17.08	6.06	2	B
	74	1.41	2.52	19.65	5.37	2	B
	94	2.04	2.78	21.68	7.82	2	B
	76	1.46	3.12	24.33	13.42	2	B
	73	1.39	3.63	28.30	10.69	2	B
	86	1.74	3.99	31.11	10.02	2	B
	48	0.90	4.3	33.53	25.38	1	C
	14	0.26	5	38.99	41.02	1	C
	17	0.32	5.96	46.47	138.49	1	C

REFERENCES:

Bai, T., & Pollard, D. D. 2000a. Fracture spacing in layered rocks: a new explanation based on the stress transition. *Journal of Structural Geology*, **22**: 43–57.

Bai, T., Pollard, D. D., & Gao, H. 2000b. Explanation for fracture spacing. *Letters to Nature,* **403**: 753–756.

Baird, G. B., & Hudleston, P. J. 2007. Modeling the influence of tectonic extrusion and volume loss on the geometry, displacement, vorticity, and strain compatibility of ductile shear zones. *Journal of Structural Geology*, **29**(10), 1665–1678.

Beaumont, C., Jamieson, R. A., Nguyen, M. H., & Lee, B. 2001. Himalayan tectonics explained by extrusion of a low-viscosity crustal channel coupled to focused surface denudation. *Nature*: ***414***: 738–742.

Bemis, S. P., Micklethwaite, S., Turner, D., James, M. R., Akciz, S., Thiele, S. T., & Bangash, H. A. 2014. Ground-based and UAV-Based photogrammetry: A multi-scale, high-resolution mapping tool for structural geology and paleoseismology. *Journal of Structural Geology*, **69**: 163–178.

Bhattacharyya, P., & Czeck, D. M. 2008. Using network analyses within geographic information system technologies to quantify geometries of shear zone networks. *Geosphere*: **4**(4), 640-656.

Bhattacharyya, P., & Hudleston, P. 2001. Strain in ductile shear zones in the Caledonides of northern Sweden: a three-dimensional puzzle. *Journal of Structural Geology*, **23**, 1549–1565.

Bussy, F., Krogh, T. E., Klemens, W. P., & Schwerdtner, W. M. 1995. Tectonic and metamorphic events in the westernmost Grenville Province, central Ontario: new results from high-precision U-Pb zircon geochronology. *Canadian Journal of Earth Sciences*, ***671***: 660–671.

Carr, S. D., Easton, R. M., Jamieson, R. a., & Culshaw, N. G. 2000. Geologic transect across the Grenville orogen of Ontario and New York. *Canadian Journal of Earth Sciences*, ***37***(2–3): 193–216.

Carreras, J. 2001. Zooming on Northern Cap de Creus shear zones. *Journal of Structural Geology*, ***23***(9): 1457–1486.

Carreras, J., Druguet, E., & Griera, A. 2005. Shear zone-related folds. *Journal of Structural Geology*, **27**(7): 1229–1251.

Carreras, J., Czeck, D. M., Druguet, E., & Hudleston, P. J. 2010. Structure and development of an anastomosing network of ductile shear zones. *Journal of Structural Geology*, ***32***(5): 656–666.

Carreras, J., Cosgrove, J. W., & Druguet, E. 2013. Strain partitioning in banded and/or anisotropic rocks: Implications for inferring tectonic regimes. *Journal of Structural Geology*, **50**: 7–21.

Corrigan, D., Culshaw, N.G., and Mortensen, J.K. 1994. Pre-Grenvillian evolution and Grenvillian overprinting of the Parautochthonous Belt in Key Harbour, Ontario: UPb and field constraints. *Canadian Journal of Earth Sciences*, **31**(3): 583–596.

Culshaw, N. 2005. Buckle folding and deep-crustal shearing of high-grade gneisses at the junction of two major high-strain zones, Central Gneiss Belt, Grenville Province, Ontario. *Canadian Journal of Earth Sciences*, **42**(10): 1907–1925.

Culshaw, N. G., Ketchum, J. W. F., Wodicka, N., & Wallace, P. 1994. Deep crustal ductile extension following thrusting in the southwestern Grenville Province, Ontario1. *Canadian Journal of Earth Sciences*, ***31***: 160-175.

Culshaw, N. G., Slagstad, T., Raistrick, M., & Dostal, J. 2013. Geochemical, geochronological and isotopic constraints on the origin of members of the allochthonous Shawanaga and basal Parry Sound domains, Central Gneiss Belt, Grenville Province, Ontario. *Precambrian Research*, ***228***: 131–150.

Culshaw, N., Beaumont, C., & Jamieson, R. A. 2006. The orogenic superstructure-infrastructure concept: Revisited, quantified, and revived. *Geology*, **34**(9): 733-736.

Culshaw, N., Gerbi, C., & Marsh, J. 2010. Softening the lower crust: Modes of syn-transport transposition around and adjacent to a deep crustal granulite nappe, Parry Sound domain, Grenville Province, Ontario, Canada. *Tectonics*, ***29***(5): TC5013.

Culshaw, N., Gerbi, C., Marsh, J., & Plug, L. 2011. Heterogeneous amphibolite facies deformation of a granulite facies layered protolith: Matches Island shear system, Parry Sound domain, Grenville Province, Ontario, Canada. *Journal of Structural Geology*, **33**(5), 875–890.

Culshaw, N., Jamieson, R. A., Ketchum, J. W. F., Wodicka, N., Corrigan, D., & Reynolds, P. H. 1997. Transect across the northwest Grenville orogen, Georgian Bay, Ontario: Polystage convergence and extension in the lower orogenic crust. *Tectonics*, **16(**6): 966–982.

Culshaw, N.G., Check, G., Corrigan, D., Drage, J., Gower, R., Haggart, M.J.,Wallace, P.,and Wodicka, N. 1989. Georgian Bay geological synthesis: Dillon to TwelveMile Bay, Grenville Province of Ontario. *Current Research, Part C*, 89-1C: 157–163.

Culshaw, N.G., Corrigan, D., Ketchum, J.W.F., and Wallace, P. 1990. Georgian Bay geological synthesis: Twelve Mile Bay to Port Severn, Grenville Province of Ontario. *Current Research, Part C,* 90-1C: 107–112.

Culshaw, N.G., Foster, J., Marsh, J., Slagstad, T., Gerbi, C. 2016. Kiosk domain, Central Gneiss Belt, Grenville Province, Ontario: a Labradorian palimpsest preserved in the ductile deep crust. *Precambrian Research,* **280**: 249-278.

Davidson, A. 1986. New Interpretations in the Southwestern Grenville Province. *In The Grenville Province, edited by J.M.Moore, A. Davidson, and A.J. Baer, Geological Association of Canada Special Paper,* **31**: 61-74.

Davidson, A., Culshaw, N.G., and Nadeau, L. 1982. A tectono-metamorphic framework for part of the Grenville Province, Parry Sound region, Ontario. *Current Research Geologic Survey of Canada*, 82-1A: 175-190.

Davidson, C., Schmid, S. M., & Hollister, L. 1994. Role of melt during deformation in the deep crust. *Terra Nova*, **6**: 133-142.

Dickin, A.P. and McNutt, R.H. 2003. An application of Nd isotope mapping in structural geology: delineating an allochthonous Grenvillian terrane at North Bay, Ontario. *Geological Magazine*, **140**(5): 539-548.

Fossen, H., & Cavalcante, G. C. G. 2017. Shear zones – A review. *Earth-Science Reviews*, **171**: 434–455.

Fossen, H. 2010. Structural Geology. *Cambridge: Cambridge University Press*.

Fusseis, F., Handy, M. R., & Schrank, C. 2006. Networking of shear zones at the brittle-to-viscous transition (Cap de Creus, NE Spain). *Journal of Structural Geology*, ***28***(7), 1228–1243.

Gapais, D., Bale, R., Choukroune, P., Cobbold, P., Mahjoub, Y., Marquer, D., 1987. Bulk kinematics from shear zone patterns: some field examples. Journal of Structural Geology 9, 635e646.Gerbi, C., Culshaw, N., & Marsh, J. (2010). Magnitude of weakening during crustal-scale shear zone development. *Journal of Structural Geology*, ***32***(1), 107–117.

Gapais, D. 1989. Shear structures within deformed granites: Mechanical and thermal indicators. *Geology*, **17**: 1144-1147.

Godin, L., Grujic, D., Law, R. D., & Searle, M. P. 2006. Channel flow, ductile extrusion and exhumation in continental collision zones : an introduction The Himalaya-Tibetan plateau system. *Geological Society, London, Special Publications*, **268**, 1–23.

Gower, R., & Simpson, C. 1992. Phase boundary mobility in naturally deformed, high-grade quartzofeldspathic rocks: evidence for diffusional creep. *Journal of Structural Geology*, **14**(3): 301-313.

Grant, J. A. 1986.The isocon diagram; a simple solution to Gresens' equation for metasomatic alteration. *Economic Geology*, **81**(8): 1976–1982.

Harris, L. B. (2003). Folding in high-grade rocks due to back-rotation between shear zones. *Journal of Structural Geology*, **25**: 223-240.

Hanmer, S. and McEachern, S. 1992. Kinematical and rheological evolution of a crustalscale ductile thrust zone, Central Metasedimentary Belt, Grenville orogen, Ontario. *Canadian Journal of Earth Sciences*, **29**(8): 1779–1790.

Hoffman, P. F. 1988. United plates of America, the birth of a craton: Early Proterozoic assembly and growth of Laurentia. *Annual Review of Earth and Planetary Sciences*, **16**: 543-603.

Hollister, L. S., & Crawford, M. L. 1986. Melt-enhanced deformation : A major tectonic process. *Geology*, **14**: 558-561.

Horsman, E., & Tikoff, B. 2005. Quantifying simultaneous discrete and distributed deformation. *Journal of Structural Geology*, **27**(7), 1168–1189.

Hudleston, P. (1999). Strain compatibility and shear zones: is there a problem? *Journal of Structural Geology*, **21**(8–9), 923–932.

Hull, J. 1988. Thickness-displacement relationships for deformation zones. *Journal of Structural Geology*, **10**(4): 431-435.

Hynes, A., & Rivers, T. 2010. Protracted continental collision-evidence from the Grenville Orogen. *Canadian Journal of Earth Sciences*, **47**(5), 591–620.

Indares, A. and Rivers, T. 1995. Textures, metamorphic reactions and thermobarometry of eclogitized metagabbros: a Proterozoic example. *European Journal of Mineralogy,* **7**: 43–56.

Jamieson, R. A., Culshaw, N. G., & Corrigan, D. 1995. North-west propagation of the Grenville orogen: Grenvillian structure and metamorphism near Key Harbour, Georgian Bay, Ontario, Canada. *Journal of Metamorphic Geology,* **543**: 185–207.

Jamieson, R.A., Beaumont, C., Nguyen, M.H., and Culshaw, N.G. 2007. Synconvergentductile flow in variable-strength continental crust: Numerical models with applicationto the western Grenville orogen. *Tectonics*, **26**(5): TC5005.

Jamieson, R.A., Beaumont, C., Warren, C.J., and Nguyen, M.H. 2010. The GrenvilleOrogen explained? Applications and limitations of integrating numerical models with geological and geophysical data. *Canadian Journal of Earth Sciences*, **47**(4): 517–539.

Ketchum, J. W. F., and Krogh, T. E. 1997. U-Pb constraints on high-pressure metamorphism in the Central Gneiss Belt, southwestern Grenville orogen. *Geological Association of Canada, Abstract Volume*, **22**: A78.

Ketchum, J. W. F., Heaman, L. M., Krogh, T. E., Culshaw, N. G., Jamieson, R. A. 1998. Timing and thermal influence of late orogenic extension in the lower crust: a U-Pb geochronological study from the southwest Grenville orogen, Canada. *Precambrian Research*, **89**: 25–45.

Kretz, R. (1983), Symbols for rock ‐ forming minerals, Am. Mineral., 68,277‐279.

Krogh, T. E., and Kwok, Y. Y. 2005. The age enigma in the Moon River structure and the Parry Sound domain connection, Grenville Province. *Geological Association of Canada Abstracts with Program*, 30, 106.

Mancktelow, N. S., & Pennacchioni, G. 2005. The control of precursor brittle fracture and fluid–rock interaction on the development of single and paired ductile shear zones. *Journal of Structural Geology*, **27**(4): 645–661.

Lamouroux, C., Ingles, J., & Debat, P. 1991. Conjugate ductile shear zones. *Tectonophysics*, 185: 309–323.

Mandl, G. 1984. Rotating parallel faults the "book shelf' mechanism. *American Association of Petroleum Geologists Bulletin*, **68**: 502-503.

Marsh, J. H., & Culshaw, N. G. 2014. Timing and conditions of high-pressure metamorphism in the western Grenville Province: Constraints from accessory mineral composition and phase equilibrium modeling. *Lithos*, *200–201*, 402–417.

Marsh, J. H., Gerbi, C. C., Culshaw, N. G., Johnson, S. E., Wooden, J. L., Clark, C. 2011b. Using zircon U–Pb ages and trace element chemistry to constrain the timing of metamorphic events, pegmatite dike emplacement, and shearing in the southern Parry Sound domain, Grenville Province, Canada. *Precambrian Research*, ***192–195***: 142-165.

Marsh, J. H., Gerbi, C. C., Culshaw, N. G., Potter, J., Longstaffe, F. J., & Johnson, S. E. 2011a. Initiation and development of the Twelve Mile Bay shear zone: the low viscosity sole of a granulite nappe. *Journal of Metamorphic Geology*, **29**(2), 167–191.

Marsh, J. H., Grew, E. S., Gerbi, C. C., Yates, M. G., & Culshaw, N. G. 2013. The petrogenesis of the Garnet Menzerite-(Y) in Granulite Facies Rocks of the Parry Sound Domain, Grenville Province, Ontario. *The Canadian Mineralogist*, **50**(1), 73–99.

Means, W. D. 1995. Shear zones and rock history. *Tectonophysics*, **247**(1–4): 157–160.

Mitra, G., 1992. Deformation of granitic basement rocks along fault zones at shallow to intermediate crustal levels. *In: S. Mitra and G.W. Fisher (Editors), Structural Geology of Fold and Thrust Belts. Johns Hopkins University Press, Baltimore, MD*: 123-144.

Mohanty, S., & Ramsay, J. G. 1994. Strain partitioning in ductile shear zones: an example from a Lower Pennine nappe of Switzerland. *Journal of Structural Geology*, **16**(5): 663-676.

Pennacchioni, G., & Mancktelow, N. S. 2007. Nucleation and initial growth of a shear zone network within compositionally and structurally heterogeneous granitoids under amphibolite facies conditions. *Journal of Structural Geology*, **29**(11): 1757–1780.

Ponce, C., Druguet, E., & Carreras, J. 2013. Development of shear zone-related lozenges in foliated rocks. *Journal of Structural Geology*, **50**: 176–186.

Ramsay, J. G., & Graham, R. H. 1970. Strain variation in shear belts. *Canadian Journal of Earth Sciences*, **786*:*** 786–813).

Ring, U., Geowissenschaften, I., & Gutenberg-universität, J. 1999. Volume loss, fluid flow, and coaxial versus noncoaxial deformation in retrograde, amphibolite facies shear zones. *GSA Bulletin*, **111**(1): 123-142.

Rivers, T. 1997. Lithotectonic elements of the Grenville Province: review and tectonicimplications. *Precambrian Research*, **86**(3-4): 117–154.

Rivers, T. and Corrigan, D. 2000. Convergent margin on southeastern Laurentia during the Mesoproterozoic: tectonic implications. *Canadian Journal of Earth Sciences*, **37**: 359–383.

Rivers, T. 2012. Upper-crustal orogenic lid and mid-crustal core complexes: signature of a collapsed orogenic plateau in the hinterland of the Grenville Province. *Canadian Journal of Earth Sciences,* **49**(1): 1-42.

Rivers, T. 2008. Assembly and preservation of lower, mid, and upper orogenic crust in the Grenville Province—Implications for the evolution of large hot long-duration orogens. *Precambrian Research*, **167**(3–4), 237–259.

Rivers, T., Ketchum, J., Indares, A., and Hynes, A. 2002. The High Pressure belt in the Grenville Province: architecture, timing, and exhumation. *Canadian Journal of Earth Sciences*, **39**(5): 867–893.

Rivers, T., Martignole, J., Gower, C.F., and Davidson, A. 1989. New tectonic divisions ofthe Grenville Province, Southeast Canadian Shield. *Tectonics*, **8**(1): 63–84.

Sassier, C., Leloup, P. H., Rubatto, D., Galland, O., Yue, Y., & Lin, D. 2009. Direct measurement of strain rates in ductile shear zones: A new method based on syntectonic dikes. *Journal of Geophysical Research*, **114**(B1), B01406.

Schrank, C. E., Handy, M. R., & Fusseis, F. 2008. Multiscaling of shear zones and the evolution of the brittle-to-viscous transition in continental crust. *Journal of Geophysical Research*, **113**(B1), B01407.

Schwerdter, W.M. 2005. *Orillia ' 05 - 25th Workshop of the Canadian Tectonics Group Field Trip Guide : Geological structure and lithology in in parts of the Muskoka Region, southwestern Central Gneiss Belt, Grenville Province of Ontario:* 1–37.

Slagstad, T., Hamilton, M. A., Jamieson, R. A., & Culshaw, N. G. 2004. Timing and duration of melting in the mid orogenic crust: Constraints from U – Pb (SHRIMP) data, Muskoka and Shawanaga domains , Grenville Province, Ontario. *Canadian Journal of Earth Sciences*, **41**: 1339–1365.

Srivastava, H. B., & Hudleston, P. 1995. Strain and possible volume loss in a high-grade ductile shear zone. *Journal of Structural Geology*, **17**(9): 1217-1231.

Tavani, S., Granado, P., Corradetti, a., Girundo, M., Iannace, a., Arbués, P., Mazzoli, S. 2014. Building a virtual outcrop, extracting geological information from it, and sharing the results in Google Earth via OpenPlot and Photoscan: An example from the Khaviz Anticline (Iran). *Computers & Geosciences*, **63**: 44–53.

Trap, P., Faure, M., Lin, W., Augier, R., & Fouassier, A. 2011. Syn-collisional channel flow and exhumation of Paleoproterozoic high pressure rocks in the Trans-North China Orogen: The critical role of partial-melting and orogenic bending. *Gondwana Research*, **20**(2–3), 498–515.

Tuccillo, M.E., Mezger, K., Essene, E.J., and van der Pluijm, B.A. 1992. Thermobarometry, Geochronology and the Interpretation of PTt Data in the Britt Domain, Ontario Grenville Orogen, Canada. *Journal of Petrology*, **33**(6): 1225–1259.

Twiss, R. J. & Moores, E. M. 2007. Structural Geology, 2nd edition. *New York: W. H. Freeman*. ISBN 9780 7167 4951 6

van Breemen, O., Davidson, A., Loveridge, W.D., and Sullivan, R.W. 1986. U-Pb ZirconGeochronology of Grenville Tectonites, Granulites and Igneous Precursors, ParrySound, Ontario.

van Gool, J.A.M. 1992. The Grenville Front foreland fold-and-thrust belt in southwestern Labrador: Mid-crustal structural and metamorphic configuration of a Proterozoic orogenic thrust wedge. *Ph.D, Memorial University of Newfoundland, St. John's*.

Vollgger, S. A., & Cruden, A. R. (2016). Mapping folds and fractures in basement and cover rocks using UAV. *Journal of Structural Geology*, **85**: 168-187.

Wodicka, N., Ketchum, J. W. F., & Jamieson, R. A. 2000. Grenvillian metamorphism of monocyclic rocks, Georgian Bay, Ontario, Canada: Implications for convergence history. *The Canadian Mineralogist*, **38**, 471–510.

Wodicka, N., Parrish R. R., and Jamieson, R. A. 1996. The Parry Sound domain; a far‐travelled allochthon? New evidence from U-Pb zircon geochronology. *Canadian Journal of Earth Sciences*, **33**,1087‐1104.

Wynne-Edwards, H.R. 1972. The Grenville Province. In Variations in tectonic styles in Canada. *Geological Association of Canada Special Paper 11*, 263–334.